Doctoral School in Environmental Engineering

An investigation of the *Ora del Garda* wind by means of airborne and surface measurements

Lavinia Laiti

UNIVERSITY OF TRENTO - Italy
Department of Civil, Environmental and Mechanical Engineering

2013

Doctoral thesis in Environmental Engineering, XXV cycle

Department of Civil, Environmental and Mechanical Engineering, University of Trento

Academic year 2011/2012

Supervisor: Dino Zardi, University of Trento

On the cover: view of the northern shoreline of Lake Garda from the panoramic trail between Busatte and Tempesta.

This thesis is partially based on:

Laiti, L., Zardi, D., de Franceschi, M., Rampanelli, G., 2013. Residual kriging analysis of airborne measurements: application to the mapping of atmospheric boundary-layer thermal structures in a mountain valley. *Atmos. Sci. Lett.* 14, 79-85.

Laiti, L., Zardi, D., de Franceschi, M., Rampanelli, G., 2013. Atmospheric boundary-layer structures associated with the *Ora del Garda* wind in the Alps as revealed from airborne and surface measurements. [submitted to *Atmos. Res.*]

University of Trento
Trento, Italy
2013

“Den 13. September, abends.

Heute früh um drei Uhr fuhr ich von Torbole weg mit zwei Ruderern.

Anfangs war der Wind günstig, daß sie die Segel brauchen konnten.

Der Morgen war herrlich, zwar wolkig, doch bei der Dämmerung still.

(...) so waren wir schon an Malcesine vorbei, als der Wind sich

völlig umkehrte, seinen gewöhnlichen Tagweg nahm

und nach Norden zog. Das Rudern half wenig gegen

die übermächtige Gewalt, und so mußten wir

im Hafen von Malcesine landen.”

J. W. Goethe, Italienische Reise (1861)

Aknowledgements

I would like to thank my supervisor, prof. Dino Zardi, for his support during these years. Thanks also to Dr. Massimiliano de Franceschi for the fruitful discussions, and for providing the data of the field campaign of summer 2001.
Thanks to the Trento University Sport Center (CUS Trento) for providing the motorglider, and to the pilot Fabrizio Interlandi for performing the flights.
The GIS and Remote Sensing Unit of the Edmund Mach Foundation, the Meteorological Office of the Autonomous Province of Trento (Meteotrentino), the Environmental Protection Agency of the Autonomous Province of Trento (APPA), the National Center for Meteorology and Climatology of the Italian Airforce, the Austrian Aeronautical Meteorological Office (Austro Control) and the Department of Atmospheric Science of the University of Wyoming are kindly acknowledged for providing the data from their surface weather stations and sounding stations.

Contents

List of Figures

List of Tables

Summary

On fair-weather summer days an intense southerly lake breeze blows across the northern shorelines of Lake Garda (Italy). This wind, known as *Ora del Garda*, arises regularly in the late morning, and then channels northward into the adjacent Sarca Valley and Lakes Valley, coupling with the local up-valley flow. In the early afternoon, after flowing over an elevated (~400 m high) saddle, the *Ora del Garda* wind breaks into the Adige Valley north of Trento city; there it flows down on the valley floor, interacting with the local up-valley wind and creating a strongly turbulent flow. The characteristic diurnal cycle of surface meteorological variables determined by the lake-valley coupled circulation is rather well-known, on the basis of climatological analyses of data from surface automatic weather stations operated in the area by local institutions; on the contrary, the valley upper atmosphere structure, i.e. the structure of the atmospheric boundary-layer (ABL), associated with the *Ora del Garda* development has not yet been investigated. Indeed, in such a complex terrain area, the characterization of the typical structure, spatial variation and depth of the ABL, as well as a sound knowledge of local atmospheric circulation patterns, are of crucial importance for the understanding of the local climate and of air pollution transport and dispersion processes.

To meet this lack of knowledge, a series of targeted measurement campaigns, including both intensive surface observations and research flights, were carried out by the Atmospheric Physics Group of the University of Trento in the study area between 1998 and 2001, providing the database for the present work. Five flights of an instrumented motorglider explored specific sections of the valley atmosphere, namely at Lake Garda's shoreline, in the lower Sarca Valley, in the Lakes Valley, and where the *Ora del Garda* and the Adige Valley up-valley flow interact. Position, pressure, temperature and relative humidity were measured along spiralling trajectories performed over the above mentioned target areas. Surface observations from a number of weather stations disseminated along the valley floor provided a picture of the diurnal cycles of meteorological quantities determined at the surface by the development of the investigated wind on the flight days.

The preliminary processing of the experimental dataset included the application of a suitable procedure to correct airborne temperature data for the time-delay effect induced by the slow-response behavior of the sensor, and required the determination of a proper time constant. The dominant vertical structure of the valley ABL was then deciphered on the basis of vertical "pseudo-soundings" (i.e. mean vertical profiles) of potential temperature and water vapour mixing ratio extracted from airborne data. Shallow mixed layers, surmounted by deeper stable layers, likely to be produced by local subsidence associated with up-slope flows, were detected up-valley. This characteristic pattern is indeed in good accord with ABL

structures typically observed in deep Alpine valleys in connection with up-valley winds, as reported in the literature. On the other hand, closer to the lake the potential temperature profile was typically stabilized down to lower heights, due to the onshore advection of colder air from above the water surface.

A residual kriging (RK) technique was adopted to map potential temperature fields over 3D high-resolution grids for each explored section of the valley atmosphere, integrating both surface and airborne observations. Exploiting a test-bed database, RK method was preliminarly tested against the interpolation methods commonly used in the literature for mapping airborne data, namely inverse distance, inverse squared distance and natural neighbor methods. The predictive performance of the different methods was assessed by means of a cross-validation procedure, and a critical comparison of the different interpolation results was carried out. Finally, RK resulted the best-performing technique for the specific application.

RK-interpolated fields revealed fine-scale local features of the complex ABL thermal structures determined by the *Ora del Garda* in the study area valleys, revealing at the same time macroscopic features of the thermo-topographically driven wind field, mainly amenable to irregular topography and land cover heterogeneities. In particular, a non-homogeneous penetration of the lake-breeze front across the flat basin facing Lake Garda was detected in the morning, while in the afternoon the presence of a sharp discontinuity in the upper-level vertical stratification, originated by updrafts and downdrafts associated with the lake breeze circulation, was observed. Moreover, a strongly asymmetric potential temperature field, resulting from the contrast between the stable core of the *Ora del Garda* up-valley flow and an intense up-slope flow layer developing along a bare-rock valley sidewall, was detected in the area of Cavedine Lake in the Lakes Valley. Further up-valley, RK-interpolated fields displayed a thermal structure compatible with the occurrence of a single-cell cross-valley circulation, likely to be originated by asymmetric solar irradiation and by the local valley curvature. The valley curvature was also found to induce a preferential channeling of the up-valley flow along the northwestern sidewall at the valley end, in proximity of the elevated saddle from where the *Ora del Garda* overflows into the underlying Adige Valley, giving origin to an anomalous, strong katabatic wind that hinders the regular development of the local up-valley wind in the area north of Trento. Here the westerly inflow from the Lakes Valley feeds a denser wedge of potentially cooler air, which forces the local up-valley (i.e. southerly) wind to flow over it. Regridded potential temperature fields provided further insight into this flow pattern, revealing the occurrence in the area of a hydraulic jump structure, due to the blocking exerted on the flow by the eastern Adige Valley sidewall. This induced a pronounced deepening of the local mixed layer, which was likely produced by the highly-turbulent flow conditions that usually develop here following the *Ora del Garda* outbreak.

Chapter 1

Introduction

1.1 Introduction

During summertime an intense southerly breeze regularly blows on fair-weather days all cross the northern shorelines of Lake Garda. This wind, known as *Ora del Garda*[1], arises regularly in the late morning, and then channels northward into the adjacent Sarca Valley and Lakes Valley, interacting with their up-valley flow. Under favourable synoptic conditions, this breeze typically blows until the late afternoon, or even the early evening. The environment where this phenomenon takes place is very peculiar: the northern branch of Lake Garda is enclosed by high mountain ranges on both sides, resembling a sort of funnel-shaped fjord. The Sarca and Lakes Valleys are the northward continuation of the lake's basin. This furrow is a preferential corridor for the diurnal motion of the air masses, moving from the layers above the Po Valley and the lake surface, towards the inner Alpine valleys. After flowing over the elevated saddle of Terlago at the end of the Lakes Valley, the *Ora del Garda* breaks into the adjacent Adige Valley (which lies more than 400 meters below) north of Trento, where it mixes with the local up-valley wind, creating a strong and gusty local flow. The turbulence originated there is so intense that the old city airfield located right in this area was dismissed in the 70s.

The presence of Lake Garda confers a sub-mediterranean nature to the climate of the region. The *Ora del Garda* extends this mildening influence to the whole Lakes Valley, favouring in particular the cultivation of olive trees and vineyards in the area. Agriculture is not the only productive sector profiting from the peculiar local atmospheric circulation patterns: the coastal breeze regime puts the northern branch of the lake among the world's premier locations for sailing, windsurfing and kitesurfing. Indeed, water sport tourism provides consistent income for the local economy. Moreover, mesoscale atmospheric circulation systems play a dominant role in air pollution transport and diffusion processes at the regional scale: they are particularly relevant for areas in coastal and complex orography, like this area, where unusual interactions between the lake breeze and the up-valley wind regimes occur. During daytime, the pollutants produced or residing over the Po Valley are entrapped inside the well mixed convective boundary-layer (CBL) over the land, or in the stable air layers over the lake's surface; the development of the *Ora del Garda* circulation transport these polluted air masses along the Lake Garda basin and the adjacent Alpine valleys, resulting in a long-range pollution transport and possible harmful effects on the health of the people living in these regions. A deeper understanding of the mechanisms governing the development of the local winds in the study area is therefore expected to improve the forecasting skills and to provide more reliable weather and air quality predictions for many purposes, such as agriculture, tourism and water sports.

[1] The origin of the name "*Ora*" is not certain; it is supposed to derive from the Latin words "*aura*" or "*hora*", that mean respectively "*breeze*" and "*hour*", thus referring to the proverbial punctuality of the wind onset in the warm season.

Research on the *Ora del Garda* wind dates back to the early years of the twentieth century. In fact, a specific investigation of this wind was first performed by A. Defant. He provided a careful analysis of Lake Garda's seiches (A. Defant 1908) and of the daily-periodic pressure gradients reversal between the Po Valley and the South Tyrol Alpine reliefs (A. Defant 1909). In the years immediately preceding the pioneering slope and valley winds works by Jelinek (1937), Wagner (1938) and F. Defant (1949, 1951), that laid the foundations for the theory of thermally-driven mountain winds, the observed abnormal behaviour induced on the diurnal Adige Valley wind by the *Ora del Garda* in the area north of Trento attracted the interest of Austrian meteorologists, who investigated the phenomenon by means of balloons and double theodolite measurements, and aerologic analyses (Pollak 1924, Wiener 1929, Schaller 1936), as reported in Wagner (1938). More recently, the Atmospheric Physics Group (APG) at the University of Trento focused on the *Ora del Garda* as a specific case of valley wind. The research work started with a characterization of the *Ora del Garda* diurnal cycle from data collected by surface automatic weather station (AWS) networks operated by local institutions (Baldi et al. 1999, Daves et al. 1998, Giovannini 2012). Moreover, the APG carried out a series of targeted measurement campaigns, including not only intensive surface observations (de Franceschi et al. 2002, de Franceschi 2004, Zardi et al. 1999) but also airborne measurements by means of a light instrumented aircraft (de Franceschi et al. 2003, Rampanelli 2004), which provided the database for the present work. At present, ground level patterns of pressure, wind, temperature and moisture determined by the *Ora del Garda* development are qualitatively well known. On the other hand, the upper atmosphere structure, i.e. the structure of the atmospheric boundary-layer (ABL), associated with the wind development has not yet been investigated. Indeed, its characterization represents the main goal of the present study.

1.2 Motivation and rationale of the thesis

Up to now only a few observational, modeling and theoretical studies have been focusing on the development of thermally-driven wind systems over small lakes (lakes whose characteristic width is smaller than 50 km, according to Crosman and Horel 2012 and Segal et al. 1997) in Alpine areas, and associated ABL processes (e.g. the Lake Tekapo Experiment - LTEX, which included both intensive observations and numerical simulations; Kossmann et al. 2002, McGowan et al. 1995, McGowan and Sturman 1996, Sturman et al. 2003a, 2003b, Zawar-Reza et al. 2004). Under fair-weather conditions both slope and valley circulations arise in deep mountain valleys, like those forming the study area; from the coupling between these wind systems and local lake breezes, multi-scale, complex thermally-driven wind fields may arise, which differ from both "classical" slope/valley winds and lake breezes. Indeed, such combined airflows are known to display stronger intensity and farther inland penetration then "pure" circulations (Bergström and Juuso 2006, Kondo 1990a, 1990b,

McGowan et al. 1995), being possibly responsible for the transport of airborne pollutants on longer distances and seriously deteriorating air quality at considerable distances from primary emission sites (Carroll and Baskett 1979, Kitada et al. 1986, Wakimoto and McElroy 1986). Therefore, as already anticipated, the investigation of the typical patterns of the *Ora del Garda* wind and of the associated ABL variability is expected to be beneficial for air quality forecasting and management in the study area, for a good knowledge of the typical local circulations and ABL structure is essential to this kind of applications. In particular, the characterization of the non-trivial meteorological processes occurring at the junction between the Lakes Valley and the Adige Valley may definitely be of great interest, for the influence of such processes on the local patterns of pollution transport and dispersion in the intensely urbanized area including Trento and the villages north of the city.

Beside influencing surface heat and moisture exchanges with the soil and the vegetation canopy, in mountainous regions thermally-driven winds play also an important role in the triggering of convection and precipitation, due to the fact that the convergence they produce in the afternoon along the mountain crests locally increases the atmospheric moisture content (Barthlott et al. 2006, Bertò et al. 2004, Gladich et al. 2011, Kalthoff et al. 2009, Pucillo et al. 2009). Indeed, a more comprehensive understanding of local winds development and associated ABL processes could represent a further step towards the improvement of local-scale weather forecasting skills and of the knowledge of local micro-climatic conditions, such as for example those characterizing the urban area of Trento (Giovannini et al. 2011, 2013). This could be useful for many human activities, like agriculture, tourism, and water and mountain sports, which represent the natural economic vocation of the territory.

Accordingly, in order to explore how the *Ora del Garda* development affects temperature and moisture fields in the upper valley atmosphere, and the connections between the breeze flow at the valley floor and the thermodynamic processes occurring inside the ABL, an analysis based on both surface and airborne measurements is proposed in the present research work. This is the first time that the original database formed by the APG flights exploring the atmosphere structure in the valleys where the *Ora del Gard*a blows is analysed in full detail through a systematic approach.

While the daily evolution of the coupled lake-breeze and valley-wind circulation at the lowest levels is determined on the basis of surface observations from a number of automatic weather stations (AWSs) deployed along the valley floor, the mean vertical structure of the valley ABL is inferred from airborne measurements collected by means of a motorglider equipped to the purpose. Airborne vertical profiles of potential temperature and humidity are interpreted in the light of the conceptual framework for thermo-topographically driven circulations and ABL evolution over complex terrain (Zardi and Whiteman 2013), supplied by theoretical and experimental findings, often coming from field measurements carried out during major international research projects (such as the MAP-Riviera project, among others;

Weigel and Rotach 2004, Rotach and Zardi 2007; or the above-cited LTEX project), as well as from more recent numerical modelling studies (Antonelli and Rotunno 2007, Crosman and Horel 2012, Kuwagata and Kimura 1995, 1997, Rampanelli et al. 2004, Serafin and Zardi 2010a, 2010b, 2011, Schmidli and Rotunno 2010, 2012, Weigel et al. 2006). To gain detailed pictures of potential temperature and mixing ratio fields over the vertical sections of the valley atmosphere explored by the flights mentioned above, a residual kriging (RK) mapping technique (Ahmed and de Marsily 1987, Goovaerts 1999, Odeh et al. 1994, 1995) is applied to airborne measurements. The soundness and the strengths of the proposed method are carefully assessed, in comparison with simpler interpolation techniques previously used in the literature for similar datasets, e.g. inverse distance weighted and inverse squared distance interpolation (Egger 1983, Hennemuth 1985) or natural neighbour interpolation (De Wekker 2002, Weigel and Rotach 2004). High-resolution fields produced by RK application allow retrieving the fine-scale 3D variability of the valley ABL. As the latter partially reflects the main local features of the thermo-topographically driven wind field, some speculations about the *Ora del Garda* flow development across the study area valleys are also drawn.

1.3 Thesis outline

The plan of the thesis is as follows.

In the next chapter (**Chapter 2**) a detailed description of the geographic area where the *Ora del Garda* wind blows is provided, and the diurnal development of the coupled lake-breeze and valley-wind system is outlined. The associated typical daily cycles of wind and temperature are also characterized by analysing time series of surface observations from local AWSs, selecting four days of clear and regular development of the *Ora del Garda*.

The setup of the measurement platform, i.e. the instrumented motorglider, is introduced in **Chapter 3**, together with the adopted flight strategy and the general features of the collected airborne data. For each of the five flights forming the experimental dataset, an overview of weather conditions is given, and a detailed description of the *Ora del Garda* diurnal pattern, based on surface observations, is reported.

In **Chapter 4** the methods used for airborne data post-processing are introduced. A preliminary procedure for correcting the time-lag effect induced by the slow-response temperature sensor is described and applied. Then a brief overview of the methods previously used in the literature for mapping airborne observations over high-resolution regular grids is provided, together with an introduction to RK technique. A comparison of the performance of the different interpolation methods, based on a test-bed dataset formed by three flights, follows. Finally, strengths and weaknesses of RK are discussed, allowing further evaluations about the suitability of the different interpolation methods and the choice of the flying strategy for ABL structure exploration in complex terrain.

The dominant vertical structure of the ABL developing in the study area valleys in

connection with the *Ora del Garda* is analysed in **Chapter 5**. Vertical "pseudo-soundings", extracted from airborne potential temperature and water vapour mixing ratio observations by means of a moving-window vertical average algorithm, allow isolating the prevailing vertical structures. These are interpreted in the light of the conceptual framework for the ABL daily evolution over complex terrain, where thermally-driven slope and valley winds play a key role.

In **Chapter 6** the high-resolution 3D fields of potential temperature and mixing ratio resulting from the application of RK to the airborne dataset described in **Chapter 3** are presented and discussed. The analysis of the fine-scale variability of the ABL thermal structures displayed in the interpolated meteorological fields provides further insight into the structure of the thermo-topographically driven flow patterns developing in the study area.

The last chapter (**Chapter 7**) summarizes the key results of the proposed investigation of the *Ora del Garda* wind, and provides an outlook on possible directions for future work.

Chapter 2

The *Ora del Garda* wind

Abstract

This chapter provides a detailed description of the geographic area where the *Ora del Garda* wind blows, from the northern end of Lake Garda and the lower Sarca Valley to the Lakes Valley further north, until the saddle of Terlago, which communicates these valleys with the Adige Valley immediately north of Trento city. The diurnal development of the coupled lake-breeze and valley-wind system across the study area is then outlined. Indeed, the *Ora del Garda* arises in the late morning as an intense southerly lake breeze over the northern shorelines of Lake Garda, and then channels northward into the above mentioned valleys, where it couples with the local up-valley flows. On days of greater intensity, the wind reaches the Adige Valley in the early afternoon, after flowing over the elevated saddle of Terlago at the end of the Lakes Valley. There the *Ora del Garda* interacts in a complex fashion with the local up-valley wind, producing a strong and gusty anomalous flow that persists in the area until the late evening. The typical daily cycles of wind and temperature associated with this circulation are characterized through the analysis of surface observations from a number of automated weather stations disseminated along the valley floor, selecting four days of clear and regular development of the *Ora del Garda*.

2.1 Introduction

Daily-periodic local circulations typically arise under fair-weather conditions along coastal regions, originated by the differential heating of neighboring water and land surfaces that produces corresponding pressure differences in the air columns. These result in a system of breezes blowing across the shoreline and reversing their direction between day and night (see **figure 2.1**). After sunrise, the greater sensible heat fluxes over the land heats the air column more rapidly than over the water surface. This causes a more rapid expansion of the land columns, meaning that the pressure aloft becomes higher than at the same level over the water. This in turn results in an offshore flow at upper levels, and hence an onshore flow develops across the shoreline at lower levels, i.e. the sea/lake breeze, resulting in a complete circulation cell. On the contrary, the land breeze is initiated in the evening due to the more rapid cooling and contraction of the land air column.

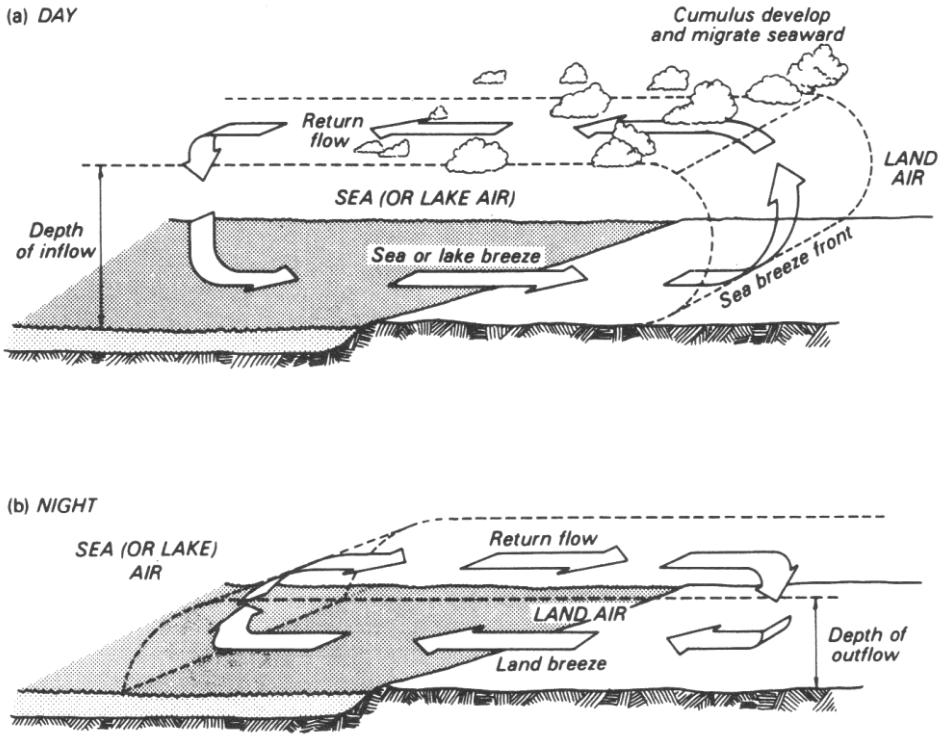

Figure 2.1. Schematic diagram of **a)** sea and **b)** land breeze circulations developing across a shoreline by day and night respectively, during fair-weather conditions. Notice the leading edge of the sea breeze, i.e. the sea-breeze front, formed by colder and more humid marine air moving onshore and wedging under the warmer land air (from Oke 1987).

Sea/lake breezes play a leading role in determining local weather and climate, as well as related processes, such as pollution transport from mesoscale down to local scale (Boyouk et al. 2011, Lyons and Olsson 1973). For this reason sea and large-lake breezes have been

extensively investigated, both theoretically and by means of field observations and numerical simulations (see, among others, the reviews by Atkinson 1981, Crosman and Horel 2010, Pielke 1984, Simpson 1994). On the other hand, less attention was paid to a systematic characterization of thermally-driven winds arising over small lakes, i.e. lakes whose characteristic width is less than 50 km according to the survey of observational studies on small lakes provided by Segal et al. (1997). As a matter of fact, the broad diversity in size, shape and surrounding land use and topography makes a comprehensive treatment of atmospheric dynamics associated with small lakes more difficult. An attempt to estimate size effects was made by Crosman and Horel (2012), who evaluated the sensitivity of lake breeze intensity and extent to lake diameter by means of idealized numerical simulations. Boybeyi and Raman (1992) also performed idealized numerical simulations of the airflow developing over a circularly-shaped lake, in order to analyse the lake-breeze sensitivity to the lake-land temperature difference, the ambient wind magnitude and direction, the lake size, the surrounding surface roughness, the Coriolis force; they identified the lake-land temperature difference and the ambient wind as the main factors influencing the lake breeze.

A variety of daily-periodic, thermally-driven winds is also observed in mountainous regions. These airflows develop as an organized and interacting system of air motions, including regional scale circulations (such as mountain-plain winds), mesoscale flows (such as valley winds), and local scale currents (such as slope winds) (see Zardi and Whiteman 2013 for a recent review of mountain wind systems). These winds are also generated by the differential heating of air masses. In particular, slope winds are produced by buoyancy forces arising from the the more rapid heating/cooling of air close to a slope than air at the same level but far from the slope. They blow up-slope during daytime and down-slope during nighttime. On the other hand, valley winds typically blow up-valley during daytime and down-valley during nighttime; they are induced by horizontal pressure gradients arising from the fact that the diurnal temperature variation range is generally larger in a valley than over the adjacent plain (Vergeiner and Dreiseitl 1987, Whiteman 1990). This is usually interpreted through geometric explanations: during daytime the same amount of energy is used to heat a smaller volume in a valley than over a plain, resulting in a greater heating of the valley air. Similarly, at night the same loss of energy cools a smaller volume, resulting in lower temperatures in a valley. This concept, which is quantified by the "topographic amplification factor" (TAF), was first proposed by Wagner (1932) and Steinacker (1984). The typical daily cycle of valley and slope winds is represented in the well-known diagram by F. Defant (1949) (**figure 2.2**), which illustrates the different stages of interaction between these two types of circulations. Thermally-driven mountain winds deeply affects the ABL processes (Rotach and Zardi 2007) and, as a consequence, local air quality conditions (de Franceschi and Zardi 2009, Gohm et al. 2009, Kalthoff et al. 2000). Moreover, they are known to play an important role also in the initiation of deep convection on mountainous terrain, for the convergence they produce along

the mountain crests increases the local moisture content in the atmosphere (Barthlott et al. 2006, Gladich et al. 2011, Kalthoff et al. 2009, Pucillo et al. 2009).

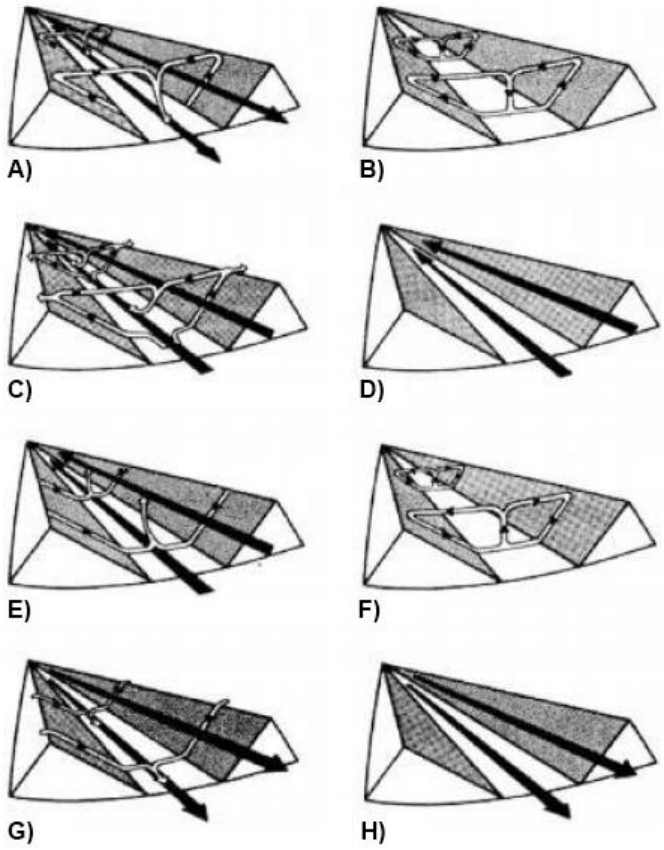

Figure 2.2. Defant's (1949) scheme of diurnal slope and valley wind regimes. From the top: **A)** at sunrise the down-valley wind still blows while up-slope winds start to develop, **B)** in the morning transition phase up-slope winds are fully developed, **C)** at noon up-slope winds weaken and the up-valley wind starts to blow, **D)** in the late afternoon the up-valley wind is fully developed, **E)** at sunset the up-valley wind weakens and down-slope winds start to develop, **F)** in the late-evening transition phase down-slope winds are fully developed, **G)** in the first hours of the night down-slope winds weaken and the down-valley wind develops, **H)** before sunrise down-slope winds cease and the down-valley wind is fully developed.

The basic mechanisms of mountain winds are well documented, as they were extensively studied since the 1930s (F. Defant 1949, 1951, Jelinek 1937, Wagner 1932, 1938). In the last decades, the increasing capabilities of numerical simulations allowed researchers to make considerable progress in the understanding of atmospheric processes involved in the development of these winds (Chow et al. 2006, Kuwagata and Kimura 1997, Rampanelli et al. 2004, Schmidli and Rotunno 2010, 2012, Schmidli et al. 2011, Serafin and Zardi 2010a,

2010b, 2011, Weigel et al. 2006, 2007a, 2007b). In particular, recent investigations by (Rampanelli et al. 2004, Schmidli and Rotunno 2010, Serafin and Zardi 2010a, 2010b, 2011, Weigel et al. 2006) revealed that the absence of heat exchange between the valley atmosphere and the free atmosphere above assumed in the TAF conceptual scheme rarely holds true, and that other mechanisms are usually involved in the heating/cooling of the valley atmosphere.

In situations where a shoreline and complex terrain combine, coastal breeze systems typically interact with topography-driven circulations. Idealized numerical simulations by Kondo (1990b) provided evidence of an effective enhancement of the sea breeze in connection with a valley outlet in front of the coast, even at many kilometers distance, leading to a regional-scale unified flow, the so-called "Extended Sea Breeze". Similarly, detailed observations around the small Lake Tekapo (25 km × 3.5 km) in New Zealand outlined the development of a complex lake-valley wind system, referred to as the "Extended Lake Breeze" (Kossmann et al. 2002, McGowan et al. 1995, McGowan and Sturman 1996). Mahrer and Pielke (1977) also showed that the combination of sea breeze and mountain circulations produce a more intense circulation than when they act separately. Indeed, a variety of site-specific phenomena are observed to arise from different combinations of coastal and orographic factors. Lidar observations in the Monterey Bay and in the Salinas Valley (California) documented the morning development of a shallow sea breeze, evolving into a deeper unified up-valley circulation in the afternoon (Banta 1995, Darby et al. 2002, De Wekker et al. 2012). During the ESCOMPTE project, Bastin et al. (2005) reported the different behavior accompanying the diurnal development of local winds in two large valleys facing the Mediterranean Sea in the area of Marsille (France): the Rhône Valley and the Durance Valley. While the former does not modify significantly the sea breeze development, the narrower Durance Valley always affects the channeled sea breeze by accelerating the flow. Indeed, Bergström and Juuso (2006), by means of numerical simulations over idealized topography, provided evidence that a lake acts as a continuous source of cold air at a valley bottom, leading to stronger up-valley winds. Furthermore, Bischoff-Gauß et al. (2006), in their investigation of the impact of a new storage lake on the arid environment of the Elqui Valley in the Andes, found that, even if a real lake breeze circulation may fail to develop, the presence of the small lake (7.6 km^2) significantly modifies the surface energy budgets, and consequently the local airflows.

The present work examines a peculiar case of lake-breeze and valley-wind interaction in the southeastern Italian Alps, the so-called *Ora del Garda* wind. This wind arises over the northern shoreline of Lake Garda, and hence blows northward up-valley for few tens of kilometers, until it breaks out, through an elevated saddle, into the adjacent Adige Valley. Here it interacts with the local up-valley wind, producing a strong and gusty flow. Various authors contributed in the past to the understanding of the mechanisms behind this particular, and in some respect anomalous, wind (A. Defant 1908, 1909, Pollak 1924, Schaller 1936,

Wagner 1938, Wiener 1929). More recently, some targeted measurement campaigns were carried out, including not only intensive surface observations (de Franceschi et al. 2002, Zardi et al. 1999), but also flights of an instrumented motorglider (de Franceschi et al. 2003), which actually provided the database for the present work. Also, climatologic characterizations of the typical patterns associated with the *Ora del Garda* were provided by Baldi et al. (1999), Daves et al. (1998) and Giovannini (2012), based on the analysis of data from a network of surface weather stations.

This chapter provides a detailed description of the peculiar and complex topographic context where the *Ora del Garda* wind develops, i.e. the northernmost part of Lake Garda basin and the Sarca, Lakes and Adige valleys in the southeastern Italian Alps. The different stages of the breeze development in the above area are also illustrated, and the typical daily cycle associated with the wind is outlined, based on the analysis of selected surface observations from a number of automated weather stations (AWSs) disseminated along the valley floor in the area.

2.2 Description of the study area

The target area for the present study is the corridor connecting the region north of Lake Garda with the Adige river Valley near the city of Trento, in the southeastern Italian Alps (**figure 2.3a**). Lake Garda is a typical subalpine lake of glacial origin, displaying a length of 52 km and a maximum width of 17 km, with a total surface area of 368 km^2. Its main tributary is the Sarca river. Indeed the southern part of the above corridor is the lower Sarca river Valley, while the northern part is the Lakes Valley (**figure 2.3b**). Actually these two valleys represent the northward extension of Lake Garda's geological basin, and run almost parallel to the adjacent Adige Valley for approximately 35 km in SSW-NNE direction. On the southern end the corridor is bounded by the northern shore of Lake Garda (65 m MSL), whereas on the northern side it joins the Adige Valley through an elevated saddle on its western sidewall, a few kilometers north of Trento. Although the topography of the valley looks rather regular at a larger scale, yet it contains many fine-scale features. In particular a wide and flat region faces Lake Garda's shoreline (65-90 m MSL), with the only exception of the isolated rocky hill of Mt. Brione (376 m MSL) (see **figure 2.4**). Up-valley to the town of Arco, the valley floor width narrows from about 4 km to 0.5 km, but then it widens again farther north into the Lakes Valley where Cavedine Lake lies (245 m MSL). Here the Lakes Valley is flanked on the eastward side by the elevated Cavedine Valley (valley floor height: 300-580 m MSL) for about 15 km. Farther north, the valley narrows again by S. Massenza and Toblino lakes (245 m MSL), where it suddenly bends eastward, becoming roughly W-E oriented and broadening out.

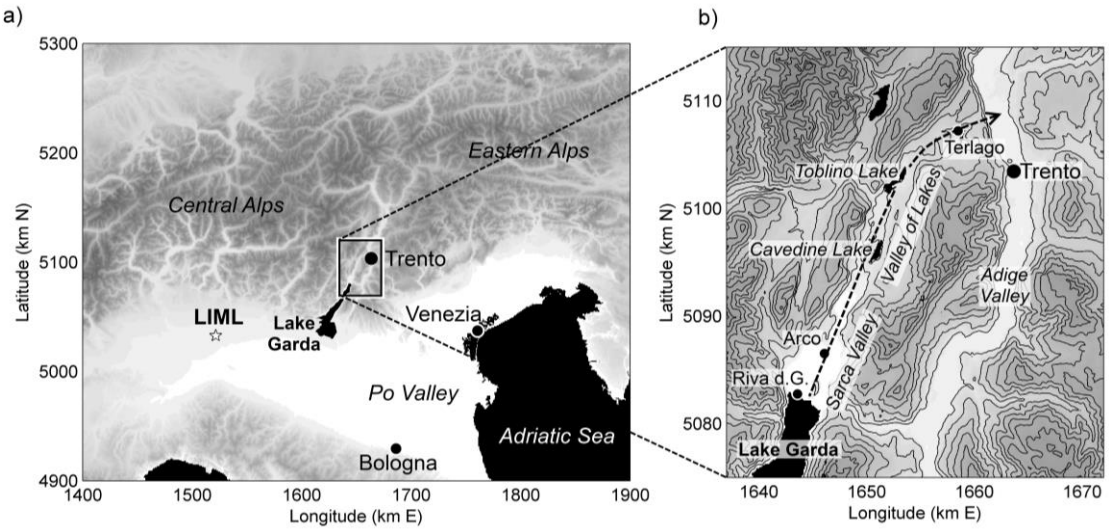

Figure 2.3. **a)** Localization of the target area (indicated by the rectangular box) near Trento city and Lake Garda, in the southeastern Italian Alps. **b)** Topography of the study area (contour interval: 200 m); the dashed arrow marks the path followed by the *Ora del Garda* wind along the lower Sarca Valley and Lakes Valley, from the northern shoreline of Lake Garda to the saddle of Terlago, and finally to the Adige Valley north of Trento. Cavedine and Toblino lakes are also indicated, as well as some reference towns in the area (Trento, Riva del Garda, Arco and Terlago). Coordinate system: Gauss Boaga, Italy East fuse.

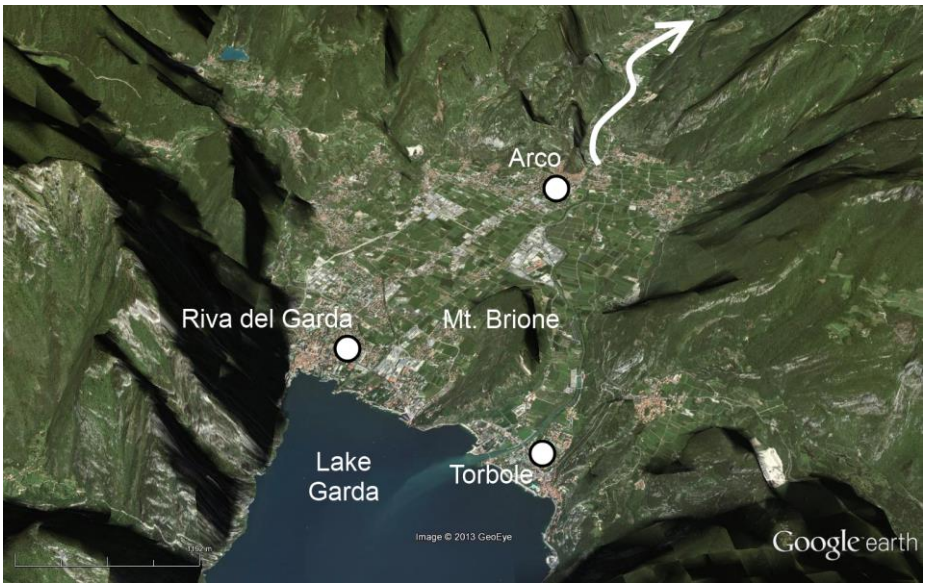

Figure 2.4. 3D view of the topography of the the lower Sarca Valley facing the northern shoreline of Lake Garda (view is from S). Mt. Brione relief is indicated. The white arrow marks the corridor communicating the lower Sarca Valley with the Lakes Valley farther north. Image © Google Earth, © 2013 GeoEye.

After an uneven series of bumps and holes, it reaches the elevated saddle of Terlago (minimum height 580 m MSL), incumbent on the adjacent Adige Valley floor (198 m MSL) through a jump of more than 400 m, immediately north of the city of Trento (see **figure 2.5**).The height of the surrounding crests ranges between 1500 and 2000 m MSL, providing an average valley depth of approximately 1500 m all along the valley. The western valley sidewalls, especially the northernmost ones, are more favorably exposed to solar radiation, due to the valley orientation, and are in general much steeper and less vegetated than the eastern sidewalls.

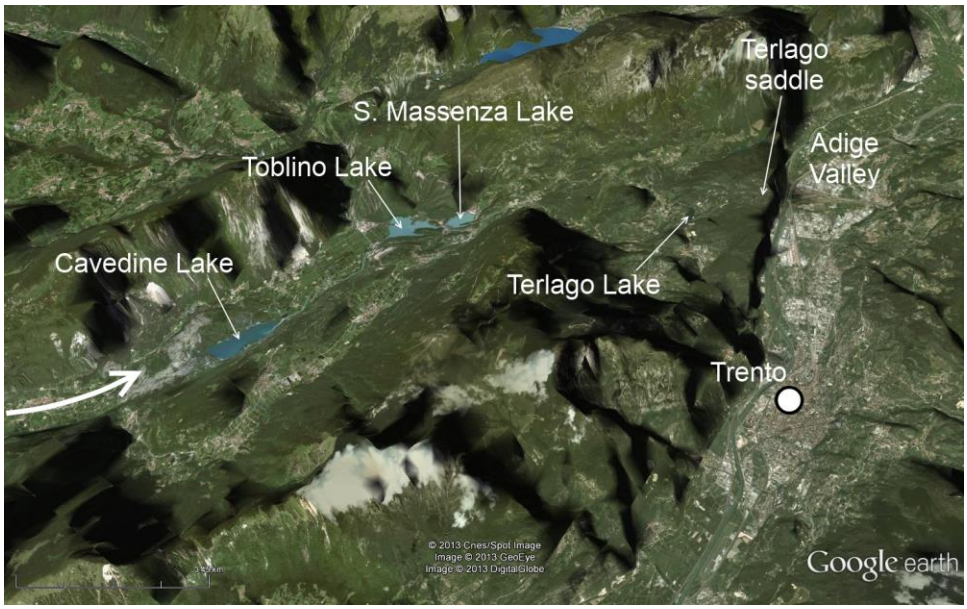

Figure 2.5. 3D view of the Lakes Valley topography, from the area of Cavedine Lake to the Terlago saddle ridge and the junction with the Adige Valley (view is from SE). Cavedine, Toblino, S. Massenza and Terlago lakes are indicated in the image, together with the city of Trento. The white arrow marks the corridor communicating the Lakes Valley with the lower Sarca Valley (cf. **figure 2.4**). Image © Google Earth, © 2013 Cnes/Spot Image, © 2013 GeoEye, © 2013 DigitalGlobe.

The altimetric profile of the valley from the Lake Garda shoreline to the junction with the Adige Valley is provided in f**igure 2.6**. The average valley floor slope increases northward, from 0.5‰ (in the lower Sarca basin) to 7% (in the upper Lakes Valley), displaying a plateau between Cavedine and Toblino lakes. As already mentioned, a number of small lakes (surface area: less than 1 km^2) are present on the valley floor: Cavedine Lake (245 m MSL) lies about 15 km inland from the Lake Garda's shore, Toblino and S. Massenza lakes (242 and 245 m MSL) are located about 10 km further up-valley, while Terlago Lake (416 m MSL) is found in the proximity of the Terlago saddle ridge. Their locations are indicated in **figures 2.3b** and **2.5**. The presence of Lake Garda, which is the largest Italian lake, consistently

marks the local climate with a mildening effect. As a consequence, the study area displays a peculiarly broad range of climates within a few kilometers range of altitude: while subalpine vegetation is present at the more elevated heights, submediterranean thermophile vegetation is found near the lake shoreline, and olive trees, vineyards and orchards are cultivated in the areas over, or slightly above, the valley floor (Keller et al. 1996).

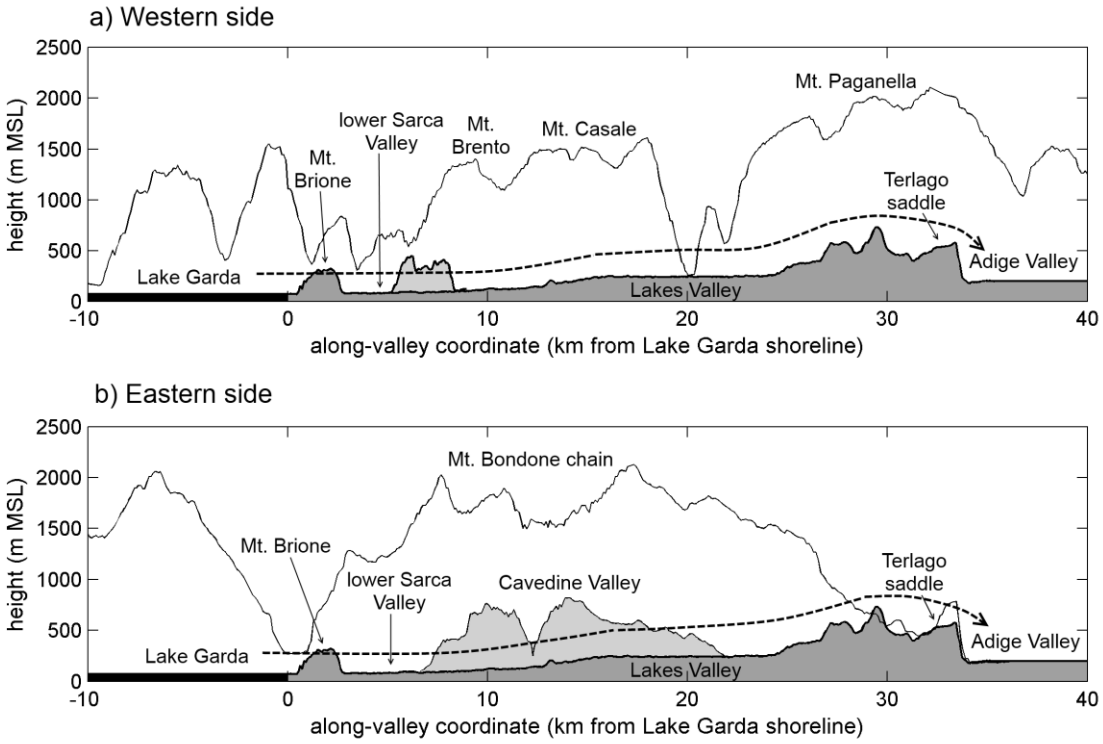

Figure 2.6. Altimetric profile of the floor of the valleys where the *Ora del Garda* wind blows (dark grey shading), from the northern shoreline of Lake Garda (black shading) to the Terlago saddle, where the wind finally breaks out into the underlying Adige Valley (the wind path is indicated by the dashed arrow). The profiles of the lateral crests are shown for both the valley sides, and the most important topographic features of the area are also reported.

2.3 The *Ora del Garda* development

On fair-weather, warm-season days, during daytime the lower atmosphere reaches higher temperatures in the Alpine valleys facing the Po Valley than on the plain itself. This temperature contrasts create pressure gradients driving plain-to-mountain and valley winds. In particular, the up-valley wind two local up-valley winds develop in the area represented in **figure 2.3b**: one along the funnel-shaped corridor formed by the northern Lake Garda basin and the valleys north of it, and the other in the parallel Adige Valley.

The former starts as an intense southerly lake breeze, arising in the late morning on the

northern shorelines of the lake, and then channels northward up-valley, resulting in the lake and valley coupled diurnal circulation known as *Ora del Garda*. When the thermal forcing is strong enough to produce an appreciable pressure gradient throughout the above mentioned valleys, connecting the area north of Lake Garda to the Adige Valley and allowing a vigorous development of the breeze, the latter spreads all along the Lakes Valley, up to the elevated saddle of Terlago. Through this saddle the *Ora del Garda* airflow breaks out into the underlying Adige Valley, where it interacts with the local up-valley wind, producing strong gusts at the the valley floor and intense turbulence in the layers aloft.

Observations of the *Ora del Garda* wind were first performed by A. Defant (1909): he carried out an aerologic analysis of the reversal of daily-periodic pressure gradients associated to the establishments of valley winds between the Po Valley and the Adige and Sarca Valley. He also was the first to report a local perturbation of valley winds in the Adige Valley at Trento, observing that in summer the development of southerly up-valley winds is completely normal both south and north of Trento, while at Trento up-valley winds rarely blow, and anomalous northwesterly winds are quite frequent at around 1400 LST.

Later on, this abnormal behavior of the diurnal valley wind at Trento was the subject of various investigations by Austrian meteorologists, which were summarized in Wagner's (1938) review on valley winds. Pollak (1924) and Wiener (1929) observed the daytime vertical distribution of the wind direction in the area of Trento by means of pilot balloons and theodolite; they found that a northerly direction prevails at the ground, gradually turning to southerly with height, until southerly winds become predominant at around 1000 m above the Adige Valley floor. A consistent explanation for this phenomenon was first outlined by Schaller (1936). He hypothesized that the potentially cooler air advected up-valley by the *Ora del Garda* wind over the saddle of Terlago pour down the western Adige Valley sidewall and slide along its floor. This spillover feeds a denser air wedge, which splits into a southward and a northward branch, and partly climbs over the opposing sidewall, forcing the main stream of the warmer local up-valley wind to flow over it (Schaller 1936, Wagner 1938). The interaction between the two circulations results in strong turbulent motions, which are typically experienced in the area throughout the afternoon.

2.4 An example of typical *Ora del Garda* diurnal cycle

Although displaying seasonal variations in strength and timing, yet the *Ora del Garda* wind is a very regular phenomenon (as foreseen by the daily periodicity typical of all thermally-driven local winds; F. Defant 1951, Zardi and Whiteman 2013), which consistently marks the local climate. Preliminary climatological analyses have been performed by Baldi et al. (1999), Daves and Zardi (1998) and de Franceschi et al. (2002), who analysed time series of observations collected from a number of local AWSs, disseminated along the valley floor. Statistics of hourly averaged values of wind speed and direction, air temperature,

relative humidity, pressure and solar radiation were computed for selected fair-weather days of clear *Ora del Garda* development, in order to characterize the wind daily cycle. From these analyses, the typical onset and offset times of the breeze fall between 1100 and 1200 LST (UTC+1), and 1900 and 2000 LST respectively. The characteristic wind intensity at Lake Garda's shoreline is around 6 m s^{-1} (measured at 5 m AGL), with maximum values being recorded around 1400-1600 LST, while the characteristic wind direction is SSW, shifting to W at the Lakes Valley outlet. After an initial heating phase in the morning, the southernmost AWSs (i.e. those closer to Lake Garda shoreline) display a local drop or at least a flattening of the temperature curve, accompanied by a wind direction reversal from a northerly (i.e. offshore and down-valley) flow to a southerly (i.e. onshore and up-valley) flow, and by an increase in wind speed. At the lake shore the wind shift is particularly rapid, and a sudden increase in water vapour mixing ratio is also observed when the lake breeze arises. All of these phenomena are typically associated with the inland penetration of cold and humid fronts produced by coastal breezes (cf. Simpson 1994, Zumpfe and Horel 2007).

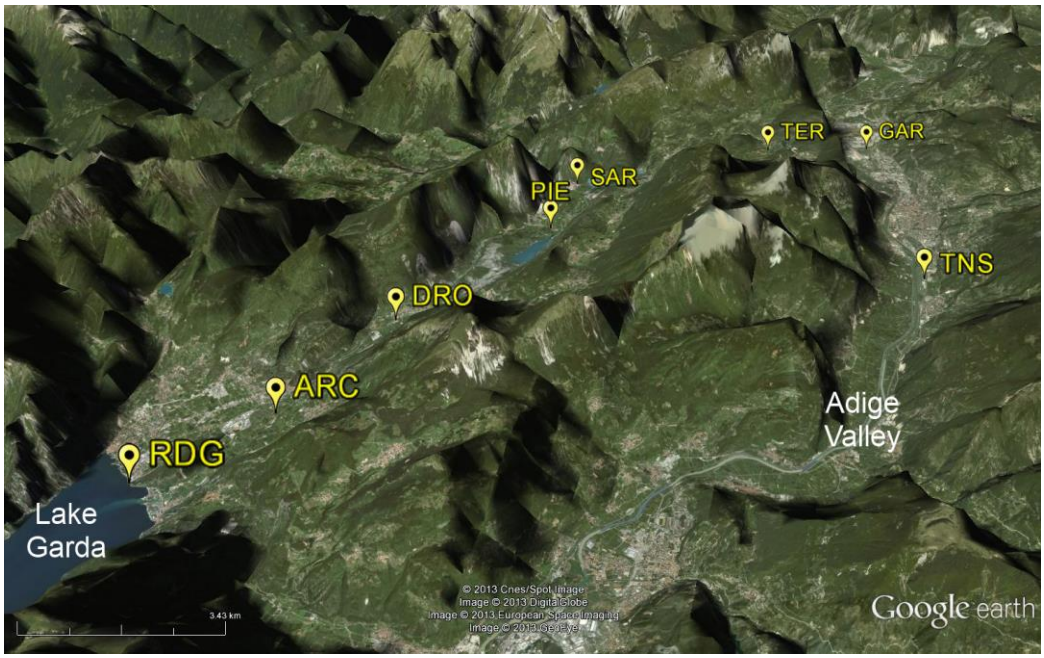

Figure 2.7. Localization of the AWSs considered in the climatologic analysis performed for the 18-21 August 2012 period, from Lake Garda shoreline to the Terlago saddle ridge, and the Adige Valley (view is from SE). Image © Google Earth, © 2013 Cnes/Spot Image, © 2013 DigitalGlobe, © 2013 European Space Imaging, © 2013 GeoEye.

To provide an example of the characteristic daily cycles of meteorological variables determined at the valley floor by the breeze, four days representative of clear *Ora del Garda*

development have been selected, namely 18, 19, 20 and 21 August 2012, when a large high-pressure system determined persistent anticyclonic conditions over northern Italy. Hourly observations of solar radiation, wind and temperature collected at the AWSs indicated in **figure 2.5** and listed in **table 2.1** have been averaged over these four days, and are shown in **figures 2.6**, **2.7** and **2.8**, and **2.9** respectively. Daily cycles of solar radiation at all stations confirm the occurrence of clear-sky and high-irradiation conditions on the selected days (**figure 2.8**), allowing the full development of thermally-driven circulations. **Figure 2.9** reports time series of wind vectors, after being projected onto the local along-valley direction for each specific AWS site.

Table 2.1. List of the AWSs considered in the climatologic analysis performed for the 18-21 August 2012 period. AWS names refer to the ones indicated in **figure 2.7**. Each AWS elevation is also reported, together with the height of the installed anemometer. All the stations are operated by Istituto Agrario di S. Michele all'Adige - Edmund Mach Foundation.

AWS name	Elevation	Anemometer height
RDG	69 m MSL	5 m AGL
ARC	83 m MSL	10 m AGL
DRO	115 m MSL	3 m AGL
PIE	242 m MSL	3 m AGL
SAR	249 m MSL	3 m AGL
TER	427 m MSL	3 m AGL
GAR	194 m MSL	3 m AGL
TNS	185 m MSL	10 m AGL

For the selected days, at RDG the wind direction suddenly changes from N to S between 1000 and 1100 LST, and the wind speed rapidly grows up to about 6 m s^{-1}, indicating the passage of the lake-breeze front. Maximum wind speed values are recorded between 1300 and 1600 LST, then the breeze gradually weakens, until the wind direction reverses again between 1900 and 2000 LST. A westward deflection of the flow is produced here by the presence of Mt. Brione relief to the E, immediately behind the shoreline. ARC station in the middle of the flat basin facing Lake Garda displays more gradual transitions, with a morning clockwise rotation and an evening counter-clockwise rotation of the wind vectors. On the contrary, at DRO the up-valley flow appears to be very well channelled into the narrow corridor which communicates the lower Sarca Valley with the Lakes Valley. Farther north at PIE and SAR the *Ora del Garda* blows from 1200 LST until respectively 1900 LST and 1800 LST. Close to the ridge of the saddle of Terlago, at TER station, the up-valley wind regime

begins only at 1300 LST, but persists until 2200 LST, longer than at AWSs further down-valley, for in this specific area the local pressure gradient vanish later (in accord with previous observations by de Franceschi et al. 2002).

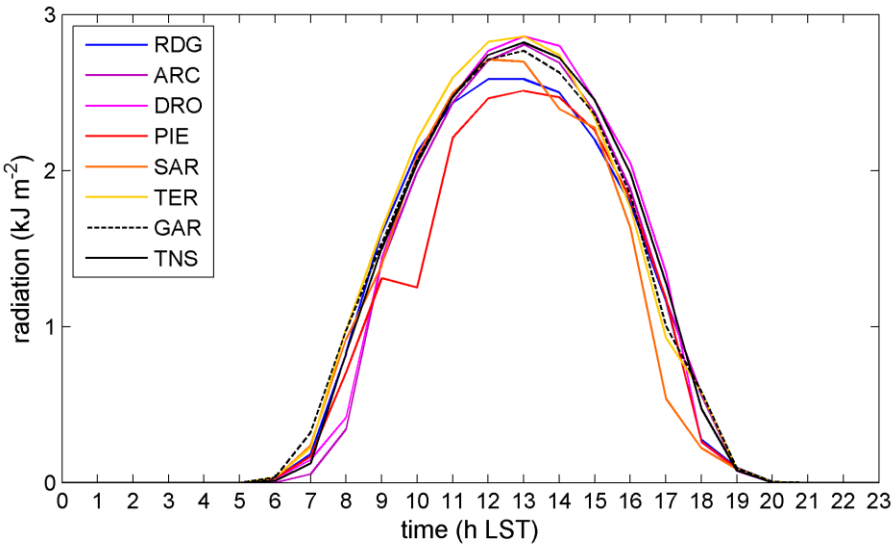

Figure 2.8. Daily cycles of solar radiation at the AWSs considered in the climatologic analysis performed for the 18-21 August 2012 (see **figure 2.7** for locations). Notice that all the cycles present a very regular pattern, (except at PIE, where the shadowing by some obstacle, possibly a tree, causes a morning radiation deficit occurring everyday), indicating very clear-sky conditions for the selected days.

In general the *Ora del Garda* intensity maximum is observed to occur later when moving up-valley from the lake's shoreline to the Lakes Valley end: at 1300 LST at RDG, ARC and DRO, at 1400 LST at PIE and SAR, and at 1600 LST at TER (**figure 2.10**). On the other hand, at TNS in the adjacent Adige Valley the local up-valley wind blows from 1400 to 2100 LST, displaying an intensity peak beween 1600 and 1700 LST. Accordingly, a weak up-valley wind is detected at 1400 LST also at GAR, which is located exactly in front of the Terlago saddle, before the wind direction abruptly shift to W when the potentially colder *Ora del Garda* air overflows from the Lakes Valley at 1500 LST. The westerly current gradually strengthens, reaching an intensity of approximately 4.5 m s^{-1} between 1700 and 1900 LST, then slowly weakens until ceasing at 2200 LST, when the inflow from the Lakes Valley stops (cf. TER) (**figure 2.9** and **2.10**).

Average temperature daily cycles in **figure 2.11** show the effects of the lake-breeze inland propagation: at RDG the *Ora del Garda* onset induces a pronounced drop after 1100 LST (clearly marking the breeze front passage), while at the AWSs further up-valley the temperature curve is evidently flattened during the up-valley flow hours. This reveals the

important role of the lowest-atmosphere cooling process associated with the up-valley advection of cold air from above Lake Garda surface.

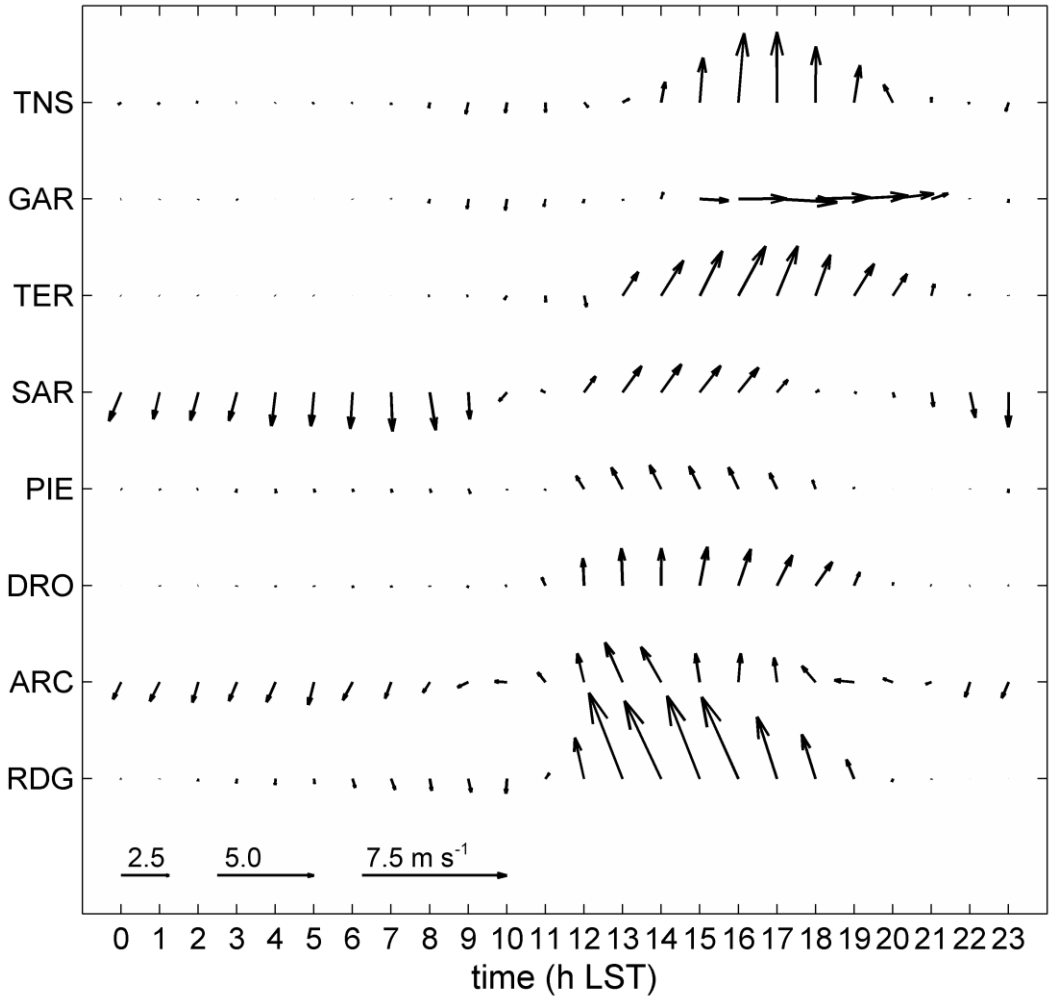

Figure 2.9. Daily cycles of wind speed and direction as time series of wind vectors at the AWSs considered in the climatologic analysis performed for the 18-21 August 2012 (see **figure 2.7** for locations and **table 2.1** for anemometer heights). Notice that the wind vectors have been projected onto the local valley axis direction (22.5° N for RDG, ARC, DRO, PIE; 45.0° N for SAR; 67.5° N for TER; -22.5° N for GAR; 0.0° N for TNS), so that in this representation vertical and horizontal components represent respectively along-valley and cross-valley wind components. The sequence is from the AWS closest to Lake Garda shoreline (RDG), at the bottom of the graph, to the farthest (TNS), at the top. Accordingly the *Ora del Garda* wind development can be followed along the Sarca and Lakes Valley until the Adige Valley, reading the graph from the bottom to the top.

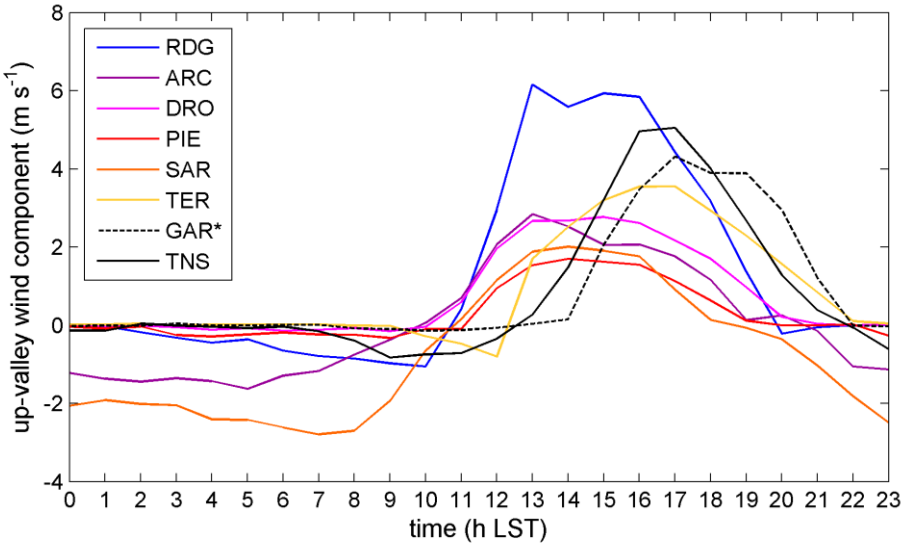

Figure 2.10. Daily cycles of down-stream wind speed (i.e. the wind component locally associated to the *Ora del Garda* and Adige Valley wind flow) at the AWSs considered in the climatologic analysis performed for the 18-21 August 2012 (see **figure 2.7** for locations and **table 2.1** for anemometer heights). The local orientation adopted for the valley axis is reported in **figure 2.9** caption. (*) Notice that for GAR the cross-valley component is displayed as down-stream component, instead of the along-valley component shown for all the other AWSs.

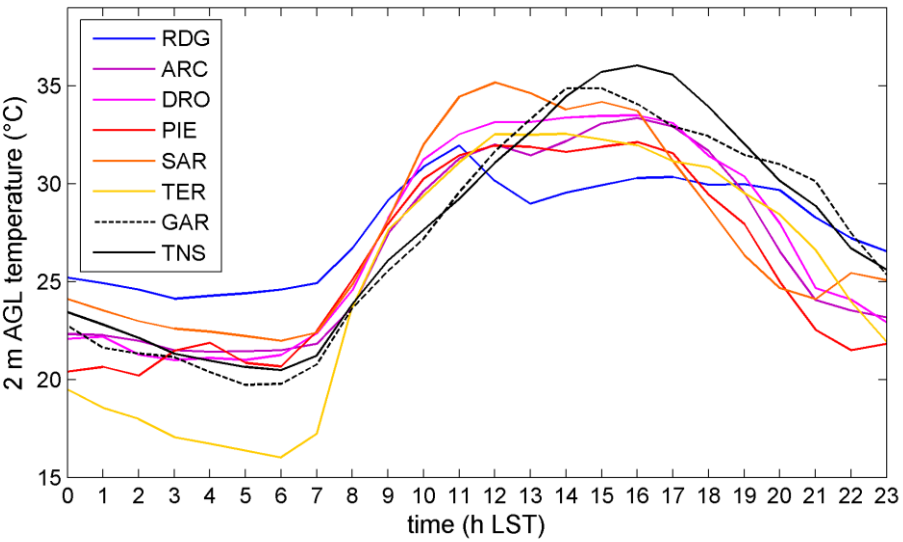

Figure 2.11. Daily cycles of 2 m AGL air temperature at the AWSs considered in the climatologic analysis performed for the 18-21 August 2012 (see **figure 2.7** for locations).

Indeed, also temperature observations from the Adige Valley floor display very different patterns for TNS and GAR. While the former displays a "standard" temperature cycle for a summer day, composed of a morning heating phase and a peak at around 1500-1600 LST, followed by a gradual cooling phase, the temperature cycle of the latter is suddenly modified by the *Ora del Garda* outbreak into the Adige Valley, and from 1500 LST deviates from the TNS "standard" cycle. From that point onward, the air temperature at GAR slowly but constantly decreases as an effect of the inflow of colder air, until the westerly flow ceases; indeed lower temperature values than at TNS are recorded until 1900 LST, while from 2000 to 2200 LST the temperature keeps slightly higher than at TNS, for the air advection from the Lakes Valley (which is still persisting in the area in the late evening) partially delays the radiative cooling process.

2.5 Summary

The lake-breeze and valley-wind coupled circulation that is the subject of the present thesis, i.e. the *Ora del Garda* wind, is introduced. This thermally-driven wind arises as a southerly, intense lake breeze from the northern shorelines of Lake Garda in the southeastern Italian Alps, in the late morning of fair-weather, warm-season days. Then it channels northward into the Sarca and Lakes valleys, coupling with their up-valley flows. On days of greater intensity, after overflowing from the elevated saddle of Terlago at the end of the Lakes Valley, the *Ora del Garda* breaks out into the Adige Valley nearby, where it interacts with the local up-valley wind in a rather complex fashion.

Indeed, the topography of the area where the *Ora del Garda* develops is very peculiar and complex. Moreover, the presence of Lake Garda at the valley inlet marks the daily cycle associated with the wind with the typical features of lake breeze circulations, especially in the lower valley (i.e. closer to the lake shoreline). The analysis of selected days of surface observations from AWSs deployed along the valley floor provided evidence of the inland penetration of a lake-breeze cold front, from the lake's shoreline across the lower Sarca Valley. Moreover, the advection of colder air produces an homogeneous suppression of the temperature rise, i.e. a flattening of the temperature curve, during the central hours of the day, which is recorded also at stations further up-valley in the Lakes Valley. On the other hand, associated with the *Ora del Garda* outbreak, an anomalous westerly flow occurs in the early afternoon in the Adige Valley, right in front of the saddle of Terlago. In this area the potentially colder air pouring from the Lakes Valley (i.e. from W) down to the Adige Valley floor produces a strong and gusty flow, which overcomes the local up-valley wind. The latter is therefore forced to flow over the denser air wedge that forms at the valley floor, and channels in both northward (up-valley) and southward (down-valley) direction. This anomalous wind pattern typically persists in the area until the late evening, i.e. a few hours after the *Ora del Garda* offset at Lake Garda shoreline.

Chapter 3

Outline of airborne and surface measurements

Abstract

Measurement platforms based on manned or unmanned light aircrafts represent very flexible tools for atmospheric research, for they are able to provide high spatial and temporal resolution observations. Indeed, they have been widely used in field campaigns whose aim was the investigation of thermally-driven slope/valley winds and sea/land breezes, and of the associated non-trivial, fine-scale 3D variability of atmospheric boundary-layer structures. In this chapter the instrumented motorglider used to perform the five flights forming the airborne dataset analysed in the present work and the five flights forming the latter are briefly presented, together with a brief overview of the weather conditions occurring on the single flight days. Moreover, for each flight the diurnal cycles of the two principal thermally-driven circulations developing in the study area, i.e. the *Ora del Garda* and the Adige Valley wind, are characterized on the basis of surface observations from local weather stations.

3.1 Introduction

Measurement platforms based on manned or unmanned light aircrafts (i.e. remotely piloted aircraft systems) represent very flexible tools for atmospheric research, for they may help to reduce the gap between ground-based and satellite observations. Indeed, they allow both vertical profiling and horizontal surveys of the atmosphere, providing high spatial and temporal resolution observations of its structure (Bonin et al. 2013, de Franceschi et al. 2003, Druilhet and Durand 1997, Neininger et al. 2001, Reuder et al. 2009). This is particularly important when meteorological processes characterized by a non-trivial 3D variability at small spatial scales are studied. Actually, light aircrafts have been largely adopted in the investigation of atmospheric boundary-layer (ABL) processes in complex terrain contexts, where the low atmosphere displays significant horizontal inhomogeneities. For example, the field campaigns of the DISKUS project (Hennemuth 1985, 1986, Hennemuth and Schmidt 1985), the MAP-Riviera project (Rotach et al. 2004, Rotach and Zardi 2007, Weigel and Rotach 2004) and the ALPNAP project (de Franceschi and Zardi 2009, Gohm et al. 2008, Harnisch et al. 2009, Heimann et al. 2007, Schnitzhofer et al. 2009), which focused on the development of thermally-driven slope/valley winds in Alpine valleys, and associated ABL structure and pollution spatial distribution, included flights of instrumented light aircrafts. Similarly, airborne measurement platforms based on light aircrafts were used by Finkele et al. (1995), Kraus et al. (1999), Stephan et al. (1999) and Wood et al. (1999) in order to characterize the front region for sea breeze circulations, and by Flamant et al. (1999) and Brooks and Rogers (2000) for the investigation of internal boundary-layers (IBLs) associated with onshore flows.

Since the aim of the present thesis is the investigation of ABL structures occurring in connection with the development of a lake-breeze and valley-wind coupled system, i.e. the *Ora del Garda*, the use of a measurement platform based on a motorglider is particularly appropriate. Indeed, the main advantage offered by such a highly manoeuvrable light airplane is the possibility of exploring the whole valley volume, both in cross- and along-valley direction. Airborne observations appears to be a necessary complement to surface measurements collected at a number of automated weather stations (AWSs) deployed along the valley floor in the study area, which show the diurnal cycle of the *Ora del Garda* at the ground surface. **Chapter 3** presents the experimental dataset analysed in this research work, starting with a description of the airborne measurement platform and of the flight strategy. Then the trajectories followed during the five flights forming the database and their timing are illustrated, including a brief overview of the weather conditions on the flight days, and a detailed analysis of the diurnal cycles of the local wind patterns as revealed by surface observations from the local AWSs.

3.2 The airborne measurement platform

Between 1997 and 2001 a series of research flights were performed by the Atmospheric Physics Group of the University of Trento in order to investigate the ABL structure in the study area and in the Adige Valley, near the cities of Trento and Bolzano (de Franceschi et al. 2003). The measurement platform was set up on a motorglider, a Scheibe Falck SF 25C (see **figure 3.1**), owned by the Trento University Sport Center (CUS Trento), a highly manoeuvrable light airplane that could be operated only for diurnal visual flight. The motorglider had a single 80HP engine, allowing a maximum speed of 42 m s^{-1}. The equipment included instruments for the measurement of standard scalar atmospheric variables, such as air pressure, temperature and relative humidity, as well as a GPS device, which was operated in continuous kinematic mode with relative positioning, to achieve a precise positioning of measurement locations. The meteorological sensors installed onboard the motorglider and their technical specifications are listed in **table 3.1**.

Figure 3.1. The Scheibe Falck SF 25C. Notice temperature and humidity sensors mounted on the left-side leg of the motorglider undercarriage (lower-right corner of the picture). Picture by courtesy of Massimiliano de Franceschi.

The use of an aerial vehicle for carrying out atmospheric measurements requires greater care in the setup of the instrumentation installed onboard, than usually required in standard atmospheric measurements. Indeed, to avoid possible measurement disturbances due to flow distortion or to temperature alteration by exhaust emissions, the positioning of the instruments on the airplane was carefully planned. Temperature and humidity sensors were mounted on the left-side leg of the undercarriage to ensure a suitable distance from the

boundary layer of the motorglider wing. Moreover, the RTD sensor was shielded against direct solar radiation by means of a specific protection, which at the same time allowed an adequate ventilation of the sensing part. The thermohygrometer fragile sensing parts were also equipped with a specific cap in order to protect them from mechanical stress during the flights. On the other hand, the barometer, the GPS receiver and the datalogger were placed inside the cockpit. The data acquisition was synchronized with the GPS system, and a sampling frequency of either 1.0 or 0.5 Hz was chosen (see de Franceschi et al. 2003 and Rampanelli 2004 a more detailed description of the measurement platform setup and operation). Notice that all sensors were slow-response with respect to the typical timescales of turbulent fluctuations. Hence they naturally filtered out high-frequency turbulent fluctuations in time and space, and recorded mean values only.

Table 3.1. List of the meteorological sensors carried by the motorglider and main technical specifications.

Sensor	Technical specifications
Barometer Vaisala Mod. PTB 101 B	Range: 600 ÷ 1060 hPa Accuracy at 20 °C: ± 0.5 hPa 100% response time: 300 ms
Temperature RTD sensor Hart Scientific Mod. 5627	Range: –200 ÷ 500 °C Accuracy: ± 0.050 °C (at 0 °C). ± 0.051 °C (at 200 °C) Time constant in water (1 m s^{-1}): ≤ 4 s
Thermohygrometer Rotronic Mod. PT 101 A	Humidity range: 0 ÷ 100% RH Temperature range: -40 ÷ +60 °C Accuracy at 23°C: ± 1% RH, ± 0.3 °C Time constant in air (23 °C, 1 m s^{-1}): ≤ 10 s for RH, ≤ 15 s for temperature

3.3 General outline of airborne measurements

For all the five flights analysed in this study, the motorglider took off from a small airfield located about 5 km south of Trento in the Adige Valley, and entered the upper Lakes Valley flying over the saddle of Terlago; then it flew in southward direction all along the study area valleys until reaching the northern shoreline of Lake Garda, and finally came back.

The aircraft followed ascending and descending spiraling trajectories over some target areas, moving around vertical planes oriented either in cross- or along-valley direction, and performing a series of long quasi-horizontal transects and small-radius curves at turning points. This flight pattern was designed taking into account some practical constraints (like

the typical climbing/diving speed allowed by the motorglider, the minimum distance required for turning, the shape of the underlying topography and the minimization of the flight duration), and also the nature of the phenomenon under investigation; indeed, this type of trajectory allowed the identification not only of the dominant vertical structure, but also of the fine-scale horizontal variability, e.g. between the valley atmosphere core and the slope layer. Specific slices of the valley atmosphere at particularly interesting locations were explored, namely the Lake Garda shore and the flat basin forming the lower Sarca Valley (site A), the area of Cavedine Lake in the Lakes Valley (site B), the upper Lakes Valley and the area of the Terlago saddle (site C), and the Adige Valley in front of the latter (site D). The flying height typically ranged from a minimum of about 170 m MSL (i.e. about 100 m above Lake Garda surface) to a maximum of about 2500 m MSL, in order to explore a few hundreds of meters above the crests of the mountain enclosing the target valleys. The typical duration of a single downward/upward spiraling leg varied on average between 15 and 25 min. This time interval is smaller than the characteristic time scale of the ABL evolution (in the order of 1 h; Stull 1988), thus the ABL structure may be reasonably considered in steady-state conditions for each single section survey. During the flights the climbing and diving speeds of the motorglider typically varied between 1.5 and 2.5 m s^{-1} respectively, while the average cruise speed was of about 25-30 m s^{-1}; as a consequence, the vertical and horizontal average spacings between subsequent observations resulted respectively of 1-3 m and 25-30 m for 1.0 Hz measurements, and of 3-5 m and 50-60 m for 0.5 Hz measurements.

3.4 24 September 1998 flight (flight #1)

3.4.1 Description of the flight

The 24 September 1998 flight included four vertical cross-valley sections in the lower Sarca Valley and Lakes Valley (see **figure 3.2**). The flight was performed in the late morning before local noon, i.e. in the early phase of the *Ora del Garda* development. A spiral explored the atmosphere over the flat basin facing the Lake Garda shoreline, immediately north of Mt. Brione (site A), while the area over Cavedine Lake was explored twice (site B). The last spiral was performed north to S. Massenza Lake in the upper Lakes Valley, where the valley changes its orientation from SSW-NNE to WSW-ENE and the valley cross section narrows before widening out to the Terlago saddle area (site C). This flight was the only flight exploring the eastern half of the valley cross section at site B, i.e. the elevated Cavedine Valley running parallel to the Lakes Valley (spiral B/e in **figure 3.2**). All the other flights investigated only the western half of the cross section (spiral B/w in **figure 3.2**). Notice that humidity measurements are not available for flight #1. Timings and characteristics of the flight trajectory are summarized in **table 3.2**.

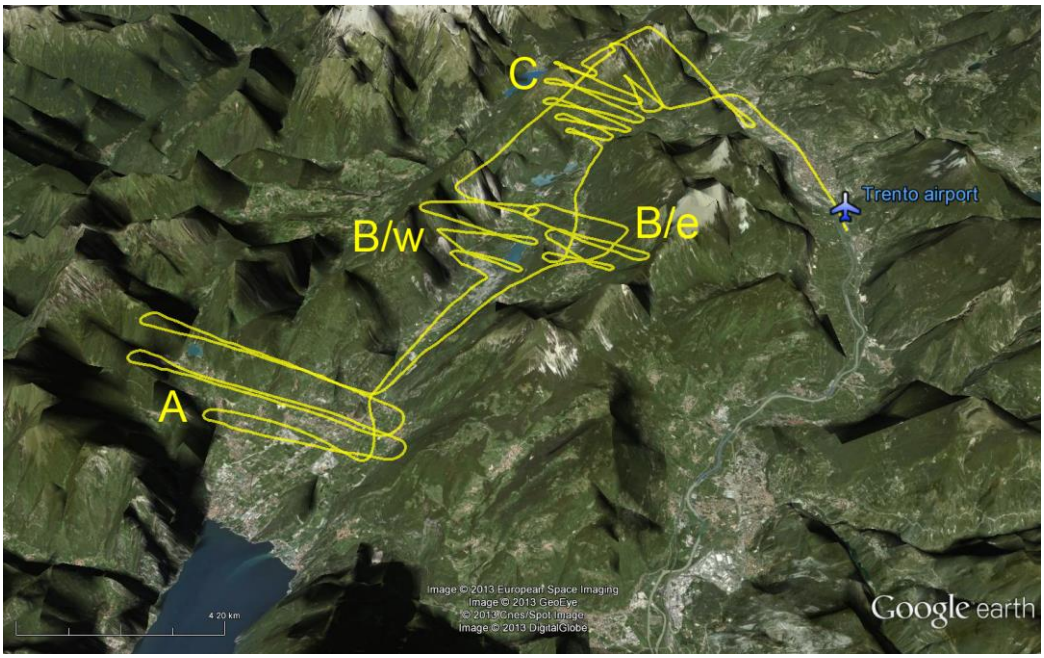

Figure 3.2. 3D representation of flight #1 trajectory (yellow line). View is from S. The name of the vertical sections explored by each single spiral are also indicated (labelled according to the site they explored). Image © Google Earth, © 2013 European Space Imaging, © 2013 GeoEye, © 2013 Cnes/Spot Image, © 2013 DigitalGlobe.

Table 3.2. Timings and characteristics of measurement flight #1. Single spirals are labelled according to **figure 3.2**. CV and AV respectively indicate whether the spiraling trajectories explored a cross- or an along-valley oriented section. D stands for a descending (downward) flight leg and U for an ascending (upward) flight leg. LST times are UTC+1 times.

Flight		Takeoff	Landing	Spiral	Start	End	Trajectory
#1	24 Sep 1998	1015 LST	1300 LST	B/w	1054 LST	1110 LST	CV D
				A	1116 LST	1143 LST	CV U
				B/e	1148 LST	1200 LST	CV D
				C	1205 LST	1228 LST	CV U

3.4.2 Weather conditions and surface observations

Flight #1 was performed on a fair-weather day of late summer, when weak synoptic forcing and completely clear-sky conditions allowed a full development of local thermally-driven wind systems. These situation is documented by surface observations from weather stations

routinely operated in the area (see **figure 3.3** and **table 3.3** for station locations and technical specifications). In particular, three key stations were selected as most representative, namely:

- RDG: right on Lake Garda shoreline, immediately up-stream (with respect to the wind flow), and on the western side of Mt. Brione;
- ARC1: about 5 km north to the lake shoreline in the middle of the lower Sarca Valley, about 1 km south to the valley narrowing north of Arco town;
- TNS: at Trento airport, a few kilometers south to the area where the *Ora del Garda* breaks into the Adige Valley.

Time series of wind, radiation, temperature and water vapor mixing ratio from these stations are shown for flight #1 in **figure 3.4**. Further input on the weather situation was obtained from inspection of additional sources (not reported here), such as synoptic charts from NCEP analyses, satellite images, and observations from PAG surface station on top of Mt. Paganella (2125 MSL; see **figure 3.3** and **table 3.3**), representative of intermediate upper levels. An overview of 24 September 1998 weather conditions, based on the above data, follows.

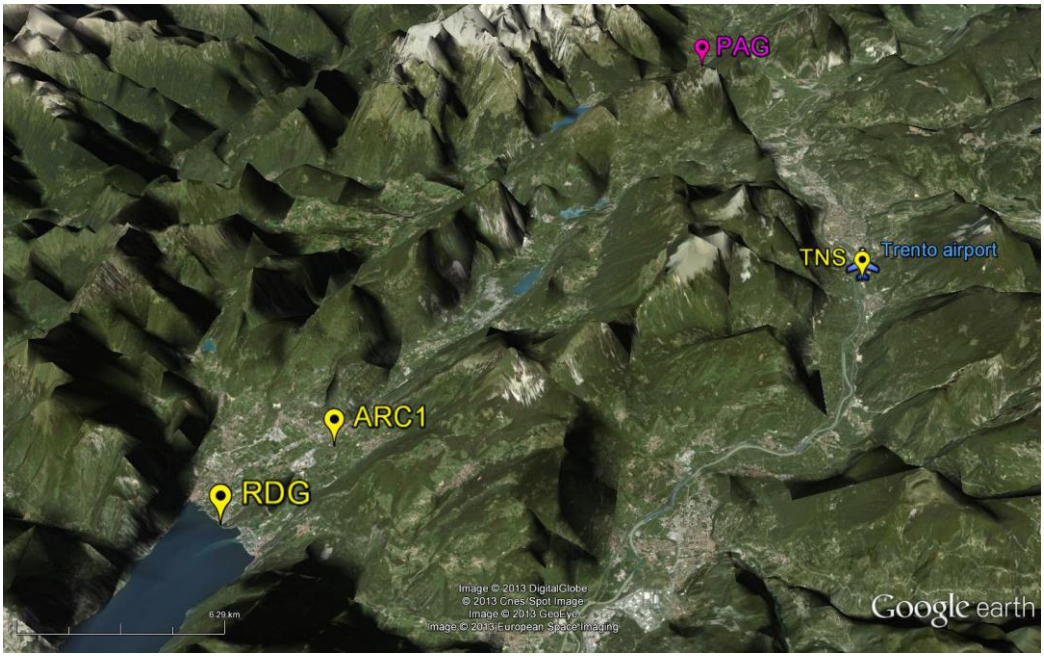

Figure 3.3. Location of RDG, ARC1, TNS and PAG surface weather stations in the study area. View is from SE. Image © Google Earth, © 2013 DigitalGlobe, © 2013 Cnes/Spot Image, © 2013 GeoEye, © 2013 European Space Imaging.

A high pressure ridge extending over Italy and central Europe induced the presence of a weak south-southwesterly synoptic circulation, which is confirmed by soundings from the nearest stations and by surface wind observations at PAG. 24 September 1998 was characterized by relatively high temperatures. Indeed satellite images and surface observations at PAG reveal the total absence of clouds over the study area and very clear-air conditions. Accordingly,

radiation time series at RDG, ARC1 and TNS display a perfectly regular pattern (cf. **figure 3.5**).

Table 3.3. List of surface weather stations considered in the discussion of weather conditions and surface observations for flights #1, #2 and #3. The operating institution is also indicated (IASMA stands for Istituto Agrario di San Michele all'Adige). The local terrain height and the height of the installed anemometer are also reported.

Station	Institution	Terrain height	Anemometer height
RDG	IASMA	69 m MSL	5 m AGL
ARC1	IASMA	83 m MSL	10 m AGL
TNS	IASMA	185 m MSL	10 m AGL
PAG	Italian Airforce	2125 m MSL	[---]

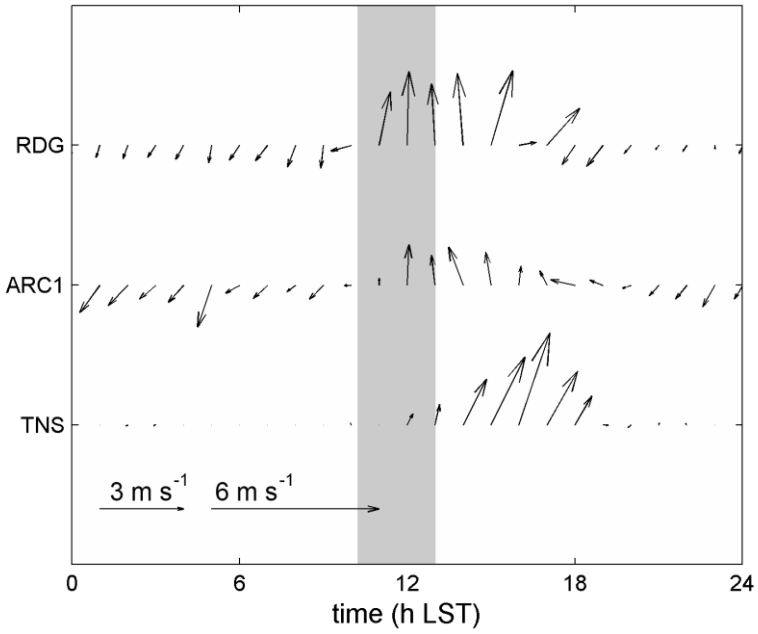

Figure 3.4. Time series of wind (vectors) observations at RDG, ARC1 and TNS surface stations for 24 Sep 1998. Flight #1 duration is indicated by the grey band. N direction is top, S is bottom, W is left, E is right.

Surface weather station observations indicate that at 1100 LST a southerly wind with 4.5 m s^{-1} average speed (associated gust speed 7.0 m s^{-1}) has already developed at RDG (**figure 3.4**). It strengthens and turns slightly eastward during the day, then it ceases at 1700 LST. The lake

breeze reaches ARC1 with a delay of one hour (at 1200 LST), displaying an intensity of about 2.5 m s^{-1}. At 1700 LST the wind starts to rotate in counter-clockwise direction, until reversing at 2100 LST, differently from RDG, where the shift in wind direction is very sharp. The propagation of the *Ora del Garda* lake-breeze front is marked by a sudden interruption of air temperature increase at RDG, and by a slowing down of the morning heating at ARC1 (**figure 3.5**). At both stations the temperature curve is flattened during the entire onshore-flow phase, due to the advection of colder air from above Lake Garda surface. The passage of the front at RDG is also accompanied by an increase in water vapour mixing ratio value (by 2.5 g kg^{-1}). On the other hand, in the Adige Valley a southerly up-valley wind blows from 1200 to 1800 LST, reaching a peak intensity of 5.5 m s^{-1}. Indeed, a fair development of the *Ora del Garda* wind is seen for 24 September 1998 despite the late time of the season, due to high irradiation conditions and light southerly (i.e. concordant) synoptic winds.

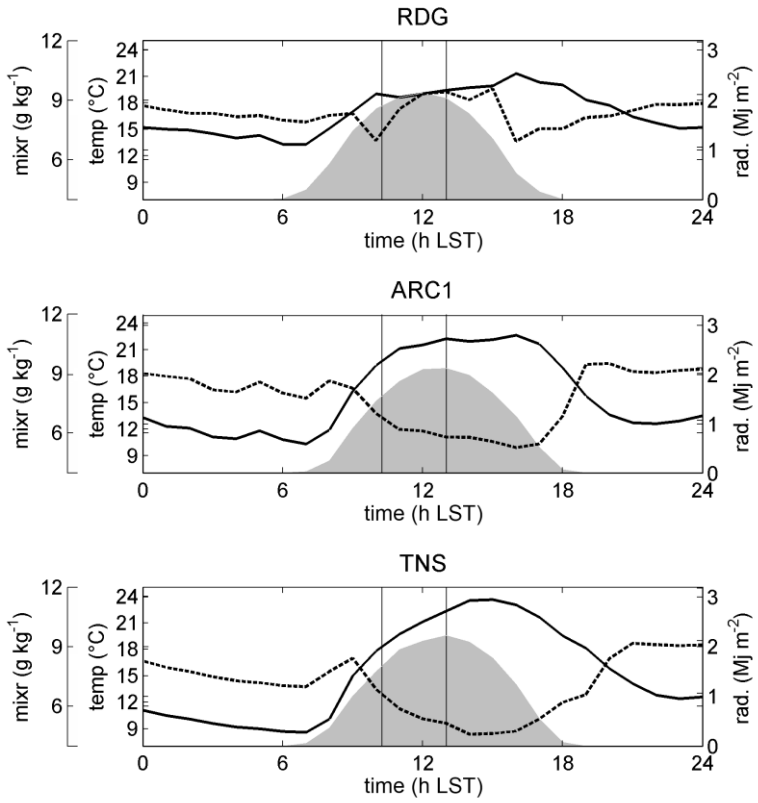

Figure 3.5. Time series of radiation (grey shading), temperature (solid black line) and water vapour mixing ratio (dashed black line) observations at RDG, ARC1 and TNS surface stations for 24 Sep 1998. Flight #1 takeoff and landing times are indicated by vertical lines.

3.5 05 August and 01 September 1999 flights (flights #2 and #3)

3.5.1 Description of the flights

The two flights of 1999 summer followed very similar trajectories, and were both performed in the central afternoon hours, when the *Ora del Garda* circulation is typically already well established. They both explored a longitudinal section over the Lake Garda northern shoreline, in the narrow corridor between the Mt. Brione relief and the eastern sidewall of the valley (site A), a cross-valley section over Cavedine Lake area (site B), and a cross-valley section at the end of the Lakes Valley over the Terlago saddle area (site C). In addition, flight #3 included a cross-valley section in the Adige Valley, in the area where the *Ora del Garda* overflow occurs (site D) (see **figures 3.6** and **3.7**). Some of the valley atmosphere slices were explored by both an ascending and a descending spiralling path (A section for flight #2, A and B section for flight #3). Timings and characteristics of the flight trajectories are summarized in **table 3.4**.

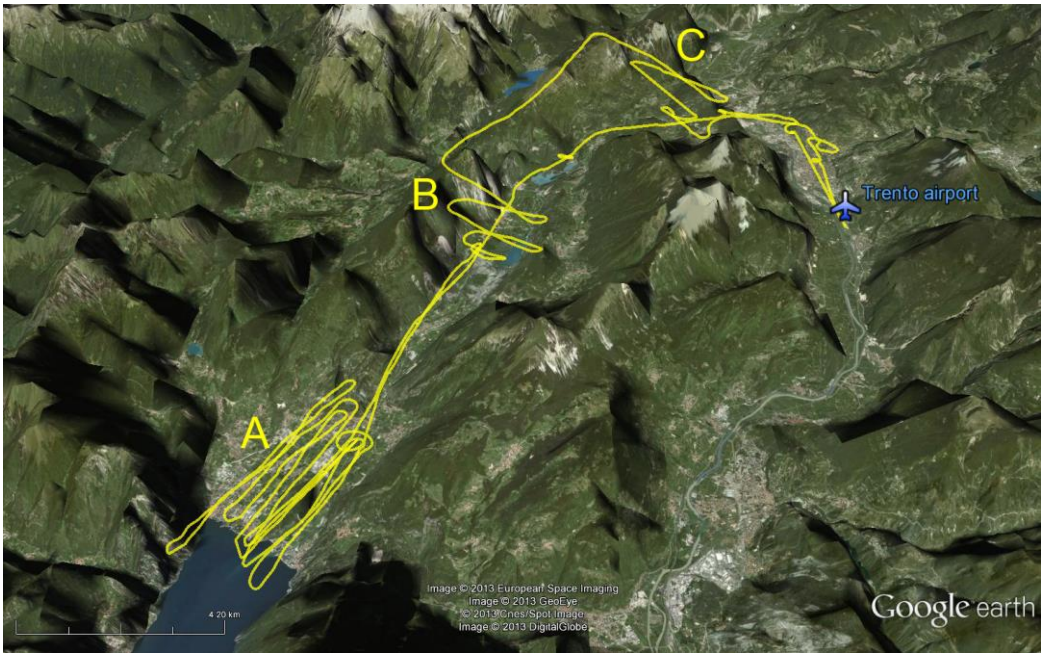

Figure 3.6. As in **figure 3.2**, but for flight #2. Image © Google Earth, © 2013 European Space Imaging, © 2013 GeoEye, © 2013 Cnes/Spot Image, © 2013 DigitalGlobe.

3.5.2 Weather conditions and surface observations

On 05 August 1999 a vast high-pressure region, covering the whole Mediterranean area, was associated with a westerly flow throughout the troposphere, very weak below the 700 hPa level. The morning hours were very sunny, while at local noon the sky turned partially clouded, as indicated by satellite images, showing stratocumulus clouds over the Alps in the

afternoon, and observations at PAG weather station, reporting visibility reduced by clouds. Despite the resulting deficit in incoming shortwave radiation, the energy input remained quite intense throughout the afternoon, and enough to warm up the valley atmosphere and allow for along-valley pressure gradients producing the lake breeze and valley winds.

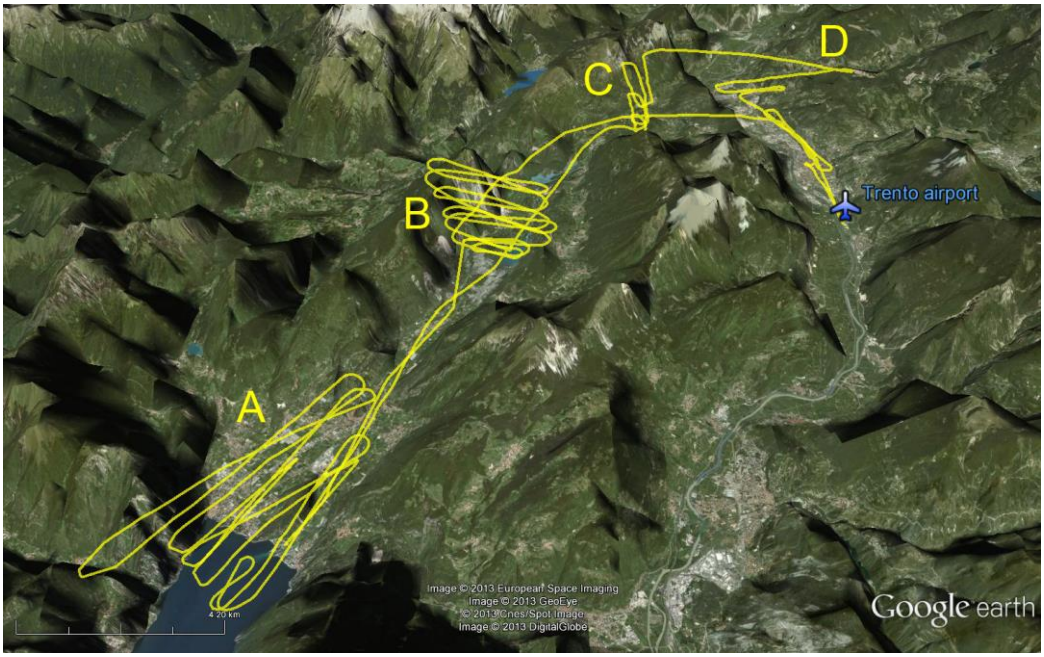

Figure 3.7. As in **figure 3.2**, but for flight #3. Image © Google Earth, © 2013 European Space Imaging, © 2013 GeoEye, © 2013 Cnes/Spot Image, © 2013 DigitalGlobe.

Table 3.4. Timings and characteristics of measurement flights #2 and #3. Single spirals are labelled according to **figures 3.6** and **3.7**. CV and AV respectively indicate whether the spiraling trajectories explored a cross- or an along-valley oriented section. D stands for a descending (downward) flight leg and U for an ascending (upward) flight leg. LST times are UTC+1 times.

Flight		Takeoff	Landing	Spiral	Start	End	Trajectory
#2	05 Aug 1999	1330 LST	1530 LST	C	1355 LST	1413 LST	CV U
				B	1420 LST	1433 LST	CV D
				A	1438 LST	1520 LST	CV U+D
#3	01 Sep 1999	1330 LST	1615 LST	B	1343 LST	1422 LST	CV U+D
				A	1428 LST	1519 LST	AV U+D
				C	1529 LST	1549 LST	CV U
				D	1550 LST	1603 LST	CV D

At RDG the *Ora del Garda* wind blew from S from 1000 to 1900 LST, reaching an intensity of 7.0 m s^{-1} (associated gust speed: 9.3 m s^{-1}); at ARC1 the lake breeze was recorded from 1100 to 1900 LST with a 4.8 m s^{-1} peak speed (see **figure 3.8**). As foreseen, the flight was therefore performed right in the hours when the breeze was strong. The timing of the passage of the lake breeze front is clearly detected from temperature and humidity surface patterns: the typical temperature drop and water vapour mixing ratio increase were detected at RDG and ARC1 at 1000 and 1100 LST respectively (**figure 3.9**). On the other hand, at TNS a robust up-valley wind was blowing between 1300 and 2000 LST, with an average 5.5 m s^{-1} intensity.

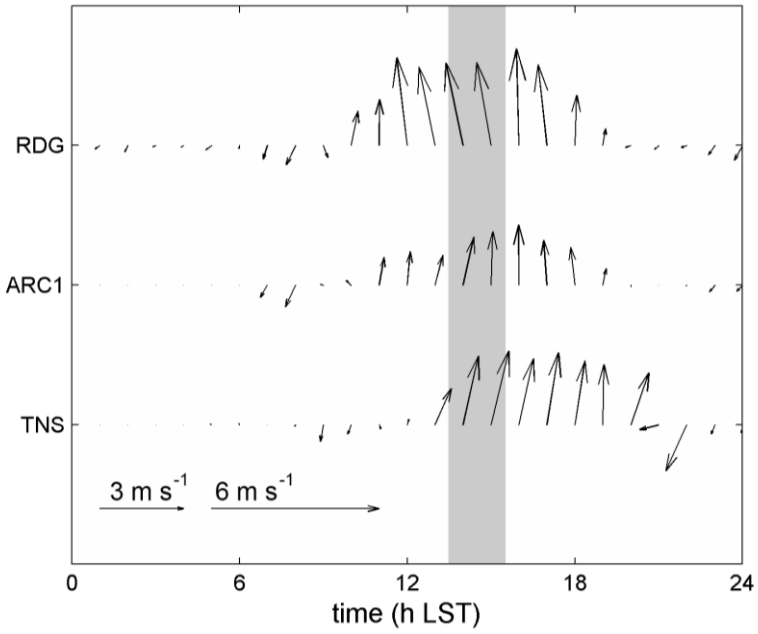

Figure 3.8. As in **figure 3.4**, but for flight #2.

On 01 September 1999 the target area was under a isobar surface slope, associated with a north-northwesterly flow. However soundings indicate very weak wind strengths everywhere below 700 hPa level. Satellite images also show a sky covered with scattered stratocumulus clouds over the eastern Alps, which resulted in a significantly reduced radiation pattern in the afternoon at RDG and ARC1 (**figure 3.11**), although no reduction in visibility was registered at Mt. Paganella station.

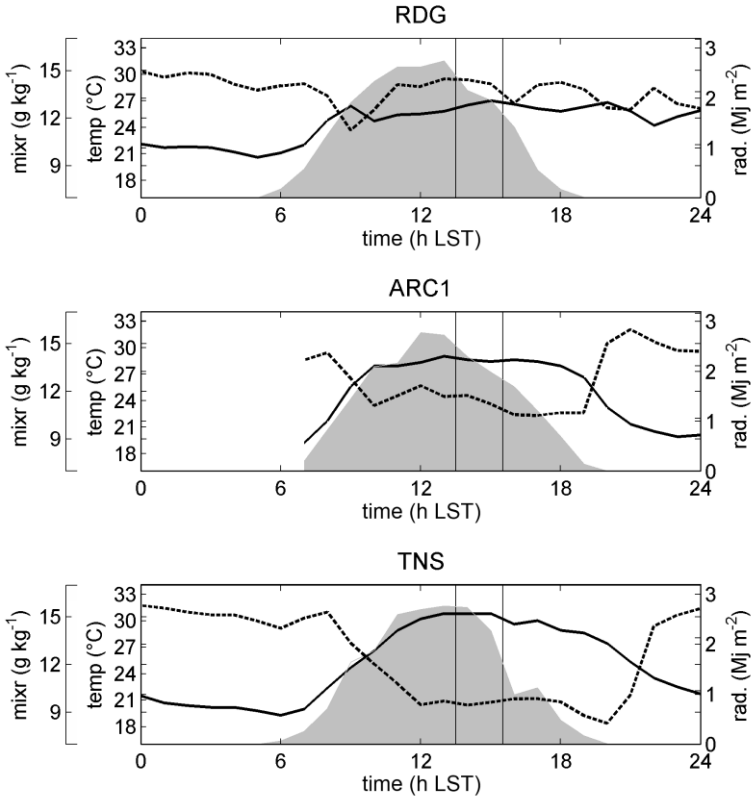

Figure 3.9. As in **figure 3.5**, but for flight #2.

Weak valley winds, somehow hindered by the contrary blowing upper ambient wind, developed. Data from surface stations (see **figure 3.10**) show that the *Ora del Garda* blew weakly from 1100 to 1700 LST, with an intensity peak at 1300 LST (4.1 m s^{-1} at RDG and 1.6 m s^{-1} at ARC1); at 1100 LST at RDG the temperature rise halted, and the mixing ratio rose by 4.5 g kg^{-1} (1200 LST), while the influence of the breeze front passage was scarcely felt at ARC1 (**figure 3.11**). Flight was therefore performed during partially disturbed *Ora del Garda* conditions. In the Adige Valley an up-valley wind was recorded only between 1300 and 1800 LST, and reached a 4.8 m s^{-1} intensity. On the other hand, the nocturnal northerly down-valley wind blew more intense than usual.

To sum up, for both the flight days the main typical features associated with the *Ora del Garda* diurnal cycle did occur, even under not completely clear-sky conditions. The disturbance induced by the contrary synoptic wind damped the breeze intensity on 01 September, while southerly synoptic winds reinforced the mentioned circulation on 05 August, as expected. The two flight days are therefore representative of opposite synoptic forcing conditions, hence offering a richer scenario for the present investigation.

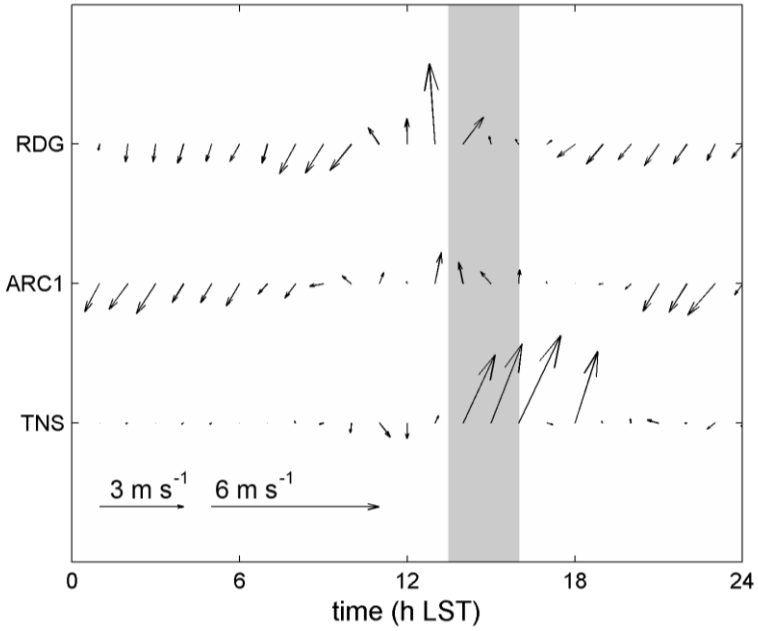

Figure 3.10. As in **figure 3.4**, but for flight #3.

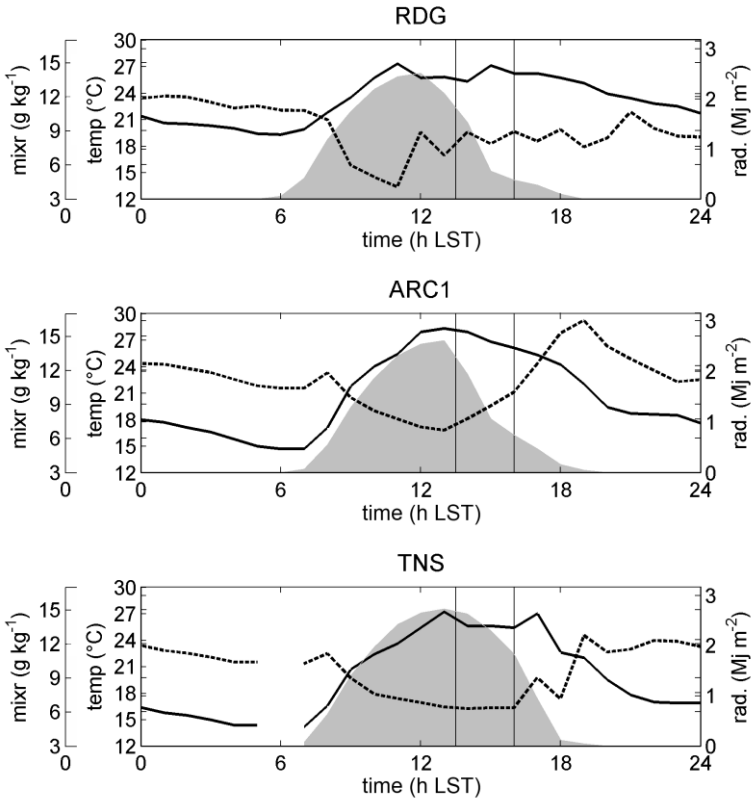

Figure 3.11. As in **figure 3.5**, but for flight #3.

3.6 23 August 2001 flights (flights #4 and #5)

3.6.1 Description of the flights

On 23 August 2001 the motorglider performed two flights over the study area. The first flight (flight #4) was carried out in the late morning, and explored the area of Lake Garda shoreline through the Terlago saddle, while the second (flight #5) flew in the early afternoon only over the area north of Trento where the *Ora del Garda* interacts with the Adige Valley up-valley wind. A total of eight spiralling trajectories were flown, exploring five different sites: the flat basin facing Lake Garda (site A), the narrow valley stretch joining the lower Sarca Valley to the southern Lakes Valley (site B1), the Lakes Valley at halfway between Cavedine Lake and Toblino Lake (site B2), the area close to the ridge of the Terlago saddle (site C), and the Adige Valley in front of the latter (site D). Flight #4 covered the four sections along the Sarca and Lakes valleys (A, B1, B2 and C sites) and explored twice site D (D1 and D2), while flight #5 explored only C and D sites (see **figures 3.14** and **3.15**). Notice that GPS data are lacking for the last two spirals of flight #4 (C and D2 sites), therefore only the vertical distribution of the measured variables is available for them. Moreover, notice that over site A both along-valley and cross-valley oriented flight legs were performed, ascending and descending over the target area, and allowing a complete exploration of the tridimensional atmosphere structure. Timings and characteristics of the flight trajectories are summarized in **table 3.5**.

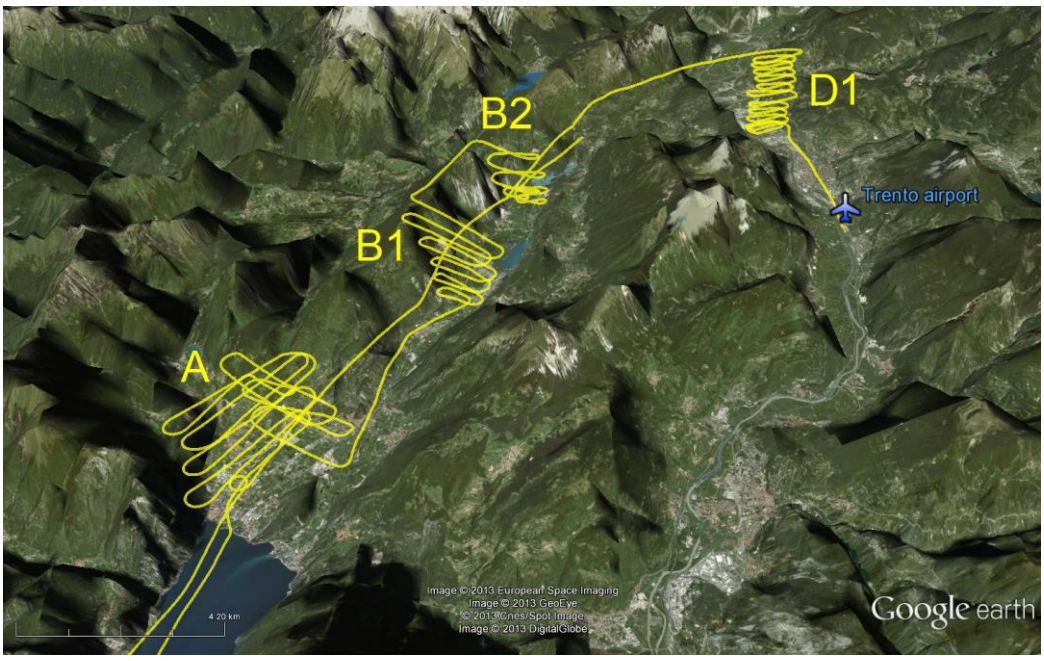

Figure 3.12. As in **figure 3.2**, but for flight #4. Image © Google Earth, © 2013 European Space Imaging, © 2013 GeoEye, © 2013 Cnes/Spot Image, © 2013 DigitalGlobe.

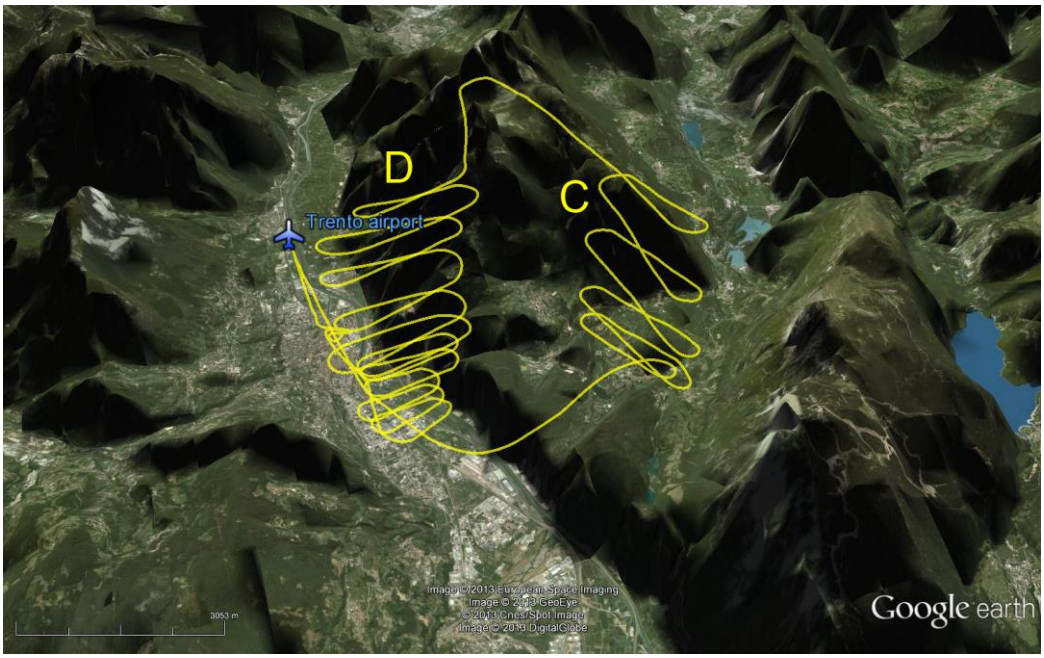

Figure 3.13. As in **figure 3.2**, but for flight #5. View is from N. Image © Google Earth, © 2013 European Space Imaging, © 2013 GeoEye, © 2013 Cnes/Spot Image, © 2013 DigitalGlobe.

Table 3.5. Timings and characteristics of measurement flights #4 and #5. Single spirals are labelled according to **figures 3.14** and **3.15**. CV and AV respectively indicate whether the spiraling trajectories explored a cross- or an along-valley oriented section. D stands for a descending (downward) flight leg and U for an ascending (upward) flight leg. LST times are UTC+1 times.

Flight		Takeoff	Landing	Spiral	Start	End	Trajectory
#4	23 Aug 2001 (morning)	0900 LST	1200 LST	D1	0918 LST	0947 LST	CV U
				A	0959 LST	1042 LST	C+AV U+D
				B1	1046 LST	1106 LST	CV U
				B2	1108 LST	1121 LST	CV D
				C	1123 LST	1143 LST	[---] U
				D2	1143 LST	1157 LST	[---] D
#5	23 Aug 2001 (afternoon)	1415 LST	1530 LST	D	1424 LST	1454 LST	CV U
				C	1458 LST	1517 LST	CV D

3.6.2 Weather conditions

Clear sky and weak-wind conditions were observed throughout all the day at PAG surface station at the crest level. The absence of cloud cover in the morning is also indicated by satellite images, while in the afternoon some cumulus clouds developed over the target area at mountain-top level, as a result of convergence produced by thermally-driven circulations. Reanalyses show a high-pressure ridge elongating over central Europe from SW, consistently with the presence of a weak northerly synoptic wind blowing across the Alps, as indicated by routine radiosoundings. Hence, it can be argued that on the flight day good conditions for the full development of the *Ora del Garda* wind occurred (which is documented by time series of surface observations; see next section).

3.6.3 *Ora del Garda* diurnal cycle from surface observations

In addition to airborne data, for flights #4 and #5 surface observations collected from several AWSs are available. These stations belong to observational networks routinely operated by local institutions, and are mainly disseminated along the floor of the study area's valleys. They are listed in **table 3.6**, together with their technical specifications. Notice that pressure, radiation and especially wind data are recorded at some stations only, and also that the observation temporal resolution is different among networks (15 min vs. 1 h). Beside routine observations, an intensive field campaign was held between 13 and 24 August 2001 in the area north of Trento, where the two airflows interact. During this campaign two additional weather stations were operated. One was installed at Monte Terlago (720 m MSL; close to the ridge of the Terlago saddle and the north-northwestern valley sidewall, where the maximum wind speed is expected), and recorded 10 min averaged values of 3 m AGL wind speed and direction, air pressure, relative humidity, global and net radiation. The second station consisted of an ultrasonic anemometer installed near a pre-existing AWS at Roncafort, on the Adige Valley floor (195 m MSL) at the foot of the Terlago saddle, to evaluate the turbulent fluxes developing in the surface layer (SL) in this area (cf. de Franceschi et al. 2002, de Franceschi 2004). The location of all surface observation sites is indicated in **figure 3.16**. On the basis of surface observations time series from the above AWSs, the different stages of the *Ora del Garda* wind diurnal cycle on 23 August 2001 are discussed in detail below. Selected wind and temperature observations are reported in **figures 3.17** and **3.18**. The AWSs are grouped according to their geographic area (cf. **table 3.6** and **figure 3.16**), namely: a) the lower Sarca Valley, b) the Lakes Valley, c) the Adige Valley south of Trento and d) the Adige Valley north of Trento. The discussion follows the same subdivision.

Table 3.6. List of surface weather stations considered in the discussion of weather conditions and surface observations for flights #4 and #5. The operating institution is also indicated ("IASMA" stands for Istituto Agrario di San Michele all'Adige; "Meteot." stands for Meteotrentino, i.e. Meteorological Office of the Autonomous Province of Trento; "APG" stands for Trento University Atmospheric Physics Group). The local terrain height and the height of the installed anemometer (when present) are also reported. (*) indicates anemometers recording only wind speed. (**) indicates the ultrasonic anemometer operated by the APG.

Group	Station	Institution	Terrain height	Time resolution	Anemometer
a	RDG	IASMA	69 m MSL	1 h	5 m AGL
	TOR	Meteot.	70 m MSL	15 min	[---]
	NAG	IASMA	223 m MSL	1 h	[---]
	TEN	Meteot.	405 m MSL	15 min	[---]
	ARC2	Meteot.	91 m MSL	15 min	[---]
	DRO	IASMA	113 m MSL	1 h	[---]
b	CAV	Meteot.	245 m MSL	15 min	[---]
	PIE	IASMA	242 m MSL	1 h	3 m MSL(*)
	MAS	Meteot.	245 m MSL	15 min	[---]
	TER	IASMA	428 m MSL	1 h	3 m MSL(*)
	Monte Terlago	APG	720 m MSL	10 min	3 m MSL
c	TNS	IASMA	185 m MSL	1 h	10 m MSL
	ROM	IASMA	184m MSL	1 h	[---]
	ALD	IASMA	183 m MSL	1 h	3 m MSL(*)
	BES	IASMA	180 m MSL	1 h	3 m MSL(*)
	VOL	IASMA	175 m MSL	1 h	[---]
	ROV	IASMA	170 m MSL	1 h	3 m MSL(*)
d	RON	Meteot.	194 m MSL	15 min	10 m MSL
	GAR	IASMA	197 m MSL	1 h	3 m MSL
	ZAM	IASMA	201 m MSL	1 h	3 m MSL(*)
	SMA	Meteot.	205 m MSL	15 min	[---]
	Roncafort	APG	200 m MSL	0.04 s	6.5 m MSL(**)

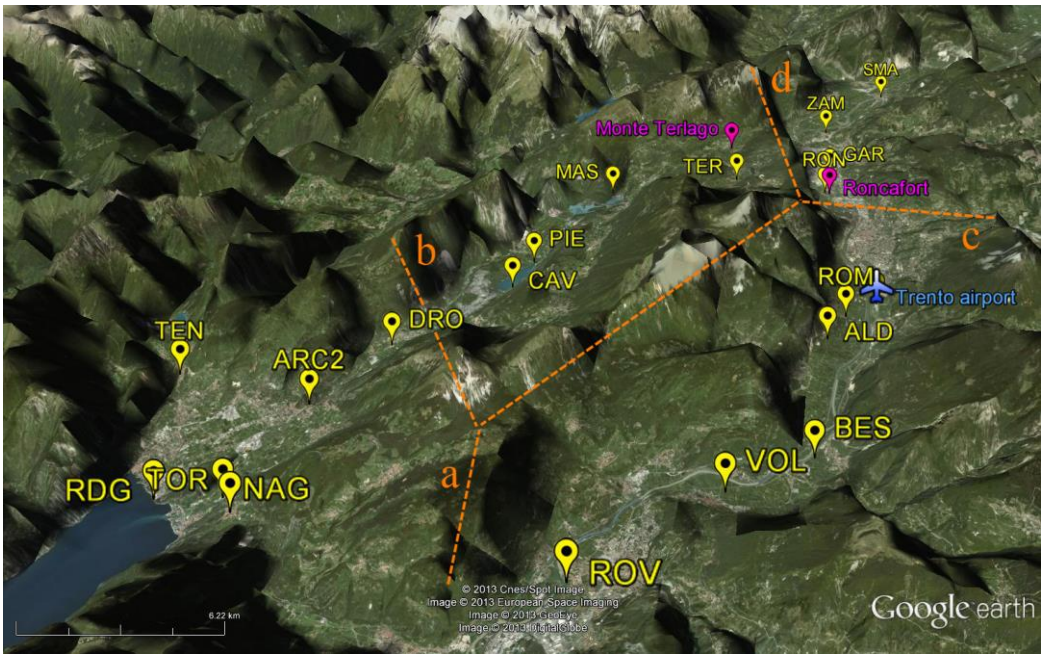

Figure 3.14. Location in the study area of the surface weather stations considered in the analysis of flights #4 and #5. Station and geographic area labels refer to **table 3.6**. View is from S. Image © Google Earth, © 2013 Cnes/Spot Image, © 2013 European Space Imaging, © 2013 GeoEye, © 2013 DigitalGlobe.

3.6.3.1 a) Lower Sarca Valley

Observations collected at RDG (**figure 3.17**) depict the wind pattern at Lake Garda's shoreline on the flight day: following a pressure maximum and a wind speed minimum, the wind direction abruptly shifts from northerly to southerly at 1000 LST indicating the onset of the lake breeze, i.e. the formation of a lake-breeze front, which is accompanied by a sudden temperature decrease (**figure 3.18a**) and increase in mixing ratio (not shown) (Simpson 1994, Zumpfe and Horel 2007). The lake breeze reinforces from 1300 LST to the maximum intensity of 6.0 m s^{-1} (corresponding gust speed: 8.8 m s^{-1}) recorded at 1400 LST, persisting until the local sunset time (1800 LST) and then rapidly ceasing. Lake Garda's water temperature (measured at RDG; see RDGw time series in **figure 3.18a**) keeps almost constant throughout all the day (~21 °C), showing rather low values with respect to daytime air temperature (which contributes to the development of a strong circulation): the average difference is around 7 °C at the breeze onset, and reduces to 5 °C when the wind strengthens in the afternoon. Actually air temperature also shows a very limited range of variation between night and day (only 6.5 °C): in the afternoon RDG temperature curve appears completely flattened around 26.5 °C.

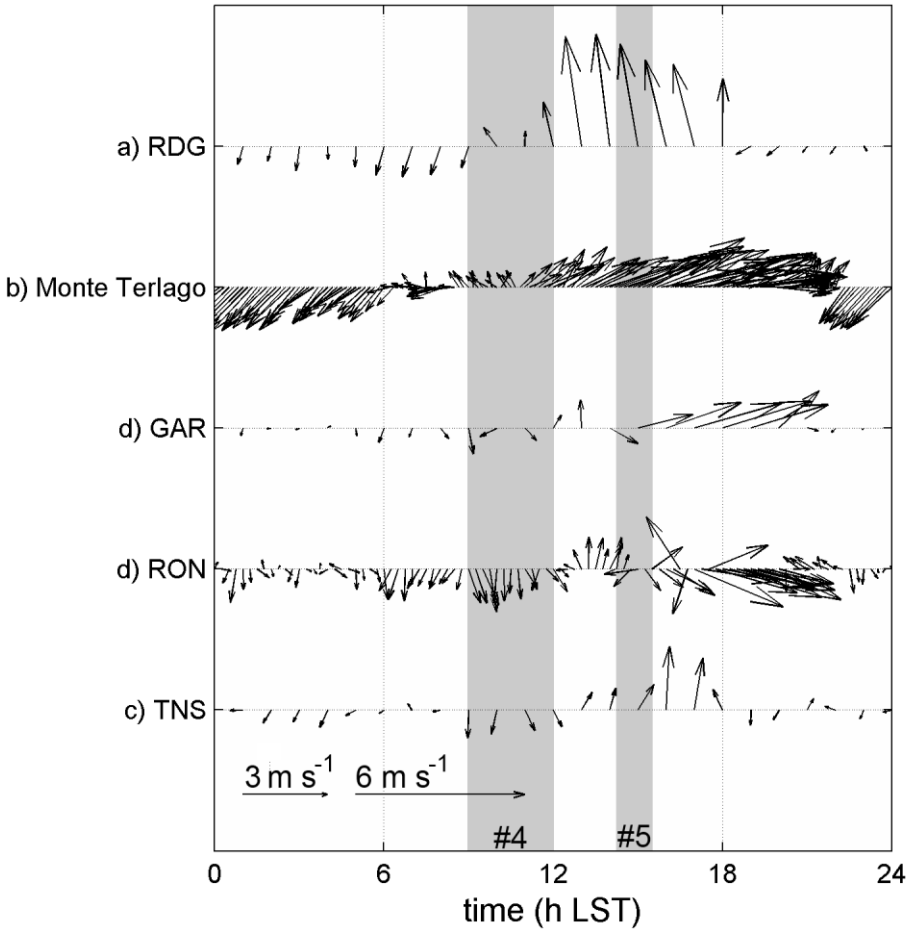

Figure 3.15. Time series of wind observations (vectors) at RDG, Monte Terlago, GAR, RON and TNS surface stations for 23 Aug 2001. The duration of flights #4 and #5 is indicated by the grey bands. The spatial development of the *Ora del Garda* wind along the lower Sarca Valley (a), the Lakes Valley (b) and finally the Adige Valley, both north (d) and south of Trento city (c), can be read from the top to the bottom of the graph. N direction is top, S is bottom, W is left, E is right.

At 1100 LST a sharp drop in the higher-resolution temperature series collected at TOR and ARC2 (respectively located ~1.5 km and ~5 km inland from the lake shoreline; see **figure 3.18a**) clearly indicates the passage of a lake-breeze cold front at both locations at the same time, despite their different distance from the shoreline. A similar signal is recorded also at 1100 LST at NAG and TEN (not shown; see **figure 3.19** for a close-up on the area topography and station position). This indicates a delayed inland propagation of the front in the easternmost part of the lower Sarca Valley, between Mt. Brione and the eastern sidewall. At DRO, which lies in the narrow corridor joining the lower Sarca Valley with the Lakes Valley, the morning heating phase ceases from 1000 LST, then the temperature curve is levelled out (to values ranging between 28 and 30 °C) until 1700 LST (**figure 3.18a**). Note that TOR, ARC2 and DRO recorded temperature higher than stations further down-stream

(i.e. up-valley; see next section) because they are situated very close to the lateral valley sidewalls, experiencing locally warmer conditions. However, at all the stations of this group the observed temperature cycle is remarkably different from a "standard" diurnal cycle of a fair-weather day, which is normally characterized by a relatively fast morning warming phase, a peak occurring about two hours after the solar radiation peak, and a slower afternoon decay. Here the temperature pattern during the central hours of the day appears to be completely dominated by the effects of the up-valley advection of cold air from above the Lake Garda surface.

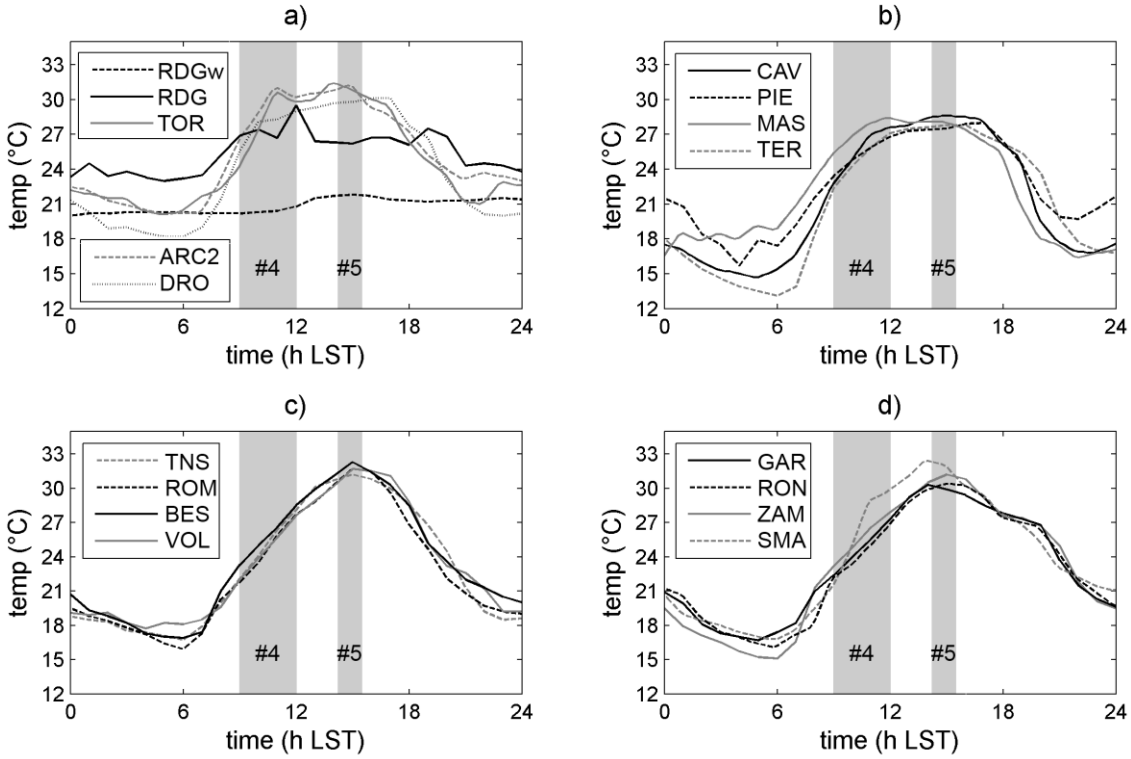

Figure 3.16. Time series of 2 m AGL temperature observations at selected surface stations (listed in **table 3.6**) for 23 Aug 2001. RDGw time series represents water temperature observations at RDG station. The duration of flights #4 and #5 is indicated by the grey bands. The stations are grouped according to their geographic area (see **table 3.6**).

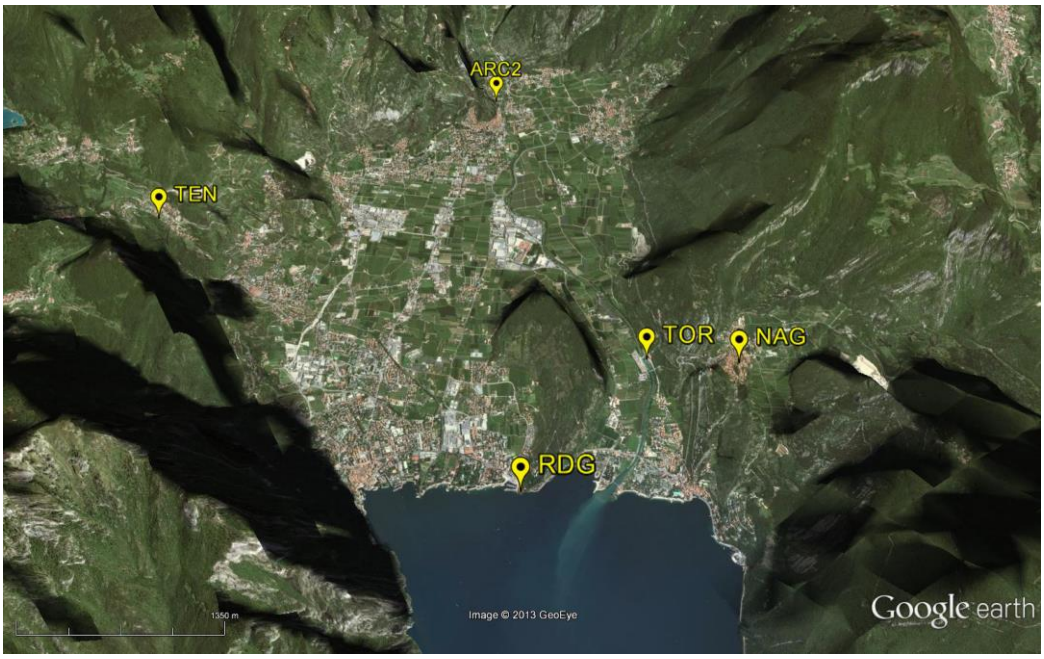

Figure 3.17. Location of the surface stations considered in the analysis of the *Ora del Garda* cycle on 23 Aug 2001 in the flat basin facing Lake Garda shore. Station labels refer to **table 3.6**. View is from SSW. Image © Google Earth, © 2013 GeoEye.

3.6.3.2 b) Lakes Valley

CAV and MAS stations lie on the shoreline of Cavedine and S. Massenza lakes respectively, while PIE is located less than 1 km north of Cavedine Lake, i.e. immediately down-stream to this small lake with respect to the *Ora del Garda* flow. In this area the valley floor displays a negligible slope, while north of S. Massenza Lake it rapidly rises up to about 600 m MSL (Terlago saddle ridge). At the same time, the valley axis turns from SSW-NNE to WSW-ENE. TER and Monte Terlago stations are both situated in this upper part of the Lakes Valley.
On 23 August 2001 PIE and TER record an increasing wind intensity from 1000 and 1100 LST respectively, peaking at 1400 and 1600 LST respectively (not shown; maximum wind speed is 3.9 m s^{-1} at TER; corresponding gust speed: 8.7 m s^{-1}) At TER the wind drops around 2200 LST (not shown). Intensive observations at Monte Terlago (located at short distance from TER, very close to the SE-exposed valley sidewall; see **figure 3.20**) show a gradual transition from up-slope to up-valley wind in the morning, completed at 1150 LST; the up-valley wind strengthens up to ~5.5 m s^{-1} between 1530 and 2000 LST and then weakens, definitely dropping at 2150 LST (**figure 3.17**). Although no clue of a well-defined lake-breeze front arrival is given by these AWSs, at all of them the evident flattening of the temperature curve (**figure 3.18b**) during the diurnal up-valley wind phase reveals the presence of a large source of cold air at the valley bottom, i.e. Lake Garda; indeed, homogenous values around 27-28 °C are recorded, even at the end of the valley at TER (428 m MSL).

Figure 3.18. Location of the surface stations considered in the analysis of the *Ora del Garda* cycle on 23 Aug 2001 in the area of the Terlago saddle. Station labels refer to **table 3.6**. View is from NE. Image © Google Earth, © 2013 Cnes/Spot Image, © 2013 DigitalGlobe, © 2013 GeoEye.

3.6.3.3 c) Adige Valley south of Trento

This group of stations is representative of pure up-valley wind conditions in the Adige Valley, free from any interference by the *Ora del Garda* (except TNS). On the flight day a southerly up-valley wind blows at ROV from 1400 to 1900 LST, with an average 2.6 m s^{-1} speed; the wind intensity peak is generally recorded around 1600 LST (3.9 m s^{-1} at VOL) (not shown). At TNS (~5 km south to Trento) a southerly up-valley wind blows from 1300 to 1800 LST (average intensity: 2.0 m s^{-1}), replaced by a weak (0.7 m s^{-1}) northerly flow between 1900 and 2000 LST (**figure 3.17**): this is very likely the effect of the *Ora del Garda* airflow channelling in southward direction along the Adige Valley. At all stations quasi-identical and rather typical diurnal temperature cycles are observed: the temperature increases up to about 32 ˚C peak value (at around 1500 LST), then it gradually decreases during the afternoon and evening phase (**figure 3.18c**).

3.6.3.4 d) Adige Valley north of Trento

Stations belonging to this group are located up to 8 km north of the area where *the Ora del Garda* first overflows from the Lakes Valley into the Adige Valley, and most directly affects the local airflow. Weak (1.5 m s^{-1}) up-valley wind conditions are detected around local noon at GAR and RON (**figure 3.17**), the two stations closest to the Terlago saddle (see **figure 3.20**

for a close-up of their position in the area). Associated with the *Ora del Garda* outbreak, a westerly wind is recorded first at GAR, which lies in the middle of the valley floor exactly in front of the lowest point of the saddle ridge (580 m MSL, i.e. ~400 m above the valley floor), from 1400 LST. Only later at 1530 LST a west-northwesterly wind is detected at RON, which is situated in a more sheltered position (1.5 km south to GAR and close to the foot of the quasi-vertical sidewall, where the height of the saddle crest touches 780 m MSL, i.e. ~600 m above the valley floor), after a short (~30 min) northerly flow phase. Indeed RON high-resolution observations are consistent with the picture of a gradual southward propagation of the denser airmass advected by the *Ora del Garda* (Schaller 1936, de Franceschi et al. 2002) from the point of the main-stream overflow, i.e. the lowest point of the saddle ridge. Then the wind speed increases gradually up to 5 m s^{-1} at both stations; this flow regime suddenly stops first at RON (2015 LST) and then at GAR (2100 LST), the maximum wind intensity values being recorded between 1600 and 1800 LST at GAR, RON and ZAM, with gusts up to 11.3 m s^{-1} at GAR (not shown).

The associated temperature daily cycle (**figure 3.18d**) presents specific features, different from those displayed by the "reference" Adige Valley AWSs (see previous section): during the central afternoon hours (1500-1800 LST) their temperature results lower; in particular, at GAR the air begins to cool down at a quasi-constant rate from 1400 LST. On the contrary, from 1800 LST onwards, at all the group stations the temperature is higher than in the southern Adige Valley, and a near constant temperature value (~27 °C) is registered until 2000 LST; then the air cools down, although keeping still warmer than south to Trento until the late evening. This behaviour is to be ascribed to the persistence of the inflow of air from the Lakes Valley in the evening: in the afternoon the air advected by the *Ora del Garda* is potentially cooler than the local (i.e. Adige Valley) air, while in the early evening phase it results warmer; this slows down the cooling of the lowest Adige Valley atmosphere due to the local radiation drop. Accordingly, the diurnal cycle of the sensible heat flux (SHF) at the Adige Valley floor (provided by eddy correlation analysis of ultrasonic anemometer data at Roncafort; see de Franceschi et al. 2002, de Franceschi et al. 2009, de Franceschi and Zardi 2003, de Franceschi 2004, Druilhet and Durand 1997) shows rather large negative values (in the order of –100 W m^{-2}) starting from the local sunset time, i.e.1700 LST, until 2030 LST (see **figure 3.21**), in connection with the climax of the strong ventilation and turbulence produced by the *Ora del Garda* in the area.

The above analysis of the *Ora del Garda* diurnal cycle on 23 August 2001 highlights that flight #4 is representative of the earlier stage of the wind development, i.e. the first three hours following the lake breeze onset at Lake Garda shoreline. In this phase a down-valley current was still blowing along the Adige Valley. On the contrary, flight #5 was performed shortly after the first outbreak of the breeze from the Lakes Valley, as it aimed at exploring the ABL structure associated with the interaction between the *Ora del Garda* and the local

up-valley wind in the area of the saddle of Terlago.

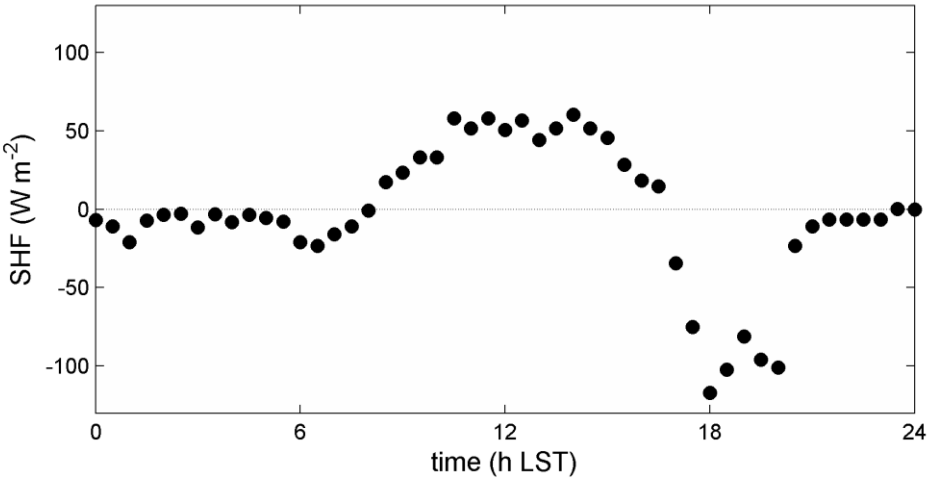

Figure 3.19. Time series of SHF from eddy covariance analysis (averaging interval: 30 min) of ultrasonic anemometer observations at Roncafort site (see **figure 3.18**) for 23 Aug 2001.

3.7 Summary

This chapter provided an outline of airborne and surface measurements that form the experimental dataset analysed in this study of the *Ora del Garda* wind. The database is primarily composed of five research flights performed by means of an instrumented motorglider in the valleys where the wind blows, and by surface observations collected from automated weather stations deployed along the valley floor in the study area.

Sections 3.2 and **3.3** presented the setup of the measurement platform used for the flights and the instrumentation carried onboard, as well as the flight strategy adopted in order to explore the fine-scale variability of the ABL at selected valley sections (de Franceschi et al. 2003, Rampanelli 2004). For each flight, a description of the trajectory followed by the equipped motorglider, including the detailed timing of the different valley sections' exploration and an overview of the weather conditions occurring on the flight day, is given (**sections 3.4**-**3.6**). Moreover, for each flight day the corresponding diurnal cycles of the two principal thermally-driven circulations developing in the study area, i.e. the *Ora del Garda* and the Adige Valley wind, are characterized on the basis of available surface observations.

In particular, this analysis outlined that flight #1 (24 September 1998) was held in the late morning of a fair-weather, late-summer day, when clear-sky conditions allowed the full development of the *Ora del Garda* wind in the area despite the late time of the season (cf. the typical diurnal cycle described in **Chapter 2**). Flight #1 explored four different valley cross sections in the lower Sarca Valley and in the Lakes Valley.

On the other hand, flights #2 and #3, whose trajectories and timings are very similar, were found to be representative of two different synoptic forcing conditions (i.e. respectively southerly synoptic wind for 05 August 1999 and northerly synoptic wind for 01 September 1999). The development of local circulations is known to be strongly dependent on the prevailing synoptic airflow (Whiteman and Doran 1993), as confirmed by time series of surface observations: indeed, intense lake breeze and up-valley wind systems were detected on 05 August 1999, while on 01 September 1999 local winds were rather weak but still blowing. Accordingly the two flights will provide parallel pictures of the afternoon ABL structure associated with the *Ora del Garda* flow under favorable (flight #2) and unfavorable (flight #3) conditions. Both flights explored the longitudinal structure of the valley atmosphere over Lake Garda shoreline, and flight #3 included also a cross section of the Adige Valley, taken in the area where the *Ora del Garda* overflows from the Lakes Valley.
For flights #4 and #5 (23 August 2001) a more detailed analysis of the *Ora del Garda* development at the surface was possible, for observations were available from a greater number of AWSs than for the other flights. Surface measurements indicate that 23 August 2001 was a "typical" *Ora del Garda* day, as the daily cycles of meteorological variables compare fairly well with those showed in **section 2.3** from **Chapter 2**. Indeed, a well-defined lake breeze front was found to move inland from the shoreline starting at around 1000 LST. Its penetration into the lower Sarca Valley was not homogenous: its propagation across the easternmost part of the flat basin was in fact delayed by at least ~1 h with respect to the western half of valley cross section. Stations further up-valley in the Lakes Valley did not show any clear evidence of the passage of a well-defined lake breeze front, however at all of them the surface temperature daily cycle markedly differed from the typical textbook pattern, as a consequence of colder air advection from a continuous source provided by Lake Garda at the valley inlet. The average breeze intensity at the shoreline was ~5.5 m s^{-1}, with gusts up to 9 m s^{-1}; the wind climax was reached at 1400 LST at RDG, and one or two hours later in the upper Lakes Valley. The *Ora del Garda* outbreak from W into the Adige Valley was first detected at 1400 LST at GAR and at 1530 LST at RON (this delay being due to the more sheltered location of RON with respect to GAR); the westerly inflow of air from the Lakes Valley continued until the late evening (2100 LST), being particularly intense in the late afternoon hours, with gusts up to 11.3 m s^{-1} at the Adige Valley floor. Indeed, at 1900 LST the *Ora del Garda* airflow channelling in southward direction along the Adige Valley even reached TNS station about 5 km south of Trento city, overwhelming the regular up-valley wind formerly recorded in the area (average intensity: ~2.5 m s^{-1}). In the light of this daily evolution, flight #4 may be considered representative of the early stage of the *Ora del Garda* development along the Sarca and Lakes valleys, while flight #5 will provide a picture of the ABL structure associated with the interaction between the two local airflows occurring in the afternoon in the area north of Trento (cf. de Franceschi et al. 2002, Pollak 1924, Schaller

1936, Wagner 1938, Wiener 1929).

Chapter 4

Methods for the post-processing of airborne data

Abstract

Measurement platforms based on manned or remotely piloted light aircrafts allow detailed observations of the non-trivial variability of the atmospheric boundary-layer (ABL) in complex terrain areas. In order to retrieve the fine-scale 3D structures of the ABL, suitable interpolation techniques need to be used for mapping airborne measurements over high-resolution regular grids. The adoption of a residual kriging (RK) technique is proposed here for this specific application. RK performance, both in terms of interpolation accuracy and likelihood of the results, is evaluated against the performance of techniques previously applied in the literature, namely inverse-distance weighted method, exponentially-weighted inverse squared distance method and natural neighbor method. As test-bed dataset observations of the potential temperature field in a mountain valley near Trento from three flights of the instrumented motorglider introduced in **Chapter 3** are used. The necessary shielding of the temperature sensor against solar radiation and mechanical stress (see **Chapter 3**) increased its time constant. The resulting slow-response effects are preliminarly removed through the application of a suitable "deconvolution" procedure to the original data. Then a leave-one-out cross-validation analysis and a critical comparison of the interpolated fields produced by the different methods are performed. Advantages and disadvantages offered by RK are discussed, and further evaluations about the suitability of the different interpolation methods.

4.1 Introduction

The structure of the ABL over complex terrain displays a great spatial heterogeneity, which is strictly associated with the inhomogeneous distribution of the surface fluxes; under such conditions, horizontal inhomogeneity may show variability length-scales even comparable to the ABL depth itself (Rotach 2012, Rotach and Zardi 2007). In complex terrain contexts surface observations and vertical soundings only are not able to capture this non-trivial, fully 3D variability of the meteorological variables. On the contrary, light instrumented aerial vehicles are able to provide temporal and spatial high-resolution datasets able to resolve the fine-scale 3D structure of the atmosphere (Finkele et al. 1995, Gohm et al. 2008, Harnisch et al. 2009, Hennemuth 1985, 1986, Weigel and Rotach 2004). In order to visualize the fully 3D spatial structure of the observed meteorological fields, suitable mapping techniques must be used for the interpolation of measurements collected at discrete points along the flight trajectory (and eventually for integrating ground-based observations, where available) over high-resolution, regularly-spaced grids. The choice of the mapping method determines the accuracy of the results, as well as the quality of further analyses of the interpolated fields. The most commonly adopted algorithms perform weighted averages of neighboring observations, where the weights are simply assigned on the only basis of the distance between the observation point and the estimate point with purely geometrical criteria. For example, Egger (1983) used an inverse distance weighted (IDW) interpolation and Hennemuth (1985) an exponentially-weighted inverse squared distance (exp-ISD) interpolation, while de Wekker (2002) and Weigel and Rotach (2004) used a natural neighbour (NN) interpolation based on a Delaunay triangulation.

The present work introduces the novel application of the geostatistical method called residual kriging (RK; firstly suggested by Ahmed and de Marsily 1987, Odeh et al. 1994, 1995, Goovaerts 1999) to the mapping of airborne measurements collected along a flight trajectory. We intend to show that RK is a very suitable technique for the retrieval of 3D high-resolution pictures of the ABL structures over complex terrain, by carrying out a systematic comparison of RK performance with the performances of the literature methods mentioned above. The test-bed database for this analysis is formed by potential temperature measurements collected by means of the instrumented motorglider presented in **Chapter 3** (de Franceschi et al. 2003, Rampanelli 2004). As mentioned in **Chapter 3**, the installation of the meteorological sensors onboard of the platform required great care. In particular, the RTD temperature sensor had to be shielded against direct solar radiation. This determined an increase of the instrument time constant, whose effect is removed from the observations by means of a suitable pre-processing procedure suggested by Rampanelli (2004). Based on the corrected data, two types of test are carried out. First a leave-one-out cross-validation analysis is performed for all the methods to assess their interpolation accuracy, then interpolated fields produced by the application of the different methods are critically analysed in terms of physical plausibility of

the results. Their characteristic features are discussed in order to outline strengths and weaknesses of the different techniques, identifying the most suitable method for the specific application.

4.2 The test-bed dataset

The test-bed dataset for the present analysis is formed by airborne observations of potential temperature collected during three flights that were performed on 01 October 1999 in the Adige Valley, a few kilometers south to the city of Trento. Position, pressure and temperature measurements were collected using a sampling frequency of 1 Hz.

4.2.1 Description of the target area

The Adige Valley is the widest and longest valley in the eastern Italian Alps; it runs perpendicularly to the main chain of the Alps, opening to the Po Valley to the south. In the target area explored by the flights the valley orientation is almost perfectly N-S; the local valley depth is rather large, being the approximate height of the lateral crests 1300 m MSL and 2100 m MSL on the western and on the eastern side respectively, while the height of the valley floor is 180 m MSL. The local width of the floor is about 1.5 km; it is entirely covered by vineyards and orchards, while the lateral slopes, whose average inclination is around 25° and 20° respectively on the western and on the eastern side, are mainly covered by woods, very homogeneously despite the consistent altitude variation (see **figure 4.1**) This particular valley section was selected because of its relatively regular morphology in terms of cross section shape and land cover, at least compared to the valleys where the *Ora del Garda* wind blows (cf. **Chapter 2**).

4.2.2 Description of the flights

All the three flights took off from Trento airport, a few kilometers north of the target area. The same cross section of the valley atmosphere was explored in detail by following an ascending and descending spiraling trajectory over the selected target area (see **figure 4.1** for an example), similarly to the flight patterns described in **Chapter 3**; long transversal transects and small-radius curves at turning points (i.e. close to the valley sidewalls) were performed, maintaining a quasi-constant vertical ascent/descent rate. The flights sampled the atmosphere up to ~2500 m MSL, i.e. a few hundreds of meters above the lateral crest height, and down to a minimum height of ~200 m AGL (due to safety regulations). Some minor parts of the flights, especially those exploring the lowest layers of the valley volume, lack the spatial coordinate information because of the reduced visibility of satellites for the GPS device, due to the steep topography. The actual average cruise-speed of the motorglider was ~30 m s^{-1} and its climbing/diving-speed was ~2 m s^{-1}, resulting in a typical spacing between subsequent observations of 30 m in horizontal direction and 2 m in vertical direction.

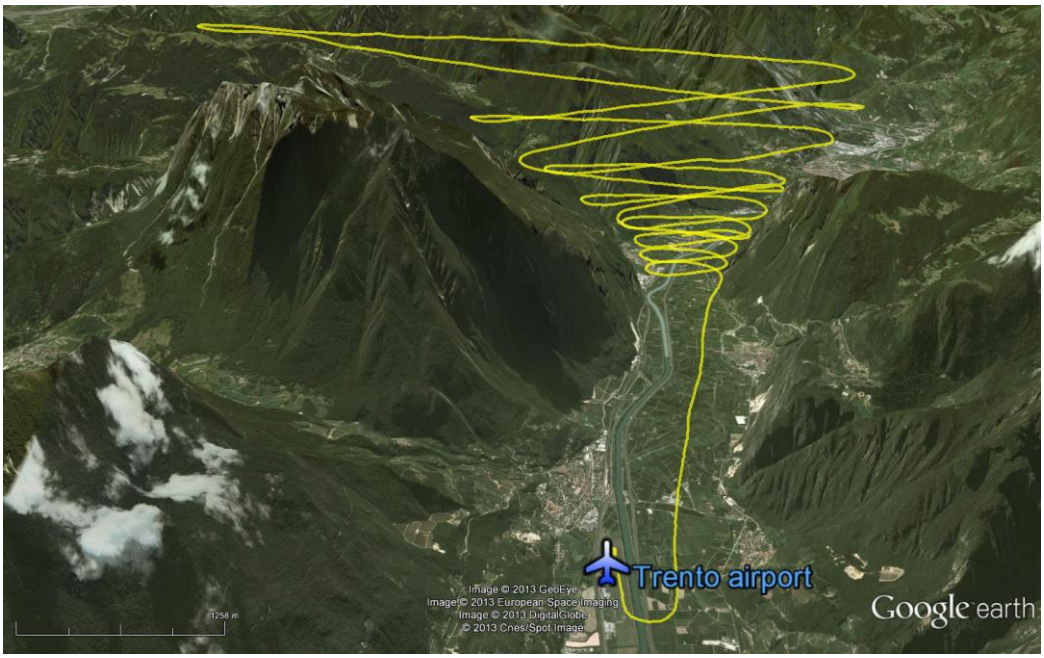

Figure 4.1. 3D representation of flight #N trajectory exploring the target Adige Valley cross section. View is from N. Image © Google Earth, © 2013 GeoEye, © 2013 European Space Imaging, © 2013 DigitalGlobe, © 2013 Cnes/Spot Image.

Table 4.1. Timing of 01 October 1999 flights forming the test-bed database (LST times are UTC+1 times).

Flight	Takeoff	Landing
#M	0830 LST	0930 LST
#N	1130 LST	1230 LST
#A	1430 LST	1530 LST

The three flights, whose average duration was of about one hour each, followed very similar trajectories, and were performed respectively during the early morning phase (flight #M), around the local noon (flight #N) and in the mid-afternoon phase (flight #A; see **table 4.1** for a detailed timing), in order to capture pictures of the valley atmosphere for different regimes of the thermally-driven wind field expected to develop in the area, i.e. the morning up-slope wind regime, the transition to the diurnal up-valley wind around noon, and the fully-developed, up-valley wind regime in the early afternoon (cf. Defant 1951, Whiteman 1990, 2000, Zardi and Whiteman 2013). Indeed, on the flight day (01 October 1999) a moderate westerly synoptic wind blew over the target area, due to the presence of a weak pressure gradient across the Alps, as confirmed by surface wind observations from local crest-level weather stations. Satellite images display completely cloudless conditions,

allowing the development of moderate thermally-driven winds in the target area despite the late time of the season, as indicated by surface observations from valley floor weather stations in the area (not shown).

4.3 Correction of the sensor time-lag effect

As anticipated, the setup of an airborne measurement platform based on an aerial vehicle requires that great care be paid to the onboard installation of the meteorological instruments, in order to avoid damages to the more fragile components and flow disturbances induced by the propeller or by the aircraft boundary-layer. In particular, the RTD thermometer installed on the measurement platform required to be shielded against direct solar radiation, while the thermohygrometer sensing parts were sheathed to protect them from the mechanical stress produced by the airflow during the flights (see **Chapter 3** and de Franceschi et al. 2003, Rampanelli 2004). However, these devices, especially the shield applied to the resistance thermometer, are expected to increase the time constant of the sensor, inducing a slow-response behavior. The resulting time-lag effect is a common problem in meteorological airborne observations of both temperature and humidity (not only from aircrafts, but also from radiosondes; cf. Mahesh et al. 1997, Tschudin and Schroeder 2013), and a variety of correction methods have been proposed in the literature (e.g. Inverarity 2000, Mahesh et al. 1997, McCarthy 1972, Shaw and Tilman 1980). Here the sensor-induced time delay for RTD observations was corrected using a "deconvolution" algorithm, specifically developed by Rampanelli (2004) for the pre-processing of the airborne datasets analysed in this thesis.

4.3.1 Theoretical framework

Original temperature observations recorded by the resistance thermometer display an hysteresis loop in the higher part of the flights, typically sampling the free atmosphere (FA) (see **figure 4.2**). In principle, in this region, which is weakly affected by the underlying ABL processes, vertical profiles are expected to be almost independent from the horizontal coordinate and nearly constant with time. As anticipated, this measured temperature pattern is produced by the time-lag associated with the slow response of the RTD sensor. Rampanelli (2004) performed a simplified conceptual experiment, which aimed at reproducing this effect for an ideal measurement flight. Steady-state and evolving convective boundary-layer (CBL) conditions were simulated, by adopting a pure "encroachment model" (Garratt 1992), which assumes that the CBL growth be sustained only by the sensible heat flux input from the ground surface. The distortion induced both by the slow-response effect and by the unsteady nature of the ABL was evaluated with reference to a simplified CBL structure, displaying a well-mixed layer of depth h with a constant potential temperature value (namely θ_m), surmounted by a stably stratified FA with constant lapse rate γ (4.0 K km^{-1}). In terms of

temperature, the lower layer displays a constant lapse rate Γ_d (9.8 K km^{-1}), while a constant lapse rate Γ (equal to the difference between Γ_d and γ) occurs above (see **figure 4.3**).

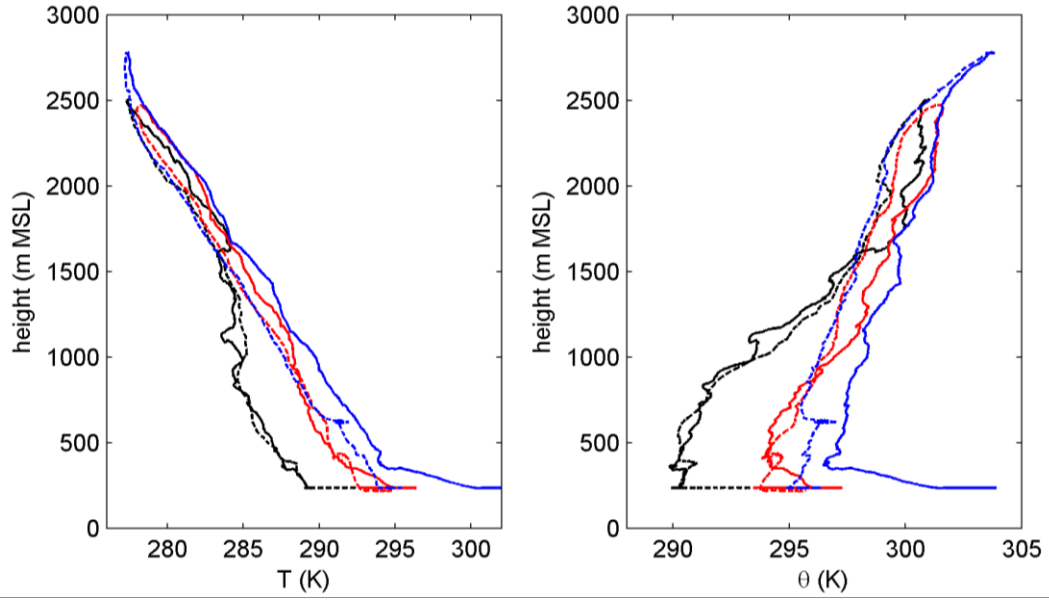

Figure 4.2. Original observations of temperature (left) and potential temperature (right) provided by the RTD sensor for flights #M (black), #N (red) and #A (blue). Solid lines indicate the flight ascents, while dashed lines represent the flight descents.

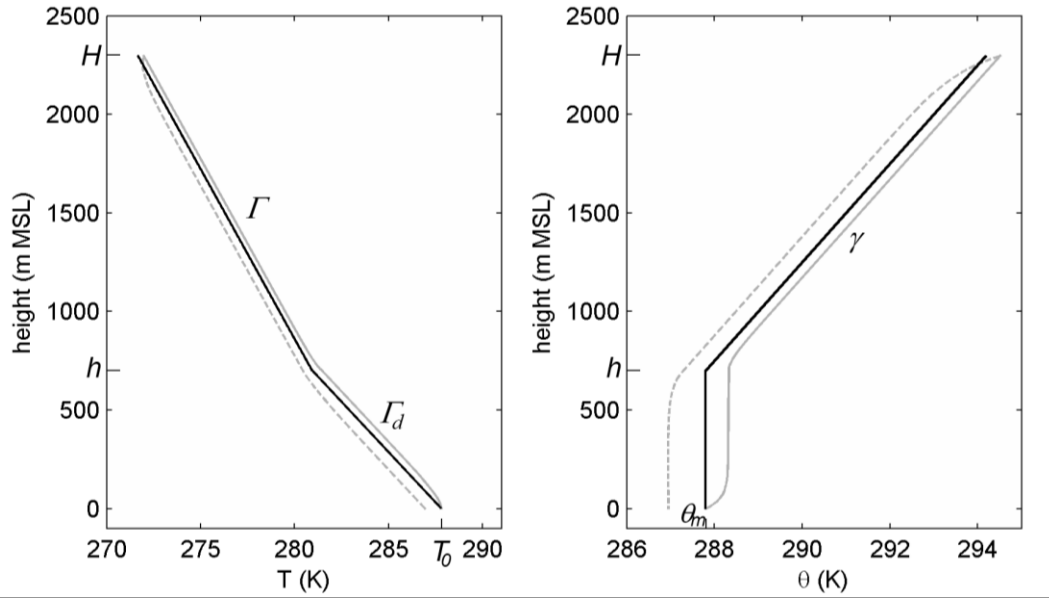

Figure 4.3. Vertical profiles of true (black line) and measured (grey line) air temperature (left) and potential temperature (right), resulting from the conceptual experiment by Rampanelli (2004), for a steady-state CBL condition. Ascents are solid lines, while descents are represented by dashed lines. Simulation parameters are: T_0 (temperature at the ground surface) = θ_m = 288 K, h = 700 m, H (maximum flight height) = 2300 m, w_a (climbing speed) = 1.5 m s^{-1}, w_d (diving speed) = –2.5 m s^{-1}, τ = 35 s.

A first-order linear differential equation in time (t) is supposed to describe suitably the heat transfer process governing the sensor dynamic:

$$\frac{dT(t)}{dt} + \frac{T(t)}{\tau} = \frac{T_a(t)}{\tau}, \qquad \text{(eq. 4.1)}$$

where $T(t)$ is the measured temperature (sensor output), $T_a(t)$ is the true ambient temperature (meteorological input) and τ is the instrument time constant. Notice that even higher-order instrument dynamics and complex dependence of τ on ambient parameters (like temperature, airflow speed, etc.) may be reasonably well approximated by a simple first-order equation, through a proper tuning of the parameters (Benedict 1984). According to a well-known result (cf. Doebelin 1990, Benedict 1984), for a linear-ramp temperature distribution the difference between indicated and true temperature values reaches a steady value after a short transient, as follows:

$$T(t) = T_a(t - \tau) \qquad \text{for } t >> \tau\,. \qquad \text{(eq. 4.2)}$$

This determines an asymptotic (maximum) error ΔT equal to:

$$\Delta T = T(t) - T_a(t) = \frac{dT_a(t)}{dz} w\tau\,, \qquad \text{(eq. 4.3)}$$

positive for the flight ascent and negative for the descent (being w the vertical speed of the aircraft).

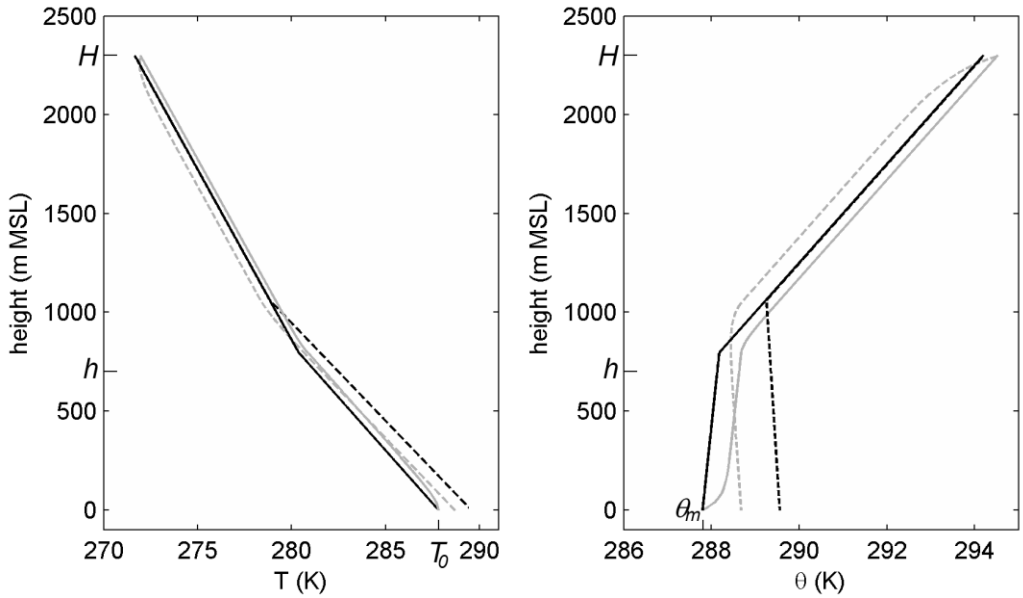

Figure 4.4. As in **figure 4.3**, but for evolving CBL conditions. Simulation parameters for the steady-state CBL are adopted here as initial conditions; a constant sensible heat flux input is prescribed at the surface. Notice the apparently homogenous (potential) temperature value detected in the lowest layers: the combination of the slow sensor response and the gradual heating of the ML with time reduces the hysteresis loop amplitude inside the lowest ABL.

Examples of theoretical temperature profiles measured during an ideal flight exploring both the CBL and the overlying FA are compared with the associated profiles of true temperature in **figures 4.3** and **4.4**, for steady-state and evolving CBL conditions respectively. Profiles of true potential temperature and of potential temperature calculated from the measured temperature are also displayed in the figures. The parameters of the simulations are chosen so as to be representative of typical values of atmospheric variables and flight characteristics of the airborne measurements. The distortion induced by the sensor delay is evident: a large hysteresis loop around the real trend is formed by the ascending and the descending branches of the flights. Its amplitude in the FA remains exactly the same for both simulations, while the change driven by the CBL unsteadiness involves in particular the mixed layer (ML) depth, apparently reducing the sensor-induced distortion. This simplified scheme seems to reproduce fairly well the pattern of real data (cf. **figure 4.2**).

Rampanelli (2004) suggested a simple "deconvolution" algorithm for processing time series of airborne measurement in order to correct the effect of the sensor time response described above and retrieve the true $T_a(t)$. This correction algorithm is based on the numerical approximation of the time derivative of $T(t)$, as explained below.

A function $y(t)$ sampled at fixed spacing in time Δt can be approximated by a suitable interpolating polynomial $L_n(t)$, calculated using n data points in the neighborhood of the location under consideration t_i. This can be done using the well-known expression of the Lagrange interpolating polynomial for equally spaced points (Quarteroni et al. 2007):

$$L_n(t) = \sum_{k=0}^{n} \frac{(-1)^{n-k} y_k}{k!(n-k)!} \frac{q^{[n+1]}}{(q-k)}, \qquad \text{(eq. 4.4)}$$

where

$$q = \frac{(t - t_i)}{\Delta t} \qquad \text{(eq. 4.5)}$$

and

$$q^{[n+1]} = q(q-1)(q-2)\ldots(q-n-1). \qquad \text{(eq. 4.6)}$$

The above expression can be differentiated to obtain the value of the approximate derivative of the function. For example, the expression for the approximate derivative y' in the central point t_i using a neighborhood of six points ($n = 6$) is:

$$y'_{n=6} \cong \frac{1}{60\Delta t}\left(-y_{i-3} + 9y_{i-2} - 45y_{i-1} + 45y_{i+1} - 9y_{i+2} + y_{i+3}\right). \qquad \text{(eq. 4.7)}$$

Finally, the discretization of the differential term in **eq. 4.1** gives the algorithm for the time series deconvolution:

$$T^i_{a,dec} = T(t_i) + \tau\, T'(t_i), \qquad \text{(eq. 4.8)}$$

where $T^i_{a,dec}$ is the retrieved value of the true atmospheric temperature T_a at time t_i, $T(t_i)$ is the temperature indicated by the sensor at t_i, and $T'(t_i)$ is the numerical derivative of the original

time series $T(t)$ calculated at time t_i through the above **eq. 4.7**.

4.3.2 Determination of the effective sensor time constant

The adoption of the above algorithm presumes the knowledge of the value of the sensor time constant τ. In our application, due to the shielding against solar radiation, the time constant of the RTD probe installed onboard the motorglider may be consistently higher than the time constant of the sensor alone, so the value declared by the instrument technical specifications, reporting a τ of 4 s for a flow speed of 1 m s^{-1} in water (see **Chapter 3**), may underestimate the real delay. Moreover, not only the density, the specific heat and the thermal conductivity of the ambient medium (air) are different from those of water, but also the flow regime around the probe is rather complex, for it results from the relative speed of the motorglider with respect to the wind field experienced during the flights. This deeply influences the dynamics of the convective heat exchange between the ambient air and the sensor. As a consequence, an analytical approach to an a priori determination of the effective value of τ cannot be pursued, and a suitable *effective* time constant, accounting for all the above factors, has to be retrieved ex post from the original airborne data.

In order to determine the effective value of τ, a simplified evaluation is first carried out, based on the loop amplitude ΔT observed in the uppermost branch of the measured profiles, i.e. in the FA, where a steady delay is likely to be reached as outlined above. Indeed, this atmosphere region displays a temperature distribution very close to a regular linear ramp, and no significant evolution is likely to be appreciated here throughout the whole flight duration. Therefore the idealized scheme of the hysteresis loop can be reasonably assumed to be valid. Ascent and descent average speeds (w_a and w_d respectively) were calculated for each flight, in order to apply the following relation (derived from **eq. 4.3**):

$$\Delta T = \frac{dT_a(t)}{dz}\left(w_a + \|w_d\|\right)\tau = \frac{dT(t)}{dz}\left(w_a + \|w_d\|\right)\tau , \qquad \text{(eq. 4.9)}$$

from which first-guess values are calculated for τ, assuming that T_a vertical gradient in the FA be well approximated by the average T vertical gradient (see **figure 4.5** for an enlarged scheme of the loop structure based on the conceptual experiment by Rampanelli 2004). All the three τ values resulting from this evaluation fall between 40 and 50 s.

Second, we tried a wide range of τ values (0-100 s) in the deconvolution algorithm, checking which value is able to remove better the hysteresis loop at the top of the trajectory, by minimizing the average absolute difference between ascent and descent $T_{a,dec}$ values. This analysis confirmed the range of values previously indicated, leading to the final choice of a τ of 45 s, which could fully account for the complex dynamic response of the sensor. Note that similar evaluations carried out for other analogous airborne datasets (i.e. the flights exploring the valleys where the *Ora del Garda* blows) confirmed the general validity of this value.

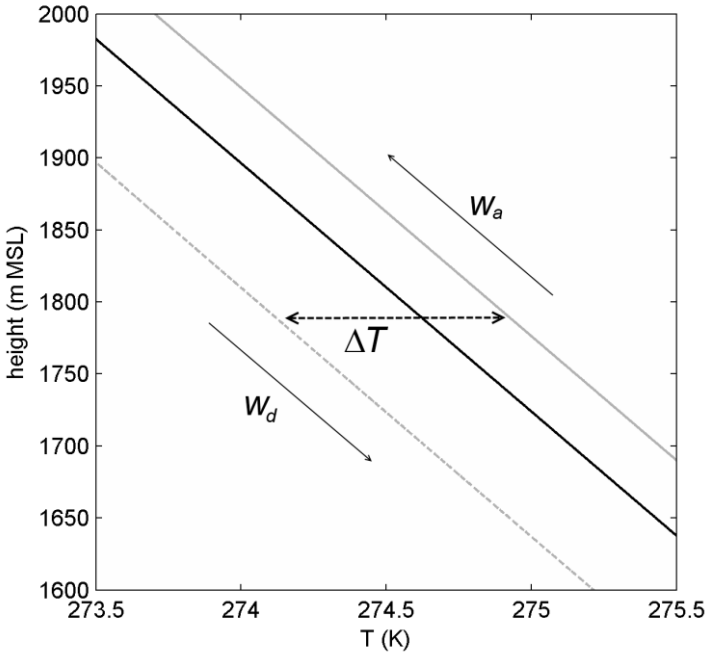

Figure 4.5. Close-up on the measured temperature hysteresis loop at the top of the ideal flight trajectory (conceptual experiment results). The black line is the true atmospheric temperature *Ta*(*t*), while the black line is the temperature indicated by the instrument *T*(*t*). Ascending and descending branch of the flight are respectively solid lines and dashed lines. The total loop amplitude ΔT is also indicated.

Second, we tried a wide range of τ values (0-100 s) in the deconvolution algorithm, checking which value is able to remove better the hysteresis loop at the top of the trajectory, by minimizing the average absolute difference between ascent and descent $T_{a,dec}$ values. This analysis confirmed the range of values previously indicated, leading to the final choice of a τ of 45 s, which could fully account for the complex dynamic response of the sensor. Note that similar evaluations carried out for other analogous airborne datasets (i.e. the flights exploring the valleys where the *Ora del Garda* blows) confirmed the general validity of this value.
The results of the final application of the deconvolution procedure discussed above to the data collected during the three measurement flights performed on 01 October 1999, and using a τ of 45 s, are shown in **figure 4.6**. Notice in particular the almost single-valued (potential) temperature profile in the uppermost part of the flights, indicating the total removal of the hysteresis loop, and the fact that the corrected profiles provide a consistent and clearer picture of the CBL structure evolution occurring between takeoff and landing at the lowest levels.

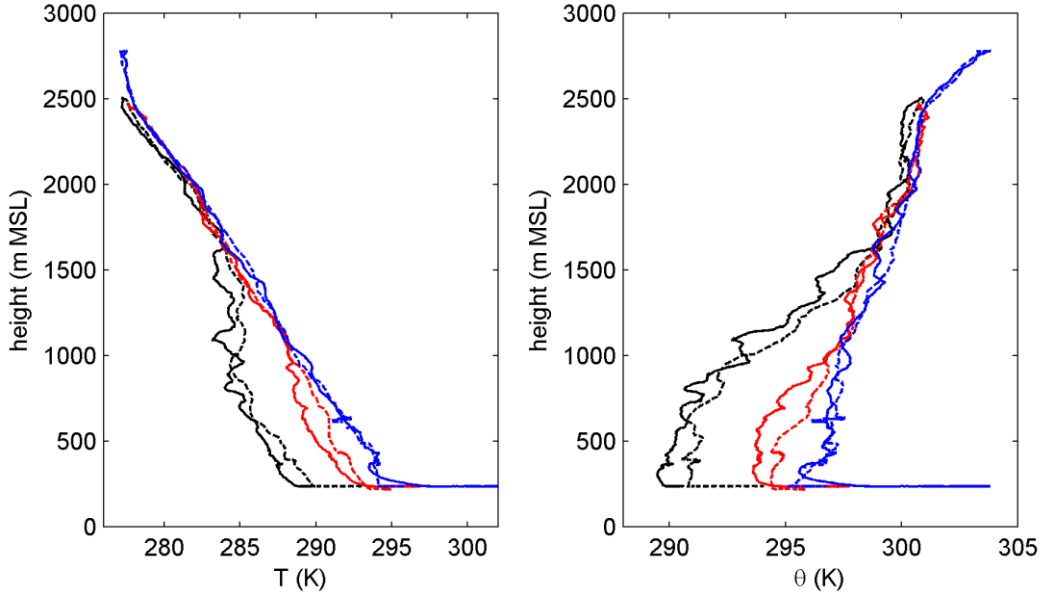

Figure 4.6. Observations of temperature (left) and potential temperature (right) after the correction of the RTD sensor time-lag effect for flights #M (black), #N (red) and #A (blue). Solid lines indicate the flight ascents, while dashed lines represent the flight descents. Notice in particular the fact that the hysteresis loops present in **figure 4.2** in the uppermost part of the profiles (i.e. FA) have been removed by the application of the deconvolution algorithm. On the contrary, the evolution of the ABL (i.e. the heating of the lowest atmosphere) during the single flight time has become evident (except for flight #A).

The application of the deconvolution algorithm also retrieves some oscillations of the temperature signal, which has been damped by the high time constant of the sensor. This variability is mainly associated with the horizontal inhomogeneity of the ABL meteorological fields, driven by the heterogeneous distribution of the surface sensible heat fluxes and by local flow patterns. Accordingly, **figure 4.7** shows that the temperature positive anomalies amplified by the sensor time-lag correction correspond very well to the western extremities of flight #M trajectory; indeed, here the motorglider experienced locally warmer conditions when flying close to the western sidewalls of the valley, which are preferentially sunlit in the early morning hours due to the valley orientation.

In general the deconvoluted temperature time series captures very well the main features of the observations from the thermohygrometer (see **figure 4.7**), which displays a faster response but a much lower accuracy (±0.3 °C vs. ±0.05 °C), although still preserving a reasonable smoothness. The thermohygrometer time constant for temperature is declared to be less than 15 s for an airflow with 1 m s^{-1} speed, but due to the higher relative velocity of the airflow experienced during the flights analyzed here (around 30 m s^{-1}) its effective value is

expected to be much lower, due to the increase of the convective heat transfer coefficient between ambient air and sensor. The excellent phase alignment with the deconvoluted RTD observations suggests that it can be reasonably considered negligible for our application. As a consequence, also relative humidity measurements can be considered free from any appreciable sensor time-lag, as the time constant declared for the hygrometer is even lower than for the temperature sensor (cf. **Chapter 3**).

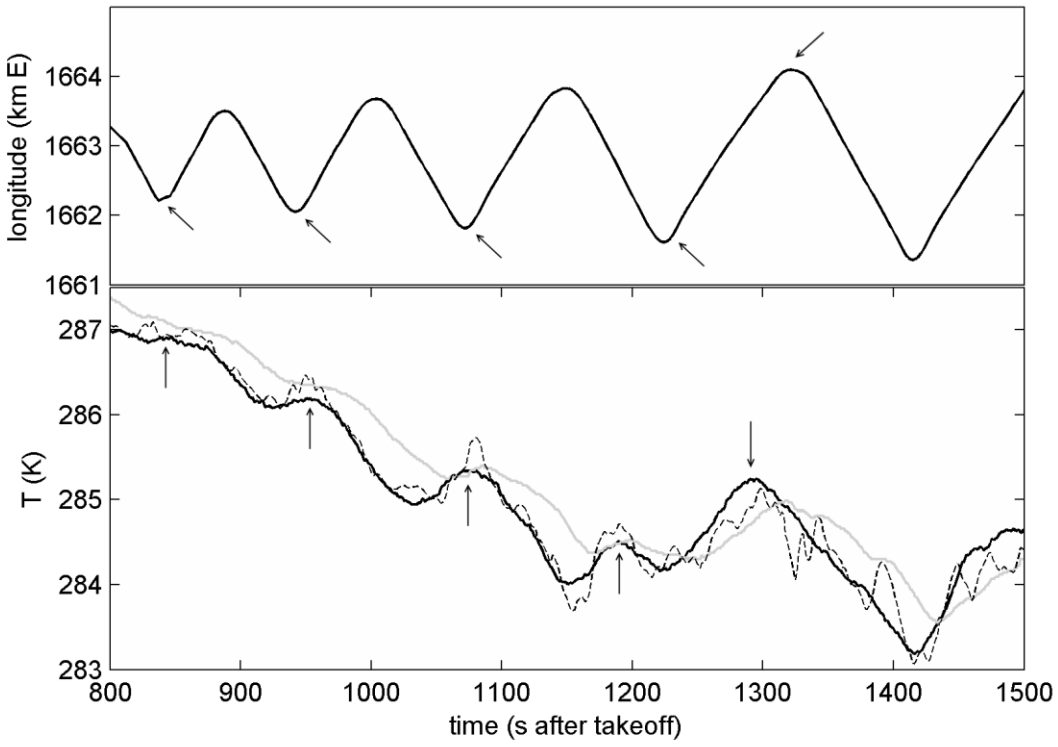

Figure 4.7. Upper panel: longitude time series for the ascending branch of flight #M (in km E; geographic coordinate system: Gauss Boaga, Italy East fuse). Lower panel: corresponding time series of original measured RTD temperature (grey line), RTD temperature corrected for the slow-response effect (solid black line) and temperature recorded by the thermohygrometer (dashed black line). The arrows highlight the good correspondence between local temperature peaks and the turning points of the flight trajectory, where the motorglider flew close to the western valley sidewall. The backward time shift (approximately equal to τ) produced by the application of the deconvolution algorithm can also be appreciated.

4.4 The interpolation methods

As anticipated, to produce easily readable, visually appealing graphical representations (i.e. contour plots) of the meteorological fields from ABL airborne measurements, a number of mapping techniques have been used in the literature to interpolate observations from the flight trajectory over high-resolution, regularly-spaced 3D grids. For instance, inverse distance weighted (IDW) and exponentially-weighted inverse squared distance (exp-ISD) methods were adopted respectively by Egger (1983) and Hennemuth (1985) to regrid the pressure and the potential temperature fields in the Dischma Valley, Switzerland, while a natural neighbor (NN) method based on a Delaunay Triangulation was used by de Wekker (2002) and Weigel and Rotach (2004) for mapping the potential temperature and wind fields in the Riviera Valley, Switzerland. Following Rampanelli (2004), Rampanelli and Zardi (2002) and Laiti et al. (2013), a residual kriging (RK) method is proposed here as a suitable technique for this specific application. In the next paragraphs a brief overview is provided for each of the above-cited interpolation methods.

4.4.1 Inverse distance methods

Methods based on the inverse of distance between points (Shepard 1968, Watson 1992) are among the most commonly adopted and computationally inexpensive weighted-average interpolation methods. In general, weighted-average methods compute the estimated value of the target field Z (denoted by the circumflex accent) at the unobserved location $\mathbf{x}_\alpha$ (i.e. an interpolation grid node) as a linear combination of a subset of N_α nearby observations at $\mathbf{x}_i$ neighboring points (i.e. neighbors):

$$\hat{Z}(\mathbf{x}_\alpha) = \frac{1}{N_\alpha} \sum_{i=1}^{N_\alpha} \lambda_i Z(\mathbf{x}_i), \qquad \text{(eq. 4.10)}$$

where an unbiasedness condition prescribes:

$$\sum_{i=1}^{N_\alpha} \lambda_i = 1. \qquad \text{(eq. 4.11)}$$

In inverse-distance based methods, the weights λ_i of the linear combination are usually assigned through a weighting power p, which controls how the relative influence of the neighboring observations $Z(\mathbf{x}_i)$ decreases with the distance r_i from the estimate point $\mathbf{x}_\alpha$:

$$\begin{cases} \lambda_i = \dfrac{(r_i)^{-p}}{\sum_{j=1}^{N_\alpha} (r_j)^{-p}} & \text{for} \quad \mathbf{x}_i \neq \mathbf{x}_\alpha \\ \lambda_i = 1, \quad \lambda_{j \neq i} = 0 & \text{for} \quad \mathbf{x}_i = \mathbf{x}_\alpha \end{cases}. \qquad \text{(eq. 4.12)}$$

Alternatively, the weights may be exponentially graduated:

$$\begin{cases} \lambda_i = \dfrac{\exp\left[-\left(r_i\right)^p\right]}{\sum_{j=1}^{N_\alpha} \exp\left[-\left(r_j\right)^p\right]} & \text{for} \quad \mathbf{x}_i \neq \mathbf{x}_\alpha \\ \lambda_i = 1, \quad \lambda_{j \neq i} = 0 & \text{for} \quad \mathbf{x}_i = \mathbf{x}_\alpha \end{cases} . \qquad \text{(eq. 4.13)}$$

In general, for small p values ($0 < p < 1$) the weights of neighboring observations result rather evenly distributed. On the contrary, as p increases ($p \geq 1$) the influence of the neighbors farthest from the estimate point diminish, and the estimate values approaches the value of the nearest point. Inverse-distance interpolators are exact (i.e. they return the observed value when applied at an observation point) and convex (i.e. they never result in an estimated value out of the range of observed values); moreover, an arbitrarily determined value of the search radius (i.e. the threshold distance for the selection of the neighbors involved in the interpolation) is commonly set to reduce the computational cost of the interpolation in large dataset applications (Watson 1992). The here considered IDW (Egger 1983) and exp-ISD (Hennemuth 1985) methods from the literature implement respectively **eq. 4.12** with $p = 1$, and **eq. 4.13** with $p = 2$ (notice that Hennemuth 1985 also used a scaling factor of 2 for the vertical coordinate).

4.4.2 Natural neighbor method

NN is also a weighted-average interpolation method. It relies on the definition of a triangulation (usually a Delaunay triangulation) to determine the natural neighbors of the estimate point and to assign them the linear combination weights (Watson 1992). A Delaunay triangulation for a set of points in a 3D volume consists in a set of tetrahedrons such that no point falls inside the circumsphere of any tetrahedron, i.e. satisfying the requirement that the circumsphere of all tetrahedrons has an empty interior. The dual of a Delaunay triangulation is a set of Thiessen polyhedrons, i.e. a set of polyhedrons whose vertices are provided by the centers of the former circumspheres; each Thiessen polyhedron contains a single observation point. If a new $\mathbf{x}_\alpha$ point (i.e. the interpolation grid node) is added to the original set of observation points, the Thiessen polyhedrons are modified and a new polyhedron $\mathbf{P}_\alpha$ is created. The natural neighbors of $\mathbf{x}_\alpha$ are then identified as the N_α points $\mathbf{x}_i$, associated with the polyhedrons $\mathbf{P}_i$, sharing a facet with $\mathbf{P}_\alpha$. The fractions of $\mathbf{P}_\alpha$ volume that were subtracted from each single pre-existing polyhedrons $\mathbf{P}_i$ are called borrowed volumes ($V_{\alpha,i}$). The weights λ_i assigned to observations collected at natural neighbors $\mathbf{x}_i$ are proportional to the corresponding borrowed volumes:

$$\begin{cases} \lambda_i = \dfrac{V_{\alpha,i}}{\sum_{j=1}^{N_\alpha} V_{\alpha,j}} & \text{for} \quad \mathbf{x}_i \neq \mathbf{x}_\alpha \\ \lambda_i = 1, \quad \lambda_{j\neq i} = 0 & \text{for} \quad \mathbf{x}_i = \mathbf{x}_\alpha \end{cases} . \qquad \text{(eq. 4.14)}$$

Note that extrapolation is not possible when using NN method, for the Delaunay triangulation cannot be defined outside the convex hull of the observation locations, i.e. outside the outline of the Thiessen polyhedrons (Watson 1992).

4.4.3 Residual kriging method

Originally developed in mining engineering for the evaluation of mineral resources in the 1950's (Krige 1951), kriging methods were mathematically formalized in the following years (see Cressie 1993, Isaaks and Srivastava 1989, Journel and Huijbregts 1978, Goovaerts 1997, Matheron 1971 among others), and are nowadays widely applied in geosciences. In the field of atmospheric sciences, they are commonly adopted to map the planimetric distribution of rainfall, temperatures and other meteorological quantities, often applying at the same time multiple regression with variables like topography elevation, slope and aspect, distance to the sea, longitude and/or latitude (see for example Alsamamra et al. 2009, Dryas and Ustrnul 2007, Hudson and Wackernagel 1994, Tveito et al. 2006). Kriging is a family of geostatistical mapping techniques, which rely on the theory of stochastic processes and assume the target field *Z* be a stochastic variable. Kriging estimates also consist in weighted averages of values observed at neighboring points, the weights being determined on the basis of the spatial covariance function of observations through the minimization of the predicted variance of the estimate at each interpolation point, not by a purely geometrical criterion as in IDW, exp-ISD and NN.

Among the various kriging options, the most appropriate for the present dataset is residual kriging (RK, also named Regression Kriging; Ahmed and de Marsily 1987, Odeh et al. 1994, 1995, Goovaerts 1999). RK assumes that *Z* can be explicitly decomposed into a deterministic drift μ and a stochastic residual component δ, as follows:

$$Z(\mathbf{x}_\alpha) = \mu(\mathbf{x}_\alpha) + \delta(\mathbf{x}_\alpha), \qquad \text{(eq. 4.15)}$$

and that the two can be estimated separately and then summed back:

$$\hat{Z}(\mathbf{x}_\alpha) = \hat{\mu}(\mathbf{x}_\alpha) + \hat{\delta}(\mathbf{x}_\alpha). \qquad \text{(eq. 4.16)}$$

4.4.3.1 The pseudo-soundings

Analytical models are usually adopted in RK as drift functions, whose coefficients are estimated from the observations by means of standard regression methods (e.g. least squares). Nevertheless, a suitable analytical formulation that could properly model the complex

vertical distribution of real ABL observations is not always available. For example, the method proposed by Rampanelli and Zardi (2004), although very useful when trying to determine the parameters of the diurnal convective boundary-layer (CBL) vertical structure, fails in detecting the presence of elevated mixed layers (MLs) or when the lapse rate is not constant with height. A moving-window vertical average algorithm is therefore used in the present work to extract the dominant vertical structure of the valley ABL, and the resulting "pseudo-soundings" (i.e. the vertically averaged profiles) are adopted as drift terms in RK implementation (see **figure 4.8**).

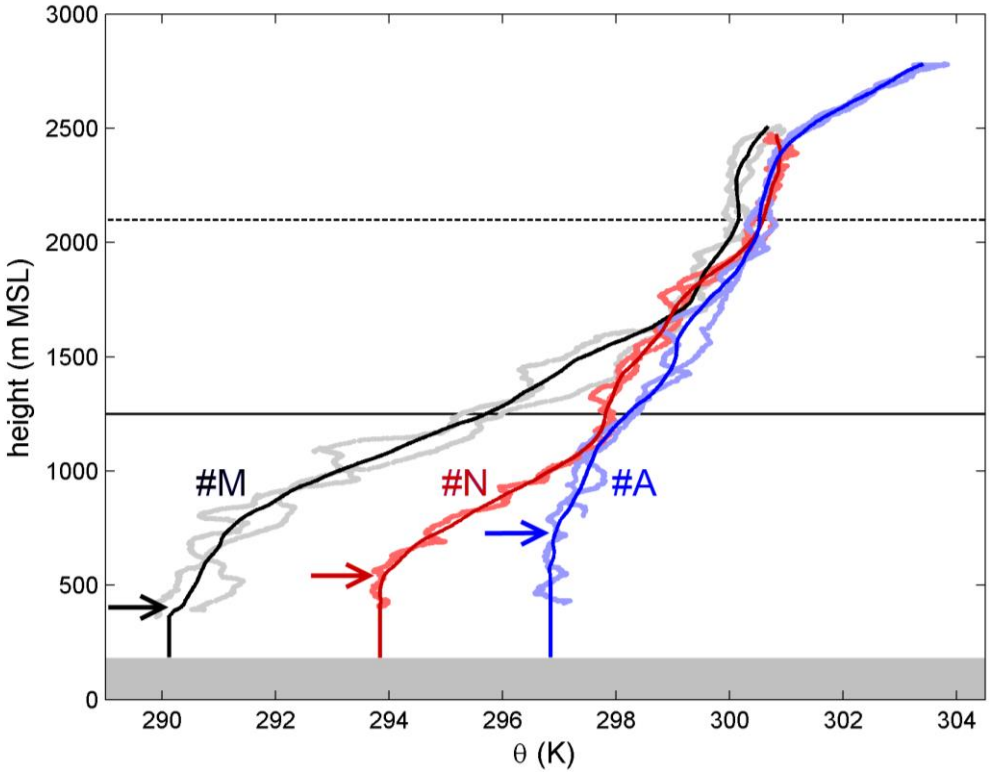

Figure 4.8. Vertical distribution of potential temperature observations for the three flights #M, #N and #A. The superimposed solid lines are the pseudo-sounding extracted from these data, and adopted as drift terms in RK for the evaluation of residuals (colors correspond to those used in **figures 4.2** and **4.6**). The arrows indicate the top of the detected MLs. The grey shading marks the local valley-floor height (180 m MSL), while the black horizontal lines report the local height of the lateral crests, respectively on the western (solid line) and on the eastern side (dashed line) of the valley.

This allows filtering out local anomalies reflecting local patterns associated with specific flow features, driven by complex topography and land cover heterogeneities. In our case, the pseudo-soundings were further extended also below the region sampled by the motorglider

under the assumption of a constant potential temperature in the lowest ABL, i.e. assuming the presence of a diurnal ML in the lowest atmosphere, as suggested by the vertical distribution of the observations (cf. **figure 4.8**). RK foresees that the separate prediction of residuals resulting from the subtraction of the drift from the original data be done by means of a standard ordinary kriging algorithm (OK; Cressie 1993, Journel and Huijbregts 1978), which requires the target variable to display at least a local second order stationarity (i.e. local stationarity of the variable mean and covariance). Accordingly, the moving-window width (200–250 m) is chosen so as to ensure that the residuals of potential temperature show a probability distribution that can be considered normal to a good degree of approximation, thus allowing the application of OK. **Figure 4.9** shows normal probability plots of the residual distribution for the three flights: except a few data in the distribution tails (especially for flight #N), the observations fit acceptably well the theoretical normal distributions. Notice that the variation range of flight #M residuals is twice the range shown by flight #N and #A. This reveals that the cross-valley thermal anomalies are more pronounced in the early morning phase than in the central hours of the day.

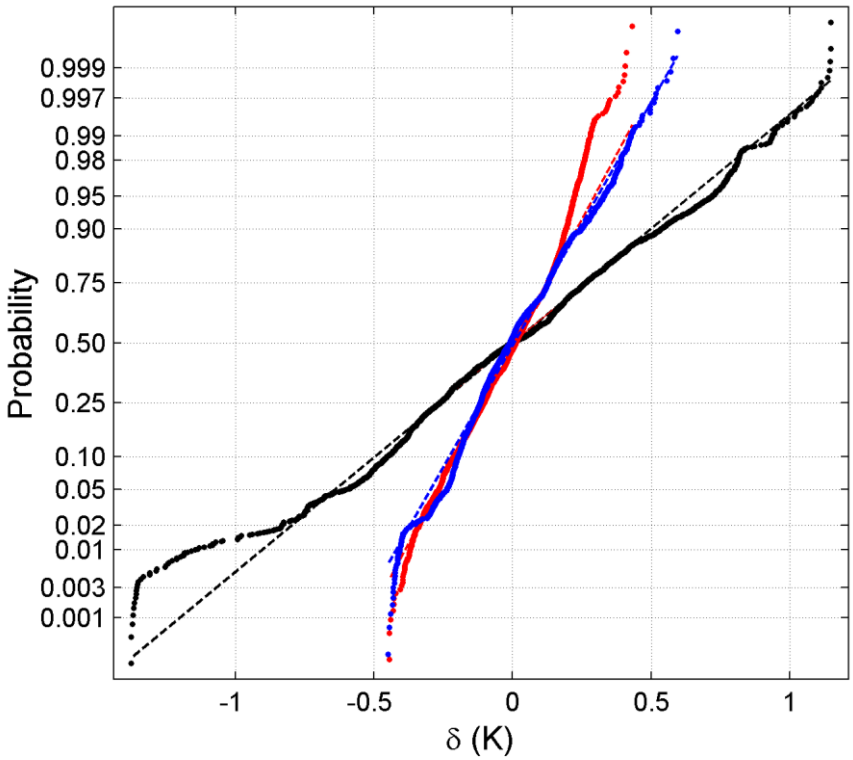

Figure 4.9. Normal probability plot of residuals (dots) from the three flights; colors correspond to those used in **fig. 4.2**, **4.6**, **4.8**. The plot graphically assesses whether a dataset is approximately normally distributed. The dashed lines represent theoretical normal distributions with same mean and standard deviation as the observations (i.e. residuals). If data are consistent with the theoretical distribution, then they should lie close to it.

4.4.3.2 The semivariogram function

OK interpolation method assumes the following expression (analogous to **eq. 4.10**) for the residual estimate, based on a linear combination of residuals evaluated at the estimate point's neighbors:

$$\hat{\delta}(\mathbf{x}_\alpha) = \frac{1}{N_\alpha}\sum_{i=1}^{N_\alpha}\lambda_i \delta(\mathbf{x}_i). \qquad \text{(eq. 4.17)}$$

Kriging techniques imply that the weights λ_i be evaluated by means of the so called semivariogram function $\gamma(\mathbf{h})$, which estimates the spatial dependence of the observations (i.e. residuals) covariance in terms of lag-averaged pairwise dissimilarity:

$$\gamma(\mathbf{h}) = \frac{1}{N_\mathbf{h}}\sum_{i=1}^{N_\mathbf{h}}\frac{1}{2}\left[\delta(\mathbf{x}_i) - \delta(\mathbf{x}_i + \mathbf{h})\right]^2, \qquad \text{(eq. 4.18)}$$

where $\mathbf{h}$ is the separation lag vector between the positions of observation pairs and $N_\mathbf{h}$ is the number of pairs separated by $\mathbf{h}$ (Goovaerts 1997). The semivariogram is a key function in geostatistics, and is defined as the variance of the difference between field values at two locations across realizations of the field itself (Cressie 1993). In practice, semivariograms may be empirically estimated by a variety of estimator functions. Here the robust estimator proposed by Cressie and Hawkins (1980) was found to give the best results in terms of semivariogram stability (see also Genton 1998):

$$\gamma(\mathbf{h}) = \frac{1}{2}\left[\frac{1}{N_\mathbf{h}}\sum_{i=1}^{N_\mathbf{h}}\left\|\delta(\mathbf{x}_i) - \delta(\mathbf{x}_i + \mathbf{h})\right\|^{\frac{1}{2}}\right]^4\left(0.457 + \frac{0.494}{N_\mathbf{h}}\right)^{-1}. \qquad \text{(eq. 4.19)}$$

The empirical semivariogram is an experimental realization of the intrinsic covariance structure of the observed field. To compute the weights, a parametric model of theoretical semivariogram must be fit to the empirical semivariogram (see Goovaerts 1997 and Isaaks and Srivastava 1989 for further details). For the present case, we used either an exponential model:

$$\begin{cases} \gamma(\mathbf{h}) = 0 & \mathbf{h} = 0 \\ \gamma(\mathbf{h}) = n + s\left[1 - \exp\left(-\dfrac{3\|\mathbf{h}\|}{r}\right)\right] & \mathbf{h} \neq 0 \end{cases} \qquad \text{(eq. 4.20)}$$

or a spherical model:

$$\begin{cases} \gamma(\mathbf{h}) = 0 & \mathbf{h} = 0 \\ \gamma(\mathbf{h}) = n + s\left[1.5\left(\dfrac{\|\mathbf{h}\|}{r}\right) - 0.5\left(\dfrac{\|\mathbf{h}\|}{r}\right)^3\right] & 0 < \mathbf{h} < r \\ \gamma(\mathbf{h}) = n + s & \|\mathbf{h}\| \geq r \end{cases} \qquad \text{(eq. 4.21)}$$

according to the specific structure of the different experimental semivariograms.

In the above **eq. 4.20** and **4.21**, the nugget n (i.e. semivariogram value at the origin) accounts

for variability at distances smaller than the shortest sampling interval or lower than the measurement resolution, the sill *s* is the asymptotic value for increasing lags, and the practical range *r* is the lag distance at which the semivariogram practically reaches the sill value (Journel and Huijbregts 1978). Beyond this distance, correlation between data is negligible. Notice however that spatial covariance may depend not only on the modulus, but also on the direction of the lag between pairs **h**. In the present case the two principal directions are along the vertical and the cross-valley coordinates respectively. Therefore horizontal and vertical directional semivariograms of residuals were evaluated separately. As an example these are shown in **figure 4.10** for flight #A. As expected, vertical and cross-valley characteristic ranges are different. Similar results are found for all the flights, with ratios between the two ranges varying between 3.5 and 4.5. The horizontal and vertical ranges also provide the appropriate scaling factors for normalizing the space coordinates to get an isotropic field. As the flight patterns were performed closely around vertical cross-valley planes, the (weak) variability in the third direction, i.e. along-valley, could not be derived from the data. Instead the same range was assumed for this direction as for the cross-valley one. Based on the above reasoning, omnidirectional semivariograms were then computed and finally used for OK mapping.

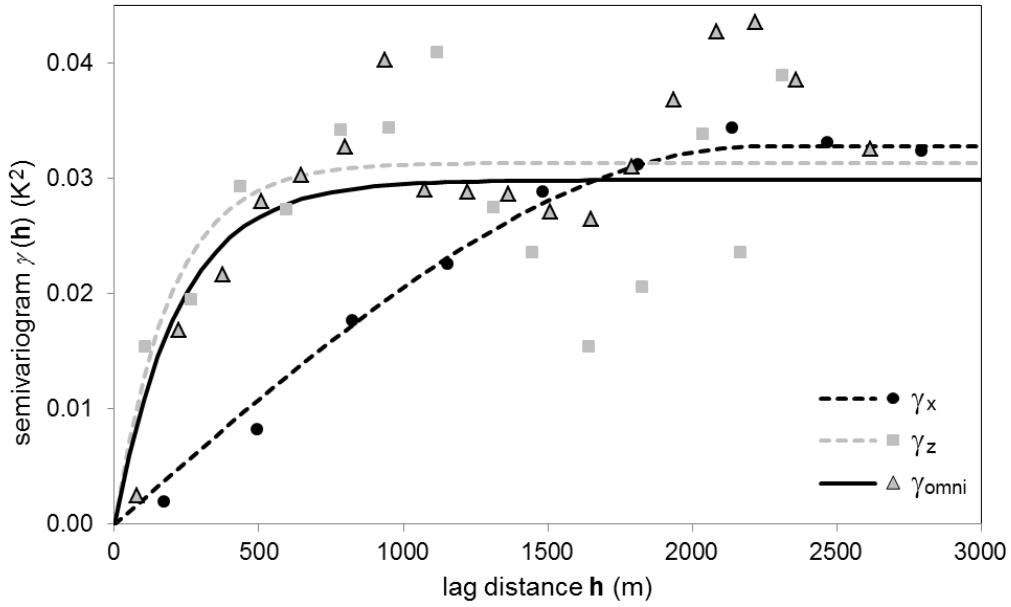

Figure 4.10. Horizontal (i.e. cross-valley) (γ_x), vertical (γ_z) and omnidirectional (γ_{omni}) empirical semivariograms of potential temperature residuals for flight #A (markers). Associated lines represent the best-fit theoretical semivariograms (spherical model for γ_x, exponential model for γ_z and γ_{omni}). Practical range values for the directional semivariograms are respectively 2230 m in cross-valley direction and 580 m in vertical direction, thus determining an anisotropy ratio of 3.8, which is used to isotropize the field before computing γ_{omni} (practical range: 650 m).

From the previous sections (**4.4.1-4.4.3**), it can be argued that RK offers a series of advantages compared to IDW, exp-ISD and NN methods. First of all, RK naturally incorporates trends underlying in the data. Second, RK linear combination weights reflect the characteristic spatial covariance structure of the specific dataset, while the other mapping methods assign them on the sole basis of the geometric configuration of the observation points. Third, it also accounts for the intrinsic anisotropy of the target field, by using appropriate, objectively determined scaling factors for the principal space directions. Moreover RK provides a value of estimate variance at each prediction point as by-product, representing an indication of the estimate confidence. However, for the sake of completeness it must be mentioned that RK is computationally more expensive than the other methods. Also the requirement that the target variable present a normal probability distribution may be a limitation of the method.

4.5 Comparison of the methods

In this section the performances of the mapping methods used in the literature (i.e. IDW, exp-ISD and NN) are compared to the performance of RK method. First a cross-validation analysis is carried out, then the results of the mapping methods application to the test-bed dataset are qualitatively discussed, highlighting weaknesses and strengths of the different techniques. Moreover, the importance of explicitly considering the underlying vertical trend component for this type of data also for IDW, exp-ISD and NN methods is assessed, testing the improvement brought to these methods by the "residual approach", i.e. the separate interpolation of drift and residuals obtained subtracting the latter from the original data as in RK.

4.5.1 Cross-validation analysis

The evaluation of the accuracy of an interpolation method is commonly carried out by means of cross-validation methods. In particular, in this work a leave-one-out cross-validation (LOOCV) was performed. As suggested by its name, in LOOCV observation points are excluded from the original dataset one at time and used in turn as validation points (Arlot and Cenisse 2010, Watson 1992). The predictive performance of the interpolation method is then assessed on the basis of the difference between the observed and the estimated value at each observation point. Scatterplots of observed vs. predicted potential temperature values in **figures 4.11-4.13** visually represent the results of the cross-validation analysis for the three flights: a dispersed distribution of the scatter points around the bisector line indicates a poor performance of the method. RK evidently results the best-performing interpolation method, at least for flights #M and #N, while for flight #A the situation is not so clear. Also exp-ISD behaves very well for flights #M and #A, neglecting a few points from flight #M where it returns very bad values (**figure 4.11**). On the contrary, NN appears to be the method giving

the worst results for all the three flights, as it performs rather poorly with respect to all the other methods. Including the separate treatment of the vertical trend component (i.e. the "residual approach", indicated by the prefix "R" before the method names) doesn't seem to improve IDW, exp-ISD and NN results to any appreciable extent, except for flight #N (**figure 4.12**), where the improved performance of R-IDW and R-exp-ISD is very evident.
Quantitative evaluations of the LOOCV results can also be done, by computing some simple statistics for the cross-validation error (i.e. the difference between the LOOCV-predicted value of the target variable *Z* and the omitted observation), like the mean bias error (MBE):

$$\mathrm{MBE} = \frac{1}{N}\sum_{i=1}^{N}\hat{Z}(\mathbf{x}_i) - Z(\mathbf{x}_i), \qquad \text{(eq. 4.22)}$$

the mean absolute error (MAE):

$$\mathrm{MAE} = \frac{1}{N}\sum_{i=1}^{N}\left\|\hat{Z}(\mathbf{x}_i) - Z(\mathbf{x}_i)\right\|, \qquad \text{(eq. 4.23)}$$

and the root mean square error (RMSE):

$$\mathrm{RMSE} = \sqrt{\frac{1}{N}\sum_{i=1}^{N}\left[\hat{Z}(\mathbf{x}_i) - Z(\mathbf{x}_i)\right]^2}, \qquad \text{(eq. 4.24)}$$

where *N* is the total number of observations in the dataset (Arlot and Cenisse 2010, Watson 1992). In **table 4.2** these statistics are reported for each flight and for each method under evaluation. These results highlight that RK performs undoubtedly better in LOOCV than the other methods: it shows always the smallest MBE (except in one single case: exp-ISD for flight #M), which assumes completely negligible values. On the contrary, IDW and both NN and R-NN show the highest MBE values, from two to three orders of magnitude higher than RK, up to ~0.1 K. The residual approach determines smaller MBEs both for R-IDW and R-exp-ISD methods. MAE and RMSE for RK method are always lower than for the literature methods, at least one order of magnitude smaller, with the residual approach allowing some improvement again for R-IDW and R-exp-ISD. In particular, literature methods RMSE is found to range from 3 to 20 times the RMSE provided by RK, which is on average around 2.5e-02 K. This good performance is a very valuable result, as an average interpolation error of a few tenths of degree Kelvin showed by the other methods appears not acceptable.

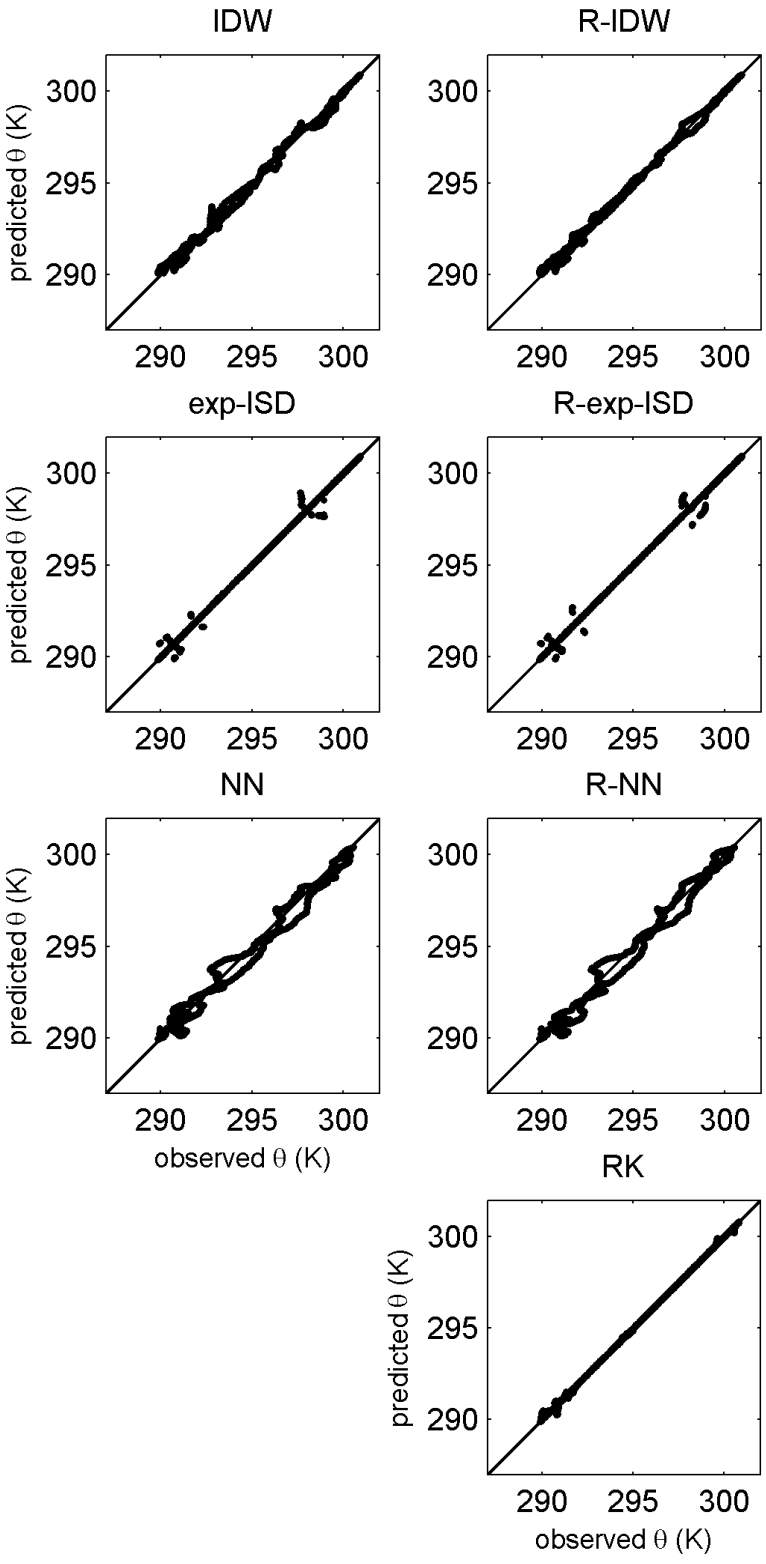

Figure 4.11. LOOCV results for flight #M: scatterplots of observed vs. predicted values of potential temperature for each interpolation method. R-IDW, R-exp-ISD and R-NN refer to the adoption of a residual approach for IDW, exp-ISD and NN methods respectively. The black lines represent identity between observed and predicted values.

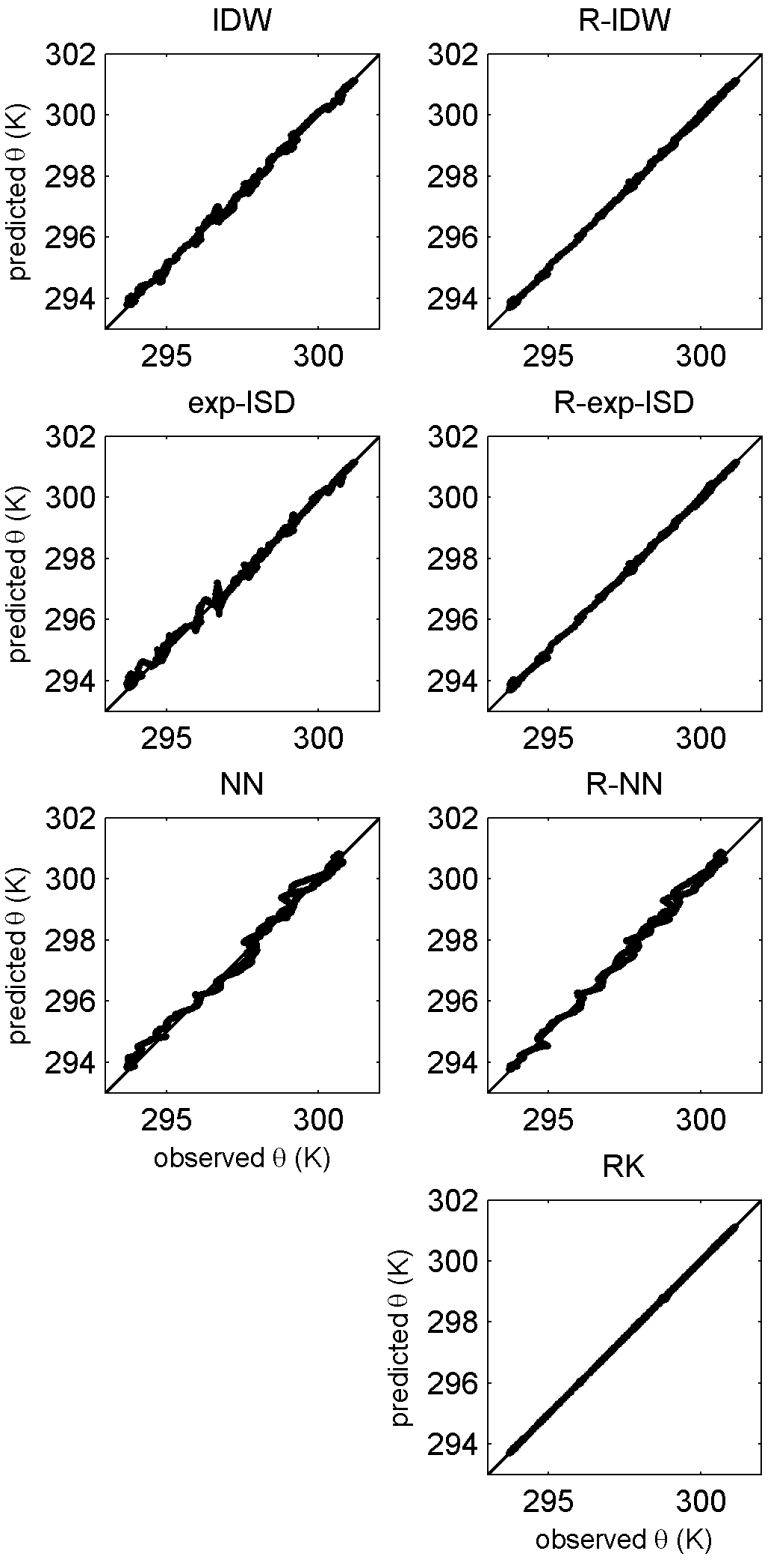

Figure 4.12. As in **figure 4.11** but for flight #N.

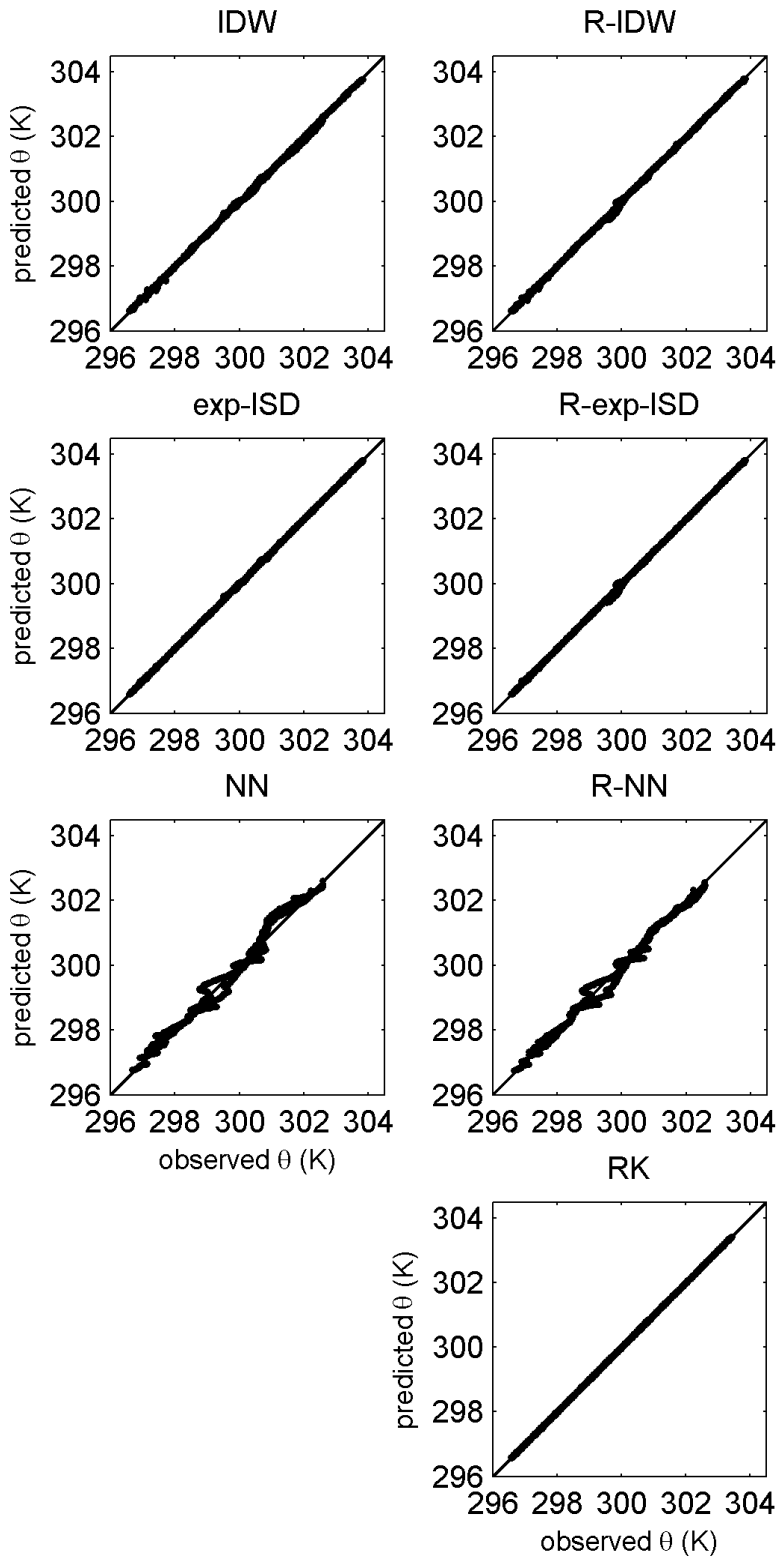

Figure 4.13. As in **figure 4.11** but for flight #A.

Table 4.2. Statistics of LOOCV error for the different methods for the three flight.

Flight	Interpolation method	MBE (K)	MAE (K)	RMSE (K)
#M	IDW	-2.40E-02	1.70E-01	2.40E-01
	exp-ISD	-7.80E-03	1.60E-01	2.40E-01
	NN	-1.30E-01	3.40E-01	4.30E-01
	R-IDW	1.60E-03	1.30E-01	1.90E-01
	R-exp-ISD	-8.60E-06	1.20E-01	1.90E-01
	R-NN	-8.80E-02	3.00E-01	4.00E-01
	RK	**3.00E-04**	**2.20E-02**	**5.30E-02**
#N	IDW	-9.70E-03	8.40E-02	1.10E-01
	exp-ISD	-6.40E-03	8.20E-02	1.20E-01
	NN	4.60E-02	1.80E-01	2.20E-01
	R-IDW	-8.40E-04	3.90E-02	5.00E-02
	R-exp-ISD	-5.00E-04	3.50E-02	5.00E-02
	R-NN	4.10E-02	1.30E-01	1.70E-01
	RK	**-2.20E-05**	**1.00E-02**	**1.40E-02**
#A	IDW	-2.30E-03	2.80E-02	4.00E-02
	exp-ISD	3.70E-04	1.50E-02	2.10E-02
	NN	4.70E-02	1.80E-01	2.30E-01
	R-IDW	-1.20E-03	2.50E-02	3.90E-02
	R-exp-ISD	-3.50E-04	1.90E-02	3.40E-02
	R-NN	-2.40E-02	1.20E-01	1.70E-01
	RK	**-2.40E-05**	**1.00E-02**	**1.30E-02**

4.5.2 Critical comparison of the interpolated fields

The best predictive performance of RK with respect to the other methods becomes even more evident when looking at the interpolated fields. In **figures 4.14-4.16** fields of potential temperature resulting from the application of the three methods from the literature (IDW, exp-ISD and NN), also using the "residual approach" (R-IDW, R-exp-ISD and R-NN), and RK are compared for the three flights. Regularly-spaced 3D grid with a 50 m resolution are built around the spiraling trajectories and used for the mapping, then their median vertical section is extracted and shown in the figures.

At first glance, it is straightforward that RK returns in general the more realistic and visually appealing potential temperature fields. NN is the method that gives the results qualitatively most similar to RK when a "residual approach" is not used, yet the fields it produces are smoother and completely miss some small-scale features revealed by RK. Moreover, in

particular for flights #N and #A (**figures 4.15** and **4.16**), NN returns isentropes with a constant slope, in contrast with the picture shown by RK-interpolated fields: this not negligible horizontal gradient would indicate the presence of a westward cross-valley flow developing over almost the whole valley cross section, which is absolutely not likely to occur. However, the most severe limitation of NN is that it cannot provide values outside the interior of the convex hull of the trajectory, i.e. it cannot extrapolate. On the other hand, IDW and exp-ISD provide similar results: they both show a very strong dependence on the geometrical configuration of the sampling path. In general, it can be said that methods assigning weights on a purely "geometrical" basis (such as the three methods here compared with RK) tend to produce reconstructed fields strongly conditioned by the flight trajectory, differently from RK; the latter appears to be less conditioned, for it includes a vertical drift term and graduates the weights also accordingly to the intrinsic spatial covariance of the observations. For example, IDW and exp-ISD produce isentropes that bend in an unrealistic way towards the lateral slopes of the valley at the lateral extremities of the trajectory (also seen in some NN results; see in particular **figure 4.14**), and when they cross the projection of the trajectory onto the vertical section. This is mainly amenable to three facts. The first is that no scaling factors have been used in the implementation of the literature methods, leading to an overestimation of the relative importance of vertical correlation between observations with respect to the horizontal one, as revealed by the anisotropy ratios inferred from the semivarograms (see **section 4.4.3.2**). The second is that the combination of the increase with height of the horizontal dimension of the flight transects (as the valley cross section widens) and of the recorded potential temperature values produces very warm areas close to the slopes, which are physically not plausible: they would imply the development of excessively thick (order of 500–1000 m) and intense up-slope currents. The third fact is that the fully 3D geometry of the spiraling trajectories determines vertical gaps of variable extent between consecutive transects, being the latter obliquely oriented and not constantly spaced out. Accordingly, the absence of an explicit vertical drift term results in not physically plausible horizontal and vertical gradients of interpolated potential temperature also in the interior of the convex hull of the trajectory points, in particular in IDW and exp-ISD interpolated fields. In this sense, the use of "residual approach" brings significant improvements (see R-IDW and R-exp-ISD results in **figures 4.14-4.16**); in fact, the appearance of the reconstructed potential temperature fields becomes qualitatively very similar for all of the four methods (R-IDW, R-exp-ISD, R-NN and RK), thus confirming a higher reliability of the results obtained through the application of the "residual approach". However, some unrealistic features of the interpolated fields, such as strong curvatures of the isentropes evidently dependent on the flight pattern geometry are still present in R-IDW, R-exp-ISD and R-NN (more evident for flight #M; **figure 4.14**), especially close to the lateral extremities of the flight trajectories.

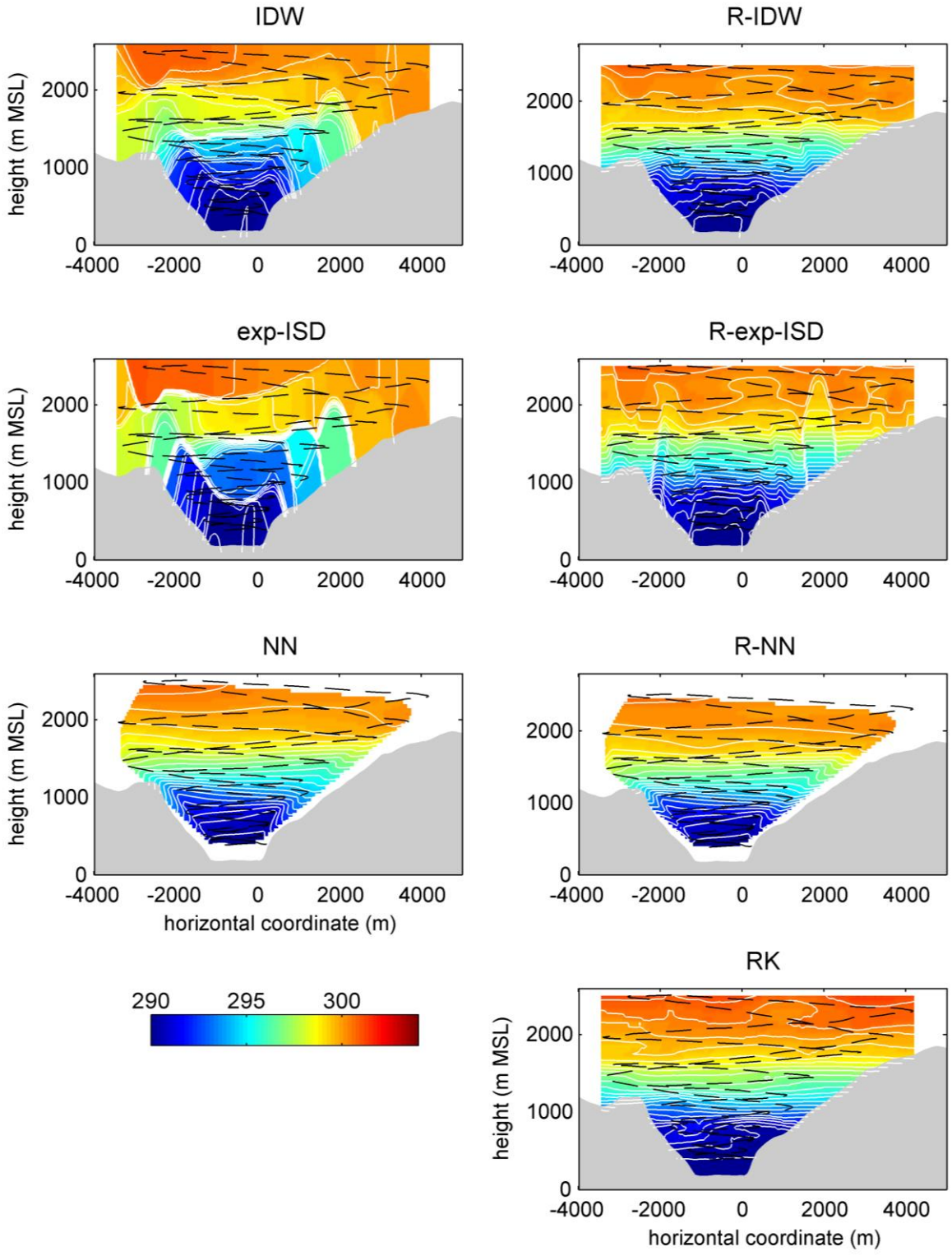

Figure 4.14. Interpolated potential temperature field (in K) from flight #M for all the interpolation methods compared. Contour interval is 0.5 K (in white). The black dashed line represents the projection of the trajectory followed by the motorglider. The local valley section topography is indicated in grey shading.

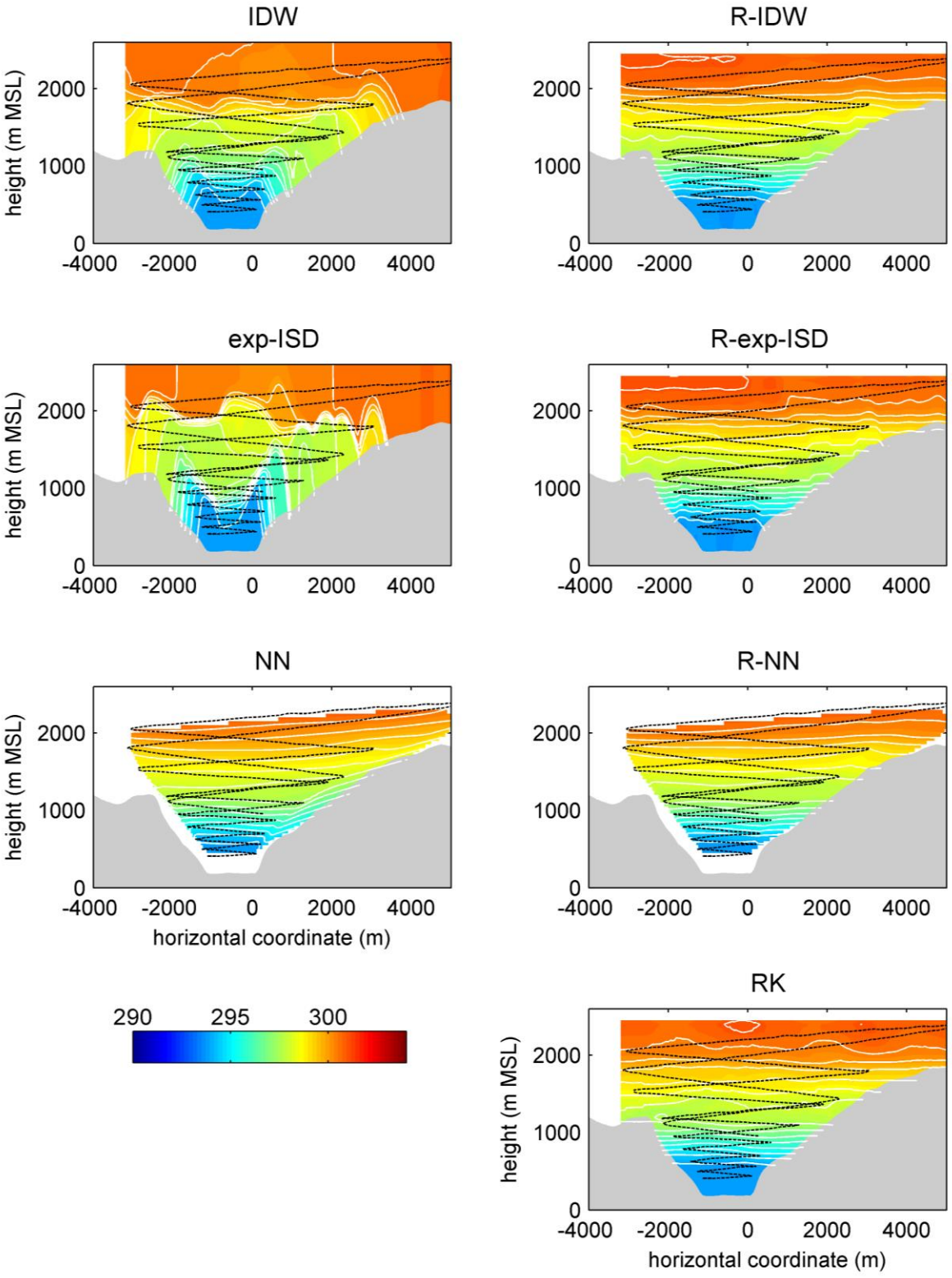

Figure 4.15. As in **figure 4.14**, but for flight #N.

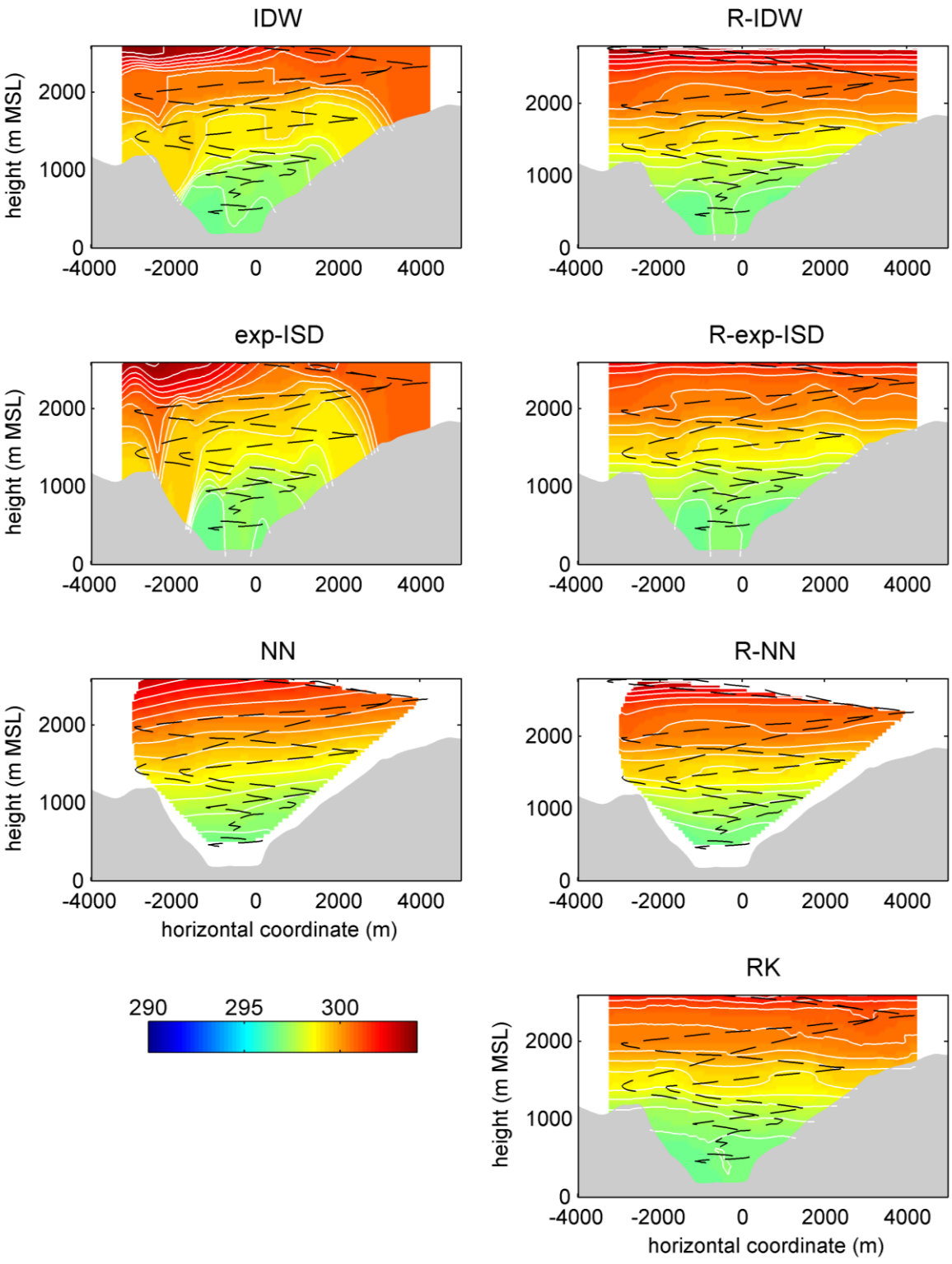

Figure 4.16. As in **figure 4.14**, but for flight #A.

Figure 4.17 shows the RK-estimated standard deviation of the interpolated potential temperature field, i.e. the square root of the RK-predicted variance, whose minimization is pursued in kriging algorithms.

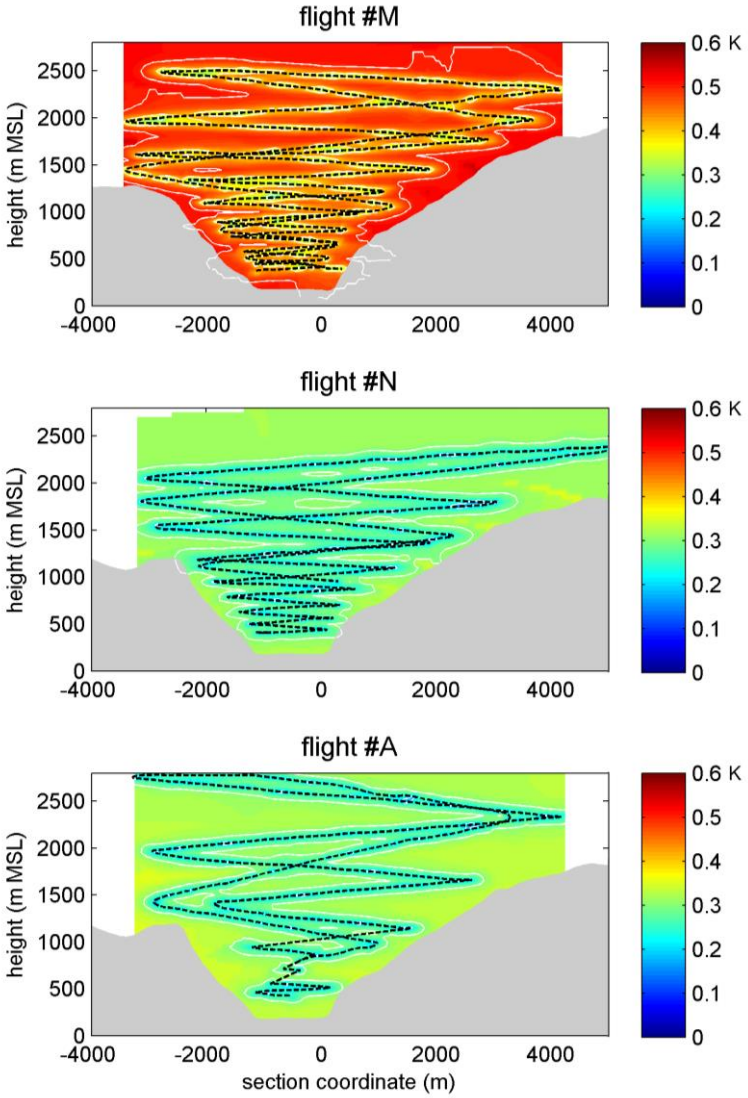

Figure 4.17. RK-estimated standard deviation of the interpolated potential temperature field for the three flights (in color). Contour interval is 0.1 K (in white). The black dashed line represents the projection of the trajectory followed by the motorglider onto the median vertical planes of the interpolation grids. The local valley section topography is indicated in grey shading.

Kriging variance is essentially a map of the distance of interpolation grid points from the nearest observation, rescaled accordingly to the adopted theoretical semivariogram function (see **section 4.4.3.1**; Cressie 1993, Journel and Huijbregts 1978). Accordingly, it represents an indication of the estimated error for the interpolated residual values, based on the

geometrical configuration of the observations. Notice that the average standard deviation is higher for flight #M, due to the larger variation range of the observed residuals (cf. **section 4.4.3.1**). Indeed at all the grid points where RK-interpolated values are shown in **figures 4.14-4.16** and **4.18-4.20**, the kriging standard deviation for flight #M is always below ~0.50 K, differently from flights #N and #A, which display maximum standard deviation values of ~0.35 K.

4.6 Evolution of the ABL thermal structure

On the basis of the pseudo-soundings extracted from the original airborne data (**figure 4.8**), it is possible to appreciate the diurnal evolution of the valley ABL for the period of time covered by the three flights. Flight #M detected the presence of a very shallow (less than 200 m deep) mixed layer (ML) above the valley floor, showing an average potential temperature of 290 K. A stable layer with a lapse rate of 3 K km^{-1} is found above (up to 750 m MSL), which in turn is surmounted by a very stably stratified layer whose lapse rate is 8 K km^{-1} (up to 1700 MSL), which has developed during night-time. In the ~3 h time interval between flight #M and flight #N, ML depth increases to 350 m and its average potential temperature grows by 4 K; moreover, an elevated quasi-mixed layer (QML) develops between 1100 and 1400 m MSL (i.e. around the approximate height of the crest of the western sidewall, which is the one receiving more solar radiation during the morning phase given the N-S orientation of the valley). This is likely due to the heating process associated with return flows compensating for the morning up-slope circulations (Kuwagata and Kimura 1995, 1997). Below this height the lapse rate is slightly reduced (to 6 K km^{-1}) by the same heating process, which also produces local subsidence of warmer air from aloft at the valley center (Rampanelli et al. 2004, Serafin and Zardi 2010a, 2010b, 2011). During flight #A, a 600 m deep ML with an average potential temperature of 297 K is seen, surmounted by a weakly stable layer (2 K km^{-1}) up to 1100 m MSL. The lapse rate changes to 4 K km^{-1} up to the height of ~1500 m MSL, where a shallow QML is still present. These patterns are consistent with the typical structure of the diurnal convective boundary-layer (CBL) observed in deep valleys (as documented in Kuwagata and Kimura 1995, 1997 and Rotach and Zardi 2007). Moreover, for all of the three flights a quasi-mixed layer persists between 2000 and 2400 m MSL (that is the approximate height of the western lateral crests). Above this height the lapse rate changes dramatically (7 K km^{-1} for flight #A), indicating the transition to the free atmosphere region where synoptic-scale flows dominate. To conclude, the top of the diurnal valley ABL, i.e. the atmosphere layer most affected by changes in the thermal structure during daytime, can be estimated to be at around 1600 m MSL, which means a maximum depth of around 1400 m. Actually, this is the layer where the most consistent heating occurs between the morning and the early afternoon, producing a maximum increase in potential temperature values of 7 K at the lowest levels.

RK-interpolated fields add further information about the fine-scale 3D thermal structures superimposed onto the mean vertical structure of the valley ABL. For flight #M for example, below ~900 m MSL the western half of the valley atmosphere is clearly warmer than the eastern one (**figure 4.18**). Considering that during the early morning hours the western slopes receive a higher amount of solar radiation (due to the S-N valley orientation), this ABL structure is likely to be associated with the presence of a cross-valley westward wind, from the shaded eastern slope (on the right in the figure) to the sunlit western slope (on the left in the figure). Moreover, around 1500 m MSL the western half of the valley atmosphere is slightly warmer than the eastern half; the local pattern of the isentropes reveals a local heating possibly induced in this layer by a return current flowing from the top of the western sunlit sidewall towards the center of the valley. On the other hand, around the local noon flight #N (**figure 4.19**) displays a very homogenous potential temperature field over the whole valley cross section, without evident horizontal temperature gradients. The RK-gridded potential temperature field from flight #A indicates a slightly warmer upper valley atmosphere close to the top level of the eastern valley sidewall (~2000 m MSL), which is indeed better sunlit than the opposite and lower one in the afternoon.

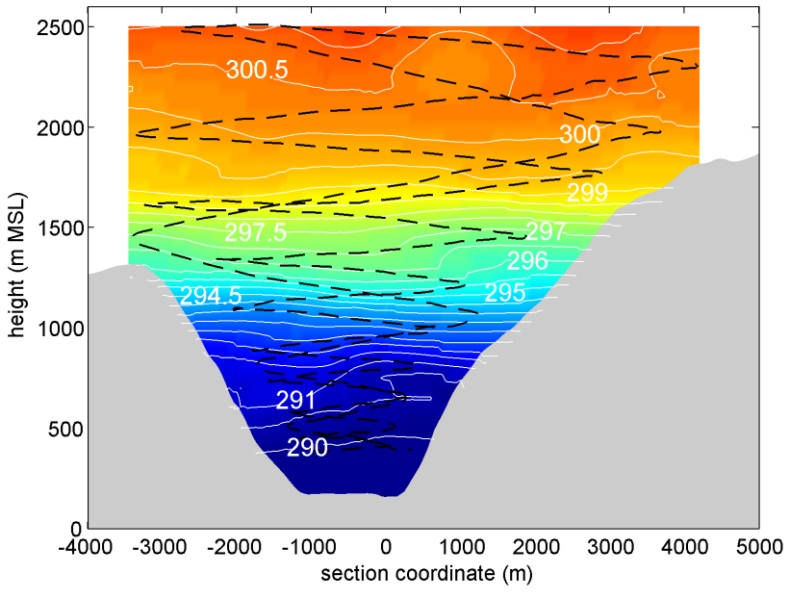

Figure 4.18. RK-interpolated potential temperature field from flight #M. Contour interval is 0.5 K (in white). The black dashed line represents the projection of the trajectory followed by the motorglider. The local valley section topography is indicated in grey shading.

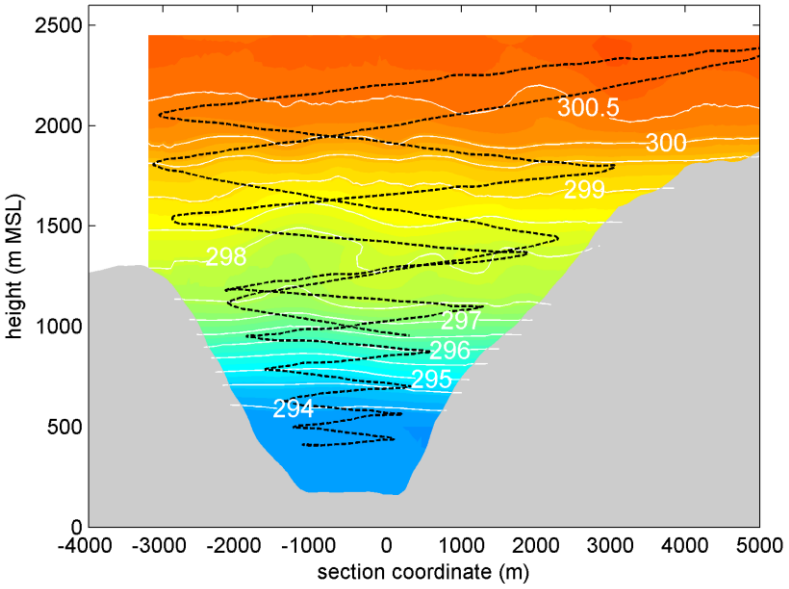

Figure 4.19. As in **figure 4.18**, but for flight #N.

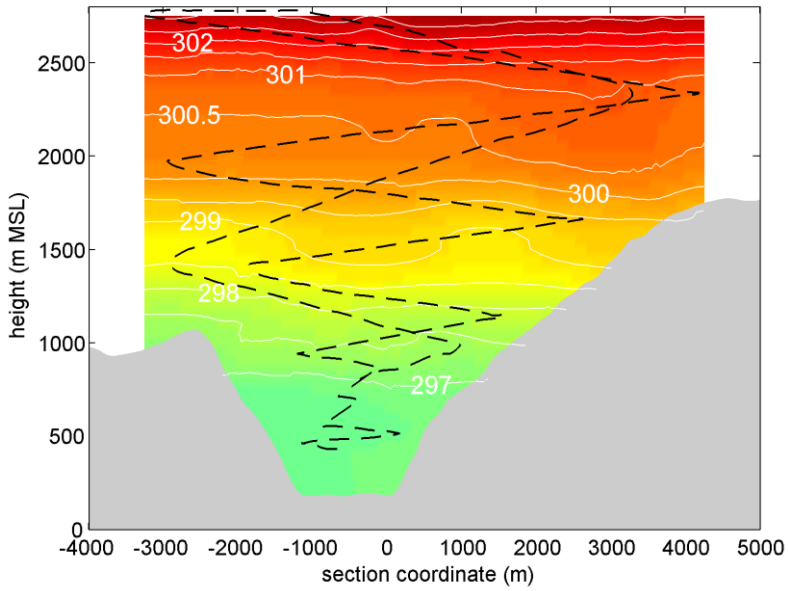

Figure 4.20. As in **figure 4.18**, but for flight #A.

4.7 Summary

Instrumented light aircrafts provide high-resolution observations of the fine-scale 3D variability of the atmosphere structure (de Franceschi et al. 2003). Various interpolation methods have been used in the literature for mapping airborne observations over regular grids; in particular Egger (1983) used an IDW method, Hennemuth (1985) an exp-ISD method, and De Wekker (2002) and Weigel and Rotach (2004) a NN technique. Indeed, re-gridded meteorological fields allow an easier interpretation of the atmosphere fine-scale structure.

Based on a test-bed dataset formed by three flights performed in an Alpine valley, the results from the application of the interpolation methods mentioned above were compared in this paper with the results from the application of a residual kriging (RK) method (Ahmed and de Marsily 1987, Odeh et al. 1994, 1995, Goovaerts 1997). First, the performance of RK was tested against the methods used in the literature by means of a leave-one-out cross-validation (LOOCV) analysis (Arlot and Cenisse 2010, Watson 1992). This highlighted that RK behaves better than all the methods from the literature. In particular IDW and NN returned the worst LOOCV results, while exp-ISD scored quite well, yet more poorly than RK. The introduction of a "residual approach" (i.e. the explicit decomposition of the target field into a drift and a residual field to be estimated separately) improved significantly the LOOCV results of IDW and exp-ISD methods, but not that of NN. However, LOOCV only measures the accuracy of the punctual estimate at observation locations, using observations as validation points one at time. Thus LOOCV doesn't say much about the reliability of the interpolation in the outer regions, where no measurements are available for validation. Indeed, a specific strength of kriging methods is that their implementation automatically returns a prediction variance value for each interpolation grid node, providing an indication of the error of the estimate (Cressie 1993, Goovaerts 1999).

RK mapping over a 3D high-resolution grid was then applied to the airborne data from each of the three flights. The results were qualitatively compared with those from the application of the literature methods, discussing the physical significance of their output. For the specific database, RK proved to be the best-performing method, for it returned the most realistic and visually appealing potential temperature fields. NN was in good qualitative agreement with RK in the interior of the convex hull of the trajectory, but it provided smoother reconstructed fields, suppressing small-scale details. On the other hand, both IDW and exp-ISD gave unrealistic thermal structures, especially close the valley sidewalls. As previously discussed for LOOCV, the application of a "residual approach" was found to bring a consistent improvement for the latter two methods, leading to interpolated fields very close to those produced by RK from a qualitative point of view. Given the physics of the sampled meteorological field, it is extremely important that the vertical drift component be explicitly accounted for. Indeed, the ABL potential temperature field usually presents a strongly

vertically-stratified structure, on which a smaller-magnitude field of local anomaly is typically superimposed. For the present dataset, for example, a variation range of approximately 1.0-1.5 K and at least 5 K can be identified for the residuals and for the drift respectively. Being the drift the primary term of the potential temperature field, RK performance strictly depends on its correct determination. A reliable identification of the drift component is essential in particular when extrapolating, i.e. when estimating values at grid nodes outside the convex envelope of the observation points (see Journel and Rossi 1989).

To summarize, from this study it is evident that RK mapping technique provides the best interpolation for the specific application. Moreover, RK presents a series of advantages with respect to the other methods used in the literature: first its implementation naturally accounts for the dominant drift term underlying in the data, as well as for the characteristic anisotropy of the target field and its characteristic spatial covariance structure. Second it provides an estimate of the prediction error, which other methods do not, thus giving an indication of the reliability of the interpolation. However, it must be said that kriging methods are computationally more expensive, and need a preliminary exploratory statistical analysis of the dataset. The requirement of second order local stationarity for the target field is also a limitation of these methods.

Unfortunately, in the present analysis the unavailability of surface observations from the valley floor and slopes hindered the possibility of getting an adequate picture for the surface and the slope-flow layer, which could not be explored by the motorglider for safety reasons. For future applications, surface measurements integration in RK mapping is desirable; the inclusion of an extensive surface dataset could possibly require that different scaling factors for the regions near the ground be determined, and that locally-estimated semivariogram functions be computed.

Finally, from this analysis some recommendations for the optimization of the flight patterns to be adopted in future field measurements in mountain valleys may be drawn. In particular, it seems preferable that quasi-horizontal transects, equally-spaced in the vertical direction be performed, so as to avoid the introduction of unrealistic cross-valley anomalies like those returned from the application of IDW and exp-ISD methods to the test-bed dataset. At the same time, it is essential that an accurate representation of the “mean” vertical profile of the ABL, to be adopted as dominant drift term in data post-processing, be available; it could eventually be provided also by independent measurements from accordingly calibrated instruments, performing a reliable profiling of the target variable above the valley floor.

Chapter 5

Deciphering the dominant vertical structure of the valley atmospheric boundary-layer

Abstract

The typical vertical structure of the diurnal atmospheric boundary-layer (ABL) over complex terrain appears rather different from the "textbook" convective boundary-layer (CBL) picture commonly found over plain uniform terrain Heterogeneities in terrain elevation and slope, sun exposure, land use and soil moisture affect the spatial distribution of the surface sensible heat fluxes, being responsible for the development of local thermally-driven circulations, like slope and valley winds and sea/lake breezes, which produce strong modifications of the ABL. In this chapter, the dominant vertical structures of the ABL occurring in connection with the *Ora del Garda* development in the study area valleys are discussed, based on pseudo-soundings of potential temperature and water vapour mixing ratio extracted from the airborne dataset presented in **Chapter 2**. Associated with the breeze flow, rather shallow mixed layers (~500 m), surmounted by deeper slightly stable layers and/or elevated warm layers up to the surrounding crest height (~1500 m MSL), are detected. In addition, the up-valley advection of potentially colder air from above Lake Garda surface further stabilizes the potential temperature profiles down to very low heights close to the lake's shoreline, and suppresses the temperature rise in the lowest valley atmosphere. In the area north of Trento, where the *Ora del Garda* and the Adige Valley wind interact, a significant deepening of the mixed layer, mainly driven by the strong local mixing, is observed in the afternoon after the *Ora del Garda* outbreak. Moreover, in this area the strong ventilation and the advective cooling induced by the anomalous afternoon flow have also the effect of stabilizing the surface layer stratification.

5.1 Introduction

Vertical structure and extent of the atmospheric boundary-layer (ABL; the lowest part of the atmosphere directly affected by the interaction with the Earth surface) depend heavily, but not exclusively, on nature and characteristics of the underlying surface, which modulates mass, momentum and heat exchanges between ground and air. In particular, over plain uniform terrain a typical convective boundary-layer (CBL) structure develops during daytime, whose growth is primarily driven by surface sensible heat fluxes from below (Oke 1987, Stull 1988). The classic "textbook" CBL includes three sub-layers (cf. **figure 5.1**):

- a surface layer (usually 50-200 m deep) that directly responds to changes in the surface forcing; here atmospheric quantities displays rapid fluctuations and strong vertical gradients, and vertical turbulent mixing is very intense;
- a mixed layer (ML), where buoyant plumes rising from the surface layer produce an efficient convective mixing, leading to the CBL depth increase and causing atmospheric quantities to be relatively constant with height; over plain areas MLs may reach vertical extents up to 2 km;
- a thin inversion layer (in the order of 100 m) that inhibits the vertical turbulent mixing and forms the interface between the CBL and the free atmosphere (FA) aloft; here also an entrainment processes of air from the FA occurs, producing further growth of the CBL.

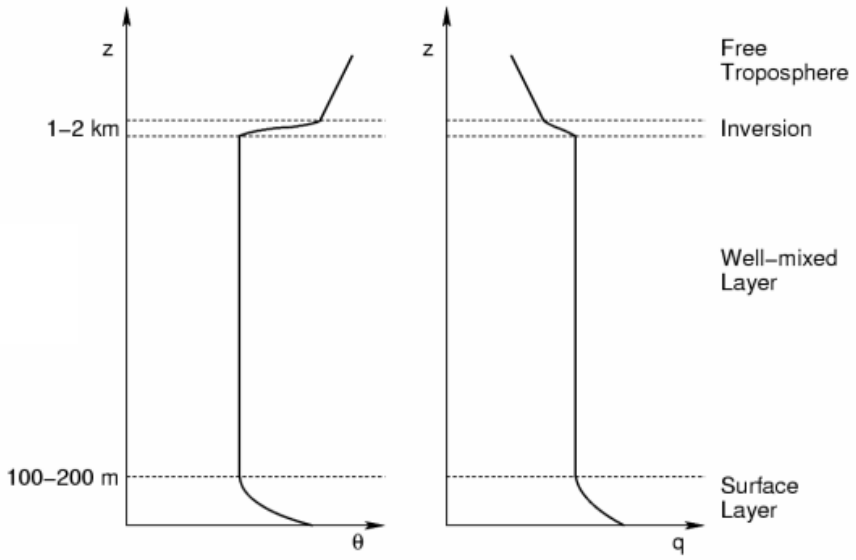

Figure 5.1. Typical vertical profiles of potential temperature (left) and water vapour mixing ratio (right) for a "textbook" CBL structure. Notice the constant values of both variables in the deep ML, extending from above the unstable surface layer to the basis of the strongly-stable inversion layer capping the ABL (modified from Kaimal and Finnigan 1994).

Diurnal ABL processes over complex terrain are known to be remarkably different from those commonly found over plain uniform terrain, i.e. from the "textbook" CBL structure, as they reflect the heterogeneities of terrain elevation and slope, sun exposure, land use and soil moisture; all these factors affect the spatial distribution of the surface sensible heat fluxes that drive the convective growth of the ABL from below (Rotach and Zardi 2007, Kossman et al. 1998). The heterogeneous distribution of sensible heat fluxes in complex terrain is also responsible for producing local thermally-driven circulations, like slope and valley winds and sea/lake breezes. In turn the development of these diurnal winds plays an important role in the daily evolution of the ABL vertical structure over complex terrain. Indeed, up-slope winds contribute together with turbulent heating from the bottom to the erosion of the morning inversion layer preceding the diurnal CBL growth in a valley (Whiteman 1982, Zardi and Whiteman 2013). For a deep Alpine valley Weigel and Rotach (2004) found that the potentially colder air advection following the onset of up-valley winds could stop the ML growth and even stabilize the potential temperature profile through the entire valley depth. This may lead to a valley ABL structure displaying shallow, or even absent, MLs surmounted by deeper weakly stable layers (Rampanelli et al. 2004). This pattern is also associated with the heating of the middle layers due to local subsidence of potentially warmer, stably-stratified air from the FA at the valley center. This effect is induced by the return flows compensating for the removal of air from the valley bottom by up-slope winds; it stabilizes the upper part of the valley ABL and, at the same time, limits the extent of the ML (Kuwagata and Kimura 1995, 1997, Rampanelli et al. 2004, Serafin and Zardi 2010a, 2010b, 2011). A similar subsidence mechanism can be originated also by a strong secondary cross-valley circulation induced by the curvature of the valley (Weigel and Rotach 2004). Moreover, the horizontal advection of heat from the summit of the slopes towards the valley center operated by return flows produces warmer elevated layers around the crest height (De Wekker 2002, De Wekker et al. 2005), called quasi-mixed layers (QMLs; Kuwagata and Kimura 1995, 1997).

In the study area a very complex orographic context, characterized by an irregularly-shaped, deep valley ending abruptly at the elevated saddle of Terlago, combines with the presence of Lake Garda at the valley inlet. The presence of this large source of potentially colder air is likely to affect to some extent the diurnal ABL structure seen in the area (McElroy and Smith, 1991). For instance, this additional cooling term could enhance the stabilization of the potential temperature profile outlined for valley winds by Weigel and Rotach 2004. Furthermore, the development of a lake breeze circulation driven by the land-water contrast may produce an internal boundary-layer (IBL; see the review by Garratt 1990) associated with the onshore flow at the surface. Indeed, Lieman and Alpert (1993) highlighted that steep ABL height gradients may be found in complex terrain areas close to coastlines, associated with sea-breeze fronts and enhanced by topography. Accordingly, in the Alpine basin of Lake

Tekapo (New Zealand), Kossmann et al. (2002) observed the local formation of an IBL, characterized by shallower CBLs than far from the small lake's shoreline, associated with a lake breeze circulation embedded in the mesoscale up-valley flow. They also detected elevated QMLs generated by advective heating from the surrounding basin and valley sidewalls by up-slope winds.

In the next sections the dominant vertical structure of the ABL occurring in the study area valleys in connection with the *Ora del Garda* development is analysed and discussed in the light of the framework presented above, based on the vertical "pseudo-soundings" extracted from the airborne dataset introduced in **Chapter 3**. Following the procedure described in **section 4.4.3.1**, for each single spiral "mean" vertical profiles of potential temperature and water vapour mixing ratio were determined from airborne observations by means of a moving-window vertical average algorithm, and extended below the minimum sampling height down to the local valley floor assuming the occurrence of well-mixed layers (i.e. constant potential temperature or mixing ratio values). This allowed isolating the prevailing vertical structure of the ABL, filtering out the fine-scale variability reflecting local features of the atmospheric fields arising from complex orography and strong surface inhomogeneities. The adopted window width (between 200 and 250 m for all flights) has been determined as a compromise between two goals: on one hand the resulting profiles have to be as smooth as possible, and on the other hand they should still preserve a nearly Gaussian distribution of deviations around the average, as required by the kriging method adopted for interpolation (see **section 4.4.3.1**). Notice that since flying each spiral required on average about 30 min, which is half the typical timescale of ABL structure daytime evolution (cf. Stull 1988), the temporal variability over the single section can be neglected, reasonably assuming that the lowest atmosphere can be considered in quasi-steady state during overflight time.

5.2 24 September 1998 (flight #1)

Figure 5.2 shows potential temperature profiles obtained from plotting airborne data vs. height (i.e. neglecting horizontal coordinates) for each valley section explored during flight #1 (see **table 5.1** and **Chapter 3** for a detailed flight timing and description). Notice that, for the sake of clarity, the number of the flight was included in the pseudo-sounding label. Gray lines are the pseudo-soundings obtained from moving-window (width: 230 m) vertical averages of airborne data, and extended below the sampled region under the assumption of a constant potential temperature in the lowest ABL, the diurnal ML. Also reported in **figure 5.2** are observations recorded around the overflight time at the surface weather stations closest to the area flown over by each spiral (see **figures 3.3** and **3.16** for name and location of the stations). As anticipated, the pseudo-soundings represent the dominant vertical structures of the valley ABL. Small-scale anomalies, reflecting local patterns associated with

specific flow features, are superimposed as a stochastic component on these "mean" vertical profiles.

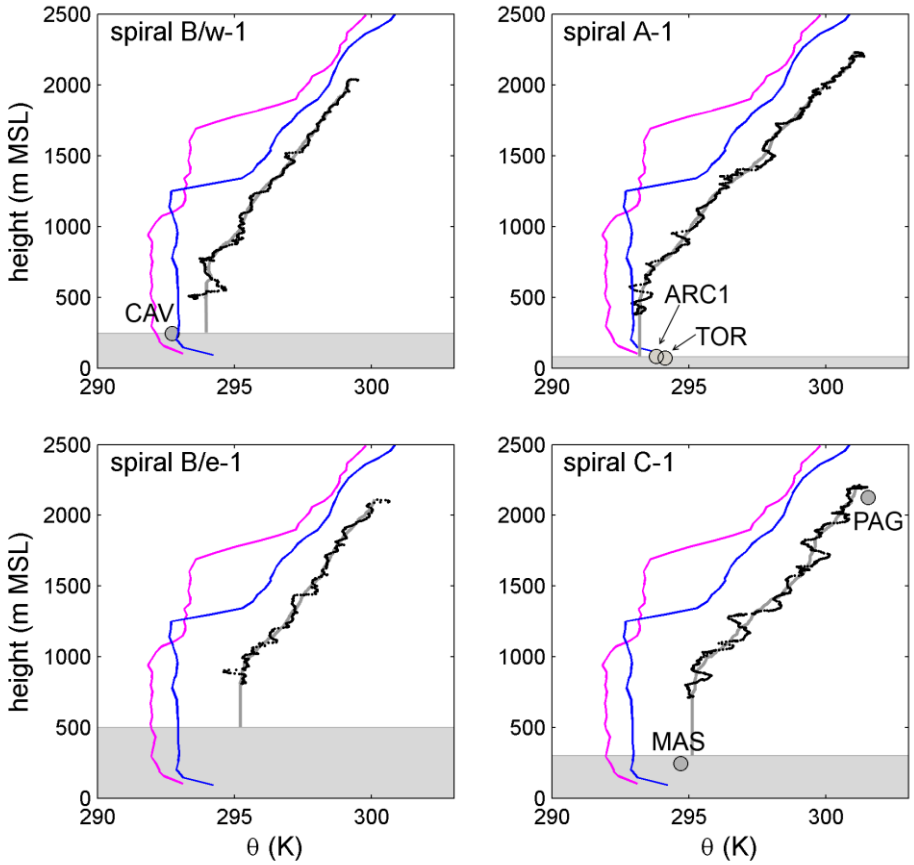

Figure 5.2. Potential temperature measurements (black dots) at each valley cross section for flight #1 compared to routine surface observations from nearby stations (grey bullets; see **section 3.4.2** and **3.6.3** for station labels and positions). Grey lines are the pseudo-soundings representative of the mean vertical structure, and used as drift terms for the evaluation of residuals in the residual kriging procedure (labeled as in **table 5.1**). Magenta and blue lines represent 1200 UTC (i.e. 1300 LST) soundings from LIML and LIPD stations respectively (see **figure 5.3**). The local valley-floor height for each cross section is indicated by the grey shading.

The vertical structure of the valley ABL associated with the *Ora del Garda* development is also compared to the corresponding ABL structure detected over the plain, i.e. over the Po Valley, represented by routine soundings launched at Milano-Linate (LIML) and Udine-Campoformido (LIPD) airports (see a map of the considered sounding stations in **figure 5.3**).

Table 5.1. Timings of the pseudo-soundings shown in **figure 5.2**. LST time is UTC+1.

Flight	Takeoff	Landing	Spiral	Start	End
#1	1015 LST	1300 LST	B/w-1	1054 LST	1110 LST
			A-1	1116 LST	1143 LST
			B/e-1	1148 LST	1200 LST
			C-1	1205 LST	1228 LST

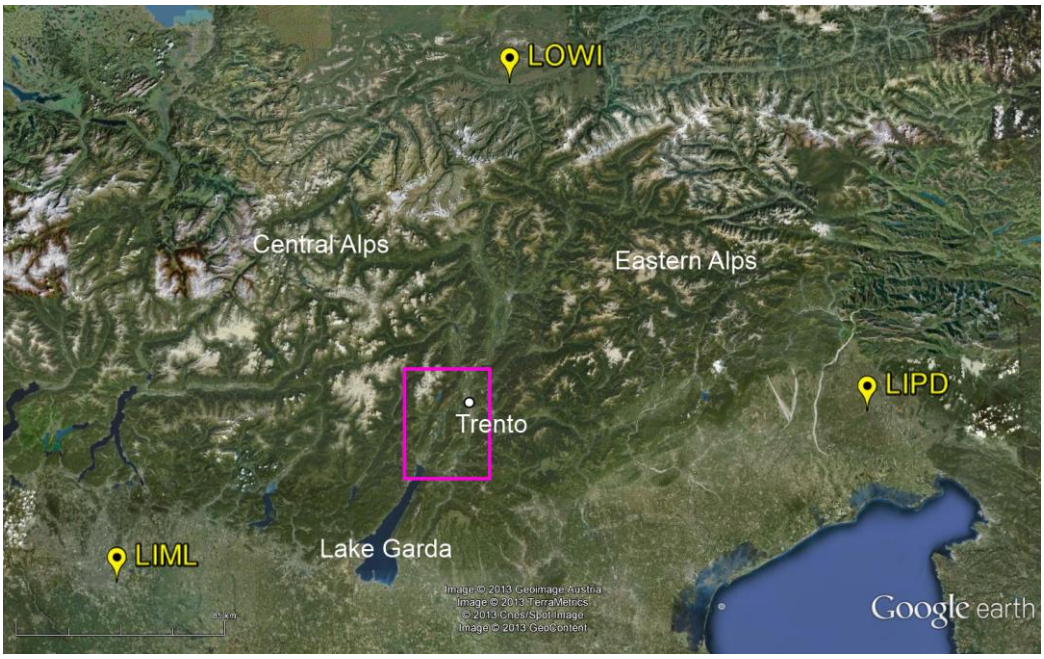

Figure 5.3. Location of the stations (yellow placemarks) providing routine soundings for the comparison with the pseudo-soundings extracted from the airborne data. LIML is Milano-Linate airport, LIPD is Udine-Campoformido airport, LOWI is Innsbruck-Kranebitten airport. The study area is delimited by the rectangular box. Image © Google Earth, © Geoimage Austria, © 2013 TerraMetrics, © 2013 Cnes/Spot Image, © 2013 GeoContent.

Some common features of the ABL structures detected in the explored valleys can be outlined from the pseudo-soundings shown in **figure 5.2**. In particular, at all the cross sections the vertical thermal structure displays a rather shallow ML (depth in the order of ~500 m), surmounted by a deep stable layer (lapse rate ~5 K km^{-1}). Such a structure has been observed in many other valleys (Weigel and Rotach 2004), and is associated with daytime subsidence of potentially warmer air from the free atmosphere. Indeed the latter compensates for the air removed at the valley floor by thermally-driven upslope winds occurring at the valley sidewalls. Subsidence stabilizes the upper part of the profile, and also inhibits the convective ML growth (Kuwagata and Kimura 1995, 1997, Weigel and Rotach 2004,

Rampanelli et al. 2004, Rotach and Zardi 2007, Serafin and Zardi 2010a, 2010b, 2011). Accordingly, the depth of the MLs observed on 24 September 1998 over the Po Valley (i.e. over the plain) is consistently larger than observed in the valleys of the study area, being in the order of 1000-1200 m. Moreover, the valley ABL structure is markedly different from the typical CBL structure (Oke 1987, Stull 1988) displayed by routine soundings at LIML and LIPD, for it doesn't include any pronounced capping inversion layer at the top of the ABL (cf. **figure 5.1**). The upper stable layer for section A displays an overall stability (~5 K km^{-1}) slightly larger than the other ones (~4 K km^{-1}): this is consistent with the stronger downward velocity associated with subsidence in narrower valley sections (B-1 and C-1). Despite the relatively early stage of the CBL, the incipient development of a warmer mixed layer at the crest level (between 1500 and 2000 m MSL) can be envisaged from C-1 pseudo-sounding. This is very likely produced by the reconnection to the valley centre of the airflow generated by upslope flows at the sidewall crests, as outlined by Kuwagata and Kimura (1995, 1997), De Wekker (2002) and De Wekker et al. (2004). Surface observations at TOR and ARC1 in the flat basin facing Lake Garda (spiral A-1) demonstrate the unstable stratification of the surface layer in the area, while CAV (spiral B/w-1) and MAS (spiral C-1) surface data indicates the occurrence of slightly stable local conditions associated with the presence at the valley floor of the small Cavedine and S. Massenza lakes respectively. The two surface weather stations are indeed located at the shoreline of the two small lakes, and recorded potential temperature values lower than the ML mean potential temperature (θ_m), and constant for all the daytime phase (not shown).

5.3 05 August and 01 September 1999 (flights #2 and #3)

In **figures 5.4** and **5.5** potential temperature and water vapour mixing ratio pseudo-soundings extracted from airborne measurements are shown for the two flights performed during summer 1999, along with 1200 and 1800 UTC (i.e. 1300 and 1900 LST) routine soundings from Milano (LIML) and Udine (LIPD) airports, both representative of the Po Valley atmosphere, and also from Innsbruck airport (LOWI) in the Inn Valley, on the northern side of the Alps (see **figure 5.3**). Surface observations recorded around the flight time by the AWSs closest to the area explored by the single spirals are also displayed (see **figures 3.3** and **3.16** for label and position of the stations).

5.3.1 General features of the valley ABL

On the flight days, all the vertical profiles from airborne measurements show a lower atmosphere sensibly warmer than over the Po Valley (i.e. over the plain), with differences up to 4-6 K in the upper part of the CBLs found over the plain (around 1500-2000 m MSL). On the contrary, the 1200 UTC Innsbruck sounding (available only for flight #2) looks

essentially comparable to airborne measurements.

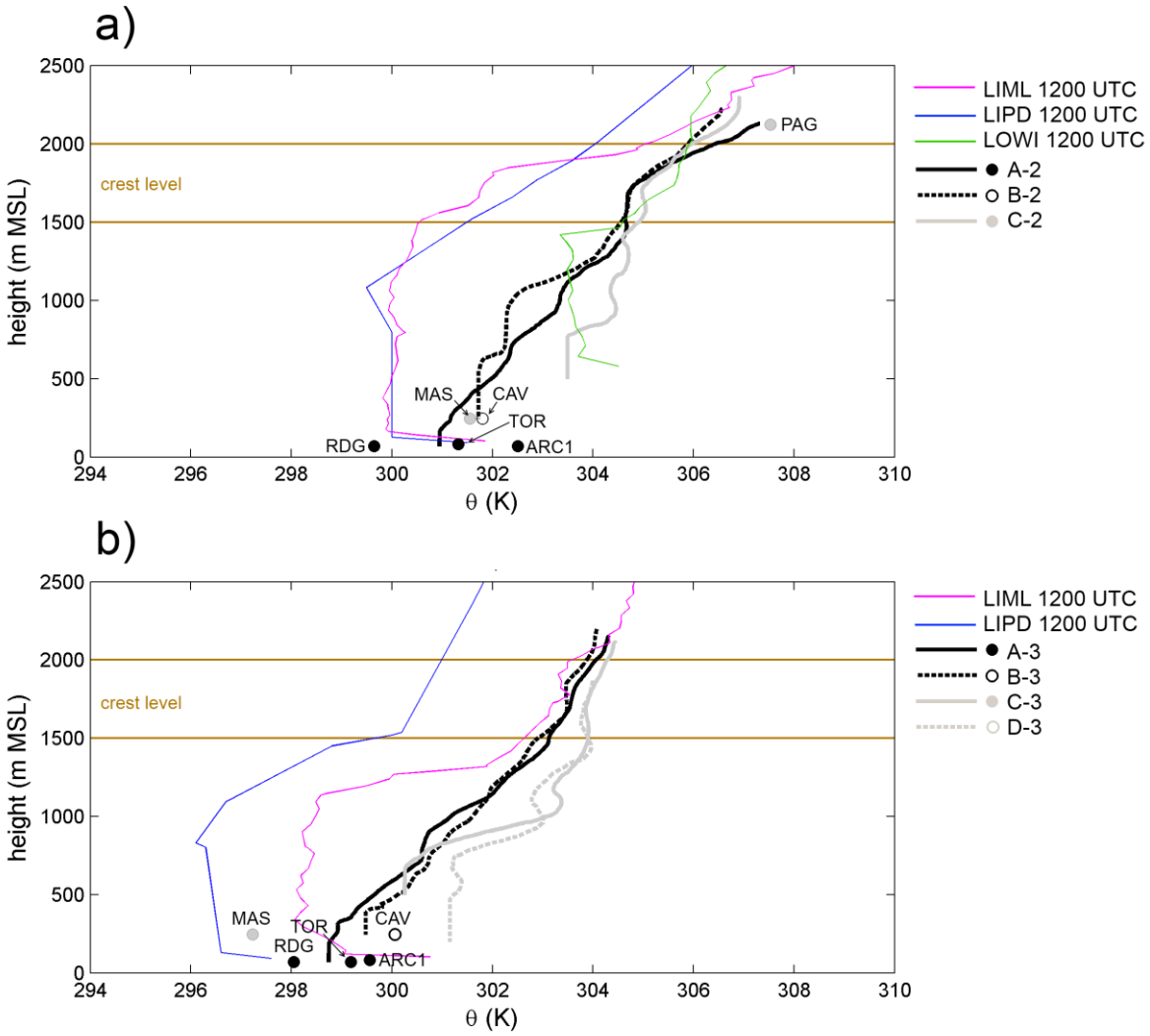

Figure 5.4. Observed pseudo-soundings of potential temperature, compared to routine soundings and surface observations for a) flight #2 and b) #3. Black and grey lines are airborne pseudo-soundings for each single explored valley section, labeled as in **table 5.2**. Color lines are associated with symbols indicating observations from the surface stations nearest to the respective spirals (see **section 3.4.2** and **3.6.3** for station labels and positions); RDG, CAV and MAS stations are located on a lake shore. Thinner lines are 1200 UTC (i.e. 1300 LST) soundings from LIML, LIPD and LOWI stations (see **figure 5.2**).

This picture is consistent with findings about the development of the daytime CBL in a valley, compared to the standard "textbook" picture of CBL over flat uniform terrain (cf. Weissmann et al. 2005, in particular their Figure 4; cf. **figure 5.1**). Such a temperature difference is the basic factor producing diurnal up-valley winds: in the daytime, the stronger heating of the

atmosphere over mountain valleys than over plain areas is responsible for the establishment of regional pressure gradients and resulting thermally-driven circulations (Defant 1951, Zardi and Whiteman 2013). Indeed, the pressure differences at equal levels between the flight measurements and the soundings over the Po Valley are always negative at all the levels explored by the flight, ranging from –2 hPa to –1 hPa at the top of the flight trajectory (about 2200 m MSL), and further gradually decreasing on average by about 2 hPa down to the lower levels, where maximum values of –4 hPa are found near the surface (not shown). In this layer, whose top is likely to exceed the surrounding ridge-top elevation (1500-2000 m MSL), diurnal plain-to-mountain and up-valley circulations are expected to occur (Weissmann et al. 2005).

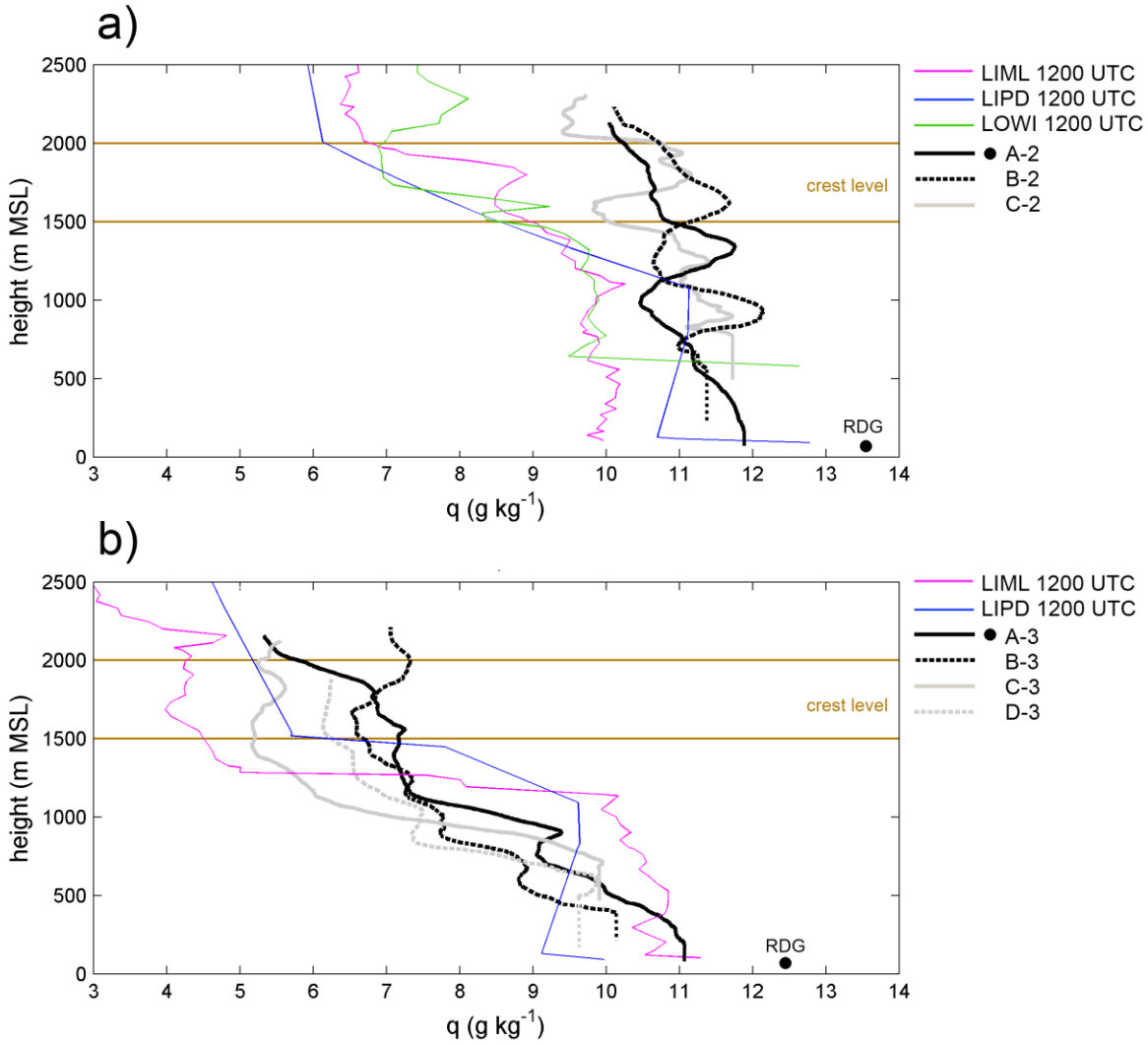

Figure 5.5. As in **figure 5.4**, but for water vapour mixing ratio.

Table 5.2. Timings of the pseudo-soundings shown in **figure 5.4** and **5.5**. LST time is UTC+1.

Flight	Takeoff	Landing	Spiral	Start	End
#2	1330 LST	1530 LST	C-2	1355 LST	1413 LST
			B-2	1420 LST	1433 LST
			A-2	1438 LST	1520 LST
#3	1330 LST	1615 LST	B-3	1343 LST	1422 LST
			A-3	1428 LST	1519 LST
			C-3	1529 LST	1549 LST
			D-3	1550 LST	1603 LST

As anticipated, the vertical thermal structure of the ABL emerging from the flight measurements reflects typical features of a valley atmosphere. In particular MLs are typically rather shallow (in the order of 500 m or less) with respect to those shown by Po Valley soundings (1.0-1.5 km), and surmounted by deeper, stable layers (3 K km^{-1} lapse rate) with a basis at much lower altitudes than the capping inversion layer occurring over the plain. In some cases a ML cannot be clearly identified. A well-defined inversion layer is often absent, except in the pseudo-soundings from the upper Lakes Valley and the adjacent Adige Valley (more pronounced for flight #3: C-3 and D-3 pseudo-soundings), where weakly stable profiles (1 K km^{-1} lapse rate) are detected above the ML on both flights. This ABL pattern is common to most diurnal valley winds and can be ascribed to the local subsidence of potentially warmer air from the FA, induced by upslope winds to compensate for air removal they operate from the valley floor. This is an important mechanism in the heating of the atmosphere core during the morning transition phase (Rampanelli et al. 2004), which also inhibits the convective ML growth and stabilizes the upper part of the profile (Kuwagata and Kimura 1995, 1997, Rotach and Zardi 2007, Serafin and Zardi 2010a, 2010b, 2011, Weigel and Rotach 2004).

On the other hand, mixing ratio pseudo-soundings display very different behaviours on the two flight days. On 05 August 1999 the water vapour concentration is rather homogeneous almost up to the lateral crest height (1500-2000 m MSL; **figure 5.5a**), while on 01 September 1999 (**figure 5.5b**) its distribution is more similar to the "classic" CBL picture (**figure 5.1**), which foresees a sharp humidity content decrease above the ML top height. This difference in vertical stratification may indicate that under unfavourable conditions (flight #3) the lowest atmosphere layers, i.e. the more humid and potentially colder up-valley flow layers, are not coupled with the upper valley atmosphere, while under favourable conditions (flight #2) the up-valley flow probably develops over the entire valley volume, up to the surrounding crests.

5.3.2 Local features of the valley ABL

The lower atmosphere over the lake region displays a stable stratification throughout the ABL height (A-2 and A-3 pseudo-soundings). This feature can be explained in terms of onshore advection of potentially colder air from above the lake by the *Ora del Garda*, which concurs in further stabilizing the lower atmosphere and inhibiting the CBL growth, while suppressing the surface temperature rise in the flat region facing the lake shore. The potentially colder air is advected further downstream, i.e. up-valley, along the significantly up-sloping floor of the Lakes Valley, up to the saddle of Terlago. Hence it flows down into the Adige Valley, where it interacts with the potentially warmer air of the local up-valley flow. Indeed, at the lowest levels ML potential temperature mean values (θ_m) gradually grow up-valley from site A to site C (respectively by 2.5 K on flight #2 and 1.5 K on flight #3). On the other hand, in the northernmost Lakes Valley (C pseudo-soundings) θ_m is on average lower (by ~1.5 K on flight #2 and ~1.0 K on flight #3 respectively) than in the adjacent Adige Valley, whose floor lies more than 300 m lower. At the upper levels, C and D pseudo-soundings show a lapse rate considerably smaller than the other ones (1 K km^{-1} versus 3 K km^{-1}), thus revealing an appreciable heating excess throughout the layer extending from about 1000 to 1800 m MSL. This suggests that a more intense subsidence of air from the FA, possibly associated with cross-valley circulations, occurs in the area of the northern Lakes Valley and Adige Valley.

Potential temperature values measured at weather stations on the valley floor are in general a few degrees (up to 1.5 K) higher than the mean ML temperatures (θ_m) detected from airborne data, with the exception of stations located very close to a lake (RDG, CAV and MAS), which recorded lower temperatures. In particular, MAS shows values up to 2.5 K lower than the above ML, suggesting local near-surface stable conditions (C-2 and C-3 pseuso-soundings). This fact is amenable to two possible explanations: one is the cooling effect of the nearby water surface, the second is a temperature drop associated with an earlier entering the shade. Indeed, a GIS-based analysis, carried out in order to assess the time evolution of the expected surface radiation input, shows that MAS gets shaded shortly after local noon.

5.4 23 August 2001 (flights #4 and #5)

This section discusses the vertical structure of the ABL associated with the *Ora del Garda* wind development on 23 August 2001, as revealed from the vertical pseudo-soundings of potential temperature and mixing ratio extracted from flight #4 and flight #5 data. The two flights were performed respectively in the morning and in the early afternoon of the flight day, and both of them explored the atmosphere structure over the area of the Terlago saddle and the Adige Valley, allowing the investigation of the ABL daily evolution in the area.

In **figure 5.6** and **5.7** airborne pseuso-soundings of potential temperature and mixing ratio are compared to routine soundings from Milan (LIML) and Udine (LIPD) stations in the Po

Valley.

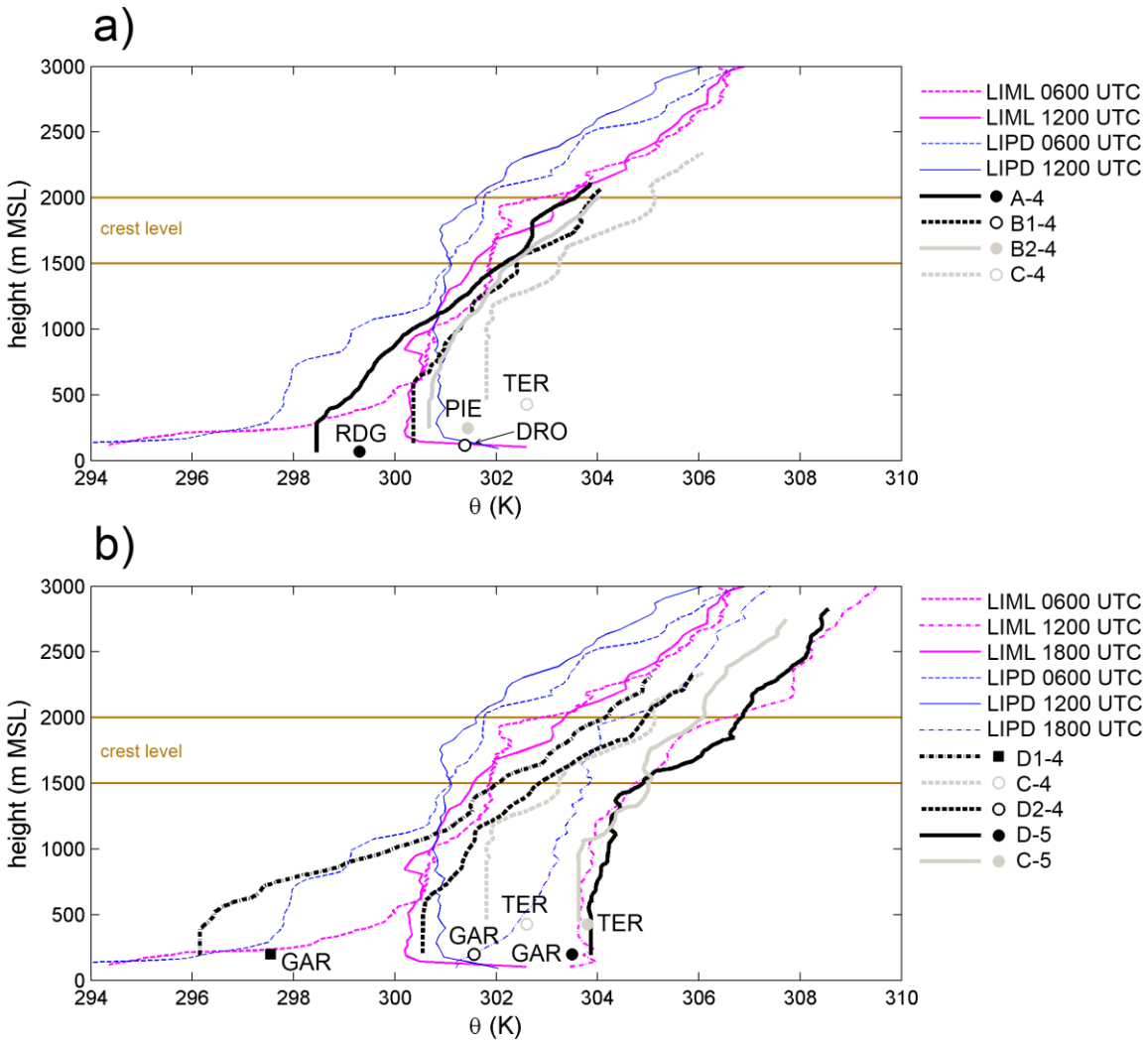

Figure 5.6. Observed pseudo-soundings of potential temperature, compared to routine soundings and surface observations for flight #4 and #5: **a)** lower Sarca Valley and Lakes Valley (flight #4) **b)** upper Lakes Valley and Adige Valley (i.e. interaction area; flights #4 and #5). Black and grey lines are airborne pseudo-soundings for each single explored valley section, labeled as in **table 5.3**. Lines are associated with symbols indicating observations from the surface stations nearest to the respective spirals (see **section 3.6.3** for station labels and positions). Color lines are 0600, 1200 and 1800 UTC (i.e. 0700, 1300 and 1900 LST) soundings from LIML and LIPD stations (see **figure 5.3**).

In particular pseudo-soundings from flight #4 (0900–1200 LST) are compared to 0600 and 1200 UTC soundings (i.e. 0700 and 1300 LST), while pseudo-soundings from flight #5 (1415–1530 LST) are compared to 1200 and 1800 UTC (i.e., 1300 and 1900 LST) soundings.

Surface measurements from the AWSs closest to the area explored by each single spiralling trajectory are also reported in the figure, as representative of the surface layer conditions. The timing relative to each pseudo-sounding is also reported in **table 5.3**. Both in the morning and in the afternoon the typical diurnal heating excess between mountain valley air masses and airmasses over the plain (i.e. the Po Valley) is observed: the upper valley atmosphere is at least ~1 K potentially warmer throughout the whole explored depth (i.e. up to ~1 km above the average height of the lateral crests). Only A-4 and D1-4 pseudo-soundings are colder than 0600 and 1200 UTC LIML soundings below ~1300 m MSL, for in the early morning hours the atmosphere in the Adige Valley and above the Lake Garda is still very stably stratified.

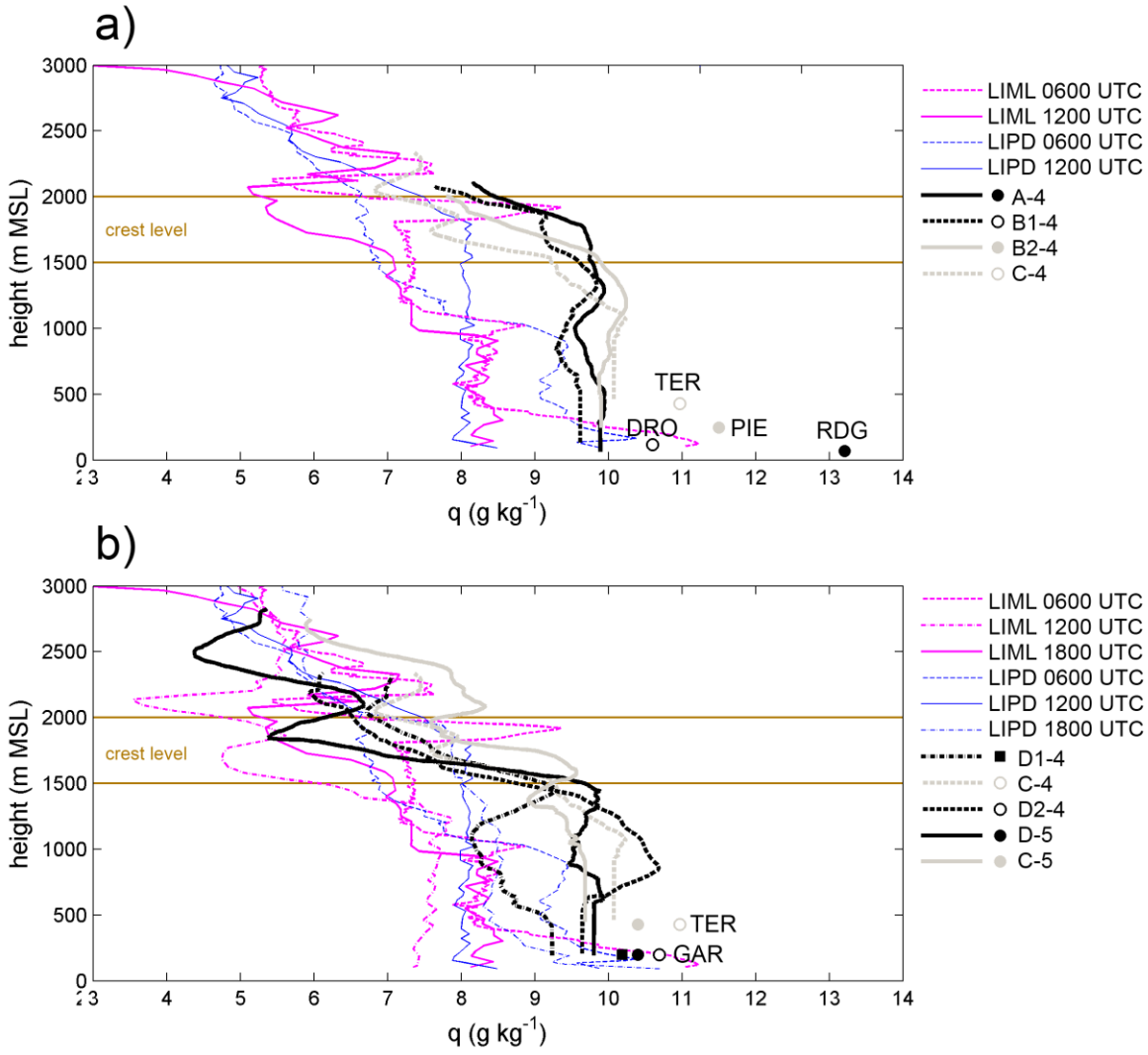

Figure 5.7. As in **figure 5.6**, but for water vapour mixing ratio.

Table 5.3. Timings of the pseudo-soundings shown in **figures 5.6** and **5.7**. LST time is UTC+1.

Flight	Takeoff	Landing	Spiral	Start	End
#4	0900 LST	1200 LST	D1-4	0918 LST	0947 LST
			A-4	0959 LST	1042 LST
			B1-4	1046 LST	1106 LST
			B2-4	1108 LST	1121 LST
			C-4	1123 LST	1143 LST
			D2-4	1143 LST	1157 LST
#5	1415 LST	1530 LST	D-5	1424 LST	1454 LST
			C-5	1458 LST	1517 LST

5.4.1 ABL structure in the lower Sarca Valley and Lakes Valley

Flight #4, which explored four different sites in the valleys where the *Ora del Garda* flows, was performed during the very initial stages of the breeze development, before its outbreak into the Adige Valley (cf. **Chapter 3**).

A-4 pseudo-sounding is representative of the flat basin facing the Lake Garda northern shoreline; at the upper levels it is rather consistent with 0600 and 1200 UTC LIML soundings; it is also colder than the following pseudo-soundings at all levels; an elevated QML driven by the return flows associated to up-slope circulations (De Wekker 2002, De Wekker et al. 2004, Kuwagata and Kimura 1995, 1997) extends between 1500 and 1800 m MSL; below that height the stratification is stable (3 K km^{-1} lapse rate) almost down to the minimum flying height (~250 m MSL, i.e. ~185 m above the lake's surface) (**figure 5.6a**). Further up-valley B1-4 and B2-4 pseudo-soundings in the Lakes Valley look very similar: they show a warmer atmosphere than A-4, especially below 1500 m MSL, where the lapse rate is reduced to 2 K km^{-1}, due to the subsidence that is locally induced by cross-valley compensation circulation (Kuwagata and Kimura 1995, 1997, Rampanelli et al. 2004, Serafin and Zardi 2010a, 2010b, 2011). At both locations a less than 500 m deep ML is detected, slightly warmer at B2-4 than at B1-4 (ML mean potential temperature θ_m: 300.7 K and 300.4 K respectively; see **table 5.4**). At the end of the Lakes Valley, C-4 pseudo-sounding is on average ~1 K warmer than B1-4 and B2-4 above 1150 m MSL height, and shows two distinct elevated QMLs around 1500 and 2000 m MSL respectively; the 750 m deep ML has a θ_m of 301.8 K (cf. **table 5.4**). More than three hours later (C-5 pseudo-sounding in **figure 5.6b**), the ML depth is reduced to 600 m, θ_m has increased by ~2 K, and the lapse rate in the layer below 1750 m MSL has been consistently modified by the heating process associated to local subsidence (from 3.5 to 2.0 K km^{-1}). Differently from pseudo-soundings further up-stream (i.e. down-valley), both C-4

and C-5 display a weak inversion layer at the top of the ML.

To summarize, close to Lake Garda the valley atmosphere is stable down to very low heights or even to the ground, while moving further up-valley (i.e. down-stream) a gradual transition to a rather typical valley ABL pattern occurs: shallow MLs (displaying depths in the order of 500 m) with weak or even absent capping inversion layers are detected, surmounted by deep, weakly stable layers and/or elevated QMLs extending up to the lateral crests height. Such a structure is likely to be originated by the local subsidence driven by downward motions compensating for up-slope circulations, according to conceptual framework presented in **section 5.1** (Kuwagata and Kimura 1995, 1997, Rampanelli et al. 2004, Rotach and Zardi 2007, Serafin and Zardi 2010a, 2010b, 2011). Mixing ratio pseudo-soundings (**figures 5.7**) further confirm this ABL pattern: unlike in standard CBL schemes, the water vapour appears rather uniformly distributed well above the top of the MLs detected at the valley floor, i.e. over the whole valley atmosphere volume up to the average height of the lateral crests (1500 m MSL). This is very likely associated with the vertical transport and possible redistribution of humidity operated by up-slope winds, exporting water vapour from the valley floor along the lateral sidewall of the valley (Kuwagata and Kimura 1995, Weigel et al. 2006).

Table 5.4. Key parameters of the valley ABL thermal structure for each explored valley section for flights #4 and #5. θ_m is ML mean potential temperature. See the name of pseudo-soundings indicated in **table 5.3** and displayed in **figures 5.6** and **5.7**.

Spiral	Valley floor height	ML depth	θ_m
D1-4	195 m MSL	200 m	296.15 K
A-4	70 m MSL	200 m	298.45 K
B1-4	130 m MSL	470 m	300.35 K
B2-4	245 m MSL	400 m	300.70 K
C-4	450 m MSL	750 m	301.80 K
D2-4	195 m MSL	400 m	300.55 K
D-5	195 m MSL	1200 m	304.00 K
C-5	450 m MSL	600 m	303.60 K

5.4.2 ABL structure and evolution in the interaction area

Three pseudo-soundings are available for the Adige Valley section situated right in front of the saddle of Terlago, allowing an analysis of the diurnal evolution of the valley ABL vertical structure in the area. From time series of surface observations discussed in **Chapter 3** (GAR and RON weather station), it can be argued that each one of them is representative of a

different wind regime: a well-developed down-valley wind (D1-4), the transition between down-valley and up-valley wind (D2-4), the westerly wind regime following the first *Ora del Garda* outbreak into the Adige Valley (D-5). Between the first two stages (D1-4 and D2-4; **figure 5.6a**), the cold airmass accumulated on the valley floor during nighttime is eroded: the heating results particularly intense in the layer extending from the ground surface up to ~1200 m MSL, while the atmosphere above maintains the same lapse rate (~4 K km^{-1}) and its potential temperature grows only by about 1 K. At the same time, θ_m increases from 296.2 K to 300.6 K, while the ML depth increases only from 200 m to 400 m. On the other hand, between noon (D2-A) and afternoon (D-5) a 2-3 K heating takes place throughout the whole depth of the explored valley atmosphere, the ML depth increases to 1200 m, and θ_m further grows by 3.5 K. Within a slightly longer time interval, over the saddle of Terlago (C site) a consistently smaller heating occurs, especially above 1750 m MSL height, and θ_m increases by only ~1.8 K (cf. C-4 and C-5 pseudo-soundings in **figure 5.6b**); this suppression of the temperature rise in the valley atmosphere during daytime is likely to be amenable to the presence of a large, continuous source of cold air at the valley inlet, i.e. Lake Garda and to the up-valley advection associated with the *Ora del Garda* flow.

Morning pseudo-soundings at C-4 (local valley floor: ~500 m MSL) and D2-4 (local valley floor: ~200 m MSL) look very similar in their upper part, while below 1150 m MSL C-4 is ~1 K warmer than D2-4 (θ_m: 301.8 vs. 300.6 K respectively). On the contrary, in the afternoon D-5 pseudo-sounding is ~1.5 K potentially warmer than C-5 above 1500 m MSL, while the two profiles show almost equal values below that height, with θ_m slightly lower at C-5. The similar mixing ratio values of C-5 and D-5 below 1500 m also suggest that this is the layer where the strong mixing between the *Ora del Garda* and the Adige Valley air occurs during the afternoon interaction phase, while airmasses with different characteristics are present in the layers above (**figure 5.7b**). A marked difference between morning and afternoon conditions is also highlighted by surface data collected at the closest AWSs (cf. **figure 5.6b**): while in the morning all surface weather stations display values on average ~1 K higher than the θ_m value from the corresponding airborne pseudo-sounding, in the afternoon surface potential temperature measurements at C and D sites are almost equal to, or even lower than, the associated θ_m. This fact suggests that the intense ventilation produced in the afternoon by the *Ora del Garda* has cooled down the ground in the area, and that surface sensible heat fluxs are no longer feeding the ML convective growth process in this phase (cf. **section 3.3.3**). Indeed, as this transition from an unstably-stratified surface layer (which is consistent with the typical diurnal CBL structure) to stably-stratified conditions immediately above ground occurs before the local sunset time (i.e. around 1800 LST at the Adige Valley floor), it cannot be produced by the radiative cooling of the ground surface.

5.5 Summary

The dominant thermal structure of the lower atmosphere accompanying the development of the *Ora del Garda* lake-valley coupled breeze at selected valley sections (from above the Lake Garda northern shorelines to the Adige Valley) has been discussed in **Chapter 5**, on the basis of pseudo-soundings of potential temperature and water vapour mixing ratio extracted from the five flights described in **Chapter 2**.

Associated with the *Ora del Garda* flow, a well-defined pattern for the vertical structure of the valley ABL emerged from airborne pseudo-soundings in the lower Sarca Valley and in the Lakes Valley (A, B and C sites); rather shallow MLs, displaying depths in the order of 500 m, develop above the valley floor, surmounted by slightly stable layers and/or elevated QMLs, extending almost up to the surrounding crest height (~1500 m MSL). This common ABL structure was observed for all the four flight days, in the late morning as well as in the afternoon hours. Moreover, similar features of the ABL vertical structure were revealed by flights #2 and #3, exploring situations representative of favorable and unfavorable synoptic forcing conditions respectively, despite the fact that thermally-driven local circulations (and associated ABL processes) are strongly dependent on the prevailing synoptic airflow. Hence, it can be concluded that such structures are tipically occurring in the valleys where the *Ora del Garda* breeze flows, in good accord with the ABL structure observed in analogous contexts in the literature (e.g. Kossmann et al. 2002, Kuwagata and Kimura 1995, Rotach and Zardi 2007, Weigel and Rotach 2004). In deep Alpine valleys this ABL pattern is primarily determined by the development of up-slope winds during the morning heating phase, whose compensation flows produce elevated QMLs (Kuwagata and Kimura 1995, 1997) and local subsidence of potentially warmer air from the FA at the center of the valley (Rampanelli et al. 2004, Serafin and Zardi 2010a, 2010b, 2011). In addition, the up-valley advection of potentially colder air from above Lake Garda surface operated by the *Ora del Garda* wind is also likely to be responsible for a further stabilization of the potential temperature profiles down to very low heights and inhibition of the growth of convective MLs, particularly closer to the lake shoreline (at site A). Indeed, the ML depth and especially its mean potential temperature θ_m gradually increase up-slope along the valley axis from Lake Garda shoreline to the valley end (very clear in flight #4 results). This behaviour is compatible with the development of an IBL associated with the onshore (i.e. up-valley) wind (cf. Arritt 1987, Kossman et al. 2002, Venkatram 1977). As expected, θ_m grows also with time, but not as fast as in the nearby Adige Valley. The limiting factor is again the advective cooling associated with the *Ora del Garda*, which suppresses the temperature rise in the lowest valley atmosphere.

Concerning the daily evolution of the ABL structure in the area north of Trento where the two local airflows interact (sites C and D), the comparison between pseudo-soundings from flights #4 and #5 provides an interesting picture. In the late morning unstable surface layers

surmounted by ~500 m deep MLs are detected in this area as well as further down-valley (i.e. at sites A and B), while in the afternoon the ML depth results consistently increased at D site, as its vertical extent almost triples (from 400 to 1200 m). This deepening appears primarily associated with the strong mixing that follows the outbreak of the *Ora del Garda* into the Adige Valley. On the contrary, the ML depth at C site is slightly reduced (from 750 to 600 m) between morning and afternoon. Moreover, afternoon observations from local surface stations reveal the establishment of neutrally- or even stably-stratified surface layers (respectively at C and D sites). This suggests that, differently from the morning, in the afternoon the surface sensible heat fluxes are no more sustaining the convective growth of the ML in the area. As this transition occurs before sunset, it cannot be induced by the radiative cooling of the ground surface. On the contrary, it is consistent with the cold air advection and the strong ventilation locally produced by the *Ora del Garda* at the valley floor.

Chapter 6

Deciphering the fine-scale structure of the valley atmospheric boundary-layer

Abstract

In complex terrain areas non-negligible horizontal inhomogeneities of the atmospheric boundary-layer (ABL) structures, primarily associated with local-scale, thermally-driven circulations, may arise from local features of the topography, such as for example the irregular shape of a valley cross section, as well as from land use discontinuities. Moreover, shading by surrounding orography may also produce differential heating of opposing valley sidewalls, resulting in asymmetric cross-valley circulations and different ABL patterns. Based on high-resolution 3D fields of potential temperature, resulting from the application of a residual kriging (RK) interpolation to the airborne dataset presented in **Chapter 3**, the fine-scale variability of the ABL structures associated with the *Ora del Garda* development in the study area was retrieved. The analysis of fine-scale features of the atmosphere thermal field allowed also some speculations about local patterns of the thermally-driven wind field, providing further insight into the wind flow structure. In particular, aspects related to the land-water discontinuity at the shoreline, or to the different insolation between two opposing sidewalls, further enhanced by land cover differences, were detected. Furthermore, a pronounced deflection of the up-valley airflow towards one of the lateral sidewalls, due to the local valley curvature, was observed in proximity of the saddle of Terlago. In the underlying Adige Valley, the *Ora del Garda* overflow was discovered to originate a hydraulic jump structure down-stream, arising from the impingement of the strong katabatic flow from the Lakes Valley on the opposing Adige Valley sidewall.

6.1 Introduction

Differently from the atmospheric boundary-layer (ABL) structures commonly found over flat and uniform terrain, which usually display similar vertical profiles at any point over large surfaces, complex orography (such as that characterizing the study area) produces additional 3D variability in the ABL structure. Indeed, the mean ABL vertical structure usually observed in valleys in fair-weather conditions significantly differs from the "standard" picture of the convective boundary-layer (CBL) provided by the textbook knowledge (Stull 1988, Oke 1987), primarily as an effect of heating/cooling processes associated with the thermally-driven circulations developing along the lateral slopes and the valley itself, as discussed in the introduction to **Chapter 5**.

However, in real complex-terrain contexts (such as the study area presented in **Chapter 2**) irregular topographic features and land use heterogeneities locally modify both thermally-driven wind patterns and the associated fine-scale structure of the ABL, introducing non-negligible horizontal inhomogeneities. For instance, in the lowest atmosphere of real valleys complex situations different from the two-cells, symmetric cross-valley circulation foreseen for idealized straight valleys by classic conceptual schemes (Defant 1951) are often found. Actually, Hennemuth (1985, 1986) and Hennemuth and Schmidt (1985) identified a strong cross-valley asymmetry for the diurnal potential temperature field of the narrow Dischma Valley, corresponding to the development of a unified, single-cell cross-valley circulation, driven by the different insolation of the two valley sidewalls. Similarly, in the circularly-shaped Arizona's Meteor Crater thermally-driven cross-basin winds, forming closed circulation cells at the crater floor, were found to occur as an effect of asymmetric solar heating (Lehner et al. 2011, Lehner and Whiteman 2012); strongly asymmetric temperature fields observed inside the basin showed a well-defined diurnal cycle, reflected by the variation of the cross-basin flow direction throughout the day. Moreover, in the Riviera Valley both aircraft observations and high-resolution numerical simulations gave evidence of an asymmetric ABL thermal structure over the valley cross section, originated this time by a cross-valley secondary circulation arising as an effect of the valley axis curvature. This circulation was found to be strong enough to produce an anomalous down-slope wind along the more insolated slope, enhancing at the same time the stability of the lowest ABL in that region (Rotach et al. 2008, Weigel and Rotach 2004, Weigel et al. 2006). Furthermore, also diurnal sea/lake breezes may produce characteristic fine-scale horizontal inhomogeneities in ABL structures, especially in proximity of the shoreline, where internal boundary-layers (IBLs) are likely to develop due to water-land surface discontinuity (Arritt 1987, Garratt 1990, Lieman and Alpert 1993), and in the breeze-front region, where very strong horizontal gradients of potential temperature and other meteorological quantities are typically found (Simpson 1994, Zumpfe and Horel 2007). Both features can be appreciated in full detail when looking at results from

high-resolution numerical modeling of coastal circulations, like those carried out by Antonelli and Rotunno (2007), Crosman and Horel (2012) and Porson et al. (2007a, 2007b) among others.

Chapter 6 analyses the fine-scale 3D structure of the ABL occurring in the study area valleys in connection with the *Ora del Garda* wind development, based on high-resolution fields of potential temperature produced by the residual kriging (RK) interpolation of the airborne observations collected during flights #1 to #5 (see **Chapter 3**). Indeed, the fine-scale variability of the valley ABL thermal structure emerging from RK results offers also the opportunity to infer some local features of the associated thermally-driven wind field.

Following the procedure described in **Chapter 4**, for each explored valley section pseudo-soundings representing the dominant vertical structure of the ABL were extracted from airborne observations (see **Chapter 5**), using a moving-window vertical average algorithm. Then the residual field obtained subtracting this vertical drift from the original data was mapped by means of RK on regular grids (50 m × 50 m × 50 m spacing) built around the single spiralling trajectory. The mapping volumes included only grid points where the interpolation can be reliably trusted (i.e. nodes whose distance from observation points is smaller than the characteristic semivariogram range, i.e. the maximum range of correlation between observations; cf. **section 4.4.3.2**), and were further restricted to the interior of each valley basin. In general, directional semivariograms of potential temperature residuals (see **section 4.4.3.2**) provided typical correlation ranges of about 1000-2000 m and 350-550 m respectively for the horizontal and the vertical direction, leading to anisotropy ratios typically varying between 3.5 and 5.5. These were adopted as scaling factors in order to isotropize the spatial coordinates before the application of the RK interpolation (cf. **section 4.4.3.2**).

Concerning the uncertainty to be associated to the estimated temperature values, RK-estimated standard deviation (i.e. the square root of the RK-predicted variance of the estimates; cf. **section 4.4.3.2**) turned out to be typically smaller than ~0.35 K at almost all the interpolation grid nodes, and tended to vanish when approaching trajectory points, as expected on the basis of theoretical properties of kriging (Cressie 1993, Goovaerts 1997). It should also be emphasized that kriging must be used very carefully to extrapolate values outside the region where data are available. This is particularly true for non-stationary fields, where the correct modeling of the drift is rather relevant (cf. **Chapter 4**; Journel and Rossi 1989). In the present case potential temperature terms (i.e. pseudo-soundings) were estimated below the minimum sampling height of flights assuming a well-mixed layer, i.e. a constant value for the vertical drift. Indeed, this assumption is consistent with the structure of the ABL reasonably expected over the valley floors at the time of the flights on the basis of the vertical distribution of the airborne data (see **Chapter 5**). For compliance to safety regulations the equipped motorglider was not allowed to fly very close to the sidewalls and the valley floor. As a consequence, the atmosphere volume more directly influenced by surface heat fluxes

was only partially explored by the flight trajectories. In order to complement the airborne dataset for the lowest layers not covered by the flights, for each valley section the basis for RK application was provided not only by the airborne data residuals, as explained above, but also by surface observations from the closest weather stations, where available. Unfortunately, the limited availability of surface measurements, especially along the lateral slopes, hindered the possibility of adequately integrating the database to make up for this lack.

6.2 24 September 1998 (flight #1)

Selected vertical sections were extracted from the potential temperature fields interpolated by means of RK over regular grids. The latter were constructed around each of the four spiraling trajectories forming flight #1, and exploring four cross-valley slices of the valley atmosphere (see **Chapter 3**). These reference vertical planes are shown in **figure 6.1**, and labeled according to the names used in **section 5.2** for the corresponding pseudo-soundings.

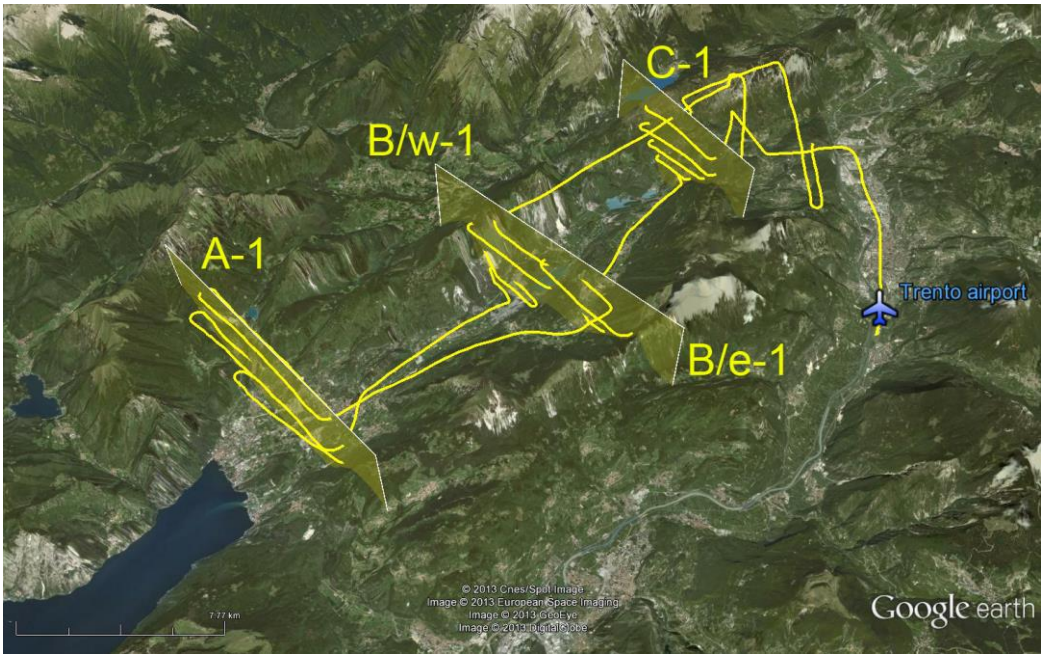

Figure 6.1. 3D representation of flight #1 trajectory (yellow line). The vertical planes adopted for displaying the RK-interpolated potential temperature fields in **figure 6.2** are also indicated. Image © Google Earth, © 2013 Cnes/Spot Image, © 2013 European Space Imaging, © 2013 GeoEye, © 2013 DigitalGlobe.

Figure 6.2a shows the RK-interpolated potential temperature field for the vertical cross section A-1. The lowest layers display a uniform temperature distribution up to 590 m AGL throughout the cross-valley section, consistently with the occurrence of a well-mixed layer on the wide (~5 km) valley floor. A minor E-W asymmetry is detected in the intermediate

layer below ~1650 m AGL, reasonably associated with up-slope flows stronger on the E-facing sunlit sidewall at the time of the flight.

Figure 6.2b shows the cross sections including both the area over Cavedine Lake on the western side (spiral B/w-1), and the elevated Cavedine Valley on the eastern half of the valley section (spiral B/e-1). Interpolated fields clearly highlight an asymmetric thermal structure: on the western side the sunlit steep sidewall in bare rock is likely to be warmer than the valley centre: here Cavedine Lake seems to favour colder conditions, as suggested by time series of local surface measurements at CAV (not shown). In section B/e-1 again a 400 m deep ML occurs above the elevated valley floor, and at upper levels a minor asymmetry, detectable from depressed isentropes, is likely to be promoted by downward subsidence at the valley centre.

Figure 6.2c shows the potential temperature field at spiral C-1. The thermal structure displays remarkable cross-valley asymmetries, clearly reversing around 1300 m MSL. This picture reflects a different heating on the two sidewalls: indeed the NW-facing sidewalls are never directly sunlit during the day, whereas the opposite side of the valley gets direct solar radiation since early morning. Such a contrast is expected to produce a cross-valley circulation with an up-slope flow occurring on the SE-facing sidewall, and a down-slope flow on the opposite side, similarly to what described for the Dischma Valley by Hennemuth (1985, 1986). The two circulations are part of a unique cross-valley cell, which tilts isentropes downward towards the sunlit side.

Such an asymmetric pattern is confirmed by the complementary view offered by horizontal sections at different levels (**figure 6.3**). Possible interference from upper winds may be excluded, on the basis of synoptic observations clearly showing a high-pressure situation and a light SW wind over the area (cf. **Chapter 3**). Instead the local eastward bending of the valley axis may enhance the purely thermally-driven cross-valley flow. Indeed local curvatures force along-valley winds to develop secondary circulations over the whole valley cross sections. In the MAP Riviera project (Weigel and Rotach 2004, Weigel et al. 2006) such an effect was invoked to explain the anomalous down-slope flow on a sunny sidewall. Differently from that case, where the dynamically-driven secondary flow was acting to contrast the thermally-driven slope-flow, here it would be in favour of the cross-valley circulation produced by the thermal asymmetry.

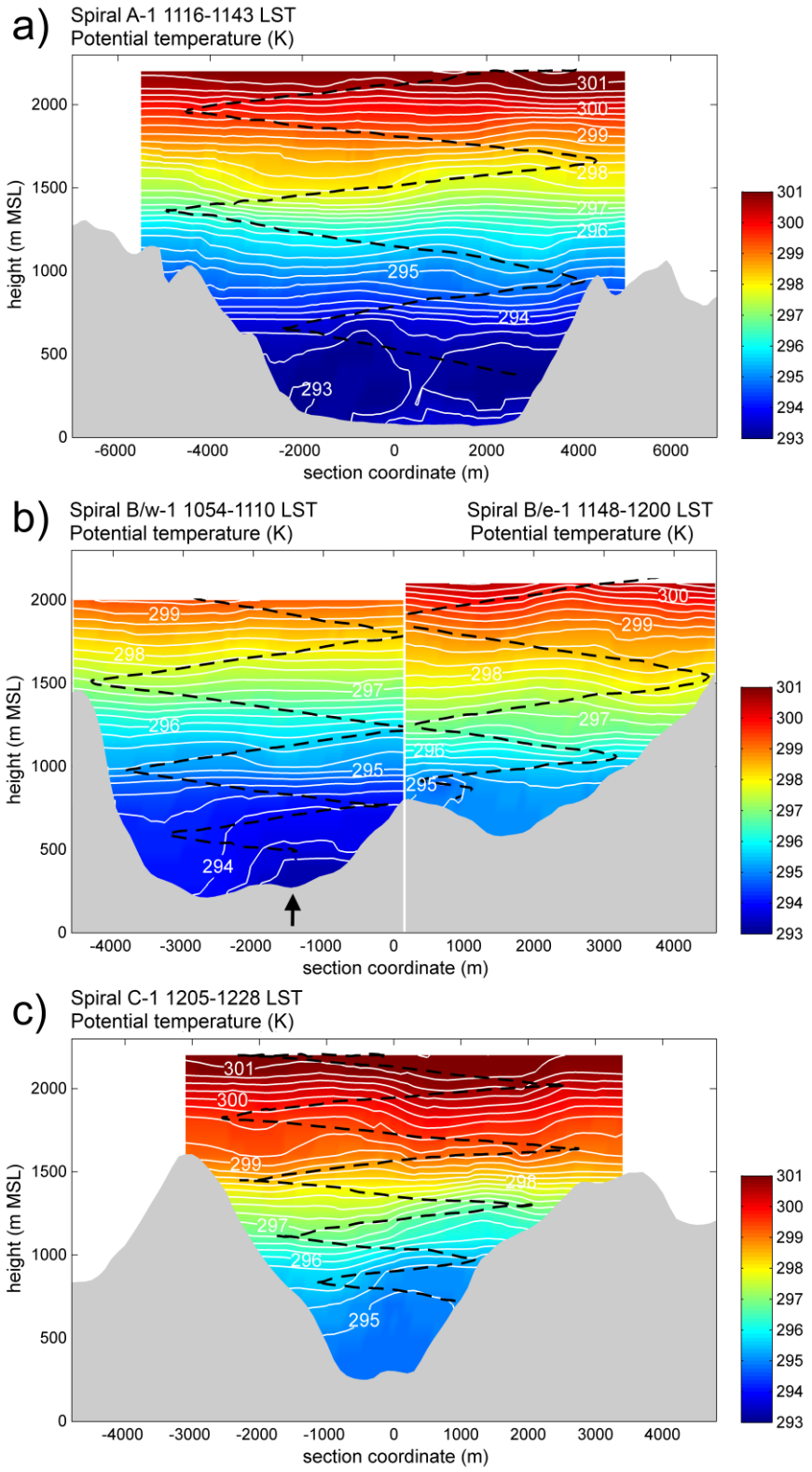

Figure 6.2. RK-interpolated potential temperature field for **a)** spiral A-1. Contour interval is 0.25 K (in white). The black dashed line represents the motorglider trajectory. The valley section topography is indicated in grey shading. **b)** As in panel **a)**, but for spirals B/w-1 (left) and B/e-1 (right). The black arrow indicates Cavedine Lake's position at the valley bottom. **c)** As in panel **a)**, but for spiral C-1.

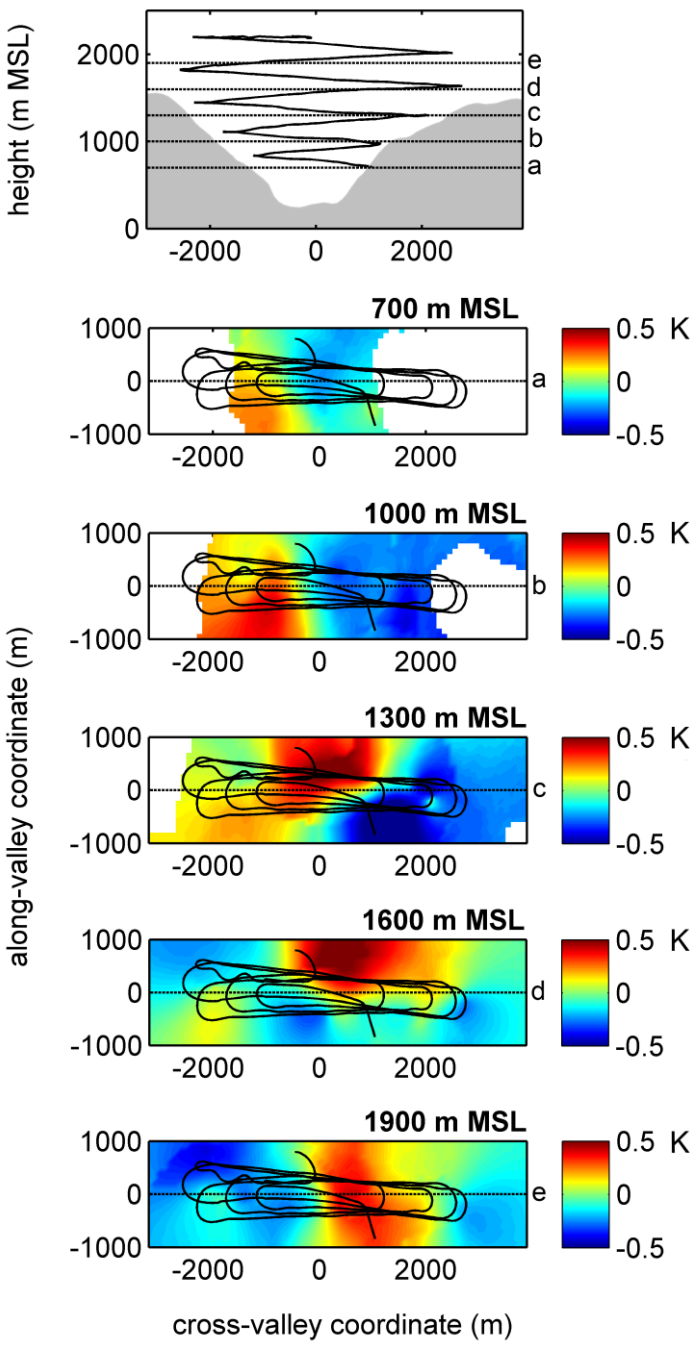

Figure 6.3. RK-interpolated anomalies of potential temperature (i.e. deviations from pseudo-sounding values) on horizontal planes at various vertical levels for spiral C-1 (**figure 6.2c**). The upper panel shows the profile of the underlying topography on a vertical cross section. The latter intersects each horizontal plane at the dotted line labelled with the corresponding letter. White areas denote regions where the topography elevation exceeds the height of the horizontal plane, or regions outside the maximum acceptable interpolation distance. The black curve is the projection of the flight trajectory on the planes. The abscise axis is the same as in **figure 6.2c**.

6.3 05 August and 01 September 1999 (flights #2 and #3)

In the following paragraphs selected views of RK-interpolated meteorological fields at the vertical planes indicated in **figure 6.4** are shown and discussed for flights #2 and #3. The order follows the up-valley development of the *Ora del Garda* wind from the Lake Garda shore to the Adige Valley, and the labels adopted for the different spirals are the same used in **section 5.3**.

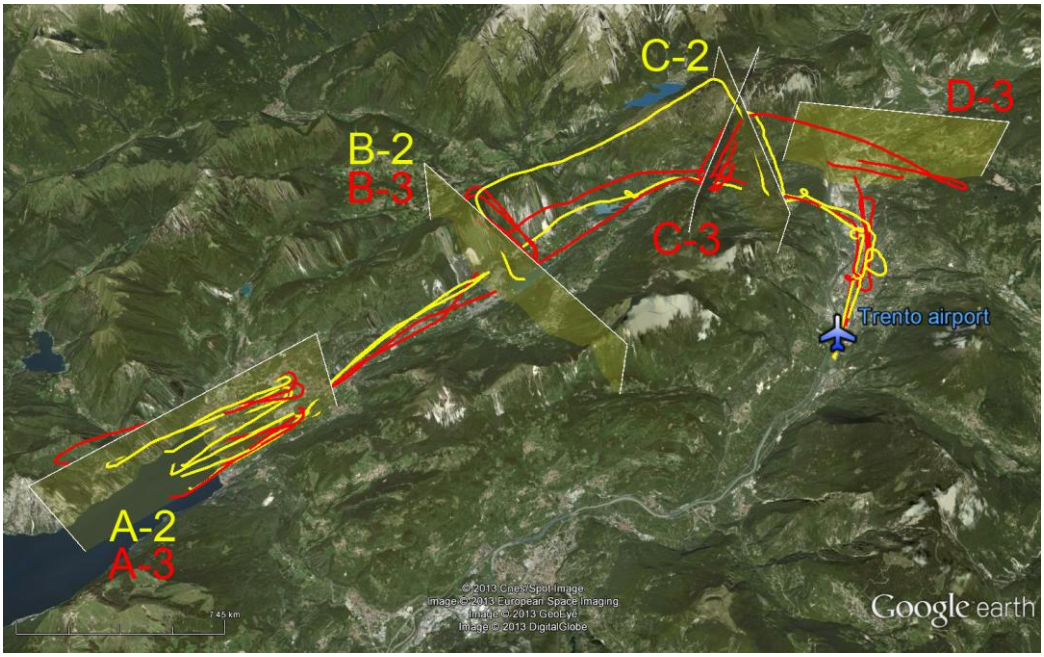

Figure 6.4. 3D representation of flight #2 (yellow line) and #3 (red line) trajectories. The vertical planes adopted for displaying the RK-interpolated potential temperature fields in **figures 6.5-6.11** are also indicated. Image © Google Earth, © 2013 Cnes/Spot Image, © 2013 European Space Imaging, © 2013 GeoEye, © 2013 DigitalGlobe.

6.3.1 Lower Sarca Valley - Lake Garda shoreline area

The vertical thermal structure of the atmosphere at the transition between water and land surface was explored by spirals A of flights #2 and #3 (**figures 6.5** and **6.6** respectively). In the shoreline proximity the bending of the lowest isentropes towards the ground reveals a rather small positive gradient in the temperature of the air mass penetrating inland (more evident for flight #3; **figure 6.6**), interrupted by a warmer region where the Mt. Brione relief rises. The localized increase in near-surface potential temperature and deceleration of the upstream flow (indicated by the spacing out of isentropes below 1000 m MSL) are very likely associated with the rocky hill: the presence of an obstacle on the valley floor reduces the flow

section at the lowest levels, and induces both a thermal and a dynamical perturbation of the lake-breeze flow in the narrow corridor (~500 m wide) between the eastern valley sidewalls and the hill.

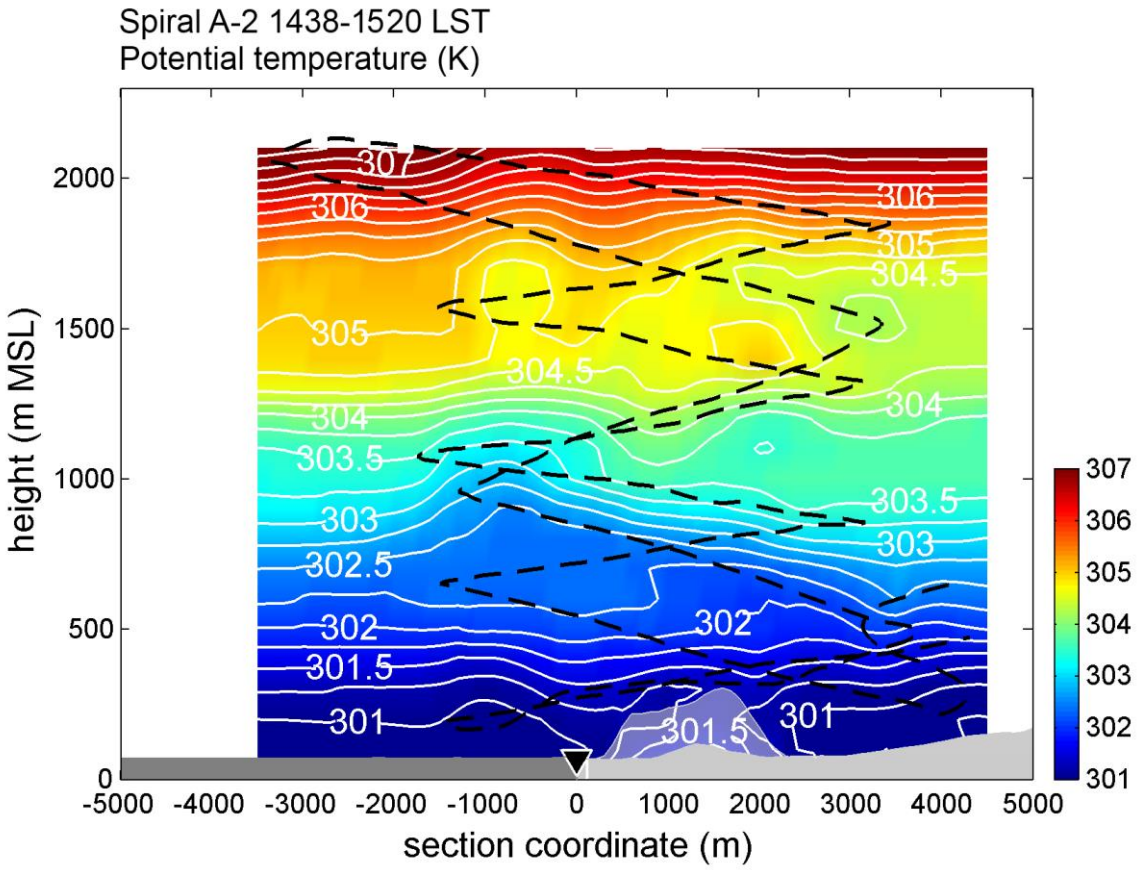

Figure 6.5. Vertical section of RK-interpolated potential temperature field for spiral A-2 from flight #2 (see corresponding vertical plane in **figure 6.4**); contour interval is 0.25 K (in white). The black dashed line indicates the trajectory followed by the motorglider over the considered section. The correspondent valley topography is indicated in light grey (Mount Brione profile is also reported), while dark grey indicates Lake Garda. The black triangle shows Lake Garda shoreline (accordingly, the horizontal coordinate can be read as distance from shoreline in SSW-NNE direction).

At the upper levels, both flights show a rather sharp discontinuity in the vertical stratification occurring right above the shoreline (cf. 304.5 and 303.5 K isentropes for flight #2 and #3 respectively), between 1300 and 1800 m MSL approximately. A similar structure was found from numerical simulations by Porson et al. (2007a) (see in particular their figure 2), Antonelli and Rotunno (2007) (see their figure 5) and Crosman and Horel (2012) (see their figures 2-4 and 9). Such a structure is typically originated at the shoreline by the offshore

downdraft and onshore updraft occurring at upper levels in association with the development and propagation of a lake-breeze front at the lower levels, and, for a pure sea/lake breeze, marks the upper boundary of the return flow layer.

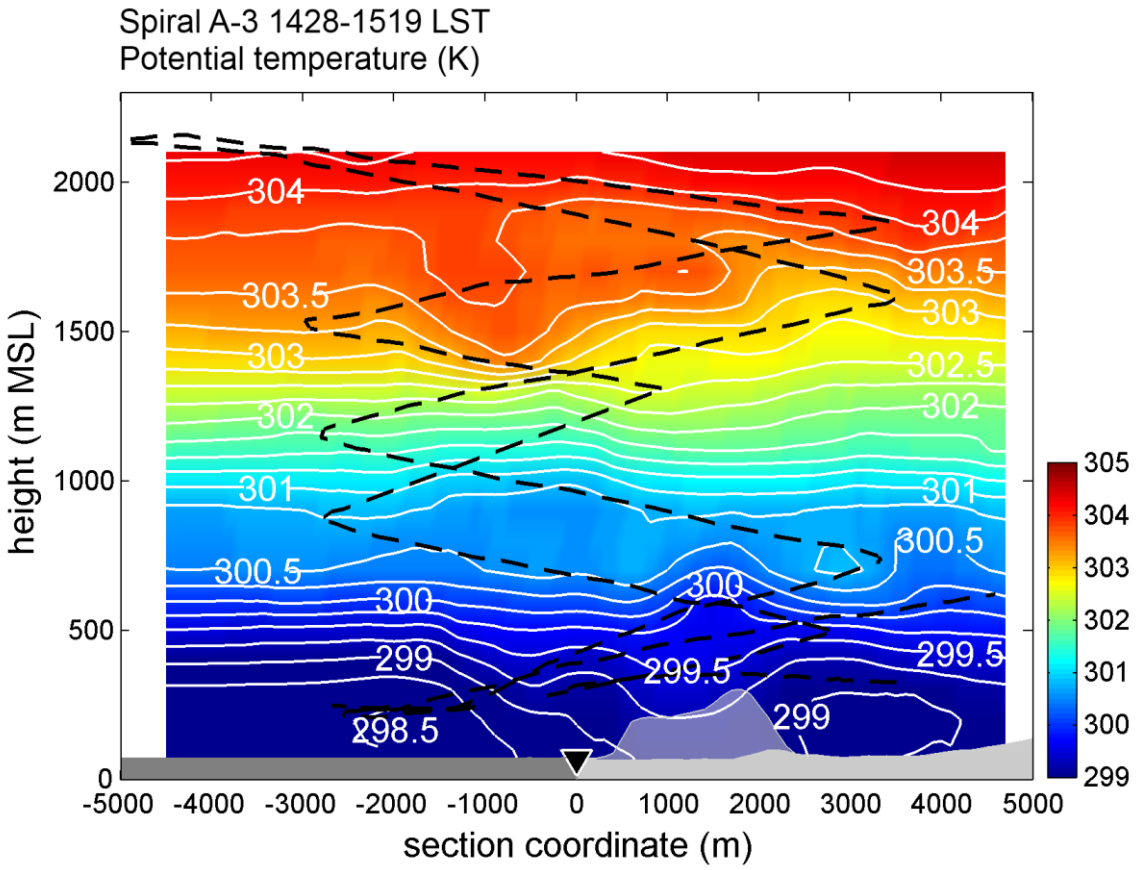

Figure 6.6. As in **figure 6.5**, but for spiral A-3 from flight #3.

6.3.2 Lakes Valley - Cavedine Lake area

In the area of Cavedine Lake the cross section is shaped in two different subsections, but only the western, deeper subsection was explored by both research flights.

Figure 6.7 shows RK-interpolated potential temperature field from flight #2: a quasi-neutral layer, likely to be the layer most affected by the local subsidence associated to the morning-phase upslope winds (cf. **Chapter 5**; Rampanelli et al. 2004) fills the levels between 1250 and 1700 m MSL. The valley atmosphere below 1100 m MSL appears rather decoupled from the layer aloft, from which it is separated by a 1.5 K inversion, and is likely to represent the *Ora del Garda* up-valley airflow (depth: ~850 m). A ~300 m deep colder airmass is also found at the valley floor in the center of the (sub)section. Accordingly to the dual nature observed by Banta (1995) and De Wekker et al. (2012) for circulations arising from the coupling of sea breezes and valley winds, this near-surface potentially colder layer

may be identified as the body of a shallow lake-breeze produced by the water-land temperature difference, being the upper airflow mainly related to valley-scale gradients.

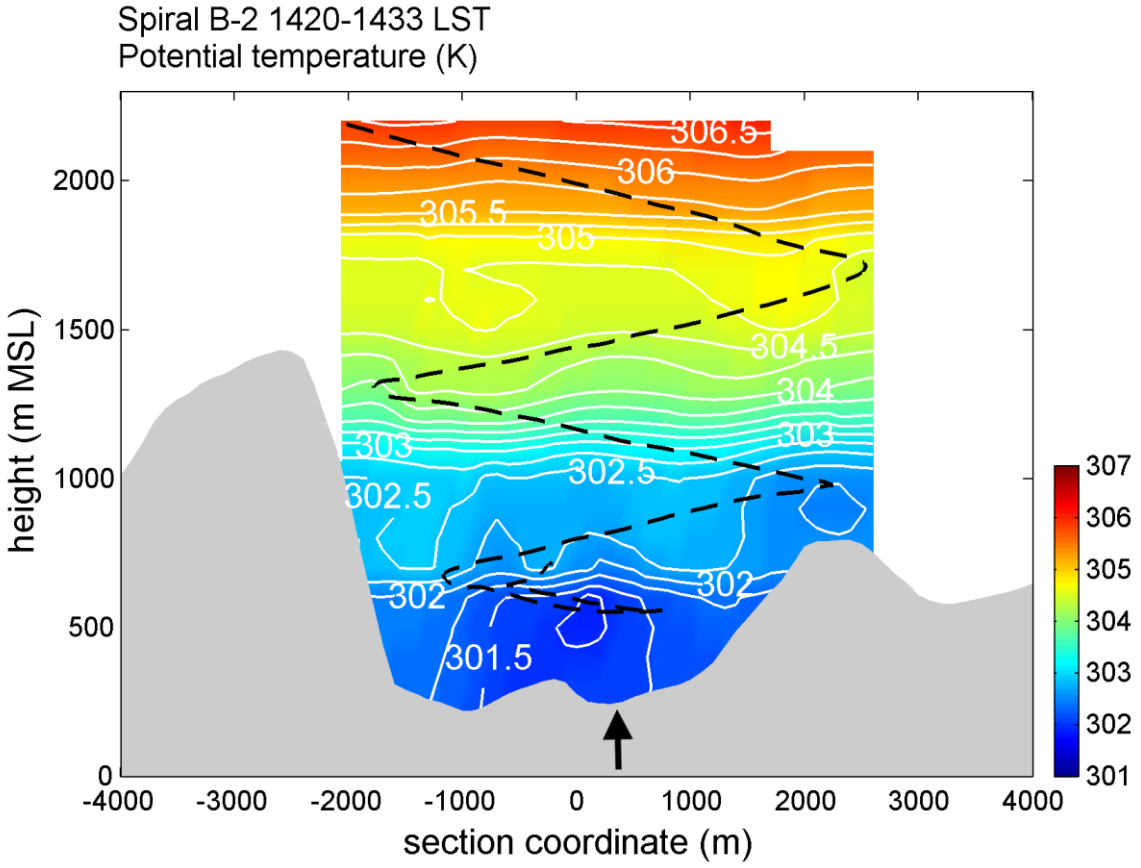

Figure 6.7. As in **figure 6.5**, but for spiral B-2 from flight #2 (B-2 plane in **figure 6.4**). The black arrow shows the position of Cavedine Lake. Horizontal coordinate marks the cross-valley direction (Lakes Valley; WNW-ESE direction).

On the other hand, results from flight #3 (**figure 6.8**) reveal that a very stably stratified, potentially cold air mass (less than ~500 m deep) fills the lowest layers, probably identifying the *Ora del Garda* airflow. A pronounced thermal asymmetry also occurs in this layer: the western half of the valley, whose floor is mainly covered with bare rocks, is clearly warmer (by more than 2 K) than the valley center, where Cavedine Lake lies (indicated by an arrow in the figure). The contrast between the very steep and rocky western sidewall and the densely wooded eastern sidewall is reasonably responsible for the mentioned thermal contrast, which is probably associated with the occurrence of a more intense upslope circulation and associated compensating downward motion (Rampanelli et al. 2004) along the western sidewall, despite both slopes were equally sunlit at the overflight time (as determined by means of a GIS analysis of solar incoming radiation patterns). At the lowest levels locally colder, stably-stratified conditions persist throughout the diurnal phase, especially above the

small Cavedine Lake, as indicated by time series of surface observations at CAV weather station (not shown; see also **Chapter 5**).

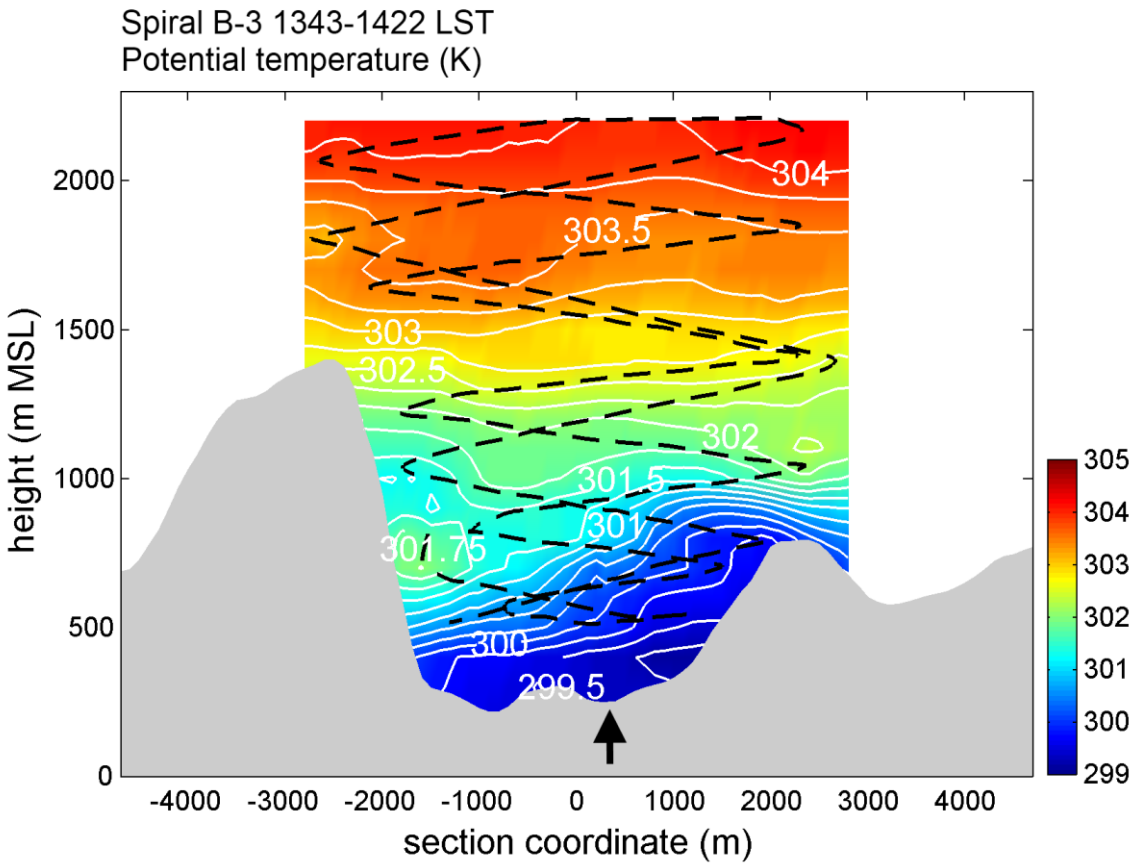

Figure 6.8. As in **figure 6.5**, but for spiral B-3 from flight #3 (B-3 plane in **figure 6.4**). The black arrow shows the position of Cavedine Lake. Horizontal coordinate marks the cross-valley direction (Lakes Valley; WNW-ESE direction).

6.3.3 Lakes Valley - Terlago saddle area

Sections C of the flights explored the northernmost area of the Lakes Valley, downstream to the eastward bending of the valley axis and upstream to the *Ora del Garda* outbreak into the Adige Valley (see **Chapter 2**).

Flight #2 (**figure 6.9**) detected a ~600 m deep, well-defined core of cold and stably stratified air filling the lowest levels (below 1200 m MSL height) of the northwestern half of the valley cross section. At the time of the flight, the rocky and steep northwestern sidewall has received much more solar radiation throughout the day than the opposite (N-facing) one, which is more gently-sloping and densely vegetated. So this apparently anomalous feature may be attributed to the local change in the valley orientation: as the breeze fully developed that day, the inertia of the intense up-valley *Ora del Garda* flow forces the cold air mass to

impinge against the western sidewalls (i.e. the external side of the curve). At the upper levels a quasi-neutral stratification (~1 K km^{-1}) appears over the whole cross section up to almost the height of the lateral crests (1750 m MSL): this is the layer where the return flows associated with the morning upslope circulations induce the subsidence of warmer air from aloft (Rampanelli et al. 2004). A much more stable stratification (~4 K km^{-1}) is found further above, marking the upper limit of the up-valley flow region (total depth: 1250 m).

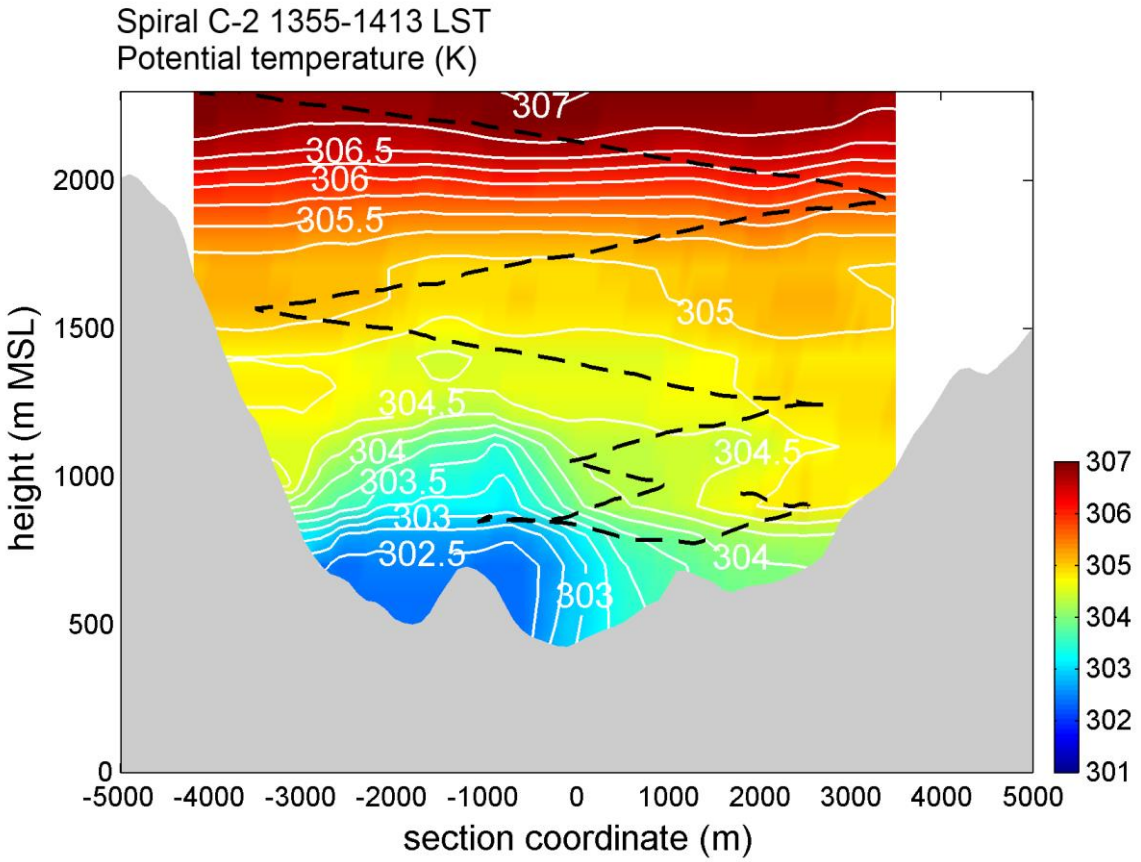

Figure 6.9. As in **figure 6.5**, but for spiral C-2 from flight #2 (C-2 plane in **figure 6.4**). Horizontal coordinate marks the cross-valley direction (Lakes Valley; WNW-ESE direction). Note that the intermediate levels (between 800 and 1500 m MSL) of the northwestern half (i.e. left) of the valley cross section were not entirely explored by the flight; as a consequence, potential temperature values in this region result from an extrapolation process and thus present poor reliability.

Flight #3 (**figure 6.10**) on the other hand detected a much shallower (less than 400 m deep) and very stable cold air mass below 1000 m MSL in the center of the valley, surmounted by a quasi-neutrally stratified layer extending up to height of the crests. Differently from flight #2, between 1000 and 1500 m MSL the northwestern half (directly sunlit sidewall side) of the valley atmosphere is found to be clearly warmer (~1 K) than the southeastern half, which is

amenable to stronger subsidence being produced here by upslope winds (Rampanelli et al. 2004) developing along the northwestern sidewall, because of the different radiation income and surface coverage. The flow in this layer appears to be completely decoupled from the flow in the lowest layers, as a strong potential temperature gradient (2.5 K) separates the two regions.

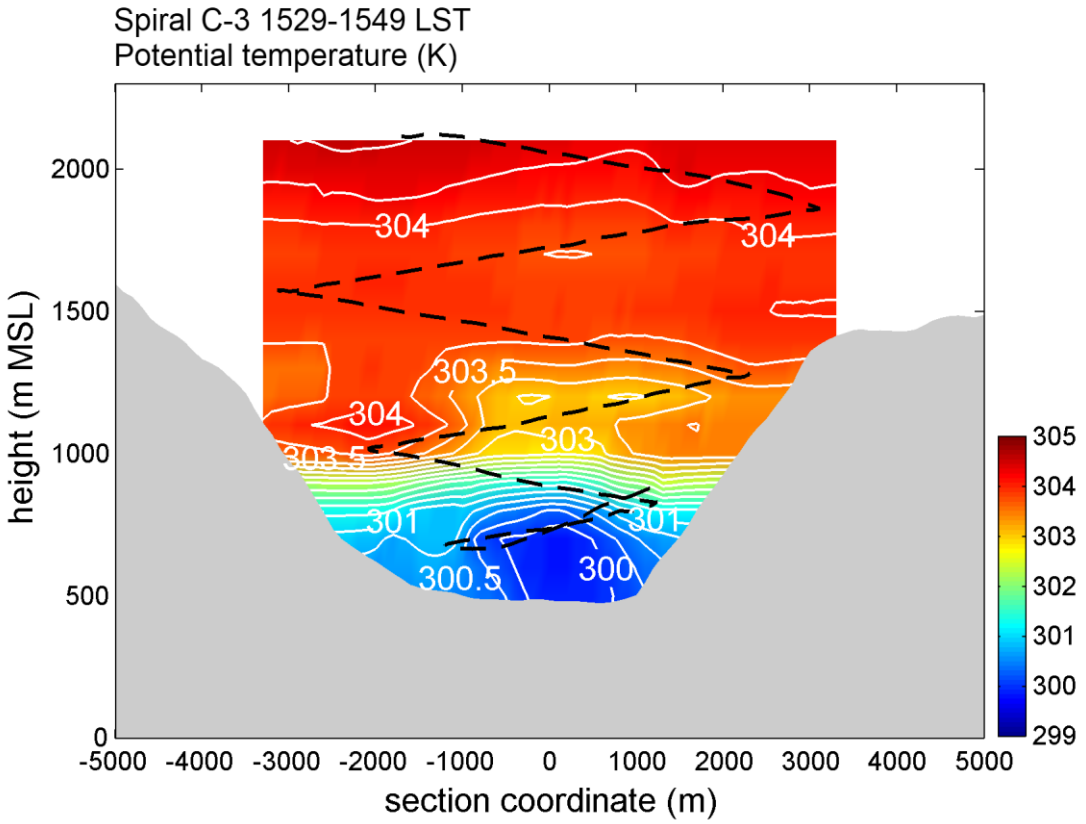

Figure 6.10. As in **figure 6.5**, but for spiral C-3 from flight #3 (C-3 plane in **figure 6.4**). Horizontal coordinate marks the cross-valley direction (Lakes Valley; WNW-ESE direction).

6.3.4 Adige Valley - interaction area

Flight #3 explored the area where the *Ora del Garda* breaks-in into the Adige Valley. The wind conditions were seriously prohibitive for safe flying through this valley section, due to strong turbulence, so it could be explored only along three transecting flight legs. Nevertheless, the following analysis highlights various interesting features.

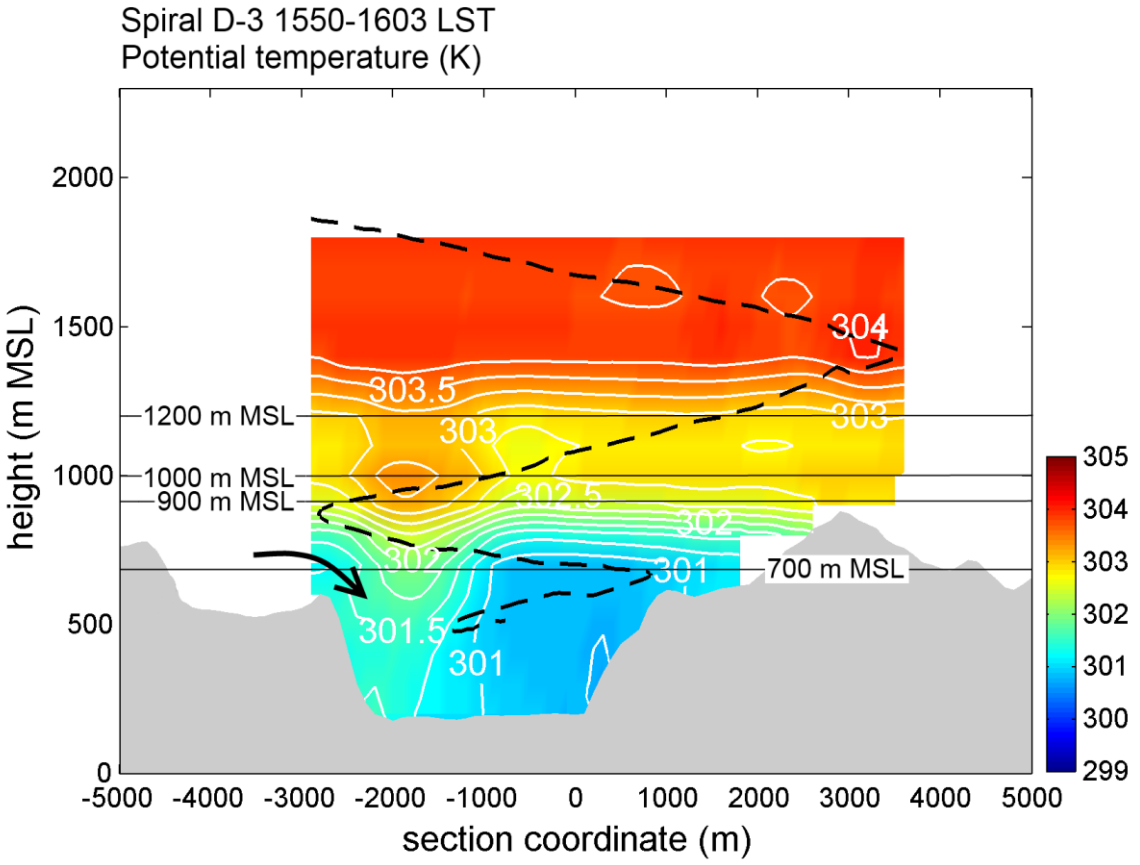

Figure 6.11. As in **figure 6.5**, but for spiral D-3 from flight #3 (D-3 plane in **figure 6.4**). The black arrow shows the point from where of the *Ora del Garda* wind overflows from the Lakes Valley, i.e. the saddle of Terlago. Horizontal coordinate marks the cross-valley direction (Adige Valley; W-E direction).

In **figure 6.11** isentropes 301.5-302.5 K (which can be assumed here as streamlines) outline an overflow of potentially colder air through the saddle of Terlago, down into the Adige Valley along its western side, and again up the opposite slope, filling the eastern side of the Adige Valley cross section up to 900 m MSL (i.e. 700 m AGL). On the other hand, the homogeneous layer (302.5-303.0 K) extending from 900 to 1250 m MSL in the eastern half of the valley cross section is likely to be associated with the mainstream of the local up-valley wind forced to flow above the denser air from the Lakes Valley; in fact this air results potentially colder than air found at the same level above the saddle of Terlago, i.e. section C-3 (**figure 6.10**). Unfortunately no wind velocity measurements are available to confirm this flow pattern. However, we speculate that this structure is consistent with the picture of the local flow emerging from previous investigations reported in **Chapter 2** (de Franceschi et al. 2002, Schaller 1936, Wagner 1938). The airflow in the area is indeed similar to the spillover of water over a barrier, followed by a weir downstream: actually a gap flow develops across the elevated saddle of Terlago, accelerating into a down-slope jet. This

characteristic feature is not completely captured by the present airborne observations, but is supported by surface observations reported in **Chapter 2** and in de Franceschi et al. (2002).

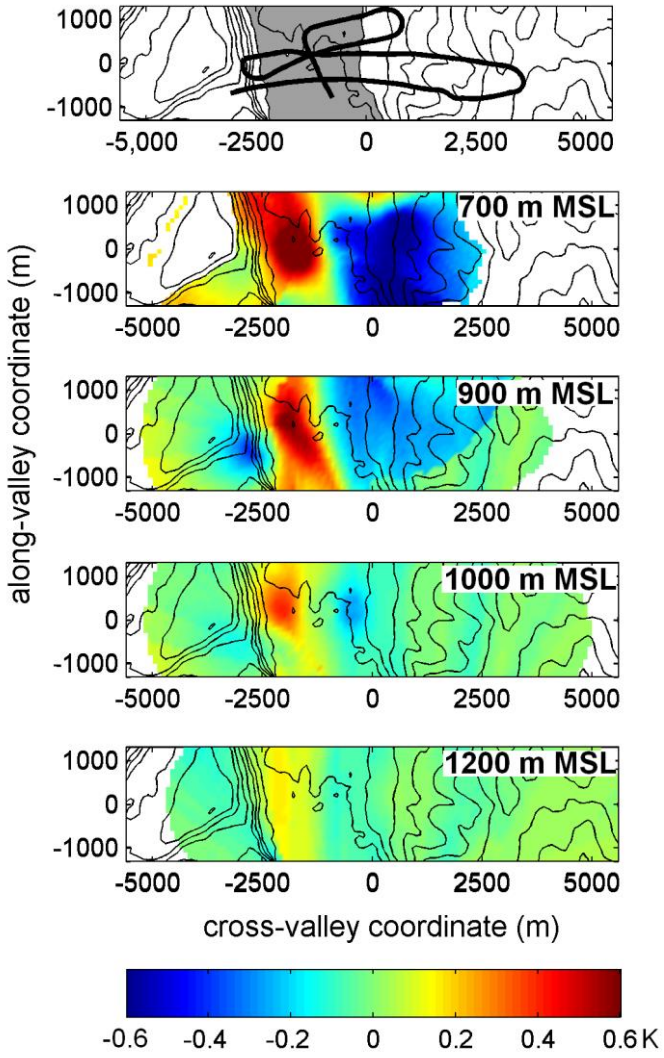

Figure 6.12. RK-interpolated potential temperature anomaly (in colors) at different height levels (indicated in **figure 6.11**) for section D-3 from flight #3. The upper panel shows the underlying Adige Valley topography: contour interval is 100 m, the valley floor (~200 m MSL) is colored in grey; the valley sidewall on the left is the saddle of Terlago. The black line is the horizontal projection of the motorglider trajectory. Abscise coordinates correspond to cross-valley coordinates in **figure 6.11** (W-E direction).

A hydraulic jump is likely to occur downstream, due to the blocking exerted by the opposite sidewall of the Adige Valley, where a potentially warmer air mass is initially encountered. Similar flow conditions, have been investigated in the Alps by Armi and Mayr (2007), Flamant et al. (2002), Gohm and Mayr (2004), Mayr et al. (2007): they investigated föhn

winds descending along the Wipp Valley (Austria) and producing clear hydraulic jump structures when they impinge on the Nordkette mountain range near Innsbruck. The reduction in the spacing between isentropes (~streamlines), which is maximum between –2500 and –2000 m in the cross-valley coordinate, i.e. in the overflow area, reflects the local acceleration of the falling airflow. Horizontal sections of potential temperature anomaly with respect to the mean potential temperature vertical profile (shown in **figure 6.12**) help to visualize these features of the local flow. By the saddle crest (cross-valley coordinate: –2500 m), the transition from potentially colder air upstream (i.e. above the saddle) to warmer air immediately downstream of the saddle ridge is associated with the downward tilting of the isentropes in the area where the *Ora del Garda* pours down the vertical sidewall below the saddle. Instead, the sharp discontinuity identifying the hydraulic jump position, where the flow depth abruptely increases and the isentropes suddenly rise again, is localized at around –1000 m cross-valley coordinate: it appears stronger (~1 K difference) at the lowest levels, thus still detectable up to 1200 m MSL (~1000 m above the Adige Valley floor); indeed, the 303.0 K isentrope (which also delimits the strongly stable airmass forming the *Ora del Garda* flow at section C-3, **figure 6.10**) marks the upper boundary of the volume involved in this complex flow pattern, i.e. around 1100 m above the Adige Valley floor.

6.4 23 August 2001 (flights #4 and #5)

RK-gridded potential temperature fields from flights #4 and #5, allowing the identification of fine-scale 3D features of the thermal structure of the ABL at the valley sections explored by the flights (see corresponding vertical planes in **figure 6.13**), are presented and discussed below. The order follows the up-valley development of the *Ora del Garda* wind from the Lake Garda shore to the Adige Valley, and the labels adopted for the different spirals are the same used in **section 5.4**.

6.4.1 Lower Sarca Valley

The high-resolution 3D potential temperature field from spiral A-4 (**figures 6.14** and **6.15**) reveals a non-uniform propagation of the lake-breeze front from Lake Garda shoreline across the lower Sarca Valley: at the time of the site's overflight (~1000-1045 LST) colder air is present at the lowest layers in the western half of the valley cross section, compared to the area of Mt. Brione (**figure 6.14**).

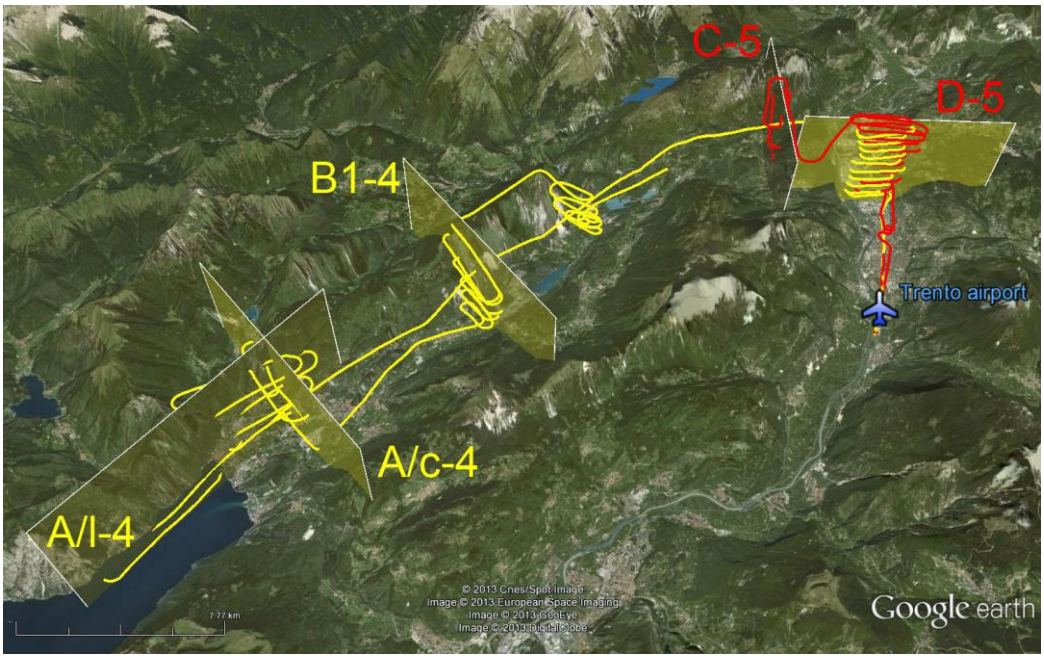

Figure 6.13. 3D representation of flight #4 (yellow line) and #5 (red line) trajectories. The vertical planes adopted for displaying the RK-interpolated potential temperature fields in **figures 6.14-6.18** are also indicated. Image © Google Earth, © 2013 Cnes/Spot Image, © 2013 European Space Imaging, © 2013 GeoEye, © 2013 DigitalGlobe.

Surface observations at TOR and ARC substantiate the hypothesis of an earlier penetration of the lake breeze in the eastern half of the valley: at both AWSs the front passage is detected at 1100 LST, although the first lies at only 1.5 km from the coastline, between the Mt. Brione relief and the eastern valley sidewall, while the second is situated 5 km inland, at the northern side of the wide basin (see **section 3.6.3.1**). A possible explanation for this behaviour is provided by the ~1.5 h delay between local sunrise times at the two lateral extremities of the valley bottom (0605 LST and 0745 LST respectively for the western and the eastern extremity of the basin, as determined by means of a GIS analysis, which was performed to evaluate the diurnal cycle of the incoming solar radiation in the area). Topographic shadowing delays the establishment of the water-land temperature contrast that produces the lake breeze. As a consequence, the onset of the latter is retarded in the area close to the eastern valley sidewalls. Moreover, the narrow corridor between Mt. Brione relief and the eastern slopes (width: ~500 m) is known to receive a strong drainage flow of cold air during the night until the morning, as this is the last portion of the basin to be sunlit in the morning. This fact could further delay the penetration of the *Ora del Garda* front in the area. On the other hand, in the upper atmosphere (above 1500 m MSL) a contrary thermal asymmetry is detected: the western half of the valley cross section results warmer than the eastern one (**figure 6.14**), suggesting that more intense compensating downward motions are induced

here by up-slope flows (Rampanelli et al. 2004) that develop earlier along the sun-facing western sidewalls.

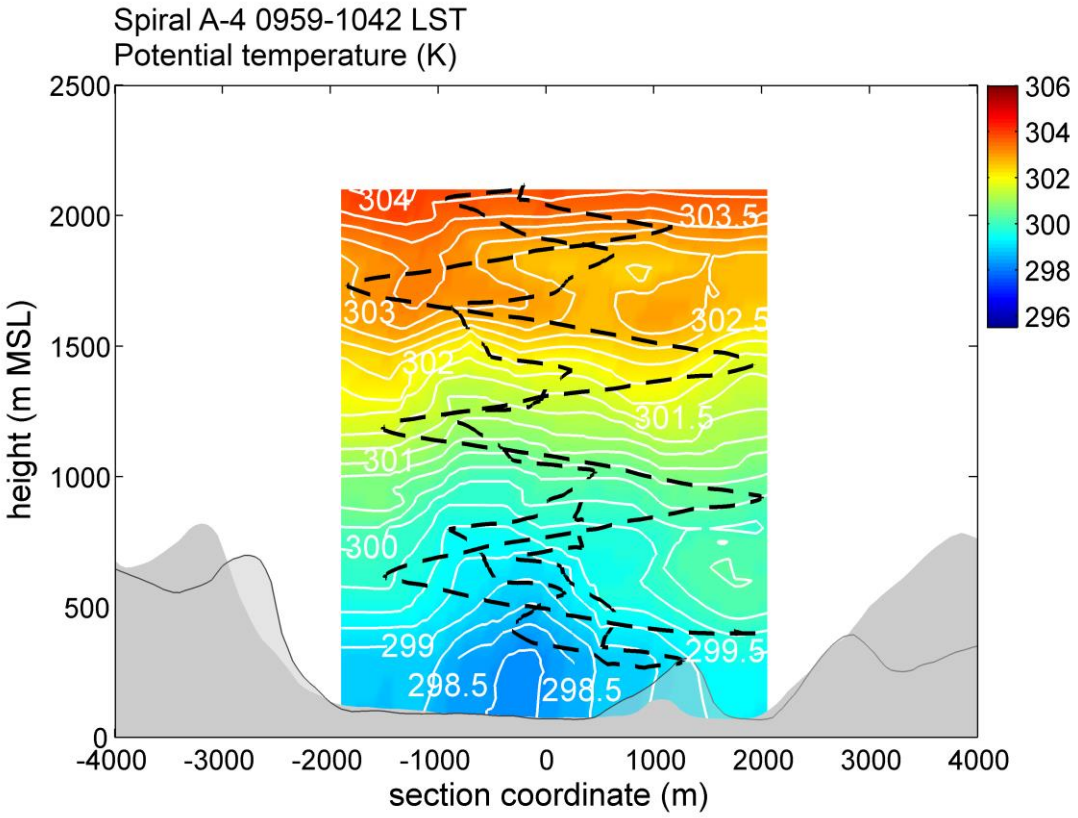

Figure 6.14. Transversal (i.e. cross-valley) vertical section of RK-interpolated potential temperature field for spiral A-4 from flight #4 (see corresponding vertical plane A/c-4 in **figure 6.13**); contour interval is 0.25 K (in white). The correspondent valley topography is indicated in grey. The cross section is taken immediately down-stream of the Monte Brione relief (semi-transparent shading), i.e. ~3 km inland from the Lake Garda shoreline. Accordingly, the horizontal coordinate marks the cross-valley direction (lower Sarca Valley; WNW-ESE direction). The black dashed line indicates the trajectory followed by the motorglider over the considered section.

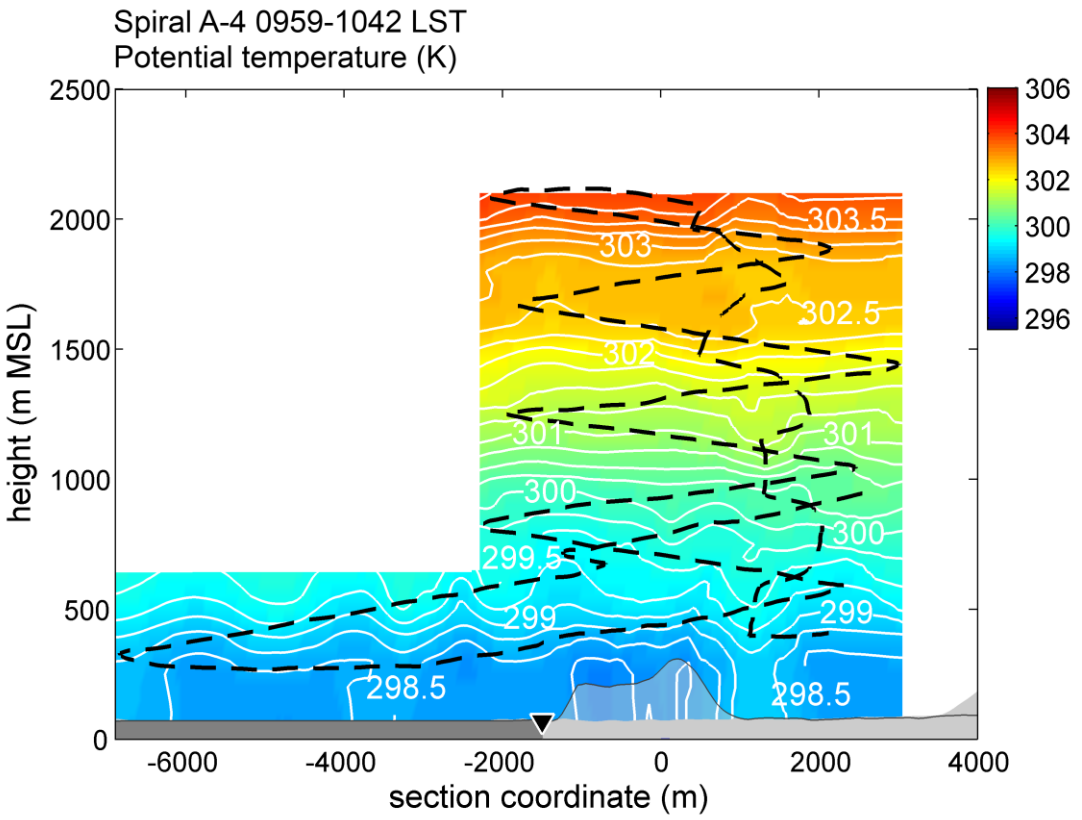

Figure 6.15. Longitudinal (i.e. along-valley) vertical section of RK-interpolated potential temperature field for spiral A-4 from flight #4 (see corresponding vertical plane A/l-4 in **figure 6.13**); contour interval is 0.25 K (in white). The correspondent valley topography is indicated in grey, while dark grey indicates Lake Garda. The longitudinal section is taken immediately west of the Monte Brione relief (semi-transparent shading), i.e. in the middle of the lower Sarca Valley. The black dashed line indicates the trajectory followed by the motorglider over the considered section. The black triangle shows Lake Garda shoreline. Accordingly, the horizontal coordinate marks the along-valley direction (lower Sarca Valley; SSW-NNE direction.

6.4.2 Lakes Valley

An analogous cross-valley thermal asymmetry is observed on the sections extracted from fields interpolated around spirals performed further up-valley, i.e. B1-4 and B2-4. The downward tilting of the isentropes around 1500 m MSL height (i.e. average crest level) is close to the western valley sidewalls, which directly face the sun in the morning hours. This is particularly evident for section B1-4 (**figure 6.16**), where a pronounced potential temperature cross-valley horizontal gradient is detected also at lower heights, almost down to the lowest point of the flight trajectory (~350 m above the local valley floor height); the

nearly N-S orientation of the valley axis then turns out to affect to a large extent the thermal structure of the ABL during the morning heating phase. Moreover, the local cross section is very narrow, and the (morning) sun-facing western slopes are also steeper and less vegetated than the opposite ones, being partly covered by bare rock; this land cover dissimilarity is likely to enhance the local temperature contrast between the two halves of the valley atmosphere, further contributing to the development of asymmetric slope circulations in the area.

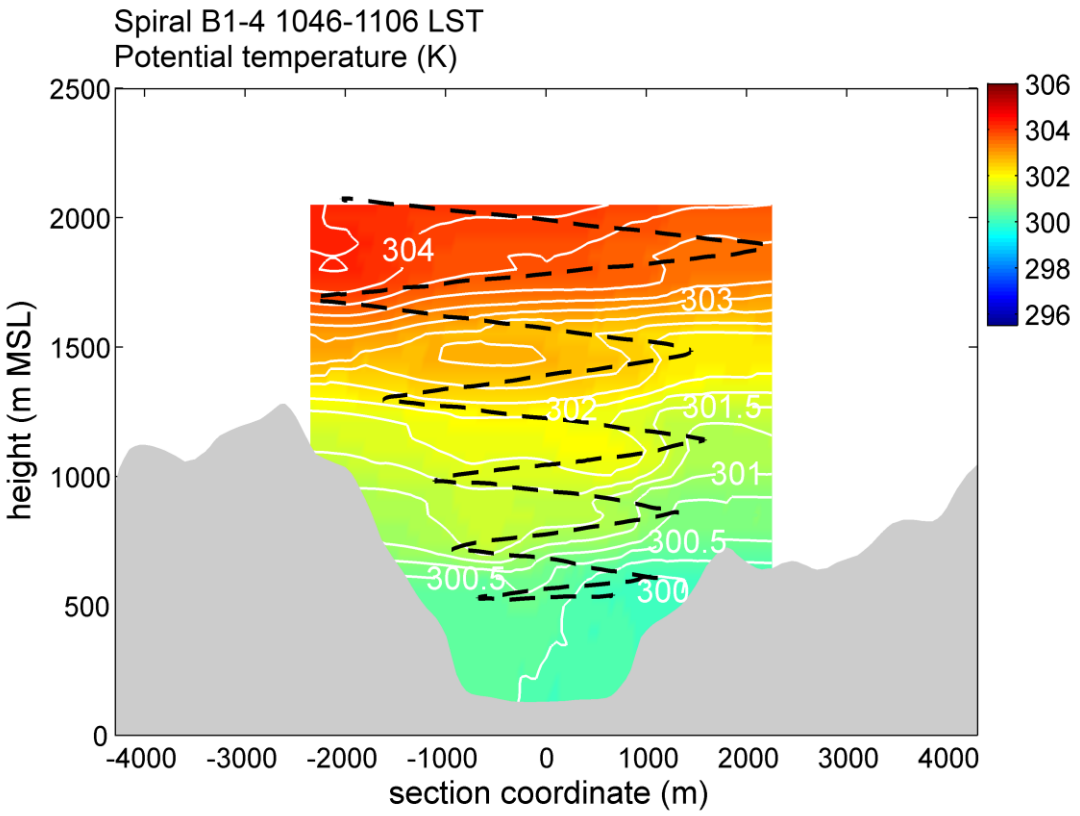

Figure 6.16. As in **figure 6.14** but for spiral B1-4 from flight #4 (see corresponding vertical plane B1-4 in **figure 6.13**). Accordingly, the horizontal coordinate marks the cross-valley direction (WSW-ENE direction).

6.4.3 Interaction area

The analysis of high-resolution potential temperature 3D fields from the afternoon flight provides some insight also on the flow patterns characterizing the interaction between the *Ora del Garda* and the Adige Valley up-valley wind in the area of the saddle of Terlago, at the Lakes Valley end.

Figure 6.17 displays the cross-valley thermal structure of the valley atmosphere in the Terlago basin, ~2 km up-stream (i.e. down-valley) with respect to the saddle ridge: the denser

air which forms the core of the breeze flow is localized in the northwestern half of the valley cross section. The preferential channelling of the up-valley current along the northwestern sidewall is likely to depend on the fact that the valley axis bends eastward a few kilometres down-valley. The flow main stream is therefore pushed against the external side of this curve (i.e. the northwestern sidewall) by inertial forces. This phenomenon is similar to the flow pattern observed by Weigel and Rotach (2004) in the Riviera Valley: they identified a "jet" structure shifted towards the eastern slope at the valley entrance, as a result of the centrifugal acceleration driven by the local valley curvature. In the Lakes Valley, the presence in the area of a more than 200 m high hillock (reported as semi-transparent topography profile in **figure 6.17**) may further contribute to the northward deflection of the lowest atmosphere airflow, which is funnelled towards the lowest point of the ridge of the Terlago saddle (indicated by the black arrow).

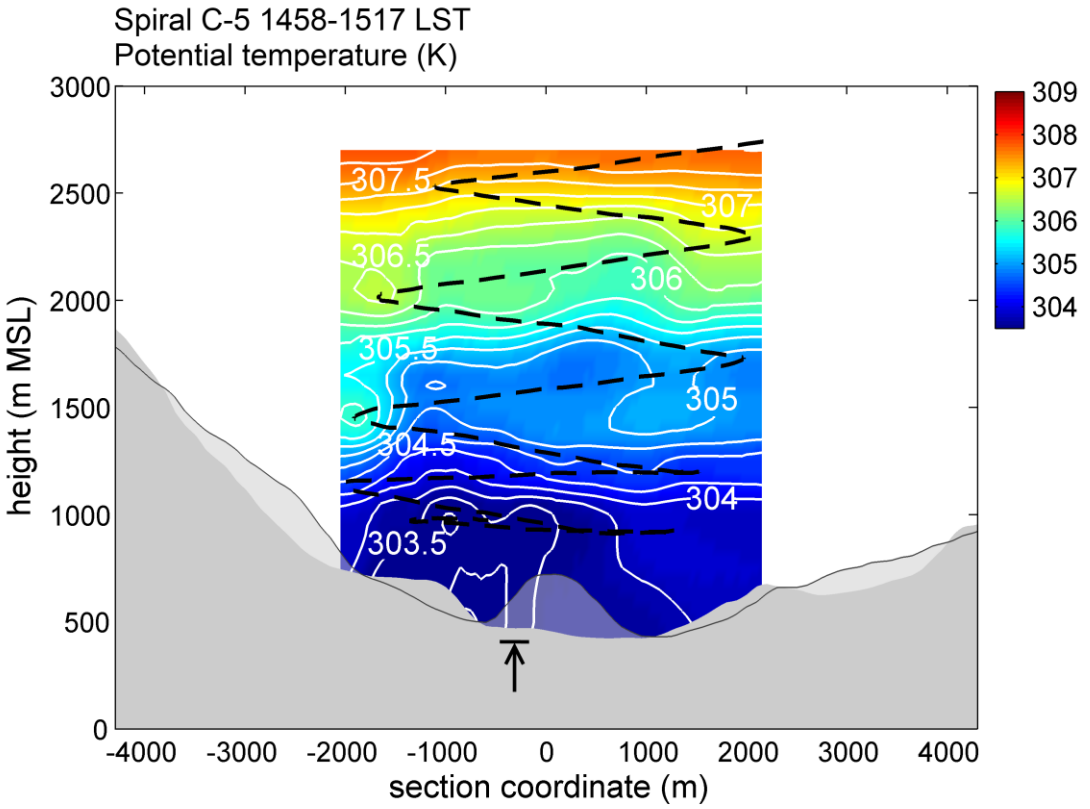

Figure 6.17. As in **figure 6.14** but for spiral C-5 from flight #5 (see corresponding vertical plane C-5 in **figure 6.13**). Accordingly, the horizontal coordinate marks the cross-valley direction (upper Lakes Valley; N-S direction).

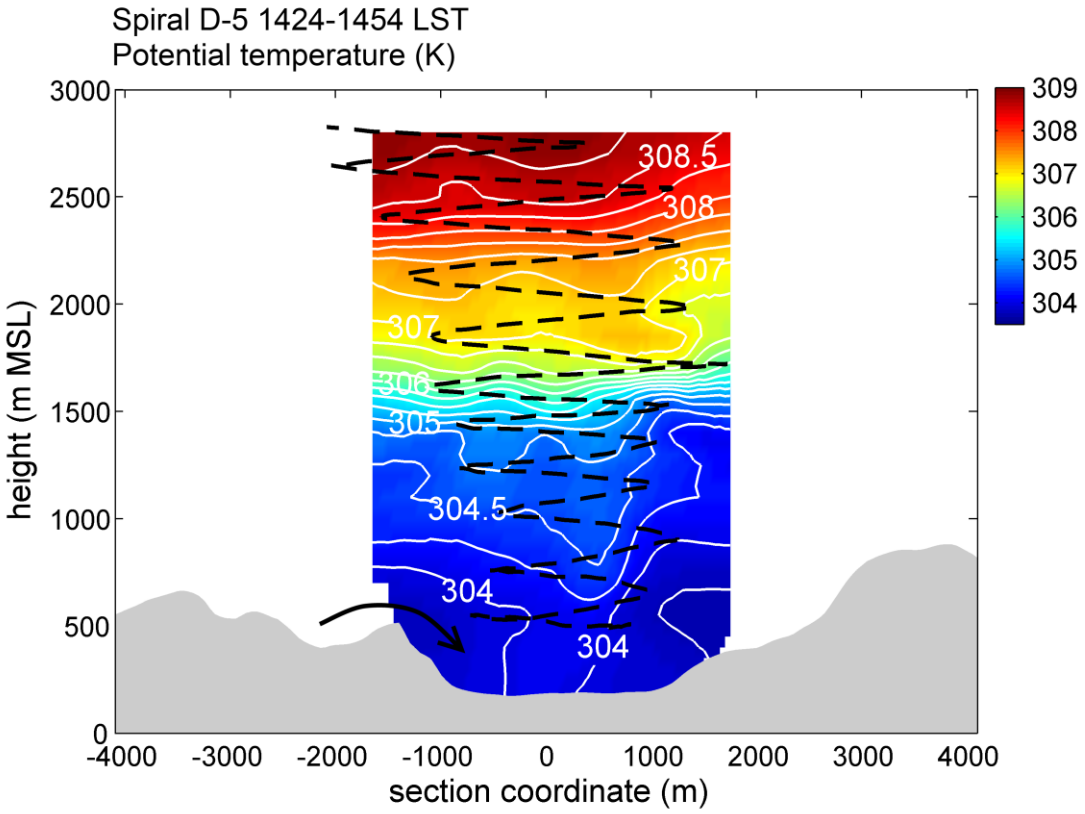

Figure 6.18. As in **figure 6.14** but for spiral D-5 from flight #5 (see corresponding vertical plane D-5 in **figure 6.13**). Accordingly, the horizontal coordinate marks the cross-valley direction (Adige Valley; W-E direction). Arrow

On the other hand, spiral D-5 (**figure 6.18**), performed slightly south to this preferential overflow point, reveals that the inlet of the *Ora del Garda* from the Lakes Valley into the underlying Adige Valley produces a complex ABL structure above the floor of the latter. 304.25 and 304.50 K isentropes (which can be roughly considered to represent streamlines) suggest the presence of a strong westerly katabatic current pouring down the saddle of Terlago, flowing down on the Adige Valley bottom, and then impinging on the opposite sidewall, as supported by surface wind observations (cf. **section 3.6.3.4**). The depth of the layer where an intense turbulent recirculation ensuing from this flow pattern is likely to occur may be estimated in approximately 1300 m (consistently with previous findings summarized in Wagner 1938), for a sharp potential temperature gradient is found above 1500 m MSL height. This marks the transition to an upper region of air warmer and drier than at the same height in the Lakes Valley (cf. the difference between the upper parts of C-5 and D-5 pseudo-soundings; **section 5.4.2** and **figure 5.5b**). This layer is likely to represent the Adige Valley up-valley flow, displaced to higher heights by the denser air overflowing from the Lakes Valley down to the Adige Valley bottom, accordingly to the findings by Schaller (1936). Results from flight #3 indicated the occurrence of a down-slope jet followed by a

"hydraulic jump" flow structure in this area (**section 6.3.4**). Actually, features similar to those of gap-flow conditions described in the Alps by Armi and Mayr (2007), Flamant et al. (2002), Gohm and Mayr (2004) and Mayr et al. (2007) among others, may be identified also in the potential temperature field of **figure 6.18**: the quasi-vertical pattern of 304.00-305.00 K isentropes (~streamlines) in the middle of the valley cross section (between 500 and 1000 m horizontal coordinate) outlines the rebound of the airflow depth to a higher height than up-stream, i.e. an hydraulic jump transition. This marks the transition between the strong westerly current pouring from the Lakes Valley and a stagnating flow regime generated by the obstruction exerted by the eastern Adige Valley sidewall in front of the saddle of Terlago.

6.5 Summary

In this chapter the fine-scale 3D structure of the ABL accompanying the development of the *Ora del Garda* wind was discussed for selected valley sections, from above the Lake Garda northern shorelines, where the wind arises as a lake breeze, to the Adige Valley, where it interacts with the local up-valley circulation. The detected fine-scale variability of ABL structures allowed some speculations about local features of the associated thermally-driven wind field.

The measurement flights described in **Chapter 3** provided the main dataset for the application of RK as an appropriate tool for mapping airborne potential temperature data on regular grids built around the above sections (cf. **Chapter 4**). The analysis of the resulting high-resolution interpolated fields cast new light on the ABL thermal structure associated with the development of the *Ora del Garda*. Indeed, the RK-reconstruction of 3D fields allowed the retrieval of further local features of the valley ABL, not detectable from vertical profiles only (which were analysed in **Chapter 5**), associated with complex terrain and surface inhomogeneities, as well as with local flow patterns that are common both to deep mountain valleys characterized by irregularly-shaped cross sections and valley axis curvatures, and to coastal environments (see **section 6.1**).

In particular, all the flights displayed the effects of the differential heating of the lateral sidewalls of the valley. In the morning, due to the roughly S-N orientation of the valley and to local differences in the land cover of lateral slopes, the local subsidence associated with morning up-slope flows is much more intense close to the directly sunlit and rocky western sidewalls than to the eastern ones, more vegetated and consistently less heated during this phase, inducing cross-valley thermal asymmetries at the intermediate levels, especially pronounced in the Lakes Valley (spirals C-1, C-3 and B1-4) but detected also in the lower Sarca Valley (spirals A-1 and A-4). In the southern Lakes Valley a strongly asymmetric cross-valley thermal structure was identified also in the lowest layers, arising from the local contrast in surface coverage between the vegetated area of small Cavedine Lake and the steep, bare-rock western valley sidewall (spirals B/w-1 and B-3). Moreover, in the area of S.

Massenza and Toblino Lakes complex asymmetric features of the potential temperature field suggested the development of a single-cell cross-valley circulation over the whole valley cross section, likely to be produced by the very different irradiation of the two lateral slopes (local valley orientation: SW-NE), and possibly favoured by the eastward bending of the valley axis in the area.

In the area of Lake Garda northern shoreline, on 23 August 2001 surface observations indicated a well-defined lake breeze front propagating inland from the shoreline starting at around 1000 LST, whose passage was clearly recorded ~1 h later at the northern end of the flat basin facing the lake (i.e. ~5 km inland). Its penetration in the lower Sarca Valley was not homogenous: in fact, its propagation across the easternmost part of the basin was found to be delayed by at least ~1 h with respect to the western half of the valley cross section (see **section 3.6.3.1**). This situation, which can be partly ascribed to the 1.5 h delay occurring between local sunrise times at the western and at the eastern extremities of the basin, was further confirmed by RK-interpolated field of potential temperature from spiral A-4. Around 1030 LST they showed the presence of potentially colder air in the lowest atmosphere west of Mt. Brione, despite the earlier heating of this area by solar radiation with respect to the region east of Mt. Brione. This proves the later penetration of the lake breeze in the narrow corridor between the small relief and the eastern valley sidewall. Here a low-level dynamical and thermal perturbation of the *Ora del Garda* onshore flow, mainly associated with the presence of the rocky hill of Mt. Brione, was also detected in the mid-afternoon phase by flights #2 and #3 (spirals A-2 and A-3). On the other hand, a sharp discontinuity in the vertical stratification, typically associated with the development of a lake-breeze circulation cell, was recognized in the shoreline region at the upper levels (around 1500 m MSL) for the two 1999 flights, both under favorable (flight #2) and unfavorable (flight #3) synoptic-forcing conditions (spirals A-2 and A-3).

Regarding the *Ora del Garda* flow depth, cold and stably-stratified airmasses less than 500 m deep were detected above the valley floor for flight #3 (spirals B-3 and C-3). On the contrary, under favorable synoptic conditions (spirals B-2 and C-2 from flight #2) the up-valley flow layer seemed to be significantly deeper (in the order of 1000 m). In general under unfavorable conditions (flight #3 day) consistently shallower airflow depths were detected for the *Ora del Garda* in the Lakes Valley, and its development at the valley floor appeared to be rather decoupled from the valley atmosphere aloft. On the other hand, under favorable conditions the up-valley flow is likely to extend up to a height almost comparable with that of surrounding mountain ranges (Zardi and Whiteman 2013).

In the upper Lakes Valley the preferential channeling of the low-level wind along the northwestern sidewall of the valley towards the lowest point of the Terlago saddle ridge, due to the eastward curvature of the valley axis in the area and to the inertia of the intense breeze flow, was revealed by RK-interpolated potential temperature fields from flight #2 and #5

(spiral C-2 and C-5). The afternoon outbreak of the *Ora del Garda* into the Adige Valley from its western sidewall, i.e. from the saddle of Terlago, produces an intense katabatic wind, with potentially cooler air rapidly descending down the underlying valley floor (cf. **sections 2.3** and **2.4**). The complex thermal structure of the ABL in the area, emerging from vertical and horizontal sections of RK-interpolated potential temperature fields for spirals D-3 and D-5, suggests that in both cases a situation similar to a gap flow developed across the Terlago saddle, followed by a hydraulic jump further down-stream, where the airflow impinged on the eastern Adige Valley sidewall facing the overflow point. The depth of the down-stream layer where the turbulent recirculation of the airflow coming from the Lakes Valley occurs was found to be around 700 and 1300 m respectively for spirals D-3 (weak *Ora del Garda* wind) and D-5 (strong *Ora del Garda* wind). Indeed, the consistent deepening of the mixed layer in the Adige Valley (from 400 to 1200 m), occurring on 23 August 2001 between 1200 and 1500 LST approximately, was produced by the *Ora del Garda* outbreak rather than by a convective growth process driven by surface sensible heat fluxes. This picture is consistent with previous investigations by Schaller (1936), de Franceschi et al. (2002) and others (reported in Wagner 1938); accordingly, the airmasses found immediately above this well-mixed layer may be identified with the local up-valley flow (whose regular development was hindered by the *Ora del Garda* overflow), being displaced at higher heights by the denser wedge of potentially cooler air that formed at the Adige Valley floor.

To summarize, high-resolution 3D fields resulting from airborne data interpolation added remarkable information to the understanding of the valley ABL patterns associated with *Ora del Garda* under different synoptic-forcing situations, in particular for what concerns the formation and propagation of the lake breeze front in the shoreline area in the late morning, and the evolution in the afternoon of the atmosphere thermal structure at the junction between the Lakes Valley and the Adige Valley. Indeed, they also provided a valuable insight into the local structure of the wind flow characterizing the *Ora del Garda* development in the valleys forming the study area.

Chapter 7

Conclusions and future developments

7.1 Conclusions

In the present work a characterization of the typical atmospheric boundary-layer (ABL) structures associated with the development of the *Ora del Garda* wind in the Sarca, Lakes and Adige valleys was achieved through the combined analysis of both airborne and surface observations, accomplishing the research objectives stated in **Chapter 1**. At the same time, further insight into the local structure of the thermally-driven flow was also obtained. The most significant results of the study are summarized below.

Based on selected observations from a number of surface weather stations deployed in the study area, the typical daily cycles of wind and temperature associated with the *Ora del Garda* development at the valley floor were outlined (**Chapter 2**). In particular, the inland propagation of a cold front was envisaged in the lower Sarca Valley, close to Lake Garda shoreline. In the Lakes Valley, a mitigation of the daytime heating and a flattening of the temperature peak were detected in connection with the flow, advecting cold air from above the lake. On the other hand, the *Ora del Garda* outbreak into the Adige Valley in the early afternoon was found to produce a sudden shift to an intense, westerly (i.e. cross-valley) flow. The latter overcomes the regular up-valley circulation, and persists in the area till the late evening, up to about two hours after the offset of the wind at the lake's shoreline.

In **Chapter 5** dominant vertical profiles of potential temperature and water vapour mixing ratio, derived from airborne observations, allowed the analysis of the "mean" vertical structure of the ABL typically accompanying the development of the *Ora del Garda*. The analysis of these profiles highlighted the occurrence of rather shallow mixed layers (MLs), displaying depths in the order of 500 m or less, surmounted by weakly stable layers, extending almost up to the surrounding crest height (~1500 m MSL), in the Sarca and Lakes valleys. Elevated warm layers were also identified around the crest height. Indeed, such ABL vertical structures are common to deep mountain valleys, and are known to be determined by up-slope winds and associated compensation currents (De Wekker et al. 2004, Kuwagata and Kimura 1995, 1997, Rampanelli et al. 2004, Rotach and Zardi 2007, Serafin and Zardi 2010a, 2010b, 2011, Weigel and Rotach 2004). Closer to the lake's shoreline the potential temperature profiles were even stabilized down to the surface, as a consequence of the up-valley advection of potentially colder air operated by the *Ora del Garda*, which also contributed to inhibit the convective ML growth and suppress the temperature rise in the lowest atmosphere.

Airborne observations at different times of the day on 23 August 2001 outlined the evolution of the ABL vertical structure at the junction between the Lakes and the Adige valleys north of Trento (**Chapter 5**). While around local noon a shallow (~400 m deep) convective boundary-layer (CBL) was detected, in the early afternoon, after the *Ora del Garda* outbreak into the Adige Valley, the ML depth increased to about 1200 m. Observations from local

weather stations revealed also a stabilization of the surface layer. The deepening of the ML was produced by the strong mechanical mixing following the arrival of the *Ora del Garda*, rather than by a classic growth process driven by sensible heat fluxes at the bottom and warmer air entrainment from above (Stull 1988). Relatively large negative values of vertical sensible heat flux observed in the late afternoon at the Adige Valley bottom confirmed the occurrence of near-surface stable-stratification conditions induced by the strong advective cooling associated with the wind flow in this area.

High-resolution fields of potential temperature resulting from the regridding of airborne observations by means of a residual kriging (RK) interpolation allowed the analysis of the fine-scale 3D structure of the ABL associated with the *Ora del Garda* (**Chapter 6**), and the inference of some local features of the thermally-driven wind field. In particular, cross-valley thermal asymmetries corresponding to a differential heating of the opposite sidewalls of the valley, due to the SSW-NNE orientation of the latter as well to land cover heterogeneities, were observed in the Sarca and Lakes valleys, both in the morning and in the afternoon. They may possibly imply the development of asymmetric cross-valley circulations, from the eastern sidewalls towards the western ones. In the lower Sarca Valley an inhomogeneous propagation of the lake-breeze cold front was detected in the late morning of 23 August 2001. This fact is supported also by surface observations, and is mainly amenable to the delay between local sunrise times at the two extremities of the flat area facing Lake Garda. In this area, the presence of a discontinuity in the vertical stratification at the upper levels, typically associated with the development of a lake-breeze circulation cell, was also observed in the afternoon. In the upper Lakes Valley the preferential channeling of the *Ora del Garda* main stream along the northwestern sidewall, produced by the local eastward curvature of the valley axis, was shown by RK-interpolated fields. Finally, the outbreak of the wind into the Adige Valley in the afternoon was found to give origin to a hydraulic jump structure, when the potentially cooler airflow pouring down the Terlago saddle from W impinges on the eastern Adige Valley sidewall. The depth of the down-stream layer, i.e. the increased-depth ML, where an intense turbulent recirculation is likely to occur, turned out to be around 700 and 1300 m respectively for weak *Ora del Garda* and strong *Ora del Garda* conditions. This picture is consistent with previous investigations by de Franceschi et al. (2002), Pollak (1924), Schaller (1936) and Wiener (1929) (reported in Wagner 1938), who speculated on the formation of a cushion of potentially cooler and denser air in the area, leading to the displacement of the regular local up-valley flow at approximately 1000 m above the valley floor.

As coupled sea/lake and valley coupled wind systems, such as the *Ora del Garda*, are known to be often responsible for the transport of airborne pollutants on longer distances than “pure” circulations (Carroll and Baskett 1979, Kitada et al. 1986, Wakimoto and McElroy 1986), a more comprehensive understanding of the typical patterns of this wind and of the fine-scale

variability displayed by the associated ABL structures, especially in the intensely urbanized and industrialized area north of Trento, may undoubtedly represent a key step towards the improvement of air quality assessment and forecasting in the area.

An ancillary result of this investigation comes from the comparison of the predictive performances of different interpolation techniques for airborne data, which was carried out in **Chapter 4**. In particular, the RK method adopted in this study (Ahmed and de Marsily 1987, Odeh et al. 1994, 1995, Goovaerts 1999) resulted to perform better than the methods previously used in the literature for similar applications, such as inverse-distance weighting (used by Egger 1983), exponentially-weighted inverse squared distance (used by Hennemuth 1985) and natural neighbour method (used by De Wekker 2002 and Weigel and Rotach 2004). A leave-one-out cross-validation analysis highlighted that RK provides the most accurate results, and also that the "residual approach" foreseen by RK may improve significantly the performance of the other methods. Moreover, RK returned the most realistic and visually appealing potential temperature fields, while the other methods generally produced physically non-plausible vertical and horizontal gradients, strictly associated with the geometry of the flight trajectory. Hence, RK was finally adopted as the most suitable tool for the regridding of airborne data. As a matter of fact, although computationally more expensive than the other methods, RK presents a series of valuable advantages:

- it explicitely and efficientely accounts for the presence of a dominant trend in the data;
- it relies on the spatial structure of the dataset-specific covariance, and does not assign the interpolation weights on the sole basis of the geometric configuration of the observation points;
- its implementation foresees the determination of the intrinsic anisotropy of the target field, and explicitly accounts for it in the interpolation procedure;
- an indication of the error of the estimate (i.e. the square root of the kriging variance, whose minimization is pursued in kriging algorithms) is inherently provided by its application.

Furthermore, RK is a very flexible technique, and data from different sources – such as point-wise surface observations, vertical profiles from ground-based remote measurements (e.g. lidar measurements) and fully 3D airborne observations – can be integrated in the interpolation process. Notice also that RK can be applied to almost any kind of measurable atmospheric quantity, such as moisture content, concentration of chemical species, aerosols and cloud particles, radiation, wind components, turbulent fluxes, etc.

7.2 Outlook on future developments

Beside the measurement flights exploring the Lakes and Sarca Valley, and primarily aiming at the investigation of the *Ora del Garda* circulation during the warm season, many other

flights were performed by the Atmospheric Physics Group of the University of Trento by means of the instrumented motorglider presented in **Chapter 3**, both in summer and winter conditions. Indeed, field campaigns similar to those providing the database for this thesis were held in different target areas, such as the Adige Valley close to the town of Besenello, around 10 km south to Trento (see for example the flights adopted as test-bed dataset in **Chapter 4**), the Adige Valley close to the city of Bolzano, about 50 km north to Trento, and, in connection with the MAP Special Observing Period (Bougeault et al. 2001), the Isarco Valley, from Trento up to Brenner Pass (de Franceschi et al. 2003). Accordingly, the application of RK post-processing technique to these further datasets is underway, in order to carry out a systematic characterization of the ABL structures and processes peculiar to these mountain areas, similarly to what has been done so far for the Sarca and Lakes valleys.

RK-interpolated meteorological fields not only provide an easier interpretation of ABL fine-scale spatial structures, but they also represent an excellent basis for the comparison and validation of high-resolution numerical simulations of the investigated phenomena. Indeed, the degree of spatial detail they offer is fully comparable to the characteristic spatial scale of the ABL structures explicitely resolved in recent large-eddy simulations (LES) of sea/lake and slope/valley winds (e.g. Antonelli and Rotunno 2007, Catalano and Cenedese 2010, Catalano and Moeng 2010, Chow et al. 2006, Crosman and Horel 2012, Lehner and Whiteman 2012, Serafin and Zardi 2010a, 2010b, 2011, Weigel et al. 2006). As the progress in high-resolution atmospheric modeling appears closely linked to a satisfactory reproduction of ABL processes (Baklanov et al. 2011, Texeira et al. 2008), which is especially problematic in complex terrain, the availability of datasets suitable for model testing and validation is essential. Both mesoscale Reynolds-averaged Navier Stokes (RANS) and LES numerical simulations have proven very useful for the simulation of real cases of thermally-driven flows over complex terrain (see for example the contributions of Bischoff-Gauß et al. 2006, 2008, Chow et al. 2006, De Wekker et al. 2005, Weigel et al. 2006, 2007a, 2007b, Zängl 2004, Zhong and Fast 2003). In particular they allowed a better comprehension of the thermodynamic processes involved in the development of these circulations and of the associated ABL structures. However, in order to get accurate model outputs, displaying a good agreement with experimental observations, high-resolution and high-quality surface datasets, including terrain height, land use and soil moisture, are needed, but are rarely available. Actually, onset time and intensity of thermally-driven winds are particularly sensitive to the initialization of these parameters, which essentially control temporal and spatial distribution of surface heat fluxes (Chow et al. 2006, Daniels et al. 2006).

In order to get a complementary view of the *Ora del Garda* phenomenon, mesoscale RANS simulations of the flight days are currently being run with the Weather Research and Forecasting model (WRF, version 3.1.1; Skamarock et al. 2008), using the setup described in

Giovannini (2012). Five two-way nested domains are used, with horizontal resolution of 500 m for the inner domain and 40 vertical levels. Initial and boundary conditions are provided by the National Center for Environmental Prediction Final Operational Global Analysis data on 1.0° × 1.0° grids and with a temporal resolution of 6 h. A topography dataset with an horizontal resolution of 30 m (http://www.viewfinderpanoramas.org/), properly smoothed, and the CORINE Land Cover 2006 dataset (horizontal resolution: 100 m; http://sia.eionet.europa.eu/CLC2006) are used respectively for terrain height and land use high-resolution initialization. Concerning physical parameterizations, the Noah land-surface model (Chen and Dudhia 2001), the Rapid Radiative Transfer Model scheme for longwave radiation (Mlawer et al. 1997), the Dudhia (1989) shortwave radiation scheme, the Bougeault and Lacarrere (1989) planetary boundary-layer parameterization with 1.5-order closure of turbulence, and the Kain and Fritsch (1990, 1993) cumulus parametrization scheme (for the three outermost domains) are adopted in these simulations. At the moment, problems due to inadequate soil moisture initialization and insufficient vertical resolution of the lowest model levels, leading to weak nocturnal inversions and inaccurate timing of the breeze onset, are being tackled. However, a preliminary analysis of the modeled atmospheric fields showed that they present a reasonably good accordance with surface and airborne observations. Moreover, the major features of the ABL structure and of the wind field outlined in this thesis on the basis of RK-interpolated fields of potential temperature, like the typical vertical structure of the ABL in the study area or the occurrence of a hydraulic jump and strong recirculation in the afternoon at the junction between the Lakes and Adige valleys, appear to be reproduced also in model results. On the other hand, the investigation of finer-scale aspects (e.g. the inhomogeneous penetration of the lake-breeze front in the lower Sarca Valley or, again, the complex flow pattern developing in the area north of Trento) is likely to require that LES simulations be performed, at least for specific key areas of particular topographic complexity or steepness (Mt. Brione and Terlago saddle areas). Indeed, they could afford a higher spatial resolution, allowing at the same time a more realistic representation of fine-scale terrain structures.

A successful validation of the above-cited numerical simulations against the surface and airborne observations presented in this study would legitimate further analyses of the completely three-dimensional, modeled atmospheric fields that were not measured during the flights, for example wind, heat and moisture surface fluxes and turbulent kinetic energy. In addition, the complete temporal and spatial evolution of the *Ora del Garda* and of the associated ABL structures could be characterized, providing further insight into the daytime coupling between the lake breeze circulation and the slope and up-valley flows along the study area valleys, as well as a more comprehensive understanding of the thermodynamic processes driving the investigated phenomenon and an evaluation of the role of the different heating/cooling mechanisms (i.e. sensible heat and latent heat fluxes from the valley floor

and the lateral sidewalls, advection terms, heat exchanges between the valley atmosphere and the free atmosphere, etc.).

Bibliography

Ahmed, S., de Marsily, G., 1987. Comparison of geostatistical methods for estimating transmissivity using data on transmissivity and specific capacity. *Water Resour. Res.* 23, 1717-1737.

Alsamamra, H., Ruiz-Arias, J., Pozo-Vazquez, D., Tovar-Pescador, R., 2009. A comparative study of ordinary and residual kriging techniques for mapping global solar radiation over southern spain. *Agric. Forest Meteor.* 149, 1343-1357.

Antonelli, M., Rotunno, R., 2007. Large-Eddy Simulation of the Onset of the Sea Breeze. *J. Atmos. Sci.* 64, 4445-4457.

Arlot, S., Cenisse, A., 2010. A survey of cross-validation procedures for model selection. *Stat. Surv.* 4, 40-79.

Armi, L., Mayr, G.J., 2007. Continuously stratified flows across an Alpine crest with a pass: shallow and deep föhn. *Quart. J. Roy. Meteor. Soc.* 133, 459-477.

Arritt, R.W., 1987. The effect of water surface temperature on lake breezes and thermal internal boundary layers. *Bound.-Layer Meteor.* 40, 101-125.

Atkinson, B.W., 1981. *Meso-scale Atmospheric Circulations*. Academic Press, London, 494 pp.

Baklanov, A.A., Grisogono, B., Bornstein, R., Mahrt, L., Zilitinkevich, S.S., Taylor, P., Larsen, S.E., Rotach, M.W., Fernando, H.J.S., 2011. The Nature, Theory, and Modeling of Atmospheric Planetary Boundary Layers. *Bull. Amer. Meteor. Soc.* 92, 123-128.

Baldi, M., Cesari, R., Tampieri, F., Tranquillini, M., Zardi, D., 1999. A study of the valley wind known as "Ora del Garda". University of Trento, Civil and Environmental Engineering Department Tech. Note, IDR 1/1999, 119 pp.

Banta, R.M., 1995. Sea Breezes Shallow and Deep on the California Coast. *Mon. Wea. Rev.* 123, 3614-3622.

Barthlott, C., Corsmeier, U., Meißner, C., Braun, F., Kottmeier, C., 2006. The influence of mesoscale circulation systems on triggering convective cells over complex terrain. *Atmos. Res.* 81, 150-175.

Bastin, S., Drobinski, P., Dabas, A., Delville, P., Reitebuch, O., Werner, C., 2005. Impact of the Rhône and Durance valleys on sea-breeze circulation in the Marseille area. *Atmos. Res.* 74, 303-328.

Benedict, R.P., 1984. *Fundamentals of Temperature, Pressure and Flow Measurements*. 3rd ed., John Wiley and Sons, New York, 560 pp.

Bergström, H., Juuso, N., 2006. A study of valley winds using the MIUU meso-scale model. *Wind Energy* 6, 109-129.

Bertò, A., Buzzi, A., Zardi, D., 2004. Back-traking water vapour contributing to precipitation event over Trentino: a case study. *Meteorol. Z.* 13, 189-200.

Bischoff-Gauß, I., Kalthoff, N., Fiebig-Wittmaack, M., 2006. The influence of a storage lake in the Arid Elqui Valley in Chile on local climate. *Theor. Appl. Climatol.* 85, 227-241.

Bischoff-Gauß, I., Kalthoff, N., Khodayar, S., Fiebig-Wittmaack, M., Montecinos, S., 2008. Model Simulations of the Boundary-Layer Evolution over an Arid Andes Valley. *Bound.-Layer Meteor.* 128, 357-379.

Bonin, T., Chilson, P., Zielke, B., Fedorovich, E., 2013. Observations of the Early Evening Boundary-Layer Transition Using a Small Unmanned Aerial System. *Bound.-Layer Meteor.* 146, 119-132.

Bougeault, P., Binder, P., Buzzi, A., Houze, R., Kuettner, J., Smith, R. B., Steinacker, R., Volkert, H., 2001. The MAP Special Observing Period. *Bull. Am. Meteorol. Soc.* 82, 433-462.

Bougealt, P., Lacarrere, P., 1989. Parameterisation of orography-induced turbulence in a Mesobeta-scale model. *Mon. Wea. Rev.* 117, 1872-1890.

Boybeyi, Z., Raman., S., 1992. A three-dimensional numerical sensitivity study of mesoscale circulations induced by circular lakes. *Meteor. Atmos. Phys.* 49, 19-41.

Boyouk, N., Léon, J.F., Delbarre, H., Augustin, P., Fourmentin, M., 2011. Impact of sea breeze on vertical structure of aerosol optical properties in Dunkerque, France. *Atmos. Res.* 101, 902-910.

Brooks, I.M., Rogers, D.P., 2000. Aircraft observatios of the mean and turbulent structure of a shallow boundary layer over the Persian Gulf. *Bound.-Layer Meteor.* 95, 189-210.

Carroll, J.J., Baskett, R.L., 1979. Dependence of air quality in a remote location on local and mesoscale transports: a case study. *J. Appl. Meteor.* 18, 474-486.

Catalano, F., Cenedese, A., 2010. High-Resolution Numerical Modeling of Thermally Driven Slope Winds in a Valley with Strong Capping. *J. Appl. Meteor. Climatol.* 49, 1859-1880.

Catalano, F., Moeng, C.H., 2010. Large-eddy simulation of the daytime boundary layer in an idealized valley using the weather research and forecasting numerical model. *Bound.-Layer Meteor.* 137, 49-75.

Chen, F., Dudhia, J., 2001. Coupling an advanced land-surface/ hydrology model with the Penn State/ NCAR MM5 modeling system. Part I: Model description and implementation. *Mon. Wea. Rev.* 129, 569-585.

Chow, F.K., Weigel, A.P., Street, R.L., Rotach, M.W., Xue, M., 2006. High-resolution large-eddy simulations of flow in a steep alpine valley. Part I: methodology, verification and sensitivity studies. *J. Appl. Meteorol. Climatol.* 45, 63-86.

Cressie, N.A.C., 1993. *Statistics for spatial data*. Revised ed., John Wiley and Sons, New York, 900 pp.

Cressie, N.A.C., Hawkins, D.H., 1980. Robust estimation of the variogram: I. *Math. Geol.* 12, 115-125.

Crosman, E., Horel, J., 2010. Sea and Lake Breezes: A Review of Numerical Studies. *Bound.-Layer Meteor.* 137, 1-29.

Crosman, E., Horel, J., 2012. Idealized Large-Eddy Simulations of Sea and Lake Breezes: Sensitivity to Lake Diameter, Heat Flux and Stability. *Bound.-Layer Meteor.* 144, 309-328.

Daniels, M.H., Chow, F.K., Poulos, G.S., 2006. Effects of soil moisture initialization on simulations of atmospheric boundary layer evolution in Owens Valley. Proc. 12th Conference on Mountain Meteorology, Santa Fe, NM.

Darby, L.S., Banta, R.M., Pielke, R.A., 2002. Comparisons between Mesoscale Model Terrain Sensitivity Studies and Doppler Lidar Measurements of the Sea Breeze at Monterey Bay. *Mon. Wea. Rev.* 130, 2813-2838.

Daves, B., Tampieri, F., Tubino, M., Zardi, D., 1998. Exchange processes in a valley system: the effects of local circulation. Proc. 25th International Conference on Alpine Meteorology, Turin, Italy.

de Franceschi, M., 2004. Investigation of Atmospheric Boundary Layer Dynamics in Alpine Valleys. PhD thesis, Doctoral School in Environmental Engineering, University of Trento, Trento, Italy, 126 pp.

de Franceschi, M., Rampanelli, G., Sguerso, D., Zardi, D., Zatelli, P., 2003. Development of a measurement platform on a light airplane and analysis of airborne measurements in the Atmospheric Boundary Layer. *Ann. Geophys.* 46, 269-283.

de Franceschi, M., Rampanelli, G., Zardi, D., 2002. Further investigations of the "Ora del Garda" valley wind. Proc. 10th Conference on Mountain Meteorology and MAP Meeting 2002, Park City, UT.

de Franceschi, M., Zardi, D., 2003. Evaluation of cut-off frequency and correction of filter-induced phase lag and attenuation in eddy covariance analysis of turbulence data. *Bound.-Layer Meteor.* 108, 289-303.

de Franceschi, M., Zardi, D., 2009. Study of wintertime high pollution episodes during the Brenner-South ALPNAP measurement campaign. *Meteor. Atmos. Phys.* 103, 237-250.

de Franceschi, M., Zardi, D., Tagliazucca, M., Tampieri, F., 2009. Analysis of second order moments in the surface layer turbulence in an Alpine valley. *Quart. J. Roy. Meteor. Soc.* 135, 1750-1765.

De Wekker, S.F.J., 2002. Structure and Morphology of the Convective Boundary Layer in Mountainous Terrain. PhD thesis, University of British Columbia, BC, Canada, 191 pp.

De Wekker, S.F.J., Godwin, K.S., Emmitt, G.D., Greco, S., 2012. Airborne Doppler Lidar Measurements of Valley Flows in Complex Coastal Terrain. *J. Appl. Meteor. Climatol.* 51, 1558-1574.

De Wekker, S.F.J., Steyn, D.G., Fast, J.D., Rotach, M.W., Zhong, S., 2005. The performance of RAMS in representing the convective boundary layer structure in a very steep valley. *Environ. Fluid Mech.* 5, 35-62.

De Wekker, S.F.J., Steyn, D.G., Nyeki, S., 2004. A Comparison Of Aerosol-Layer And Convective Boundary-Layer Structure Over A Mountain Range During Staaarte '97. *Bound.-Layer Meteor.* 113, 249-271.

Defant, A., 1908. Über die stehenden Seespiegelschwankungen (Seiches) in Riva am Gardasee [The stationary fluctuations of the lake level – seiches – at Riva del Garda]. *S. B. Akad. Wiss. Wien* 117, Abt. IIa, 697-780.

Defant, A., 1909. Berg- und Talwinde in Südtirol [Mountain and valley winds in southern Tyrol]. *S. B. Akad. Wiss. Wien* 118, Abt. IIa, 553-604.

Defant, F., 1949. Zur Theorie der Hangwinde, nebst Bemerkungen zur Theorie der Berg- und Talwinde (A theory of slope winds, along with remarks on the theory of mountain and valley winds). *Arch. Meteor. Geophys. Bioklimatol.* A1, 421-450. [English translation: Whiteman, C.D., Dreiseitl, E., 1984. Alpine meteorology: Translations of classic contributions by A. Wagner, E. Ekhart and F. Defant. PNL-5141/ASCOT-84-3. Pacific Northwest Laboratory, Richland, Washington, 121 pp.]

Defant, F., 1951. Local winds. In *Compendium of Meteorology*, T. F. Malone Ed., Amer. Meteor. Soc., 655-672.

Doebelin, E.O., 1990. *Measurement Systems: Application and Design*. 4th ed., McGraw-Hill, New York, 960 pp.

Druilhet, A., Durand, P., 1997. Experimental investigation of atmospheric boundary layer turbulence. *Atmos. Res.* 43, 345-388.

Dryas, I., Ustrnul, Z., 2007. The Spatial Analysis of the Selected Meteorological Fields in the Example of Poland. In *Spatial interpolation for climate data: the use of GIS in climatology and meteorology.* Dobesch, H., Dumolard, P., Dryas, I. (Eds), London: ISTE Ltd.

Dudhia, J., 1989. Numerical study of convection observed during the winter monsoon experiment using a mesoscale two-dimensional model. *J. Atmos. Sci.* 46, 3077-3107.

Egger, J., 1983. Pressure distributions in the Dischma Valley during the field experiment DISKUS. *Contrib. Atmos. Phys.* 56, 163-176.

Finkele, K., Hacker, J.M., Kraus, H., Byron-Scott, R.A.D., 1995. A Complete Sea-Breeze Circulation Cell Derived from Aircraft Observations. *Bound.-Layer Meteor.* 73, 299-317.

Flamant, B.C., Drobinski, P., Nance, L., Banta, R., Darby, L., Dusek, J., 2002. Gap flow in an Alpine valley during a shallow south föhn event: Observations, numerical simulations and hydraulic analogue. *Quart. J. Roy. Meteor. Soc.* 128, 1173-1210.

Flamant, C., Pelon, J., Brashers, B., Brown, R.A., 1999. Evidence of a mixed-layer dynamics contribution to the entrainment process. *Bound.-Layer Meteor.* 93, 47-73.

Garratt, J.R., 1990. The internal boundary layer. A review. *Bound.-Layer Meteor.* 50, 171-203.

Garratt, J.R., 1992. The atmospheric boundary layer. Cambridge University Press, pp.

Genton, M.G., 1998. Highly Robust Variogram Estimation. *Math. Geol.* 30, 213-221.

Giovannini, L., 2012. Urban scale phenomena and boundary layer processes in mountain valleys. PhD thesis, Doctoral School in Environmental Engineering, University of Trento, Trento, Italy, 178 pp.

Giovannini, L., Zardi, D., de Franceschi, M., 2011. Analysis of the Urban Thermal

Fingerprint of the City of Trento in the Alps. J. Appl. Meteor. Climatol. 50, 1145-1162.

Giovannini, L., Zardi, D., de Franceschi, M., 2013. Characterization of the Thermal Structure inside an Urban Canyon: Field Measurements and Validation of a Simple Model. *J. Appl. Meteor. Climatol.* 52, 64-81.

Gladich, I., Gallai, I., Giaiotti, D.B., Stel, F., 2011. On the diurnal cycle of deep moist convection in the southern side of the Alps analysed through cloud-to-ground lightning activity. *Atmos. Res.* 100, 371-376.

Gohm, A., Harnisch, F., Vergeiner, J., Obleitner, F., Schnitzhofer, R., Hansel, A., Fix, A., Neininger, B., Emeis, S., Schäfer, K., 2009. Air pollution transport in an Alpine valley: Results from airborne and ground-based observations. *Bound.-Layer Meteor.* 131, 441-463.

Gohm, A., Mayr, G.J., 2004. Hydraulic aspects of föhn winds in an Alpine valley. *Quart. J. Roy. Meteor. Soc.* 130, 449-480.

Goovaerts, P., 1997. *Geostatistics for natural resources evaluation*. Oxford University Press, New York, 483 pp.

Goovaerts, P., 1999. Using elevation to aid the geostatistical mapping of rainfall erosivity. *CATENA* 34, 227-242.

Harnisch, F., Gohm, A., Fix, A., Schnitzhofer, R., Hansel, A., Neininger, B., 2009. Spatial distribution of aerosols in the Inn Valley atmosphere during wintertime. *Meteor. Atmos. Phys.* 103, 223-235.

Heimann, D., de Franceschi, M., Emeis, S., Lercher, P., Seibert, P. (Eds.), 2007. Air pollution, traffic noise and related health effects in the Alpine space. A guide for authorities and consulters. ALPNAP comprehensive report. University of Trento, Civil and Environmental Engineering Department, Trento, Italy, 335 pp.

Hennemuth, B., 1985. Temperature field and energy budget of a small Alpine valley. *Contrib. Atmos. Phys.* 58, 545-559.

Hennemuth, B., 1986. Thermal asymmetry and cross-valley circulation in a small Alpine valley. *Bound.-Layer Meteor.* 36, 371-394.

Hennemuth, B., Schmidt, H., 1985. Wind phenomena in the Dischma Valley during DISKUS. *Arch. Meteor. Geophys. Bioklimatol.* B35, 361-387.

Hudson, G., Wackernagel, H., 1994. Mapping temperature using kriging with external drift: theory and an example from Scotland. *Int. J. Climat.* 14, 77-91.

Inverarity, G.W., 2000. Correcting Airborne Temperature data for Lags Introduced by Instruments with Two-Time-Constant Responses. *J. Atmos. Ocean. Tech.* 17, 176-184

Isaaks, E.H., Srivastava, R.M., 1989. *An introduction to applied geostatistics*. Oxford University Press, New York, 561 pp.

Jelinek, A., 1937: Beiträge zur Mechanik der Periodischen Hangwinde (Contribution to the mechanics of periodic slope winds). *Beitr. Phys. Atmos.* 24, 60-84.

Journel, A.G., Huijbregts, C.J., 1978. *Mining Geostatistics*. Academic Press, London, 600 pp.

Journel, A.G., Rossi, M., 1989. When do we need a trend model in kriging? *Math. Geol.* 21, 715-739.

Kaimal, J.C., Finnigan, J. J., 1994. *Atmospheric Boundary-Layer Flows: Their Structure and Measurement*. Oxford University Press, 289 pp.

Kain, J.S., Fritsch, J.M., 1990. A One-Dimensional Entraining/Detraining Plume Model and Its Application in Convective Parameterization. *J. Atmos. Sci.* 47, 2784-2802.

Kain, J.S., Fritsch, J.M., 1993. *Convective parameterization for mesoscale models: The Kain-Fritcsh scheme, the representation of cumulus convection in numerical models*. K.A. Emanuel and D.J. Raymond Eds., Amer. Meteor. Soc., 246 pp.

Kalthoff, N., Adler, B., Barthlott, C., Corsmeier, U., Mobbs, S., Crewell, S., Träumner, K., Kottmeier, C., Wieser, A., Smith, V., Di Girolamo, P., 2009. The impact of convergence zones on the initiation of deep convection: A case study from COPS. *Atmos. Res.* 93, 680-694.

Kalthoff, N., Horlacher, V., Corsmeier, U., Volz-Thomas, A., Kolahgar, B., Geiß, H., Möllmann-Coers, M., Knaps, A., 2000. Influence of valley winds on transport and dispersion of airborne pollutants in the Freiburg-Schauinsland area. *J. Geophys. Res.* 105, 1585-1597.

Keller, R., W. Larcher, F. Tisi, and R. Turrini, 1994. *Arco nel suo verde*. Cassa Rurale di Arco and Museo Tridentino di Scienze Naturali Ed., Grafiche Manfrini, Calliano, Trento, Italy, 240 pp.

Kitada, T., Igarashi, K., Owada, M., 1986. Numerical-analysis of air-pollution in a combined field of land sea breeze and mountain valley wind. *J. Climate Appl. Meteor.* 25, 767-784.

Kondo, H., 1990a. A Numerical experiment of the "Extended Sea Breeze" over the Kanto Plain. *J. Meteor. Soc. Japan* 68, 419-434.

Kondo, H., 1990b. A numerical experiment on the interaction between sea breeze and valley wind to generate the so-called "Extended Sea Breeze". *J. Meteor. Soc. Japan* 68, 435-446.

Kossmann, M., Sturman, A.P., Zawar-Reza, P., McGowan, H.A., Oliphant, A.J., Owens, I.F., Spronken-Smith, R.A., 2002. Analysis of the wind field and heat budget in an Alpine lake basin during summertime fair weather conditions. *Meteor. Atmos. Phys.* 81, 27-52.

Kossmann, M., Vögtlin, R., Corsmeier, U., Vogel, B., Fiedler, F., Binder, H.J., Kalthoff, N., Beyrich, F., 1998. Aspects of the convective boundary layer structure over complex terrain. *Atmos. Env.* 32, 1323-1348.

Kraus, H., Hacker, J.M., Hartmann, J., 1990. An observational aircraft-based study of the breeze frontogenesis. *Bound.-Layer Meteor.* 53, 223-265.

Krige, D.G., 1951. A statistical approach to some basic mine valuation problems on the Witwatersrand. *J. of the Chem., Metal. and Mining Soc. of South Africa* 52, 119-139.

Kuwagata, T., Kimura, F., 1995. Daytime boundary layer evolution in a deep valley. Part I: Observations in the Ina Valley. *J. Appl. Meteor.* 34, 1082-1091.

Kuwagata, T., Kimura, F., 1997. Daytime boundary layer evolution in a deep valley. Part II:

Numerical simulation of the cross-valley circulation. *J. Appl. Meteor.* 36, 883-895.

Laiti, L., Zardi, D., de Franceschi, M., Rampanelli, G., 2013. Residual kriging analysis of airborne measurements: application to the mapping of atmospheric boundary-layer thermal structures in a mountain valley. *Atmos. Sci. Lett.* [in press]

Lehner, M., Whiteman, C.D., 2012. The Thermally Driven Cross-Basin Circulation in Idealized Basins under Varying Wind Conditions. *J. Appl. Meteor. Climatol.* 51, 1026-1045.

Lehner, M., Whiteman, C.D., Hoch, S.W., 2011. Diurnal Cycle of Thermally Driven Cross-Basin Winds in Arizona's Meteor Crater. *J. Appl. Meteor. Climatol.* 50, 729-744.

Lieman, R., Alpert, P., 1993. Investigations of the planetary boundary layer height variations over complex terrain. *Bound-Layer Meteor.* 62, 129-142.

Lyons, W.A., Olsson, L.E, 1973. Detailed Mesometeorological Studies of Air Pollution Dispersion in the Chicago Lake Breeze. *Mon. Wea. Rev.* 101, 387-403.

Mahesh, A., Walden, V.P., Warren, S.G., 1997. Radiosonde Temperature Measurements in dtrong Inversions: Correction for Thermal Lag Based on an Experiment at the South Pole. *J. Atmos. Ocean. Tech.* 14, 45-53.

Mahrer, Y., Pielke, R.A., 1977. The Effects of Topography on Sea and Land Breezes in a Two-Dimensional Numerical Model. *Mon. Wea. Rev.* 105, 1151-1162.

Matheron, G., 1971. *The theory of regionalized variables and its applications*. École National Supérieure des Mines, Paris, 212 pp.

Mayr, G.J., Laurence, A., Gohm, A., Zängl, G., Durran, D.R., Flamant, C., Gaberšek, S., Mobbs, S., Ross, A., Weissmann, M., 2007. Gap flows: Results from the Mesoscale Alpine Programme. *Quart. J. Roy. Meteor. Soc.* 133, 881-896.

McCarthy, J., 1972. A method for correcting airborne temperature data for sensor response time. *J. Appl. Meteor.* 12, 211-214.

McElroy, J.L., Smith, T.B., 1991. Lidar description of mixing-layer thickness characteristics in a complex terrain/coastal environment. *J. Appl. Meteor.* 30, 585-597.

McGowan, H.A., Owens, I.F., Sturman, A.P., 1995. Thermal and dynamic characteristics of Alpine lake breezes, Lake Tekapo, New Zealand. *Bound.-Layer Meteor.* 76, 3-24.

McGowan, H.A., Sturman, A.P., 1996. Interacting multi-scale wind systems within an Alpine basin, Lake Tekapo. New Zealand. *Meteor. Atmos. Phys.* 58, 165-177.

Mlawer, E.J., Taubman, S.J., Brown, P.D., Iacono, M.J., Clough, S.A., 1997. Radiative transfer for inhomogeneous atmosphere: RRTM, a validated correlated-k model for the longwave. *J. Geophys. Res.* 102, 16663-16682.

Neininger, B., Fuchs, W., Bäumle, M., Volz-Thomas, A., Prévôt, A.S.H., Dommen, J., 2001. A small aircraft for more than just ozone: MetAir's 'Dimona' after ten years of evolving development. Proc. 11th symposium on meteorological observations and instrumentation, Amer. Meteorol. Soc., Albuquerque, NM, 123-128.

Odeh, I.O.A., McBratney, A.B., Chittleborough, D.J., 1994. Spatial prediction of soil properties from landform attributes derived from a digital elevation model. *Geoderma* 63,

197-214.

Odeh, I.O.A., McBratney, A.B., Chittleborough, D.J., 1995. Further results on prediction of soil properties from terrain attributes: heterotropic cokriging and regression-kriging. *Geoderma* 67, 215-226.

Oke, T.R., 1987. *Boundary Layer Climates*. 2nd ed., Routledge, London, 435 pp.

Pielke, R.A., 1984. *Mesoscale meteorological modeling*. 1st ed., Academic Press, New York, 612 pp.

Pollak, L.W., 1924. Berg- und Talwinde im Becken von Trient [The wind directions in Trento basin]. *Meteor. Z.* 18-21.

Porson, A., Steyn, D., Schayes, G., 2007a. Sea-breeze scaling from numerical model simulations, Part I: Pure sea breezes. *Bound.-Layer Meteor.* 22, 17-29.

Porson, A., Steyn, D.G., Schayes, G., 2007b. Sea-breeze scaling from numerical model simulations. Part II: Interaction between the sea breeze and slope flows. *Bound.-Layer Meteor.* 122, 31-41.

Pucillo, A., Giaiotti, D.B., Stel, F. 2009. Ground wind convergence as source of deep convection initiation. *Atmos. Res.* 93, 437-445.

Quarteroni, A., Sacco, R., Saleri, F., 2007. *Numerical Mathematics*. 2nd ed., Springer-Verlag, New York, 657 pp.

Rampanelli, G., 2004. Investigation of Diurnal Atmospheric Boundary Layer Dynamics in Alpine Valleys. PhD thesis, Doctoral School in Environmental Engineering, University of Trento, Trento, Italy, 133 pp.

Rampanelli, G., Zardi, D., 2002. Identification of thermal structure from airborne measurements in an Alpine valley with kriging technique. Proc. 10th Amer. Meteor. Soc. Conference on Mountain Meteorology, Park City, UT.

Rampanelli, G., Zardi, D., 2004. A method to determine the capping inversion of the convective boundary layer. *J. Appl. Meteor.* 43, 925-933.

Rampanelli, G., Zardi, D., Rotunno, R., 2004. Mechanisms of up-valley winds. *J. Atmos. Sci.* 61, 3097-3111.

Reuder, J., Brisset, P., Jonassen, M., Müller, M., Mayer, S., 2009. The small unmanned meteorological observer SUMO: a new tool for atmospheric boundary layer research. *Meteorol. Z.* 18, 141-147.

Rotach, M.W., 2012. Inhomogeneity of atmospheric boundary layers in complex terrain. European Geosciences Union General Assembly 2012, Wien, Austria.

Rotach, M.W., Andretta, M., Calanca, P., Weigel, A.P., Weiss, A., 2008. Turbulence characteristics and exchange mechanisms in highly complex terrain. *Acta Geophys.* 56, 194-219.

Rotach, M.W., Calanca, P., Graziani, G., Gurtz, J., Steyn, D.G., Vogt, R., Andretta, M., Christen, A., Cieslik, S., Connolly, R., de Wekker, S.F.J., Galmarini, S., Kadygrov, E.N., Kadygrov, V., Miller, E., Neininger, B., Rucker, M., van Gorsel, E., Weber, H., Weiss, A., Zappa, M., 2004. Turbulence Structure and Exchange Processes in an Alpine Valley:

The Riviera Project. *Bull. Amer. Meteor. Soc.* 85, 1367-1385.

Rotach, M.W., Zardi, D., 2007. On the boundary layer structure over highly complex terrain: Key findings from MAP. *Quart. J. Roy. Meteor. Soc.* 133, 937-948.

Schaller, E., 1936. Aerologische Untersuchung des periodischen Talwindsystems von Trient (Aerologic investigation of the periodic valley wind system of Trento). Dissertation, Innsbruck.

Schmidli, J., Billings, B., Chow, F.K., De Wekker, S.F.J., Doyle, J., Grubišić, V., Holt, T., Jiang, Q.F., Lundquist, K.A., Sheridan, P., Vosper, S., Whiteman, C.D., Wyszogrodzki, A.A., Zängl, G., 2011. Intercomparison of mesoscale model simulations of the daytime valley wind system. *Mon. Wea. Rev.* 139, 1389-1409.

Schmidli, J., Rotunno, R., 2010. Mechanisms of along-valley winds and heat exchange over mountainous terrain. *J. Atmos. Sci.* 67, 3033-3047.

Schmidli, J., Rotunno, R., 2012: Influence of the valley surroundings on valley wind dynamics. *J. Atmos. Sci.* 69, 561-577.

Schnitzhofer, R., Norman, M., Wisthaler, A., Vergeiner, J., Harnisch, F., Gohm, A., Obleitner, F., Fix, A., Neininger, B., Hansel, A., 2009. A multimethodological approach to study the spatial distribution of air pollution in an Alpine valley during wintertime. *Atmos. Chem. Phys.* 9, 3385-3396.

Segal, M., Leuthold, M., Arritt, R.W., Anderson, C., Shen, J., 1997. Small lake daytime breezes: some observational and conceptual evaluations. *Bull. Amer. Meteor. Soc.* 78, 1135-1147.

Serafin, S., Zardi, D., 2010a. Structure of the atmospheric boundary layer in the vicinity of a developing upslope flow system: A numerical model study. *J. Atmos. Sci.* 67, 1171-1185.

Serafin, S., Zardi, D., 2010b. Daytime heat transfer processes related to slope flows and turbulent convection in an idealized mountain valley. *J. Atmos. Sci.* 67, 3739-3756.

Serafin, S., Zardi, D., 2011. Daytime development of the boundary layer over a plain and in a valley under fair weather conditions: A comparison by means of idealized numerical simulations. *J. Atmos. Sci.* 68, 2128-2141.

Shaw, W.J., Tillman, J.E., 1980. The effect of and correction for different wet-bulb and dry-bulb response in thermocouple psychrometry. *J. Appl. Meteor.* 19, 90-97.

Shepard, D., 1968. A two-dimensional interpolation function for irregularly-spaced data. Proc. ACM National Conference.

Simpson, J.E., 1994. *Sea breeze and local winds*. Cambridge University Press, Cambridge, 234 pp.

Skamarock, W.C., Klemp, J. B., Dudhia, J., Gill, D.O., Barker, D.M., Duda, M., Huang, X.Y., Wang, W., Powers, J.G., 2008. *A Description of the Advanced Research WRF Version 3*. NCAR Technical Note.

Steinacker, R., 1984. Area-height distribution of a valley and its relation to the valley wind. *Beitraege Phys. Atmosph*. 57, 64-71.

Stephan, K., Kraus, H., Ewenz, C.M., Hacker, J.M., 1999. Sea-Breeze Front Variations in

Space and Time. *Meteorol. Atmos. Phys.* 70 81-95.

Stull, R.B., 1988. *An introduction to boundary layer meteorology*. Kluwer Academic Publishers, Dordrecht, 666 pp.

Sturman, A.P., Bradley, S., Drummond, P., Grant, K., Gudiksen, P., Kossmann, M., McGowan, H.A., Oliphant, A., Owens, I.F., Powell, S., Spronken-Smith, R., Zawar-Reza, P., 2003a. The Lake Tekapo Experiment (LTEX): an investigation of atmospheric boundary layer processes in complex terrain. *Bull. Amer. Meteor. Soc.* 84, 371-380.

Sturman, A.P., Bradley, S., Drummond, P., Grant, K., Gudiksen, P., Kossmann, M., McGowan, H.A., Oliphant, A., Owens, I.F., Powell, S., Spronken-Smith, R., Zawar-Reza, P., 2003b. Supplement to the Lake Tekapo Experiment (LTEX): An investigation of Atmospheric Boundary Layer processes in complex terrain. *Bull. Amer. Meteor. Soc.* 84, 381-383.

Teixeira, J., Stevens, B., Bretherton, C.S., Cederwall, R., Doyle, J.D., Golaz, J.C., Holtslag, A.A.M., Klein, S.A., Lundquist, J.K., Randall, D.A., Siebesma, A.P., Soares, P.M.M., 2008. Parameterization of the Atmospheric Boundary Layer: A View from Just Above the Inversion. *Bull. Amer. Meteor. Soc.* 89, 453-458.

Tschudin, M.E., Schroeder, S.R., 2013. Time constant estimates for radiosonde temperature sensors. *J. Atmos. Ocean. Tech.* 30, 40-56.

Tveito, O.E., Wegehenkel, M., Van der Wel, F., Dobesch, H., 2006. The Use of Geographic Information Systems in Climatology and Meteorology - Final Report COST Action 719.

Venkatram, A., 1977. A model of internal boundary-layer development. Bound.-Layer Meteor. 11, 419-437.

Vergeiner, I., Dreiseitl, E., 1987. Valley winds and slope winds – Observations and elementary thoughts. *Meteor. Atmos. Phys.* 36, 264-286.

Wagner, A., 1932. Der tägliche Luftdruck- und Temperaturgang in der freien Atmosphaere und in Gebirgstaelern (The daytime air- pressure and temperature variation in the free atmosphere and in mountain valleys). *Gerl. Beitr. Geophys.* 37, 315-344.

Wagner, A., 1938. Theorie und Beobachtung der periodischen Gebirgswinde (Theory and observation of periodic mountain winds). *Gerlands Beitr. Geophys.* 52, 408-449. [English translation: Whiteman, C. D., and E. Dreiseitl, 1984: Alpine meteorology: Translations of classic contributions by A. Wagner, E. Ekhart and F. Defant. PNL-5141/ASCOT-84-3. Pacific Northwest Laboratory, Richland, Washington, 121 pp.]

Wakimoto, R.M., McElroy, J.L., 1986. Lidar observation of elevated pollution layers over Los Angeles. *J. Appl. Meteor. Climatol.* 25, 1583-1599.

Watson, D.F., 1992. *Contouring: A guide to the analysis and display of spatial data*. Pergamon Press, Oxford, 321 pp.

Weigel, A.P., Chow, F.K., Rotach, M.W., 2007a. On the nature of turbulent kinetic energy in a steep and narrow Alpine valley. *Bound.-Layer Meteor.* 123, 177-199.

Weigel, A.P., Chow, F.K., Rotach, M.W., 2007b. The effect of mountainous topography on moisture exchange between the “surface” and the free atmosphere. *Bound.-Layer Meteor.* 125, 227-244.

Weigel, A.P., Chow, F.K., Rotach, M.W., Street, R.L., Xue, M., 2006. High-resolution large-eddy simulations of flow in a steep Alpine valley. Part II: Flow structure and heat budgets. *J. Appl. Meteor. Climatol.* 45, 87-107.

Weigel, A.P., Rotach, M.W., 2004. Flow structure and turbulence characteristics of the daytime atmosphere in a steep and narrow Alpine valley. *Quart. J. Roy. Meteor. Soc.* 130, 2605-2627.

Weissmann, M., Braun, F.J., Gantner, L., Mayr, G.J., Rahm, S., Reitebuch, O., 2005. The Alpine Mountain-Plain Circulation: Airborne Doppler Lidar Measurements and Numerical Simulations. *Mon. Wea. Rev.* 133, 3095-3109.

Whiteman, C.D., 1982. Breakup of Temperature Inversions in Deep Mountain Valleys: Part I. Observations. *J. Appl. Meteor*. 21, 270-289.

Whiteman, C.D., 1990. *Observations of thermally developed wind systems in mountainous terrain. Atmospheric Processes over Complex Terrain*. Meteor. Monogr., No. 45, Amer. Meteor. Soc. 5-42.

Whiteman, C.D., 2000. *Mountain meteorology. Fundamentals and applications.* Oxford University Press, Oxford, 355 pp.

Whiteman, C.D., Doran, J.C., 1993. The Relationship between Overlying Synoptic-Scale Flows and Winds within a Valley. *J. Appl. Meteor.* 32, 1669-1682.

Wiener, V., 1929. Die Windrichtungen im Becken von Trient [The wind directions in Trento basin]. Dissertation, Prague.

Wood, R., Stromberg, I.M., Jonas, P.R., 1999. Aircraft observations of sea-breeze frontal structure. *Q. J. R. Meteorol. Soc.* 125, 1959-1995.

Zängl, G., 2004. A reexamination of the valley wind system in the Alpine Inn Valley with numerical simulations. *Meteor. Atmos. Phys.* 87, 241-256.

Zardi, D., Gerola, R., Tampieri, F., Tubino, M., 1999. Measurement and modeling of a valley wind system in the Alps. Proc. 13th Symp. on Boundary Layers and Turbulence, Dallas, TX, Amer. Meteor. Soc, 28-31.

Zardi, D., Whiteman, C.D., 2013. Diurnal mountain wind systems. In *Mountain Weather Research and Forecasting: Recent Progress and Current Challenges*. F.K. Chow, S.F.J. De Wekker and B. Snyder, Eds., Springer, 35-119.

Zawar-Reza, P., McGowan, H., Sturman, A., Kossmann, M., 2004. Numerical simulations of wind and temperature structure within an Alpine lake basin, Lake Tekapo, New Zealand. *Meteor. Atmos. Phys.* 86, 245-260.

Zhong, S., Fast, J., 2003. An evaluation of the MM5, RAMS, and Meso-Eta models at subkilometer resolution using VTMX field campaign data in the Salt Lake valley. *Mon. Wea. Rev.* 131, 1301-1322.

Zumpfe, D.E., Horel., J.D., 2007. Lake-Breeze Fronts in the Salt Lake Valley. *J. Appl. Meteor. Climatol.* 46, 196-211.